ADSORPTION OF PURE AND MULTICOMPONENT GASES ON WET FRUITLAND COAL

By

FREDDIE EDDSEL HALL, JR.

Bachelor of Science

University of Central Oklahoma

Edmond, Oklahoma

May 1986

Submitted to the Faculty of the
Graduate College of the
Oklahoma State University
in partial fulfillment of
the requirements for
the Degree of
MASTER OF SCIENCE
December 1993

ADSORPTION OF PURE AND MULTICOMPONENT

GASES ON WET FRUITLAND COAL

Thesis Approved:

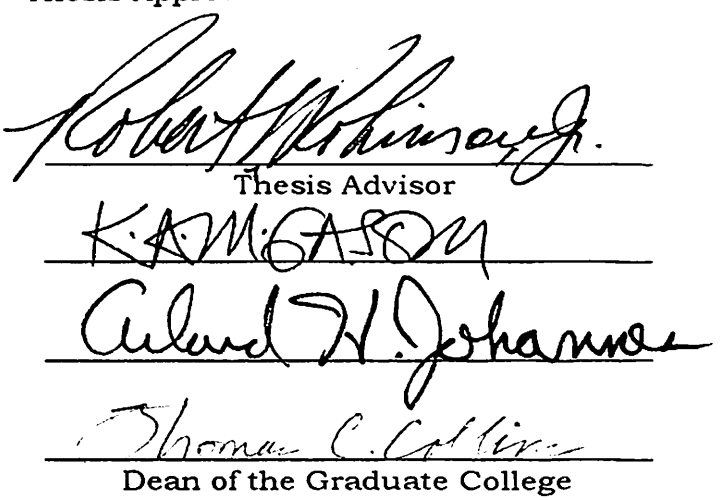

Thesis Advisor

Dean of the Graduate College

ACKNOWLEDGMENTS

There comes a time in life to decide what one has discovered about a small part of nature, and to form the thoughts derived from that experience into words. It is the hope of this author that this humble work be of some enlightenment to those that may come to read its content.

During the course of any endeavor, more than one person's effort will eventually bring about the desired end of that work. I would like to offer my sincere appreciation to my advisor, Professor Robert L. Robinson, Jr., for his guidance, expertise, and advice. I would like to thank Dr. Robinson for his patience, and giving me the opportunity to work on this project. I am deeply grateful for the opportunity to work and study under a man of such high integrity, quality and fame. I was always impressed with his ability to recall such minute details. He will remain one of the most impressive men that I have ever known.

There are not words which I may write on this page which could justly thank my friend, Dr. Khaled M. Gasem. Without his insight, wisdom and advise, this work could not have been completed. When things in the laboratory were not going as expected, Dr. Gasem was there with encouragement. I have always been impressed with his skill as a teacher, with his ability to explain even the most difficult topics.

Most of all I would like to thank my family for their love, patience, encouragement and understanding during the course of my studies, especially my mother and father, Elsie and Freddie Hall. I also love and appreciate my remaining family including brothers (Randy and Roger), sister (Gina), nephew (Dustin) and niece (Alicia).

TABLE OF CONTENTS

LIST OF TABLES

LIST OF FIGURES

Figure Page

LIST OF SYMBOLS

$\mathcal{A}$: Molar area

A : Helmholtz free energy

AAD : average absolute deviation

Ads : adsorption

A_i : chromatogram peak area of component i

A_{ash} : ash content of coal sample

B : Langmuir adsorption isotherm model constant

b : Langmuir adsorption isotherm model constant

b_{ij} : second virial expansion coefficient

B(T) : second virial coefficient

C_{ij} : binary interaction parameter

c_{ijk} : third virial expansion coefficient

C(T) : third virial coefficient

EOS : equation-of-state

G : Gibbs free energy

H : enthalpy

k : Freundlich adsorption isotherm model constant

k : Langmuir adsorption isotherm model constant

L : Langmuir adsorption isotherm model constant

L_i : Langmuir adsorption isotherm model constant (represents amount of pure component i adsorbed per unit of adsorbent upon completion of a hypothetical monolayer)

LRC : Loading Ratio Correlation

m : mass of adsorbent in Freundlich adsorption isotherm equation

n : Freundlich adsorption isotherm model constant

n : moles

n_i : moles of component i

P : pressure

PVT : pressure, volume and temperature

R : universal gas constant

R_f : relative response factor

RK : Redlich-Kwong equation-of-state

RTD : resistance temperature device

S : entropy

S_{sulfur}:sulfur content of coal sample

U : internal energy

V : volume

$V_{gas\ content}$: Freundlich/Langmuir gas content

V_{max} : maximum sorption capacity

V_p : injection pump volume reading

V_{void} : cell system void volume

v : specific molar volume

x : mass of adsorbate in Freundlich adsorption isotherm equation

x_i : adsorbed phase mole fraction of component i

y_i : gas phase mole fraction of component i

y_{pure} : mass fraction of organic (pure) coal in coal sample

Z : compressibility factor

z_k : pump section feed gas mixture composition for component k

Greek Symbols

μ_i : chemical potential of component i

ν : molar volume

π : spreading pressure

θ : fraction of monolayer adsorption coverage in Langmuir model

ρ : density

σ : uncertainty associated with experimental measurement; surface tension of a surface covered with adsorbate

σ° : surface tension of a clean surface

ω : amount of gas adsorbed per unit mass of adsorbent

ω_i : amount of pure component i adsorbed per unit mass of adsorbent

Subscripts

Abs : represents absolute adsorption

ads : represents the adsorbed phase within the cell system

ash : ash content in coal sample

att : attractive contribution to RK EOS

c : critical property

cell : cell section

f : final reading

gas : represents the unadsorbed free gas phase within the cell

Gibbs: represents Gibbs adsorption

i : initial reading

inj : amount of gas injected

mix : amount of gas mixture injected into the equilibrium cell

pump: pump section

pure : pure (organic) coal

rep : repulsive contribution to RK EOS

solu : amount of gas dissolved in water within coal

sulfur: sulfur content in coal sample

unads: amount of unadsorbed free gas within cell

Superscripts

Abs : represents absolute adsorption

ads : represents the adsorbed phase within the cell system

Gibbs: represents Gibbs adsorption

~ : partial molar property

CHAPTER I

INTRODUCTION

Large quantities of natural gas (primarily methane) are stored in coal deposits. United States coal deposits contain two to four times the amount of gas currently stored in conventional natural gas reservoirs [27]. In conventional reservoirs, the gas exists in a gaseous state stored within pores of reservoir rock, and the gas behavior can be described by the real gas law [27]. However, more gas can be stored per unit volume in coalbeds than in conventional reservoirs because the coalbed gas is stored in the form of a condensed, liquid-like adsorbed layer on the coal surface rather than in the gaseous state [4]. The adsorbed layer holds significantly more methane than an equal volume of a conventional reservoir due to the much higher density of the condensed (adsorbed) gas.

Methane has been observed in coalbeds since the beginning of underground coal mining, but only recently has coalbed methane been recognized as an economically producible energy source [5]. Coal underlies approximately 360,000 square miles of the conterminous United States, with the majority of the coal localized within thirteen coal-bearing basins [27]. The Department of Energy and Gas Research Institute estimate the potential methane resource as approximately 800 trillion cubic feet which is approximately a twenty-year supply at current consumption rates [27]. Coal resource estimates have been based on mineable coals at a depth of less than 3,000 feet. Because of a paucity of data, the deep gas resource potential is not well known.

The current state of scientific and engineering knowledge is inadequate

regarding the adsorption behavior of gases on coal [5]. Current primary production strategies recover only approximately fifty percent of the coalbed gas [5]. Amoco Production Company has an interest (and patents) in the enhanced recovery of methane [29]. Recent research at Amoco Production Company's Tulsa Research Center has shown that the recovery of coalbed methane can be enhanced by injecting gases such as nitrogen or nitrogen/carbon dioxide mixtures directly into the coal deposits, thereby displacing the methane.

The primary objective of the present work was to provide engineers with phase behavior information required to optimize the production and recovery of coalbed methane. Specific objectives of the present work included:

- Design, construct, and test an experimental facility for adsorption measurements.
- Measure the adsorption of methane, nitrogen, carbon dioxide and their binary mixtures on wet Fruitland coal at 115 °F at pressures to 1800 psia.
- Report the results in formats suitable for use in modeling of depletion behavior of coalbed methane reserves.

The adsorption research described herein was conducted jointly by Oklahoma State University's School of Chemical Engineering and Amoco Production Company's Tulsa Research Center. The experimental measurements provide data describing the adsorption characteristics of pure methane, nitrogen, carbon dioxide and their binary mixtures on wet Fruitland coal. The pure component and mixture data were used to test mathematical models for describing the adsorption behavior of mixtures of the above gases on the coal surface. The adsorption experiments were conducted at a temperature of 115 °F at pressures to 1800 psia. These conditions were chosen to be representative of the Fruitland coals commonly found in the Colorado portion of the

San Juan Basin in the four corners area of the United States [4].

Knowledge gained from this project should improve the level of understanding of coalbed gas adsorption and desorption processes. The information can be used to design optimum strategies for coalbed methane production. The information and knowledge gained from the present experimental work can impact the economics of coalbed methane production as well as help conserve this important natural resource. Environmental benefits can also occur as a result of the clean burning characteristics of methane relative to oil or coal. Minor improvements in production operations to increase coalbed gas recovery can yield tremendous economic and environmental benefits.

CHAPTER II

THEORY

Adsorption

The accumulation of particles at a solid surface is called adsorption. The substance that adsorbs on the surface is called the adsorbate with the underlying solid material known as the adsorbent or substrate [6]. Adsorption is distinguished from absorption, which involves bulk penetration of the gas into the structure of the solid by some process of diffusion [1]. Absorption is usually governed by laws of diffusion and can be differentiated from adsorption [1]. The term sorption is used when both adsorption and absorption may be occurring simultaneously [1].

Adsorption Classifications

There are two adsorption classifications based on the type of interaction occurring with the surface. In physical adsorption or physisorption, there are van der Waals molecular interactions (e.g., dispersion or dipole interactions) between the adsorbate and the substrate [6]. The formation of a physically adsorbed layer may be likened to the condensation of a vapor to form a liquid. This involves long-range but weak interactions [6]. In chemical adsorption or chemisorption, the particles bind to the surface by forming chemical (usually covalent) bonds and tend to find sites that maximize their attachment to the substrate [6]. Chemical adsorption involves the transfer of electrons between the adsorbent and the adsorbate. Other distinctions between physical and chemical adsorption include the following [1]. Physical adsorption may be multilayer while chemisorption is monolayer. The physical

adsorption process is spontaneous while the chemisorption process may require overcoming an activation energy before adsorption occurs [1].

The great majority of the adsorption isotherms (physical and chemical) observed to date can be classified into five types [37], as shown in Figure 1. Types I and II are the most frequently encountered [37]. Type I is monolayer adsorption with Types II through V involving multimolecular, multilayer adsorption [37].

Fundamental Property Relations

The theory of adsorption is based on fundamental laws of thermodynamics [1]. First and second laws of thermodynamics are used to developed "Fundamental Property Relation" for a three-dimensional open system. The equations can be used for applications in adsorption by assuming the system acts as an open system with mass and energy exchanges between the adsorbed and gas phases. The fundamental property relations for a three-dimensional, open system can be rewritten as the following [37].

$$dG = -SdT + VdP + \sum_i \mu_i \, dn_i \qquad \text{(II-1)}$$

An analogy to the above three-dimensional, open-system, Gibbs free energy fundamental property relation expression in two dimensions is shown below [37]. The two-dimensional pressure term is expressed as the spreading pressure, π, defined as the difference in surface tension between a clean surface (σ°) and a surface covered with (monomolecular) adsorbate (σ) [37].

$$\pi = \sigma^\circ - \sigma \qquad \text{(II-2)}$$

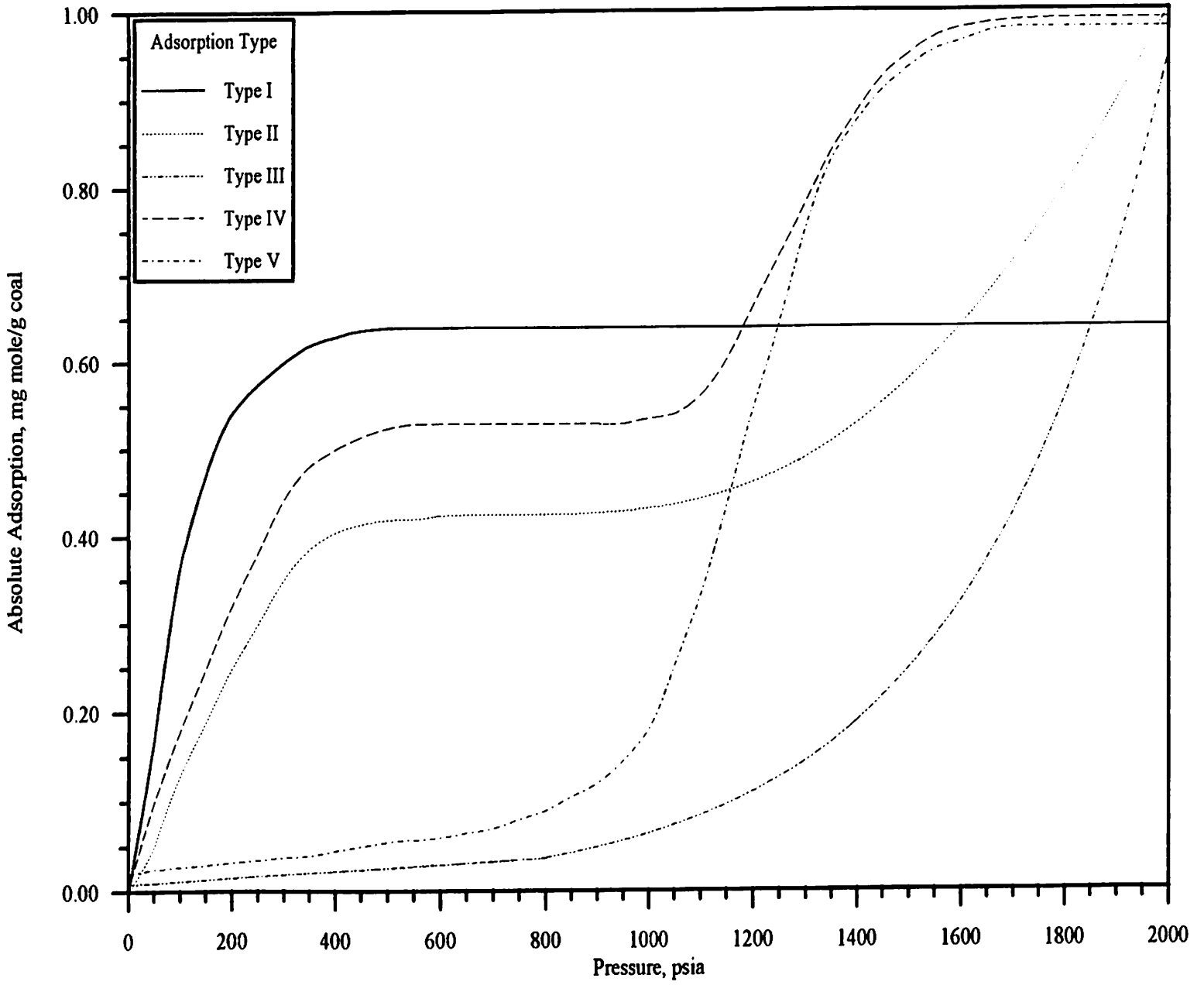

Figure 1. Five Types of Physical Adsorption Isotherms

The spreading pressure defines the lowering of the surface tension at the solid-gas interface upon adsorption [37]. The spreading pressures is defined as Equation II-3 from Equation II-2.

$$dU = TdS - \pi d\mathcal{A} + \sum_i \mu_i \, dn_i \tag{II-2}$$

$$\pi = -\left[\frac{\partial U}{\partial \mathcal{A}}\right]_{S,n_i} \tag{II-3}$$

The three-dimensional molar volume term (Equation II-1) is changed to molar area, $\mathcal{A}$.

$$dG = -SdT + \mathcal{A}\, d\pi + \sum_i \mu_i \, dn_i \tag{II-4}$$

The Gibbs free energy expression can be differentiated with respect to the moles of component i at constant temperature, spreading pressure and composition of component j to yield the following.

$$\mu_i \equiv \left[\frac{\partial G}{\partial n_i}\right]_{T,\pi,n_j} \equiv \tilde{G}_i \tag{II-5}$$

This partial differential is defined as the partial molar Gibbs property, $\tilde{G}_i$, and allows assignment of constituent contributions to a given mixture property and provides a basis for the formulation of mixture equilibrium relations.

$$G = \sum_{i=1}^{N} x_i \tilde{G}_i = \sum_{i=1}^{N} x_i \mu_i \tag{II-6}$$

Equilibrium Criteria

The equilibrium criteria are obtained from relationships furnished from the first and second laws of thermodynamics. The entropy will be a maximum at constant U, V and n. The U (S,V,n), H (S,P,n), G (T,P,n) and A (T,V,n) properties will all exist as minima at equilibrium [3]. (The properties enclosed in parenthesis are held constant for each property and are the characteristic variables in the fundamental property relation.)

For adsorption processes, the general equilibrium criteria between the gas and adsorbed phase for a two-dimensional, open system are the following. The gas phase is represented by the subscript *gas* and the adsorbed phase is denoted with *ads*.

$$dS_{gas} = \left[\frac{dU}{T}\right]_{gas} + \left[\frac{P}{T}\right]_{gas} dV_{gas} - \sum_i \left[\frac{\mu_i}{T}\right]_{gas} dn_{i_{gas}} \qquad \text{(II-7)}$$

$$dS_{ads} = \left[\frac{dU}{T}\right]_{ads} + \left[\frac{P}{T}\right]_{ads} dV_{ads} - \sum_i \left[\frac{\mu_i}{T}\right]_{ads} dn_{i_{ads}} \qquad \text{(II-8)}$$

For a system composed of two phases at equilibrium [31]

$$dS = dS_{gas} + dS_{ads} = 0 \qquad \text{(II-9)}$$

Inserting Equations II-7 and II-8 into II-9 eliminates dU_{ads}, dV_{ads} and n_i, yielding

$$dS = \left[\left(\frac{1}{T}\right)_{gas} - \left(\frac{1}{T}\right)_{ads}\right] dU_{gas} + \left[\left(\frac{P}{T}\right)_{gas} - \left(\frac{P}{T}\right)_{ads}\right] dV_{gas} - \sum_i \left[\left(\frac{\mu}{T}\right)_{gas} - \left(\frac{\mu}{T}\right)_{ads}\right]_i dn_i = 0 \qquad \text{(II-10)}$$

For the above expression to be correct for general variations in U_{gas}, V_{gas} and n_i, the

coefficients of these independent variables must be zero. This implies the following general criteria for equilibrium between heterogeneous gas and adsorbed phases for i components [31].

$$T_{gas} = T_{ads} \tag{II-11}$$

$$P_{gas} = P_{ads} \tag{II-12}$$

$$\mu_i^{gas} = \mu_i^{ads} \tag{II-13}$$

The following discussion is further demonstration that the chemical potential can be used as a criterion of phase equilibrium between the gas and adsorbed phase [31]. The assumption is made that the two phases are in equilibrium within a closed system. Within this closed system, each of the individual phases is modeled as an open system, free to transfer mass between phases. Rewriting Equation II-1 for the gas and adsorbed phase is as follows.

$$dG_{gas} = V_{gas}dP - S_{gas}dT + \sum_i \mu_i^{gas} dn_{i_{gas}} \tag{II-14}$$

$$dG_{ads} = V_{ads}dP - S_{ads}dT + \sum_i \mu_i^{ads} dn_{i_{ads}} \tag{II-15}$$

In writing these expressions, the assumption is that at equilibrium temperature and pressure are uniform throughout the entire system. The total change in the Gibbs energy of the system is the sum of these equations [31].

$$dG_{total} = dG_{gas} + dG_{ads} \tag{II-16}$$

Since the two-phase system is closed, Equation II-5 must also be valid leaving the following equilibrium expression.

$$\sum_i \mu_i^{gas} \, dn_i + \sum_i \mu_i^{ads} \, dn_i = 0 \qquad \text{(II-17)}$$

Mass conservation requires the following, assuming changes dn_i^{gas} and dn_i^{ads} results from mass transfer between phases.

$$dn_i^{gas} = -dn_i^{ads} \qquad \text{(II-18)}$$

Therefore

$$\sum_i (\mu_i^{gas} - \mu_i^{ads}) \, dn_i^{gas} = 0 \qquad \text{(II-19)}$$

Assuming the dn_i^{gas} terms are independent, the left-hand side of the above equation can be zero in general only if each term in parenthesis is separately zero, yielding the following for $i = 1$ through the number of species present in the system (k).

$$\mu_i^{gas} = \mu_i^{ads} \qquad (i = 1,2,3,\ldots,k) \qquad \text{(II-20)}$$

Thus, the gas and adsorbed phase at the same temperature and pressure are in equilibrium when the chemical potential of each specie is the same in both phases.

Relationship Between Gibbs Adsorption and Absolute Adsorption

Absolute adsorption as defined by Young and Crowell [38] is the number of moles of gas captured by the surface molecular forces. The absolute adsorption

differs from the adsorption definition by Gibbs by accounting for the volume occupied by the adsorbed phase. The relationship between absolute, *Abs*, and Gibbs adsorption, *Gibbs*, is as follows. The basic equation of our experimental work expresses the amount adsorbed as the amount injected into the cell minus the amount remaining in the gas phase at equilibrium, i.e.,

$$n_{ads} = n_{inj} - n_{gas} \tag{II-21}$$

The Gibbs adsorption definition considers the gas phase volume as the sum of the gas (V_{gas}) and adsorbed phase (V_{ads}) volumes (ignoring the reduction in gas phase volume due to presence of the adsorbed phase volume.) Rewriting the above equation in terms of vapor volume (V_{gas}) and adsorbed phase volume (V_{ads}), using the specific molar volume (of each phase), ν_{gas} and ν_{ads},

$$n_{ads}^{Gibbs} = n_{inj} - \left[\frac{V_{gas} + V_{ads}}{\nu_{gas}}\right] \tag{II-22}$$

For absolute adsorption, the amount adsorbed within the equilibrium cell is given correctly as

$$n_{ads}^{Abs} = n_{inj} - \left[\frac{V_{gas}}{\nu_{gas}}\right] \tag{II-23}$$

Thus, the Gibbs adsorption expression can be rewritten as (combining Equations II-22 and II-23)

$$n_{ads}^{Gibbs} = n_{ads}^{Abs} - \left[\frac{V_{ads}}{v_{gas}}\right] \tag{II-24}$$

but,

$$n_{ads} = \left[\frac{V_{ads}}{v_{ads}}\right] \tag{II-25}$$

so,

$$\left[\frac{V_{ads}}{V_{gas}}\right] = n_{ads}^{Abs}\left[\frac{v_{gas}}{v_{ads}}\right] \tag{II-26}$$

so Equation II-24 becomes

$$n_{ads}^{Gibbs} = n_{ads}^{Abs}\left[1-\left(\frac{v_{ads}}{v_{gas}}\right)\right] \tag{II-27}$$

At low pressures this correction is negligible but at higher pressures it becomes significant. Rewriting Equation II-27 in terms of gas (ρ_{gas}) and adsorbed (ρ_{ads}) phase densities.

$$n_{ads}^{Gibbs} = n_{ads}^{Abs}\left[1-\left(\frac{\rho_{gas}}{\rho_{ads}}\right)\right] \tag{II-28}$$

CHAPTER III

LITERATURE REVIEW

In this section, existing adsorption models (e.g., Langmuir and Gibbs) are described, including their specific assumptions, advantages, disadvantages and limitations. The assumption is made that only physical adsorption processes, with weaker forces (e.g., electrostatic, van der Waals), are encountered on which the following discussion will be focused.

Langmuir Adsorption Model

The Langmuir model is one of several models commonly used to represent the adsorption behavior of gases on adsorbents. The Langmuir model is based on a description of the dynamic equilibrium between the rates of evaporation (desorption) and condensation (adsorption). The Langmuir model was presented in 1918 by deriving the rate expressions for evaporation and condensation occurring at a gas-solid interface [37].

Langmuir derived an adsorption isotherm model which remains in wide use. Equation III-1 is shown graphically in Figure 1 as a Type I adsorption isotherm [1].

$$\theta = \left[\frac{\omega}{L}\right] = \left[\frac{BP}{1+BP}\right] \qquad \text{(III-1)}$$

The fraction of monolayer coverage is represented as θ. The amount of gas adsorbed per unit of adsorbent is ω and L is the amount adsorbed per unit of adsorbent at complete monolayer adsorption. B is the Langmuir model constant. Implicit in the

development of the Langmuir adsorption model are the following assumptions [37]:

(1) The adsorbate in the bulk gaseous phase behaves as an ideal gas.

(2) The amount adsorbed on the surface is confined to a monomolecular layer.

(3) The surface has a uniform energy of adsorption.

(4) All adsorbate-adsorbate interactions are neglected.

(5) The adsorbed molecules are localized, having definite points of attachment to the surface with equally accessible adsorption sites.

(6) The ability of a particle to bind to the surface is independent of whether or not nearby adsorption sites are occupied.

The Langmuir model [37], while insufficient, is historically important because it indicated for the first time the factors which are significant in the adsorption process. The Langmuir equation for a pure component (Equation III-2) can be extended to gas mixtures (Equation III-3), and is expressed in terms of the amount adsorbed per unit of adsorbent, ω. When written for mixtures, Equation III-3 is termed the extended Langmuir model. The Langmuir model for mixtures has historically been viewed as a correlative relation (empiricism) and not as an accurate physical model with a firm theoretical basis [4], until recently when the model has been derived by assuming a quasi-Gaussian energy distribution [36]. The Langmuir mixture expression is a two parameter model, with L_i and B_i representing Langmuir model constants for pure component i. Adsorption mixture behavior can be predicted by knowing the pressure (P), gas phase composition (y_i) and pure component model constants (L_i, B_i) [4].

$$\omega = \left[\frac{LBP}{1+BP}\right] \qquad \text{(III-2)}$$

$$\omega_i = \left[\frac{L_i B_i y_i P}{1+\sum_j B_j y_j P}\right] \qquad \text{(III-3)}$$

These expressions are confined to the above restrictions, including the monolayer adsorption limitation. The Langmuir isotherm is commonly applied to chemisorption of gases where multilayer adsorption is seldom observed. For the Langmuir isotherm at low pressures, BP is much smaller than unity and $\omega \approx BP$, so that ω increases linearly with pressure. At high pressures, BP is much greater than one, so that ω approaches unity as P approaches infinity.

The Langmuir isotherm is conveniently written in terms of gas content ($V_{gas\ content}$) expressed as volume of gas adsorbed per unit mass of substrate. V_{max} is the maximum sorption capacity (e.g., SCF/ton) with pressure typically expressed in psia and b representing the Langmuir constant in $psia^{-1}$ [37].

$$V_{gas\ content} = V_{max}\left[\frac{bP}{1+bP}\right] \qquad \text{(III-4)}$$

An early attempt by Freundlich to describe analytically the adsorption isotherm was entirely empirical. The following parabolic equation is known as the Freundlich adsorption isotherm [6]. The Freundlich isotherm is the result of an assumed failure of the above Langmuir assumptions (independence and equivalence of the adsorption sites) which suggests that the energetically more favorable adsorption sites are occupied first.

$$x/m = k\,P^{1/n} \qquad \text{(III-5)}$$

The mass of adsorbate is represented as x with m denoting the mass of adsorbent. The gas phase pressure is P; k and n are empirical model constants. A limitation of the Freundlich model is that it states that the value of x/m increases without limit as the pressure increases; in reality, the saturation of the surface with a

monomolecular layer sets an upper limit to the concentration in the "two-dimensional" adsorbed phase. The Freundlich expression is limited to monolayer adsorption as commonly seen in physical and chemical adsorption processes [6].

The Freundlich model also fails to predict the behavior observed at high pressures. The Freundlich model can be conveniently written in terms of gas content, $V_{gas\ content}$ (adsorbed volume per unit mass of adsorbent), as discussed in reference [6], where k and n are model constants.

$$V_{gas\ content} = k\,P^{1/n} \tag{III-6}$$

The combined Langmuir-Freundlich isotherm, expressed in terms of gas content, is known as the "Loading Ratio Correlation" [30] and is presented in Equation III-7.

$$V_{gas\ content} = V_{max}\left[\frac{k\,P^{n}}{1+k\,P^{n}}\right] \tag{III-7}$$

The Loading Ratio Correlation rewritten in terms of ω is similar to the extended Langmuir (Equation III-3) with the pressure raised to an exponent η. When written for mixtures, Equation III-8 is termed the extended Loading Ratio Correlation.

$$\omega_i = \left[\frac{L_i B_i y_i P^{\eta}}{1+\sum_j B_j y_j P^{\eta}}\right] \tag{III-8}$$

Gibbs Adsorption Model

The Gibbs adsorption model suggests replacing the three-dimensional, near-surface region with an idealized two-dimensional phase [9]. If the adsorbate is

treated as a two-dimensional microscopic entity, the fundamental equations of classical thermodynamics are applicable. This two-dimensional phase has its own spreading pressure, fugacity, internal energy, enthalpy, and other properties [9]. This model requires the use of two-dimensional equations of state. One of the four fundamental property relations applied to the adsorbed surface entity [9] is

$$dG = \mathcal{A}\, d\,\pi - SdT + \mu dn \qquad \text{(III-9)}$$

or the Gibbs-Duhem equation

$$SdT - \mathcal{A}\, d\,\pi + n d\,\mu = 0 \qquad \text{(III-10)}$$

where $\mathcal{A}$ is the surface area, π is the spreading pressure, and n is the number of moles of adsorbate per unit mass of adsorbent. At constant temperature, Equation III-10 yields the Gibbs adsorption isotherm [37].

$$-\mathcal{A}\, d\,\pi + n d\,\mu = 0 \qquad \text{(III-11)}$$

This expression can transform (by integration) any adsorption isotherm into the corresponding two-dimensional equation-of-state, or the corresponding isotherm can be obtained from a proposed equation-of-state. For adsorption on solid surfaces, if the assumption is made that the adsorbed species can be modeled as a two-dimensional film governed by a two-dimensional equation-of-state, Equation III-10 can be used with this equation-of-state to yield an adsorption isotherm [37]. Although not employed in this thesis, two-dimensional equation-of-state (EOS) models will be discussed in detail in a companion study [41].

Two-Dimensional Equation-of-State Models

The advantage the two-dimensional equation-of-state (EOS) models have over previous models lies in the ability to predict ideal and non-ideal mixture behavior from pure component gas adsorption equilibria data. Binary experimental data, in addition to the pure component data, allow more accurate correlations and predictions for multicomponent systems. Introducing binary interaction parameters (C_{ij} and/or D_{ij}) in an EOS to account for unlike-pair interactions is a common practice and a convenient way of employing experimental binary data. Some examples of two-dimensional EOS are the virial expansion, van der Waals, Erying and Redlich-Kwong. DeGance [9] described pure and multicomponent gas adsorption on a solid surface reasonably well by an equation of state.

Haydel and Kobayayashi [19] represented pure and binary adsorption data using a two-dimensional virial equation of state truncated after the third virial coefficient. The systems studied were methane and propane on a silica gel adsorbent at high pressures (100-1000 psia) over a temperature range of 0-40°C. The two-dimensional virial EOS model is shown below.

$$\left[\frac{A\pi}{RT}\right] = \sum_i \omega_i + \sum_i \sum_j b_{ij}\omega_i\omega_j + \sum_i \sum_j \sum_k c_{ijk}\omega_i\omega_j\omega_k \qquad \text{(III-12)}$$

The temperature dependent second and third virial coefficients are represented by b_{ij} and c_{ijk}.

The two-dimensional Erying equation was applied to the prediction of high pressure adsorption of pure and mixed hydrocarbons on charcoal by Payne and Leland [25]. The components studied were methane, propane, butane and their binary mixtures on a charcoal substrate from 20 to 2000 psia over a 10-50°C temperature range. The two-dimensional analog to the three-dimensional Erying

carbon dioxide, methane/nitrogen and methane/carbon dioxide mixtures on Fruitland coal have been collected at Amoco Production Company in Tulsa, Oklahoma [4]. These data cover the same pressure and temperature ranges of interest with current work (115°F, 0-1800 psia). These Amoco data are preliminary studies, limited to a few points along a single isotherm (115°F). Five to seven data points were measured for each pure component and three data points for each binary mixture, considerably less than in the current work. Amoco's binary mixture data are recorded at non-uniform, limited compositions. In the current work, ten data points were collected at increasing pressures to 1800 psia along an isotherm, and mixtures were studied at uniform intervals of gas-phase mole fraction (0.0, 0.2, 0.4, 0.6, 0.8, 1.0).

Experimental Techniques

There are three basic methods for measuring adsorption isotherms: volumetric, gravimetric and chromatographic [8]. The volumetric method was used to collect the adsorption data of the present work. In this technique, the amount and composition of the adsorbed phase are calculated as the difference between the amount of gas injected into an equilibrium cell and the amount which exists as an unadsorbed free gas phase at equilibrium.

The constant volume (volumetric) method uses an experimental apparatus divided into two interconnecting compartments: reservoir or pump and cell. Volume of the cell section (equilibrium cell void volume) can be predetermined by helium displacement. Gas from the injection pump is injected to the cell compartment, and equilibrium is indicated by the constancy of the pressure and composition of the gas mixture [8]. The gas-phase composition can be measured by removing a small amount of gas for analysis by the gas chromatograph. Difficulties involved with the volumetric method are due to the slow attainment of equilibrium. The equilibration

time can be reduced by circulating the gas mixture through the equilibrium cell using a recirculation pump [4].

In the gravimetric technique, total adsorption of the adsorbate is determined by difference in the equilibrium cell (vessel wherein the adsorption process occurs) mass before and after adsorption takes place [8]. The gravimetric method requires a series of constant gas mixture composition injections using premixed gases, with fixed compositions, at several total pressures [8]. The advantage is a savings in both time and experimental equipment. The total amount adsorbed can be measured by a simple flow apparatus where the sample is sealed off, disconnected, and weighed after equilibrium is attained.

The third method is the chromatographic technique involving a column packed with adsorbent to separate the flowing species [8]. The chromatographic analysis method is simple and fast in producing data but suffers from inherently larger errors [8].

CHAPTER IV

EXPERIMENTAL APPARATUS

The apparatus used in this study was designed for measuring the adsorption of pure and mixed gases on solid adsorbents. The method of measurement involves a volumetric technique wherein known amounts of a gas are injected into an equilibrium cell containing a known amount of adsorbent. By knowing (a) the amount of gas injected into the equilibrium cell and (b) the amount of gas remaining in the gas phase in the equilibrium cell when adsorption ceases, the amount of gas adsorbed on the solid surface can be determined by difference.

The basic experimental apparatus used in the adsorption experiment consists of two interconnecting sections. These two sections of the apparatus are referred to as the "pump" and "cell" sections of the apparatus, respectively. The pump section consists of a positive displacement injection pump for determining volumetrically the amount of gas injected into the equilibrium cell. The cell section consists of a high pressure vessel containing the adsorbent (moistened coal) where the adsorption process occurs. These interconnected systems are designed to function independently of each other. Knowledge of the volumetric (PVT) properties — pressure, volume and temperature— of the gases is essential to the experiment since they are used to determine (a) the amount of gas injected and (b) the amount of gas in the equilibrium cell after adsorption is complete. Measurement of pressure, volume and temperature requires instrumentation capable of yielding the greatest accuracy and resolution economically feasible. Attendant equipment, such as air and water baths, are part of the experimental apparatus and are used to isolate the

apparatus from extraneous changes in the environment.

The following is a brief overview of the equipment used to measure the adsorption of pure gases and binary gas mixtures on a wet coal substrate. More detailed equipment descriptions and illustrations can be found in the Adsorption Experiment Supplementary Material, which is a companion volume to this thesis [40]. Figure 2 is a diagram of the experimental apparatus.

Positive Displacement Injection Pump

At the heart of the pump section is a Ruska Model 1451 positive displacement injection pump (PP2, refer to Figure 2) operating on a basic piston-cylinder principle of volumetric displacement. A linear scale and a vernier dial on the pump can be read in divisions of 2.00 cc and 0.02 cc, respectively. The pump has a pressure rating of 10,000 psi and displacement volume of 500 cc. The uncertainty associated with each pump volume reading (σ_{V_p}) was estimated from experience of the principle investigators with similar equipment to be 0.02 cc [29,15]. A liquid-circulation jacket encases the barrel of the pump, permitting control of the temperature of the pump contents. The circulated liquid (distilled water) temperature was controlled using a water bath and circulator (Haake Model NB3). The temperature of the liquid jacket was maintained within ± 0.1°F.

Equilibrium Cell

The cell section of the system consists primarily of a high-pressure vessel (equilibrium cell, EC) capable of holding approximately seventy grams of substrate (wet Fruitland coal). The adsorption process occurred within this high-pressure vessel. The equilibrium cell is a thick-walled container manufactured by High Pressure Equipment (Model 2779), two inches in diameter by eleven inches in length, weighing approximately six pounds. The vessel has a pressure rating of 11,500 psi

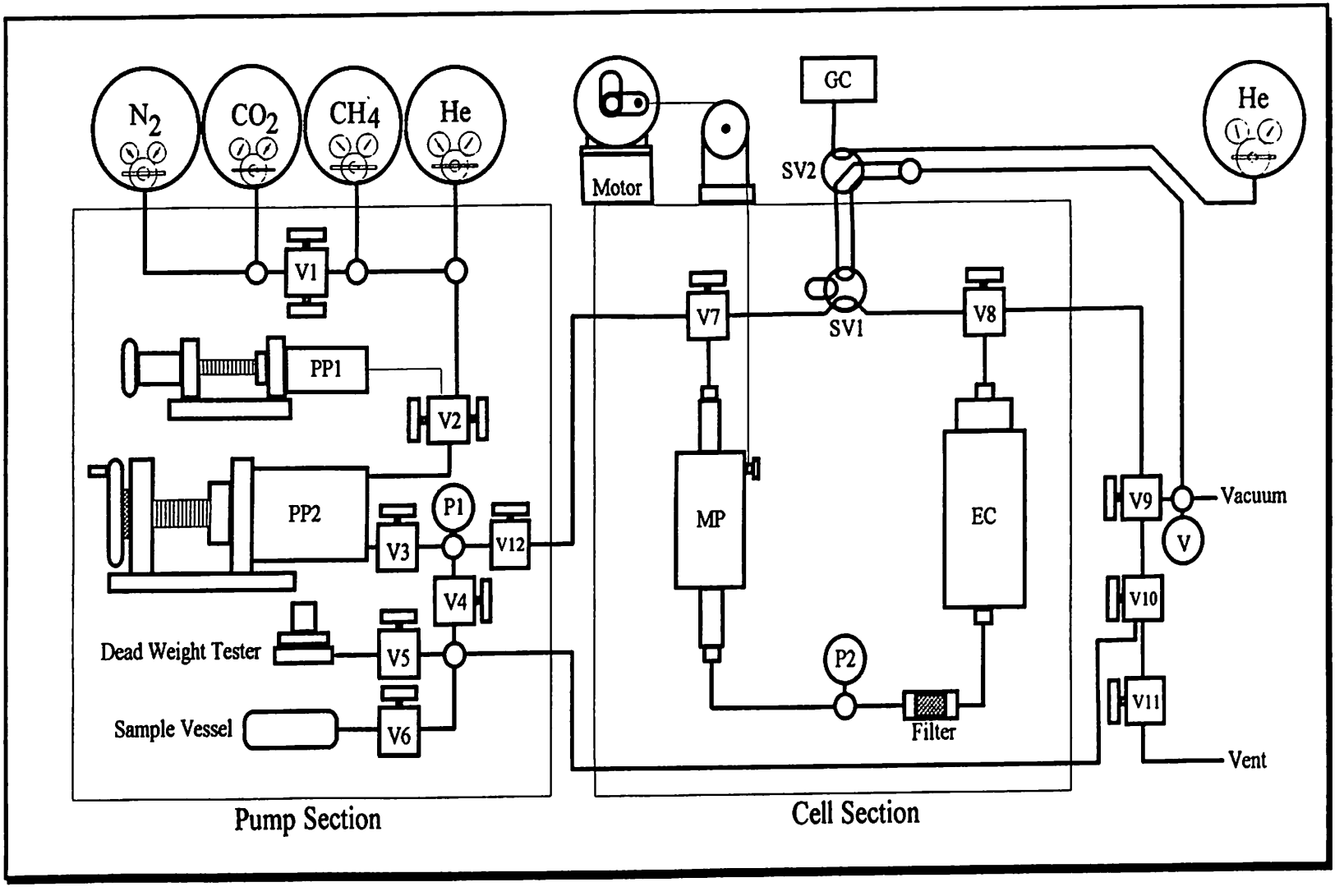

Figure 2. Schematic Diagram of Adsorption Apparatus

with an empty volume of approximately 110 cc. The coal sample was held within the cell by confining it between two porous disks. These sintered disks are about the size of a quarter and designed to allow the gas to pass but contain the coal. Loss of coal from the top of the cell is minimized by sandwiching a layer of glass wool between two additional sintered plugs placed on top of the coal within the equilibrium cell. The glass wool allows the passage of gas but retains the coal.

All fittings and tubing were purchased from Autoclave Engineering. The fittings are composed of 316 stainless steel with a low-pressure rating. The tubing is (Autoclave Engineering, Model MS15-151) 1/8 inch outer diameter (0.62 inch ID) low-pressure tubing composed of stainless steel designed for working pressures to 11,650 psi at 100°F. All tubing/fitting connections are single-ferrule, Autoclave SpeedBite connections [40]. (For detailed discussion on connections, refer to the Supplementary Material [40].)

Pressure Measurements

The equipment used to measure the pressures included two digital pressure readouts (Sensotec Model 450D) in combination with two pressure transducers (Super TJE, P1 and P2) calibrated to read absolute pressures from zero to 2000 psia. The pump section transducer (P1) was positioned at the outlet of the injection pump. The cell section transducer (P2) was installed at the bottom of the recirculation loop for the equilibrium cell. The two pressure readout instruments were positioned in the cabinet above the injection pump to allow easy access and visibility. Digital pressure readings were displayed with resolutions of 0.1 psia on the readouts. The uncertainty associated with the pressure measurements was estimated to be 0.2 psia, based on past experience [29,15] with similar equipment. The pressure transducers and digital readouts were mounted in temperature controlled air baths to reduce the effects of ambient temperature on their readings.

The pressure gauges were calibrated against a dead weight tester (Ruska Model 2470). The Ruska Dead Weight tester is a gas-lubricated piston-type pressure gage designed specifically for use with gases. A typical pressure calibration plot is shown in the Experimental Procedures section of this report. (A detailed discussion of pressure calibration procedures appears in the Supplementary Material [40].)

Temperature Measurements

The temperature of the distilled water in the circulation-jacket was monitored by a thermocouple, mounted inside the injection pump jacket and calibrated against a RTD thermometer (High Precision Hart Scientific Thermometer, Azonix Model A1011). In addition, the temperature of the injection pump contents was measured using the Azonix A1011 RTD thermometer by way of a sensor attached to the injection pump cylinder barrel. Readout for this model of thermometer is capable of displaying four temperatures, simultaneously. The entire Ruska pump assembly was enclosed in a plexiglas-covered, bench-mounted air bath with the temperature controlled within ± 0.1°F.

The temperature of the cell section was monitored using the Hart Scientific A1011 RTD Thermometer directly. The temperature of the cell section was maintained within ± 0.1°F. The Azonix A1011 RTD thermometer is microprocessor-controlled and PC programmable, capable of 0.001°F resolution and 0.01°F accuracy. The Azonix A1011 thermometer was used to monitor four sensors. The sensors are surface-mounted probes (Hart Scientific, platinum, four-wire, 100 ohm). One sensor measured the pump circulation-jacket temperature, while a second sensor was used to monitored the injection pump plunger temperature. The remaining two sensors were securely fastened to the surface of the equilibrium cell.

Cell Section

The recirculation loop of the cell section is located inside an air bath (Despatch LFD oven). The oven is a Series 1-42 with a Class-A explosion-relief rating. The oven features a horizontal airflow system for rapid, uniform distribution of heat throughout the chamber. The cell section recirculation loop can be isolated from the environment by way of valves (V7 and V8).

The adsorbing gas within the equilibrium cell was circulated using a magnetic circulating pump (Precision Manufacturing, MP) installed within the recirculation loop of the cell section. A magnetic ring assembly (1.5 inches in diameter by four inches in length) on the outside of the pump moves up and down a vertically-oriented, fixed tubing section (fitted with a floating magnetic piston) 1/2 inches in diameter by eight inches in length. The pump was manufactured at Rice University. Recirculation of the gas within the equilibrium cell loop accelerates the adsorption process and ensures that the gas is well mixed within the coal bed.

The magnetic ring assembly is driven by a gearmotor (NSH Bodine, 0.02 hp). A small diameter cable attached to the magnetic ring assembly is connected to the arm of the Bodine motor. As the arm of the motor rotates, the magnetic ring assembly moves up and down the pump body. Two check balls (sapphire) on the piston inside the tubing direct the gas through the recirculation loop (clockwise in Figure 2). The magnetic pump is housed inside a cell-section hot air bath, while the gearmotor is mounted outside and on top of the air bath. The speed of the electric motor, and thus pumping rate, is controlled by a motor speed controller mounted on the outside wall of the oven. The speed of the magnetic pump was maintained at thirty strokes per minute throughout all adsorption experiments.

A high pressure inline filter is included in the circulation loop just below the equilibrium cell to trap any coal particles which may pass through the porous disks

in the cell. The filter is composed of 316 stainless steel and holds four stainless steel filter disks with a pore size of 15 microns.

Air Bath Temperature Controllers

Air baths were used for both the pump and cell sections to maintain steady-state environments within the enclosed control volumes. Air temperatures of the pump section enclosed within the plexiglas cover and the cell section within the Despatch oven were controlled using temperature controllers (Omega CN9000). The CN9000 series controller is microprocessor based PID (Proportional-Integral-Derivative) controller for optimal control during both start-up and steady-state operation. The controller is used in conjunction with an RTD probe (Omega, three-wire, 100 ohm) mounted in an open-ended stainless steel housing with Teflon insulated leads. The probe is designed specifically for air temperature measurements and monitoring of gas streams. (Discussion of the set-up, operation and tuning procedure appears in the Supplementary Material.)

The heating element utilized is a fine-wire heater filament (Omega) capable of delivering 450 watts of power and is mounted on the outlet duct of a circulating blower. The circulating blower used to move the air within the enclosed control space (pump section) is a high-temperature blower (Dayton, Model 4C723). The fan is designed as a draft-induced, warm air circulator.

Gas Mixture Sampling

For gas mixtures, a method for analyzing the mixture composition is required. This was accomplished by installing a sampling valve (Valco Instruments, Model 6UW, SV1) in the recirculation loop. The sampling valve is a UW model Valco six-port, external volume, two position sample injector fitted with an externally-mounted twenty micro-liter sampling loop. The valve is designed with a six inch standoff

assembly for manual actuation outside the controlled area. This allows a gas sample to be taken by manually actuating the standoff assembly control knob mounted outside the oven. This sampling method does not disturb the steady-state thermal environment in the cell section. (The sampling valve flow diagram is detailed in the Supplementary Material.)

The sampling valve is used in conjunction with a switching valve (Valco Instruments, Model 6UW, SV2). By operating the sampling and switching valves in the correct sequence, the gas mixture sample is removed from the cell section recirculation loop and directed to the gas chromatograph for analysis. The switching valve (SV2) is identical to the sampling valve (SV1) except that the switching valve is used to redirect the flow of carrier gas and does not have a sample loop.

Gas Mixture Analysis

For analysis of gas mixtures, a gas chromatograph (Perkin-Elmer Sigma 2, GC) is used. The gas chromatograph uses a microprocessor based logic system with the capability to use three detector systems. The chromatograph has provisions for operating either in isothermal or two-step temperature programming modes. It has three heated-zone controls: the injectors, thermal conductivity block and detector block. For the current work, a thermal conductivity hot-wire detector was used to analyze the gas mixture samples with the gas chromatograph operating isothermally. The universal, non-destructive, thermal conductivity detector is capable of detecting parts per million of the gases of interest (methane, nitrogen and carbon dioxide).

In combination with the gas analyzer, a data reduction facility (Perkin-Elmer Sigma 1B Console) was used. The Console is a laboratory data system whereby keyboard directives and conversations can be used to establish analyzer chromatographic conditions, initiate operation of auxiliary devices, collect and reduce data and print analysis reports. The Console has the ability to link the data

source with the printer-plotter using keyboard (Plot) directives and obtain a chromatogram from that data source. A detailed report is printed immediately listing peak retention times, peak areas and response factors. Chromatographic conditions such as injector temperature, detector temperature, oven temperature and temperature programming are set by means of digital signals from the instrument console. The chromatograph accepts the analog output from the chromatograph detector amplifier through an interface (Perkin-Elmer Model 3001) which converts the output to a digital signal.

The chromatographic column used to analyze the binary mixtures was a Spherocarb column three feet in length. Spherocarb is a spherically-shaped carbon molecular sieve designed by Analabs. The column is used for analyzing light hydrocarbons (specifically C_1 through C_4), nitrogen, carbon dioxide, and stack gas mixtures (N_2O, SO_2, H_2S) [40]. The column and gas chromatograph operating conditions yielded excellent component separations with scan times of under twelve minutes. (A more detailed discussion of detectors, columns, operating conditions, etc., used in the adsorption experiments can be found in the Supplementary Material, which contains all the necessary information and procedures for set-up and operation of all the above mentioned equipment.)

CHAPTER V

EXPERIMENTAL PROCEDURE

The adsorption of pure methane, nitrogen, carbon dioxide and their binary mixtures on wet Fruitland coal was measured using the volumetric mass balance apparatus described in the previous chapter. A discussion of procedures used to measure the adsorption of these gases is given below.

The following is a general description of the procedure so that the fundamental workings of the system behind each phase of the operation can be understood. A more lengthy discussion and procedure outline for each experimental step are detailed in the Supplementary Material. Example calculations are given there for pure methane and a methane/nitrogen mixture adsorption measurement to illustrate the general equations used in the adsorption calculations and the data required to perform such calculations.

Governing Equations

The amount of pure component adsorption (n_{ads}) is determined by difference in the amount of gas injected from the positive displacement pump (n_{inj}) and the amount of gas remaining unadsorbed in the equilibrium cell (n_{unads}).

$$n_{ads} = n_{inj} - n_{unads} \qquad (V\text{-}1)$$

The amount of gas contained in the calibrated positive displacement injection pump may be written as $n = \rho_p V_p$, where ρ_p is the density of the gas in the pump and

V_p is the total volume of the pump. The amount of gas injected (by multiple injections of the gas) from the pump into the equilibrium cell from the calibrated positive displacement pump is given by

$$n_{inj} = \sum_j \left[\rho_{p_i} V_{p_i} - \rho_{p_f} V_{p_f} \right]_j \qquad \text{(V-2)}$$

where $(\rho_{p_i})_j$ and $(\rho_{p_f})_j$ are the gas densities at the initial and final conditions (pressure and temperature) in the injection pump for the *j*th injection, and $(V_{p_i})_j$ and $(V_{p_f})_j$ are the initial and final volumes in the displacement pump for the *j*th injection.

The amount of unadsorbed gas (n_{unads}) occupying the equilibrium cell void volume (free space within the cell section) is given by

$$n_{unads} = \rho_c V_{void} \qquad \text{(V-3)}$$

where ρ_c is the gas density within the cell, and V_{void} is the cell section void volume.

The actual void volume (V_{void}) is the difference between the void volume for an unadsorbed gas, as determined from the helium calibrations (V_{He}), and the adsorbed phase volume (V_{ads}). The adsorbed phase volume accounts for the fact that the condensed (adsorbed) phase occupies a finite volume within the cell. The adsorbed phase volume may be expressed as $V_{ads} = n_{ads} \nu_{ads}$, where ν_{ads} is the specific adsorbed phase volume. The void volume (V_{He}), as determined from the helium void volume tests, is given as $V_{He} = n_{He}/\rho_{He}$, where n_{He} is the amount of helium injected into the equilibrium cell from the injection pump, and ρ_{He} is helium gas density at the cell conditions (pressure and temperature). Details of the helium void volume determination appear in the Supplementary Material.

For the adsorption of multicomponent gas mixtures, a material balance

expression is written for each component k, for k components 1 through k. The expression is similar to Equation V-1 for pure components.

$$(n_{ads})_k = (n_{inj})_k - (n_{unads})_k \qquad \text{(V-4)}$$

The amount of component k injected from a mixture in the positive displacement pump is given by an expression similar to that for the pure components, except that the composition of that component (z_k) appears in the equation.

$$(n_{inj})_k = z_k \sum_j \left[\rho_{p_i} V_{p_i} - \rho_{p_f} V_{p_f} \right]_j \qquad \text{(V-5)}$$

The amount of unadsorbed component k in the free gas in the equilibrium cell is given by

$$(n_{unads})_k = y_k \rho_c V_{void} \qquad \text{(V-6)}$$

where y_k is the mole fraction of component k in the equilibrium gas mixture. The composition (mole fraction) of the injection pump gas mixture (z_k) and the equilibrium cell gas mixture (y_k) are, in general, different.

The above governing equations will be used to derive error propagation expressions for pure component and mixture adsorption experiments. Error propagation expressions determine the uncertainty associated with the experimental measurements. This is discussed in the Error Analysis Chapter, with detailed example calculations in the Supplementary Material [40].

Pressure Calibration

The pressures measured by the Super TJE pressure transducers were calibrated against a Ruska Dead Weight Gage pressure standard. The results were used to construct pressure calibration plots similar to the one illustrated in Figure 3. The pump and cell section pressure transducers were calibrated at pressures from zero to 1800 psia; typically twenty data points were collected in each calibration run. Deviations between the standard dead weight pressure and the transducer pressures were plotted as a function of the transducer pressure [40]. The pressure calibration data were fit to a second-order polynomial (although a linear function would have been sufficient, as can be seen in Figure 3) in pressure using a least squares method. Results showed root mean square errors (RMSE) deviations of the fit to be 0.10 psia. The pressure calibration regression coefficients were entered into the data reduction software routines to make the appropriate pressure corrections. (A detailed discussion of the instruments, dead weight tester, transducers and theory can be found in the Supplementary Material [40].)

Temperature Calibration

Temperatures were measured using a Hart Scientific Model A1011 Resistance Thermometer manufactured by Azonix. The platinum probe is mounted directly to the surface of the equilibrium cell for monitoring the cell section temperature. The pump section temperature is measured using a thermocouple mounted to the inside of the Ruska injection pump jacket surrounding the pump injection cylinder. The thermocouple was calibrated using the Hart Scientific RTD thermometer mentioned above with the results tabulated in the Supplementary Material. In addition, the pump section temperature is monitored using the Hart Scientific Azonix A1011 RTD thermometer mounted to the side of the injection pump. As mentioned in the

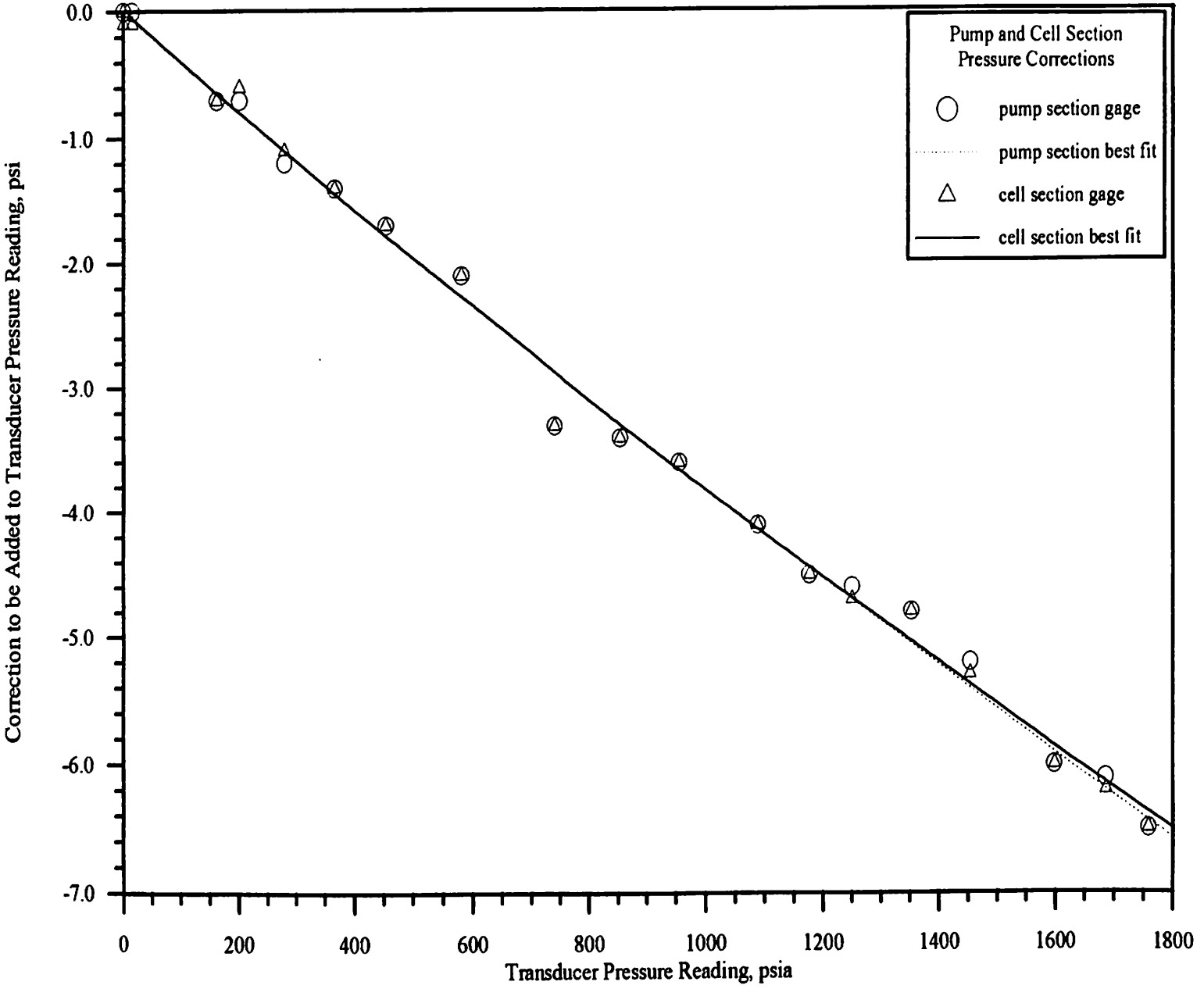

Figure 3. Pump and Cell Section Pressure Calibrations

Apparatus chapter, the Azonix thermometer is capable of measuring up to four temperatures.

Wet Coal Substrate

The equilibrium cell was filled with pre-moistened, finely ground coal substrate. The amount of gas adsorbed on a coal material is dependent upon the coal matrix characteristics for the specific coal substrate and the moisture content. The coal sample used in this work was identified as I.D. number 11344-2 and was received from Amoco Research in Tulsa, Oklahoma. Once received, the coal was kept in a nitrogen environment enclosed within an isolated glove box until used. This was done to prevent oxidation, which could alter the integrity of the coal surface. The coal material was extracted from the Ignacio Field of the San Juan Basin in La Plata County of southwestern Colorado and classified as a Fruitland coal [4]. Analysis (proximate and ultimate) of the coal is discussed and tabulated in Appendix D.

Substrate Moisture Content

The moisture content of the coal is important to the adsorption measurements [35]. The equilibrium moisture content of the coal sample was analyzed to be 2.203 weight percent, as tabulated in Appendix D. If the moisture content of the coal falls below the equilibrium value, the adsorption characteristics change, yielding an increase in the amount of gas adsorbed on the coal surface [35]. This can misrepresent the coalbed adsorption behavior in the field operations. Thus, one of the experimental constraints was to maintain a moisture content above the equilibrium moisture value [4].

The experiments were conducted with the moisture content kept between four and fourteen percent, staying well above the equilibrium moisture content. Moisture content determinations were conducted on a well-mixed sample (in duplicate) using

two separate samples. Weighings were done on an analytical mass balance, which was calibrated using known masses. The balance (Mettler) is capable of handling up to 100 grams, with readings to 0.00001 gram. Each mass reading was recorded and repeated three times with the standard deviation between readings not exceeding 0.001 gram.

After the moisture content was measured, the moist coal sample was transferred to the equilibrium cell. Since the amount of adsorption occurring within the cell is proportional to the amount of coal placed in the cell, the mass of coal in the cell must be known so the adsorption data can be reported relative to a unit mass of dry coal. The mass of coal placed in the cell was measured by two methods. The glass container containing the coal sample was weighed prior to and after filling the cell, and the difference is the amount of wet coal in the cell. As a check, the equilibrium cell was weighed prior to and after filling, and the weight difference yielded the coal mass. The coal was contained within the equilibrium cell using three sintered disks and a layer of glass wool. (Detailed procedures for filling the cell, determining the moisture content of the coal as well as how the coal is retained within the cell are discussed in more detail in the Supplementary Material [40].)

Equilibrium Cell Void Volume

The adsorption calculations require a value for the cell section void volume (equilibrium cell void volume), V_{void}. This was determined by injecting a known amount of helium from the calibrated injection pump into the cell section at sequentially higher and higher pressures (typically six data points between 100 and 1000 psia). The helium was assumed inert and not adsorbed on the coal [4]. Knowing the pump section pressure-volume-temperature data for helium, the amount injected can be calculated. By knowing the resultant cell-section pressure, the volume (void volume) of the cell section can be calculated, as follows.

$$n_{He_{inj}} = n_{He_{cell}} \tag{V-7}$$

$$\left[\frac{PV_{inj}}{Z_{He}RT}\right]_{pump} = \left[\frac{PV_{void}}{Z_{He}RT}\right]_{cell} \tag{V-8}$$

so

$$V_{void} = \left[\frac{PV_{inj}}{Z_{He}RT}\right]_{pump} / \left[\frac{P}{Z_{He}RT}\right]_{cell} \tag{V-9}$$

In the above equations, $n_{He_{inj}}$ is the number of moles of helium injected into the cell, $n_{He_{cell}}$ is the number of moles of helium unadsorbed within the cell, V_{inj} is the volume of helium injected from the pump, Z_{He} is the helium compressibility factor, R is the universal gas constant, T is the temperature, P is the pressure, and the subscripts "cell" and "pump" refer to conditions measured in these two sections of the apparatus. The pressures and temperatures may not be the same for the pump and cell sections, yielding different compressibility factors in these two sections (and in Equation V-8 and V-9).

The equilibrium cell void volume was calculated at six pressure points (150 psia intervals) over a 100-1000 psia operating range. If the average absolute deviation (AAD) of the six cell-section void volumes calculations exceeded 0.05 percent, the void volume test was repeated. Void volume tests were performed prior to and following each adsorption isotherm.

In addition to determining the void volume, the void volume tests were used to determined the moisture lost by the coal sample. The "current" void volume was compared to the "previous" void volume over the course of several runs. The difference was assumed to be the volume of water lost during the blow-down process (emptying and evacuating the cell section following completion of an adsorption isotherm). The new water mass contained within the coal sample was calculated and used to update the coal sample water mass and moisture content (required in the

adsorption calculations).

Pure Component Adsorption

After the temperature probes and pressure instruments were calibrated and cell void volume determined, the adsorption experiment was begun. The calibrated positive displacement injection pump was filled with the pure component or mixture to be tested and the pump temperature and pressure allowed to stabilize. All gas injections were made using a constant injection pressure of 1000 psia. This injection pressure (versus a variable injection pressure) was used because of a reduction in the experimental errors. Using the error propagation program, uncertainties were calculated using a variable and constant injection pressure. The constant injection pressure was shown to have lower overall errors. The cell section was evacuated prior to injection of the test fluid. The cell section was flushed several times with the test fluid to remove any contaminants (previously tested gases). The cell section was again evacuated to approximately 3.0 psia (as seen in Table XXXIII). This is the pressure of the gas remaining in the cell at the start of the adsorption experiment. Evacuating the cell section to pressures below 3.0 psia would remove too much water from the coal sample.

Data were measured at ten pressures over a range of 100 to 1800 psia while maintaining the equilibrium cell temperature at 115°F. These conditions were chosen to be representative of those associated with the Fruitland coals commonly found in the Colorado portion of the San Juan Basin [4]. The recirculation pump was used during all pure component and mixture experiments to improve the movement of the gas through the coal sample [4]. For all data points, a minimum of six to eight hours was allowed for the cell section to reach equilibrium, as evidenced by a stable pressure. Measuring a complete adsorption isotherm required three to four days.

The amount of pure component adsorbed on the coal surface was calculated

from the amount of gas injected, the amount of gas existing in an unadsorbed free gas phase within the cell at equilibrium (corrected for the solubility of the gas in the water contained in the moist coal sample). The amount of gas injected was determined from Equation V-10.

$$n_{inj} = [P\ V_{inj}/Z\ R\ T]_{pump} \qquad \text{(V-10)}$$

The amount of unadsorbed gas was calculated based on the fact that any unadsorbed gas will remain in the cell void volume. The unadsorbed gas is calculated using

$$n_{unads} = [P\ V_{void}/Z\ R\ T]_{cell} \qquad \text{(V-11)}$$

Another factor included in all adsorption and void volume calculations was the amount of gas dissolved in the moisture contained in the coal. The solubilities of helium, methane and nitrogen in water are less than one percent over the operating pressure range, but they were still considered in all calculations [4]. For carbon dioxide, the amount can exceed eight percent at higher pressures, which can greatly influence the adsorption results [4].

The solubility data for the gases of interest as a function of pressure were calculated using a proprietary properties program [43]. These data were fit to second order polynomials in pressure. The quadratic solubility equation was expressed in mole fraction of the gas dissolved in water. (For pure components, the solubility expression reduces to a function of total pressure.)

$$x = P/[a + b\ P + c\ P^2] \qquad \text{(V-12)}$$

For mixtures, the solubilities of each component was estimated by calculating the solubility at the component's partial pressure, $P\,y_i$.

The amount of gas dissolved within the water, n_{solu}, was calculated by multiplying the above mole fraction (a function of pressure) by the amount of water on the coal. This number (n_{solu}) is reported in the pure and mixture adsorption tables (Appendices B and C) as the amount of each component dissolved in water.

The amount of gas adsorbed at a given pressure is corrected for the solubility in water. Knowing the amount of gas injected (n_{inj}), the amount of unadsorbed free gas (n_{unads}) and the amount of gas dissolved in the water (n_{solu}), the amount of gas adsorbed for a given datum can be calculated according to the following expression.

$$n_{ads} = n_{inj} - n_{unads} - n_{solu} \qquad \text{(V-13)}$$

The above procedure is repeated at sequentially higher pressures until the adsorption isotherm is completed.

Binary Mixture Adsorption

In mixture adsorption studies, the procedure is slightly more complicated. A gas mixture of known composition is injected, so the total amount of each gas in the cell is known. The amount of unadsorbed free gas at each pressure is calculated from Equation V-11 with Z of the pure component being replaced with Z_{mix}, the gas mixture compressibility factor [4]. The amount of each component (for mixtures) dissolved in the water was calculated by using its partial pressure ($y_i\,P$) in Equation V-12. The equilibrium gas-phase composition in the equilibrium cell is determined by chromatographic analysis. A twenty microliter sample of the gas mixture was sent to the gas chromatograph for analysis. This allowed the total amount of unadsorbed free gas to be apportioned among various components according to their mole

fractions in the gas mixture.

Gas Chromatograph Calibration

For binary mixtures, a sample of the cell-section gas mixture at equilibrium is transferred to the gas chromatograph for analysis. The two components have different adsorption capacities depending on the composition and pressure so the feed and equilibrium gas compositions are, in general, different. The gas chromatograph measures the peak area of each component. The gas mixture compositions are determined by analyzing these peak areas. The peak area ratio is related to the composition ratio through a relative response factor (R_f) as given

$$R_f = (A_1 / A_2)/(z_1 / z_2) \qquad \text{(V-14)}$$

where A_i and z_i are the peak area and gas phase composition for component i. By knowing the relative response factor for a gas mixture as a function of the gas composition, the composition of the gas mixture can be determined. This requires calibration of the chromatograph to determine the response factors. The response factor displays a slight, but discernible, change with gas composition. Before a mixture of unknown composition can be analyzed, the response factor-composition dependence was determined.

Known compositions (pre-mixed gas mixtures) of a binary mixture were analyzed by the gas chromatograph. The pre-mixed gas mixtures were prepared using the calibrated injection pump and a sample vessel. Equation V-10 was used to determine the amount of gas injected into the sample vessel. These gas mixtures (of known composition) were used to calibrate the chromatograph. Using the data handling output device (Perkin-Elmer Console), the response factor was determined as a function of mole fraction. The calibration procedure was repeated throughout

the binary composition range. Errors associated with each measurement were determined by error propagation as discussed in the Supplementary Material [40]. A response factor (R_f)-composition plot was constructed for each binary mixture, as shown in Figure 4. Using a weighted least-square regression routine, the best-fit straight line was constructed through the data points. This straight-line expression (documented in the legend of Figure 4 for each mixture) was used to determined the composition of the gas mixture (by measuring the component peak areas) from the gas chromatograph output. (The relative response factor-composition data are tabulated in the Supplementary Material [40].)

A weighted least-squares regression method was used because the uncertainty (variance) in the measurements changed with gas composition. By weighting each datum point, a more correct evaluation of the data was accomplished.

Gibbs/Absolute Adsorption Relation

The Gibbs or apparent adsorption of a specific gas, Ads_{Gibbs}, is expressed relative to a unit mass of dry coal substrate [9]. For this work, the units for Gibbs adsorption are reported in milligram moles per gram of coal substrate. The Gibbs adsorption is the measured adsorption divided by the dry coal mass [4].

$$Ads_{Gibbs} = n_{ads}/\text{grams dry coal} \qquad \text{(V-15)}$$

Gibbs adsorption does not account for the fact that the adsorbed material occupies part of what was previously the void volume in the equilibrium cell [9]. A correction is required, based on the density of the adsorbed phase. This requires estimates for the condensed (adsorbed) phase density, ρ_{ads}. The Gibbs adsorption, Ads_{Gibbs}, can be corrected to the true absolute adsorption (for pure gas adsorption), Ads_{abs}, using the following expression [9].

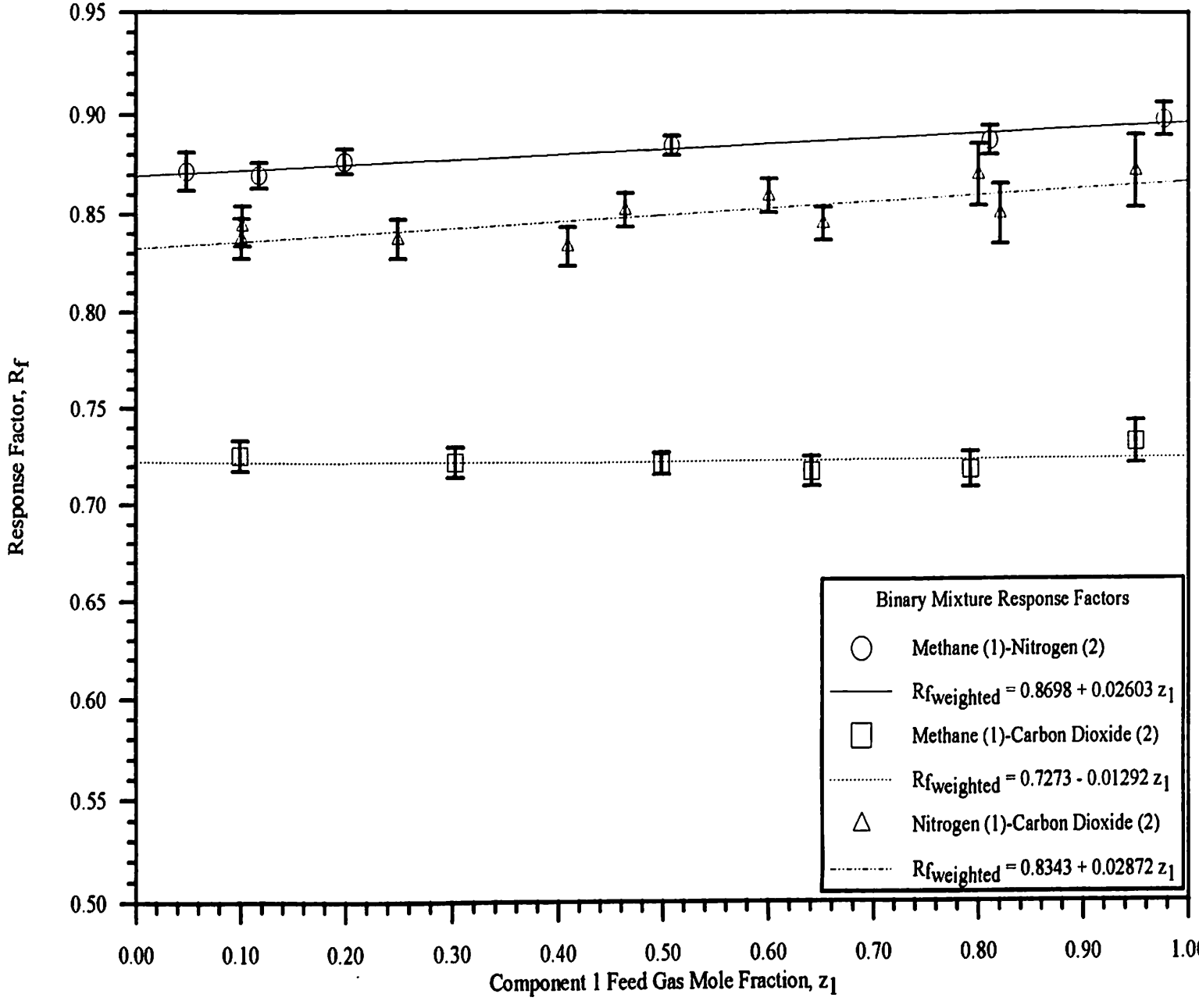

Figure 4. Concentration Dependence of Chromatograph Response Factors in Binary Mixtures

$$n_{ads}^{Gibbs} = n_{ads}^{Abs}\left[1-\left(\frac{\rho_{gas}}{\rho_{ads}}\right)\right] \qquad \text{(V-16)}$$

ρ_{gas} is the unadsorbed free gas density and ρ_{ads} is the adsorbed phase gas density. For binary adsorption (mix), the density of the sorbed gas was determined by using the molar-averaged value given by Equation V-17, [4]. This is similar to stating that the sorbed gas acts like an ideal solution [4].

$$\left[\frac{1}{\rho_{\text{adsorb}\,mix}}\right]=\left[\frac{x_1}{\rho_{\text{adsorb}\,1}}\right]+\left[\frac{x_2}{\rho_{\text{adsorb}\,2}}\right] \qquad \text{(V-17)}$$

A common approximation for the density of an adsorbed phase is to use the liquid density at the atmospheric pressure boiling point. The current work used the adsorbed phase density approximation suggested by Yee [4], reported in mass units. Methane and nitrogen adsorbed phase density estimates were 0.421 and 0.808, (grams/cc), respectively. Carbon dioxide is a solid at its atmospheric pressure boiling point. As a result, the density for a saturated liquid at the triple point was used instead, 1.18 gram/cc [4].

The pump section temperature was maintained at 96.6°F. This ensured that all pure and mixed gases (including pure carbon dioxide) were above their critical temperatures and, thus, in the gas phase at all pressures of interest.

CHAPTER VI

EXPERIMENTAL RESULTS AND DISCUSSION

Pure Component Adsorption

The experimentally determined pure component adsorption isotherms for methane, nitrogen and carbon dioxide appear in Figures 5 through 9. The figures show the absolute adsorption (mg mole adsorbate/g coal) as a function of pressure. The experimental data for all pure components are given in Tables XXXIII through XL of Appendix B. The tables include complete experimental information (void volumes, moisture content, mass of water in coal, temperatures, etc.) and are designed to contain all the data necessary to reproduce the adsorption calculations. Condensed versions of the adsorption data are in Tables I through XXI at the end of this chapter. Current work completed at Oklahoma State University are identified in the table headings as OSU followed by the experimental run number (OSU#) as documented in the laboratory notebooks.

For figures illustrating the experimental results, the best-fit lines drawn through the data points are a combination of either a third-order polynomial or a cubic-spline smoothing routine depending on which plotting routine (Grapher) software option yielded what appeared to be the most reasonable representation of the data [42].

The pure methane adsorption experiment was run twice. Figure 5 shows that the two runs agree within one percent. Methane illustrates the typical shape of a Type I monolayer physical adsorption process. The moisture contents of Runs 16 and 23 were 11.9 and 5.93 percent, respectively. The experiments produced

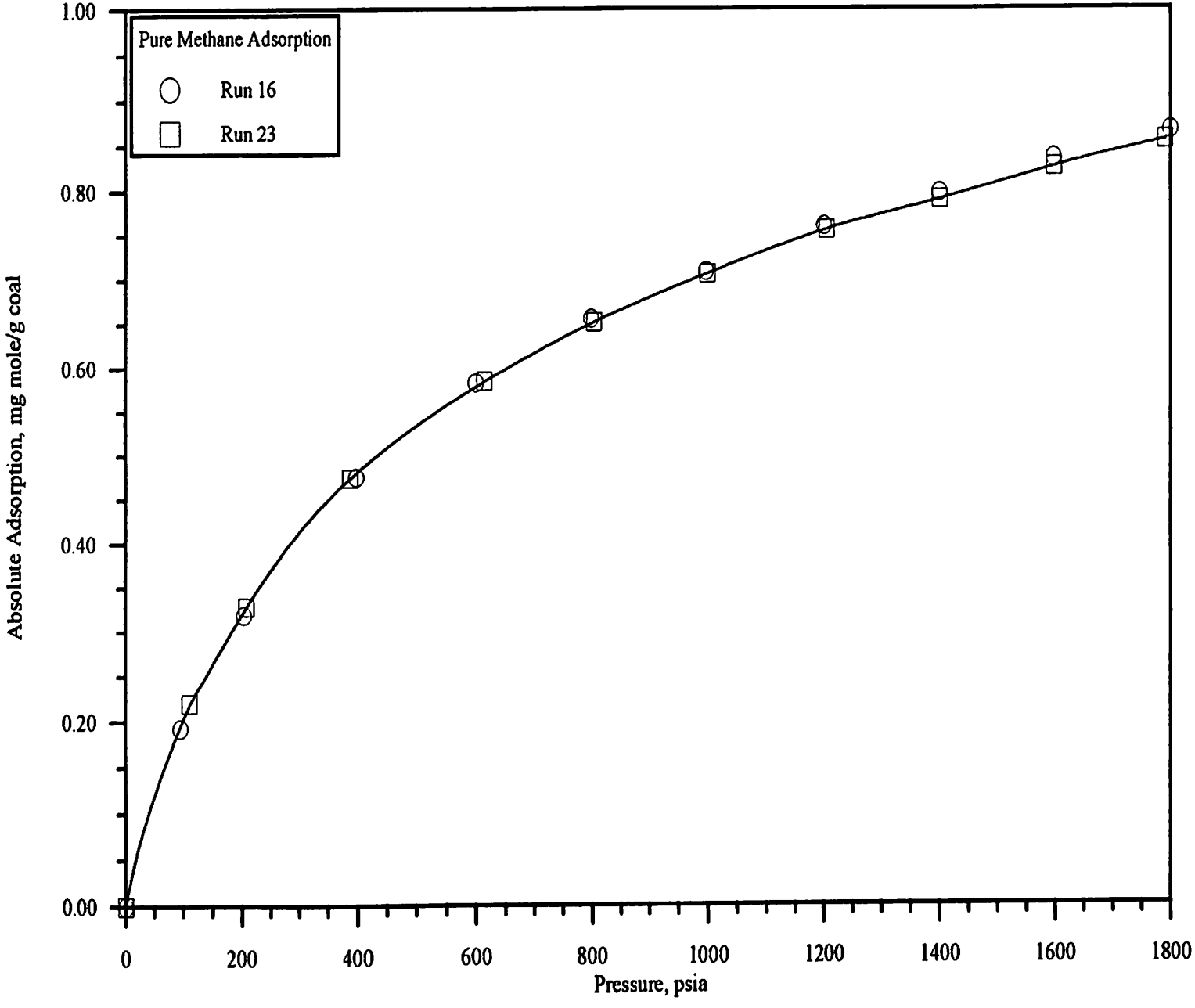

Figure 5. Absolute Adsorption of Methane at 115 °F on Wet Fruitland Coal

comparable results (within experimental uncertainty) at different moisture contents. This indicates (agreeing with the literature [37]) that the adsorption capacity is independent of moisture content, if the moisture content is above the equilibrium moisture content.

Figure 6 shows adsorption isotherms for pure nitrogen. Three replicate experiments were completed with all data agreeing within three percent (within the experimental uncertainty). The sorption capacity for nitrogen is about half that of pure methane. Nitrogen exhibits monomolecular Type I physical adsorption.

Carbon dioxide adsorption is illustrated in Figures 7 and 8. Figure 7 extends to 1800 psia while Figure 8 stops at 1200 psia. In Figure 7, the adsorption is not typical Type I monolayer adsorption. The sharp increase in sorption capacity at pressures exceeding 1200 psia is an indication that multilayer adsorption is probably occurring. Three experiments were completed with data agreeing within three percent (within the experimental uncertainty). The carbon dioxide adsorption is almost twice that of the methane and four-fold that of nitrogen. These results are consistent with the rule of thumb that the higher the boiling point, the greater the sorption capacity of the pure component gas [37].

Pure methane, nitrogen and carbon dioxide adsorption isotherms are presented together in Figure 9. Methane and nitrogen represent monolayer Type I adsorption. Carbon dioxide exhibits monolayer adsorption up to approximately 1200 psia and multilayer adsorption at pressures exceeding 1200 psia. The lines joining data points were constructed using the cubic-spline data smoothing option available with the regression routine (Grapher) software [42].

Binary Mixture Adsorption

Data for each binary mixture are plotted on separate figures. The usual adsorption information is shown as the absolute adsorption as a function of

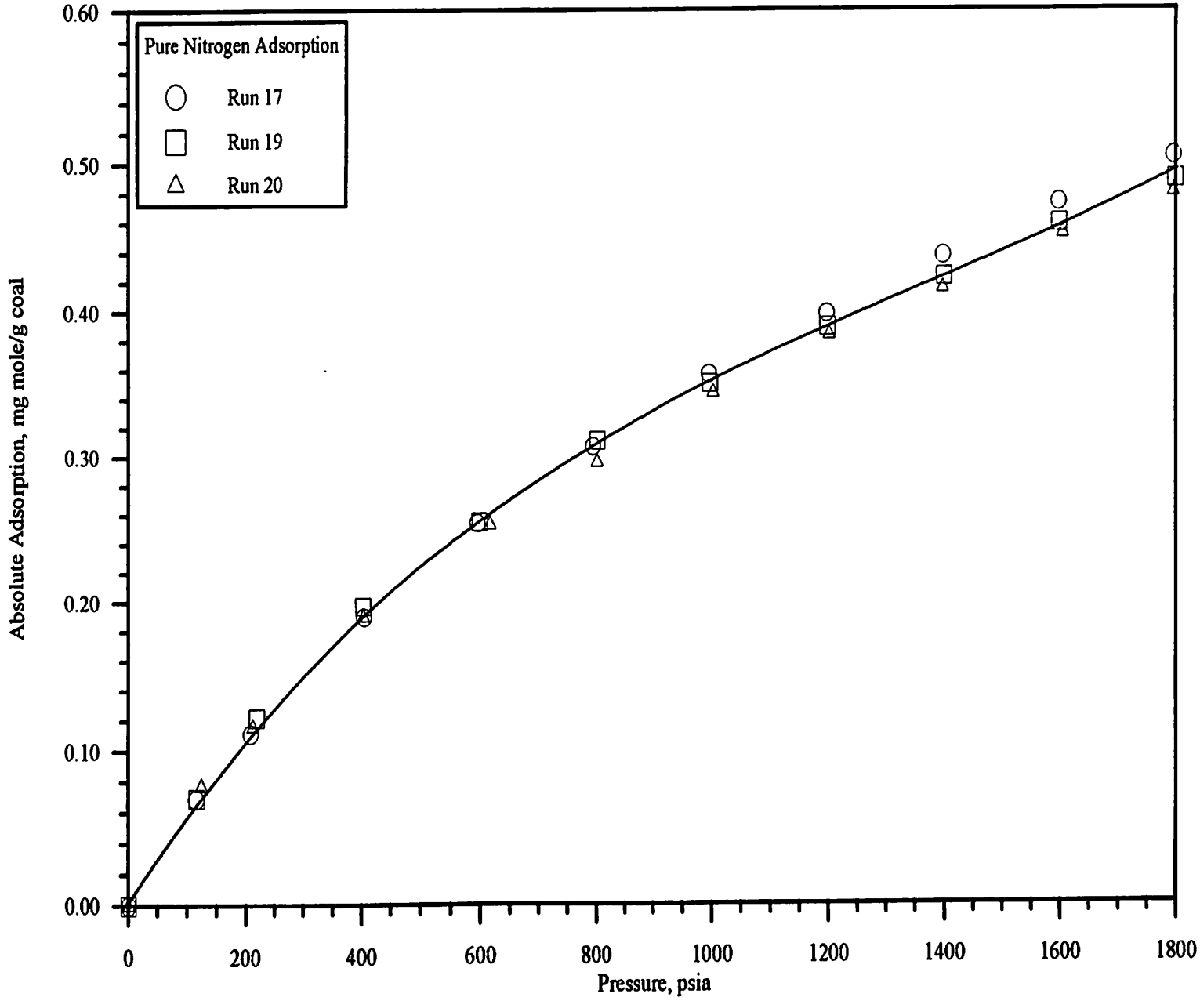

Figure 6. Absolute Adsorption of Nitrogen at 115 °F on Wet Fruitland Coal

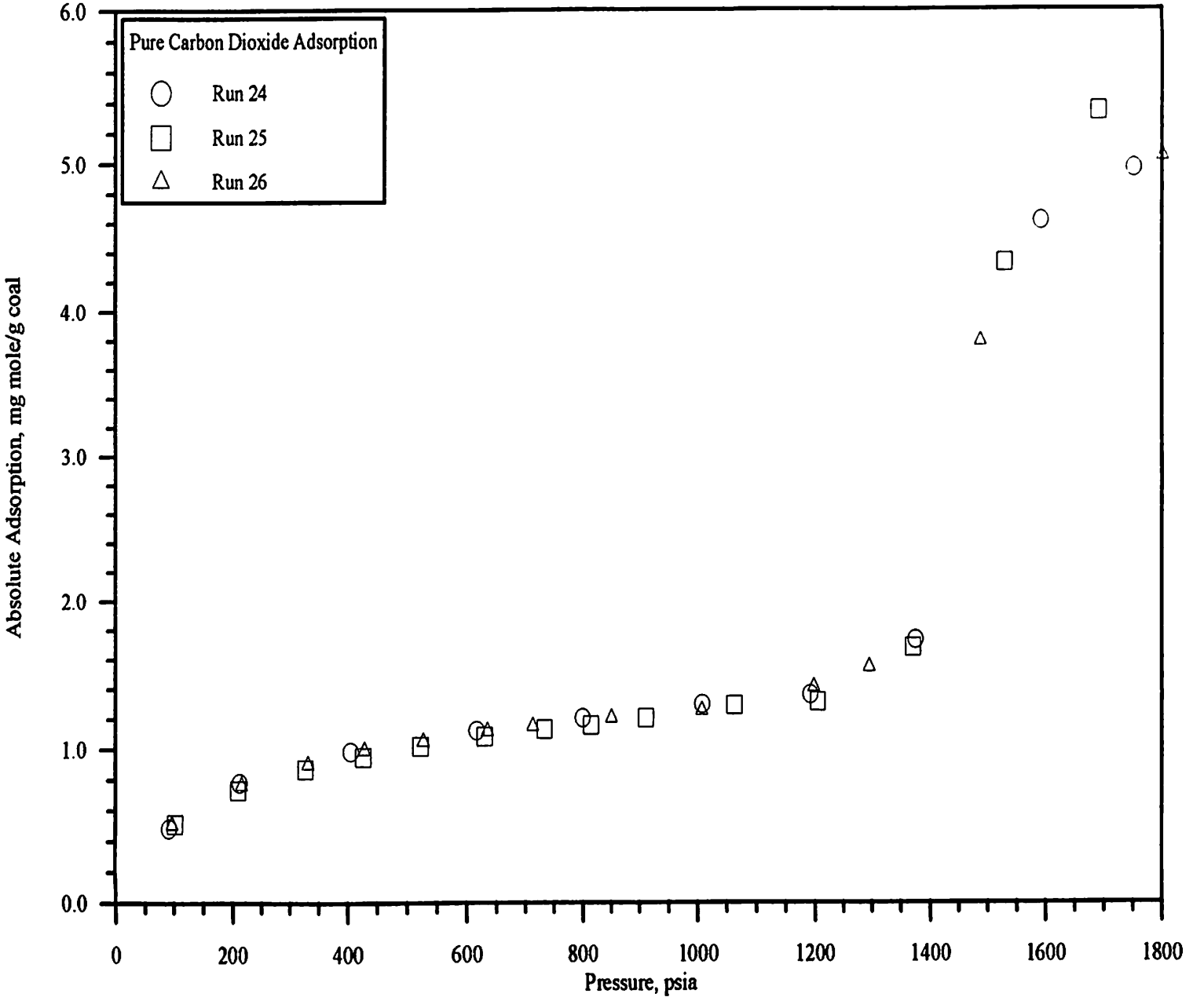

Figure 7. Absolute Adsorption of Carbon Dioxide at 115 °F on Wet Fruitland Coal

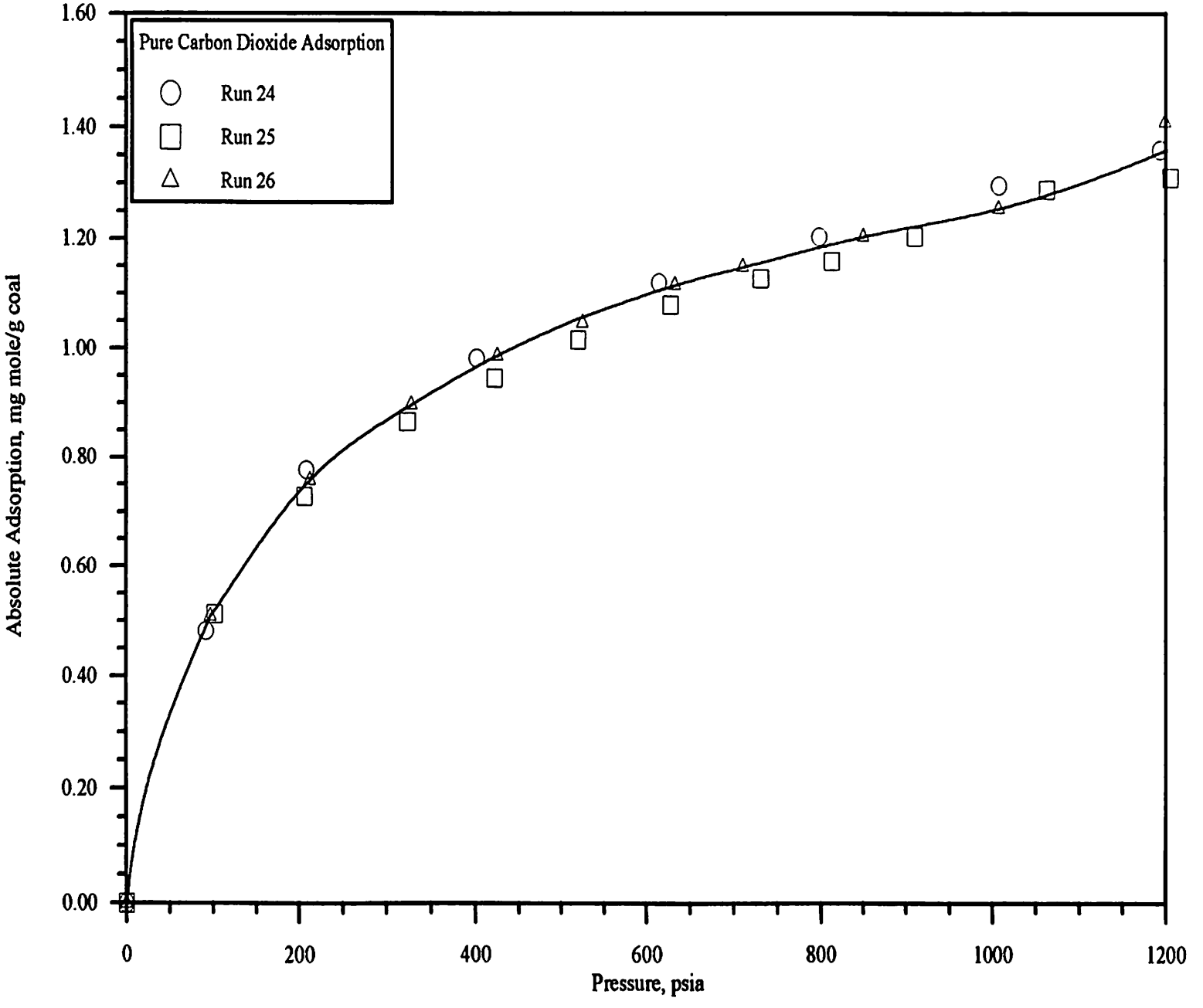

Figure 8. Absolute Adsorption of Carbon Dioxide at 115 °F on Wet Fruitland Coal

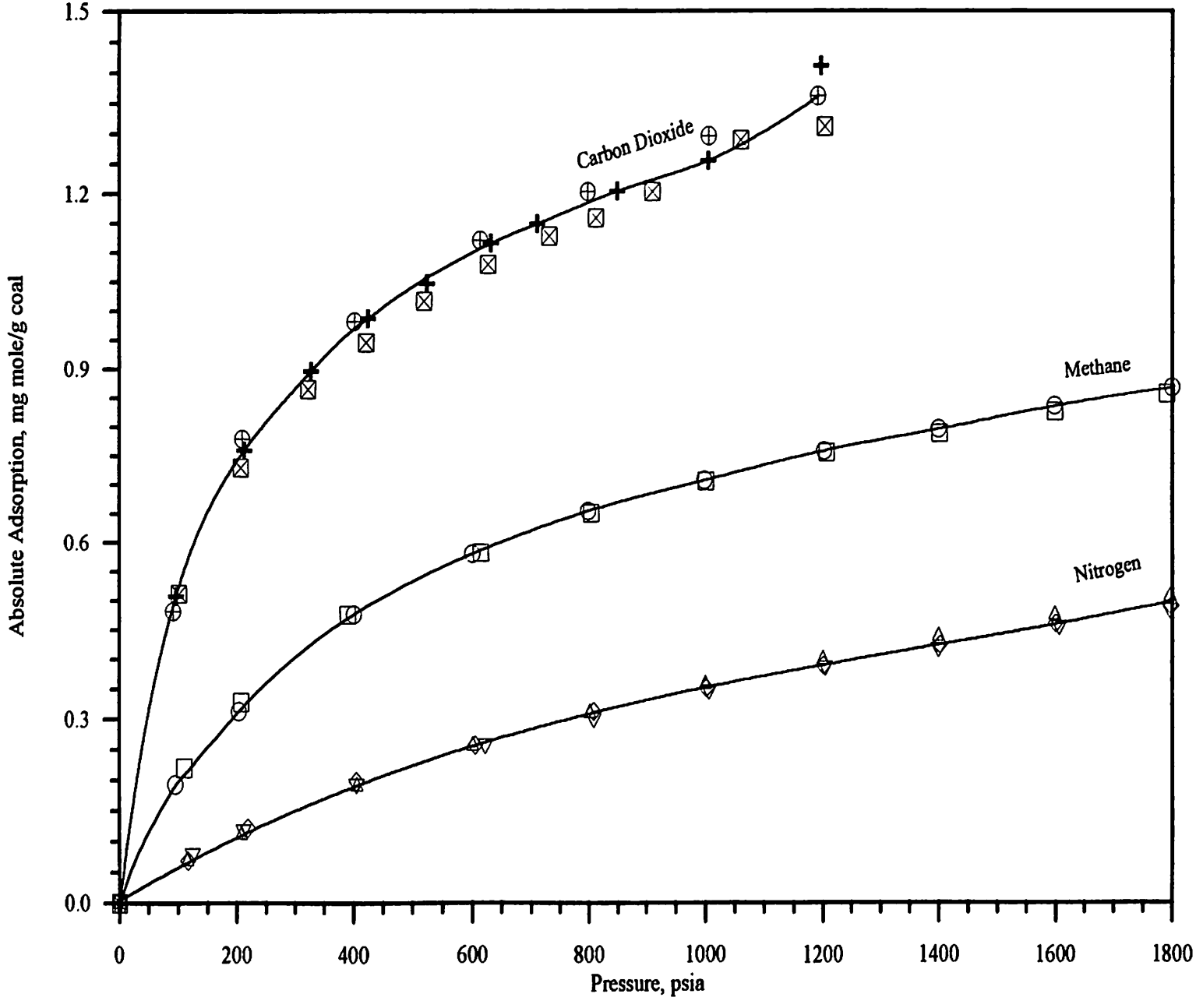

Figure 9. Absolute Adsorption for Pure Components at 115 °F on Wet Fruitland Coal

pressure. The first three figures for each binary mixture present the total absolute adsorption and the absolute adsorption of each individual component as a function of pressure. This is typically the way adsorption data appear in the literature, adsorbed mass relative to a unit mass of dry substrate as a function of pressure. The second type of figure shows the total and individual absolute adsorption data as a function of feed gas composition (mole fraction) for the individual components in the mixture. The third type of figure shows the adsorbate mole fraction as a function of the gas phase composition at equilibrium (similar to a typical y-x plot of vapor-liquid equilibrium).

Methane-Nitrogen Mixture Adsorption

Experimental data for the adsorption of binary methane/nitrogen mixtures are tabulated in Tables XLI through XLIV of Appendix C and are illustrated in Figures 10 to 16. Measurements were made for binary methane/nitrogen injection gas molar compositions of 20/80, 40/60, 60/40 and 80/20. Thus, the *overall* composition in the equilibrium cell was 20/80, 40/60, 60/40 and 80/20, although neither the equilibrium gas or adsorbate phases at equilibrium were of those compositions. Figure 10 illustrates the total absolute adsorption as a function of pressure for the methane/nitrogen mixtures, including the pure methane and nitrogen isotherms. Total adsorption varies from a minimum value corresponding to pure nitrogen adsorption extending to a maximum value corresponding to pure methane. The 80/20 mixture at higher pressures closely approach the pure methane isotherm. This is an indication that at high methane compositions, the methane and nitrogen are competing for the same adsorption sites and the methane is being preferentially adsorbed. Figure 11 illustrates the absolute methane adsorption as a function of pressure, and similar data for nitrogen appears in Figure 12. The methane and nitrogen adsorption both start low at low concentrations and progress

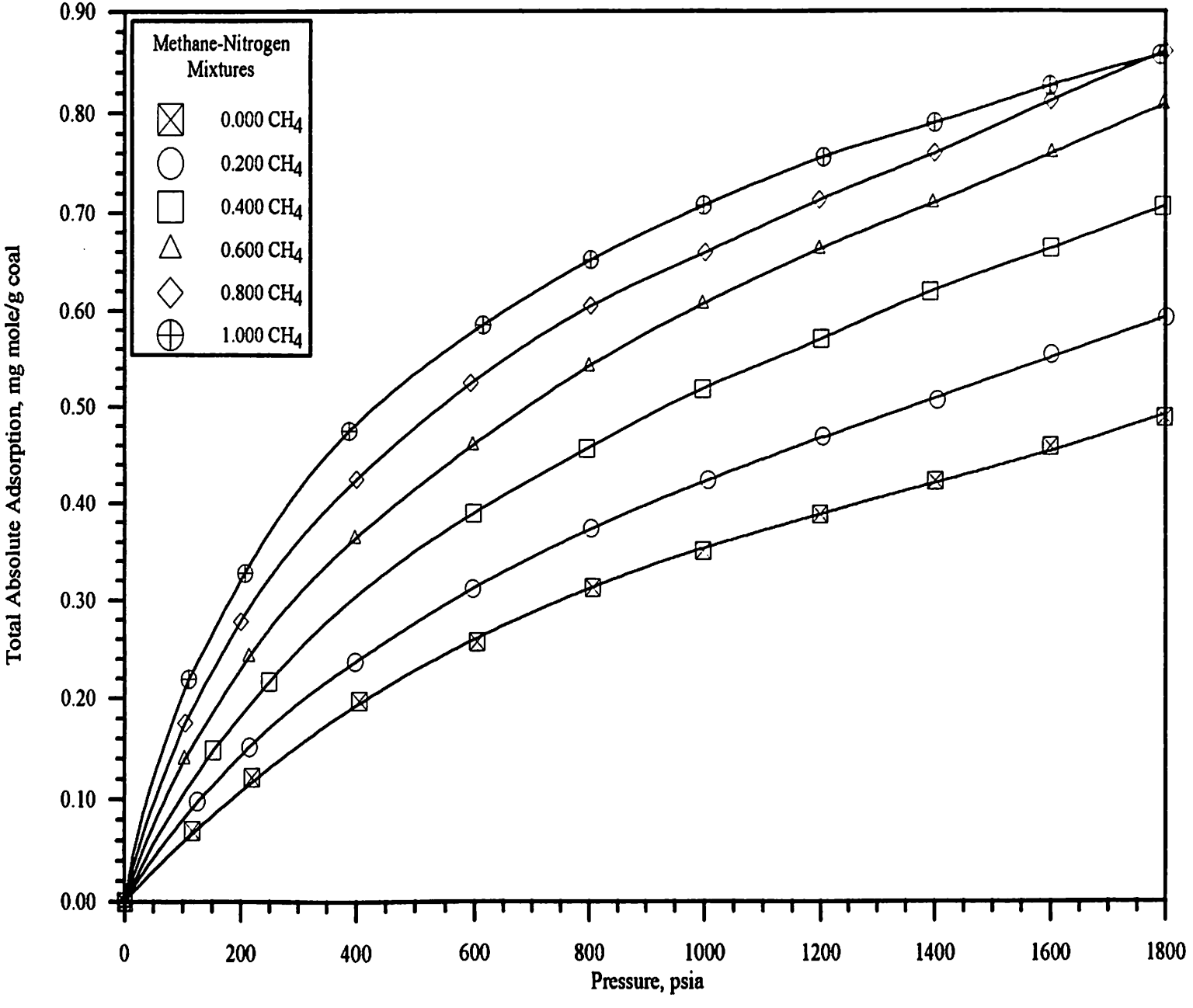

Figure 10. Total Absolute Adsorption from Methane-Nitrogen Mixtures at 115 °F on Wet Fruitland Coal

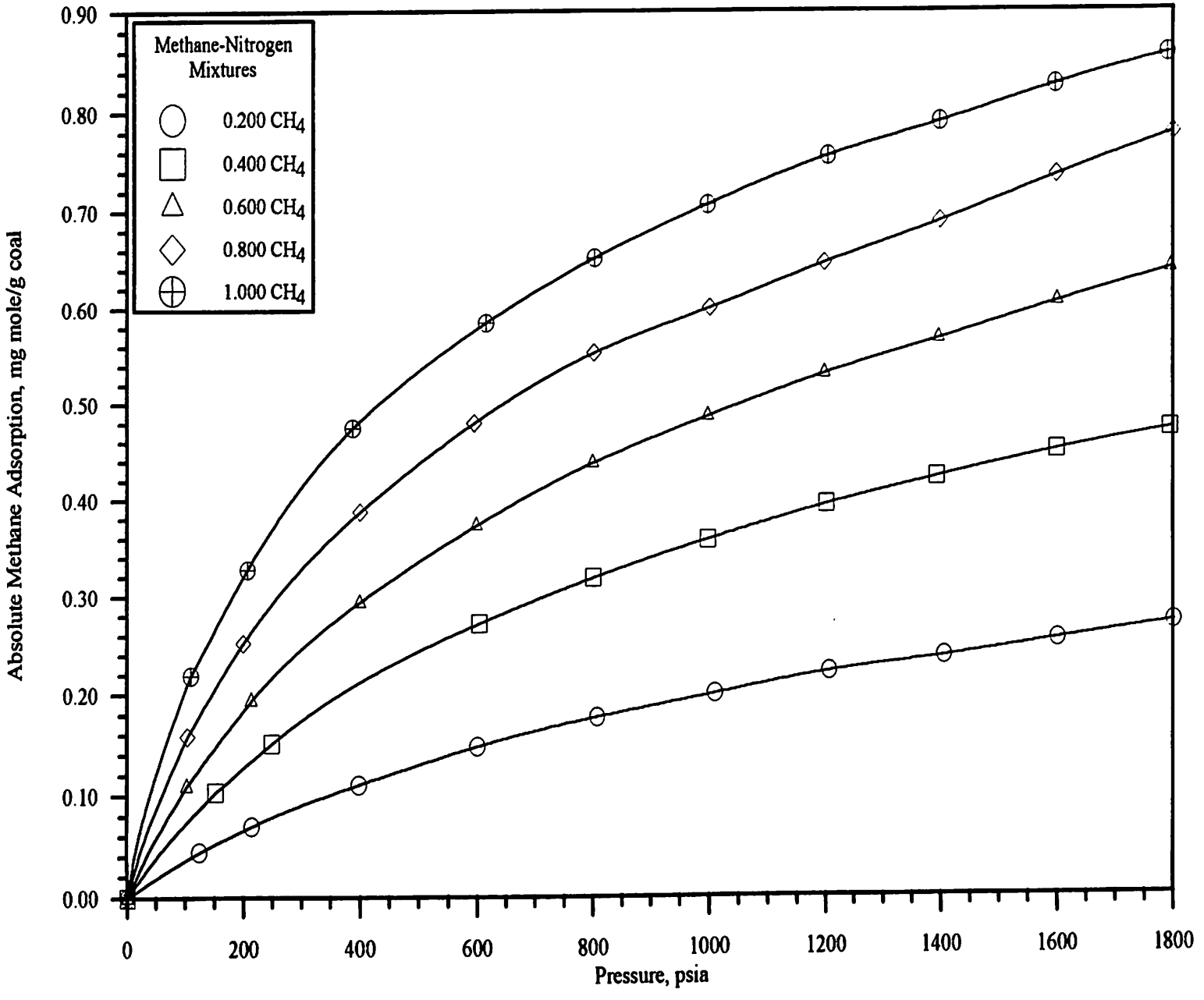

Figure 11. Absolute Adsorption of Methane from Methane-Nitrogen Mixtures at 115 °F on Wet Fruitland Coal

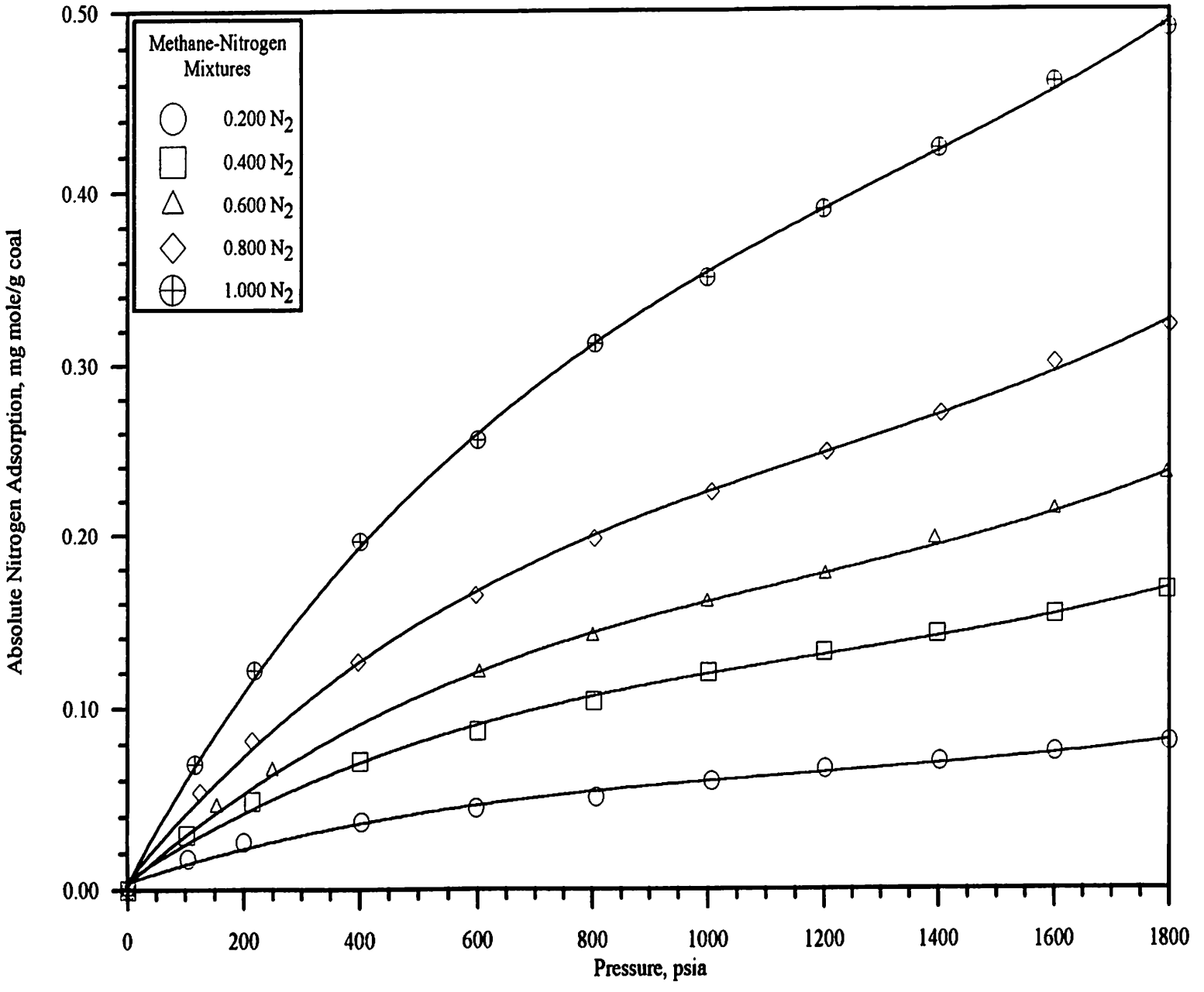

Figure 12. Absolute Adsorption of Nitrogen from Methane-Nitrogen Mixtures at 115 °F on Wet Fruitland Coal

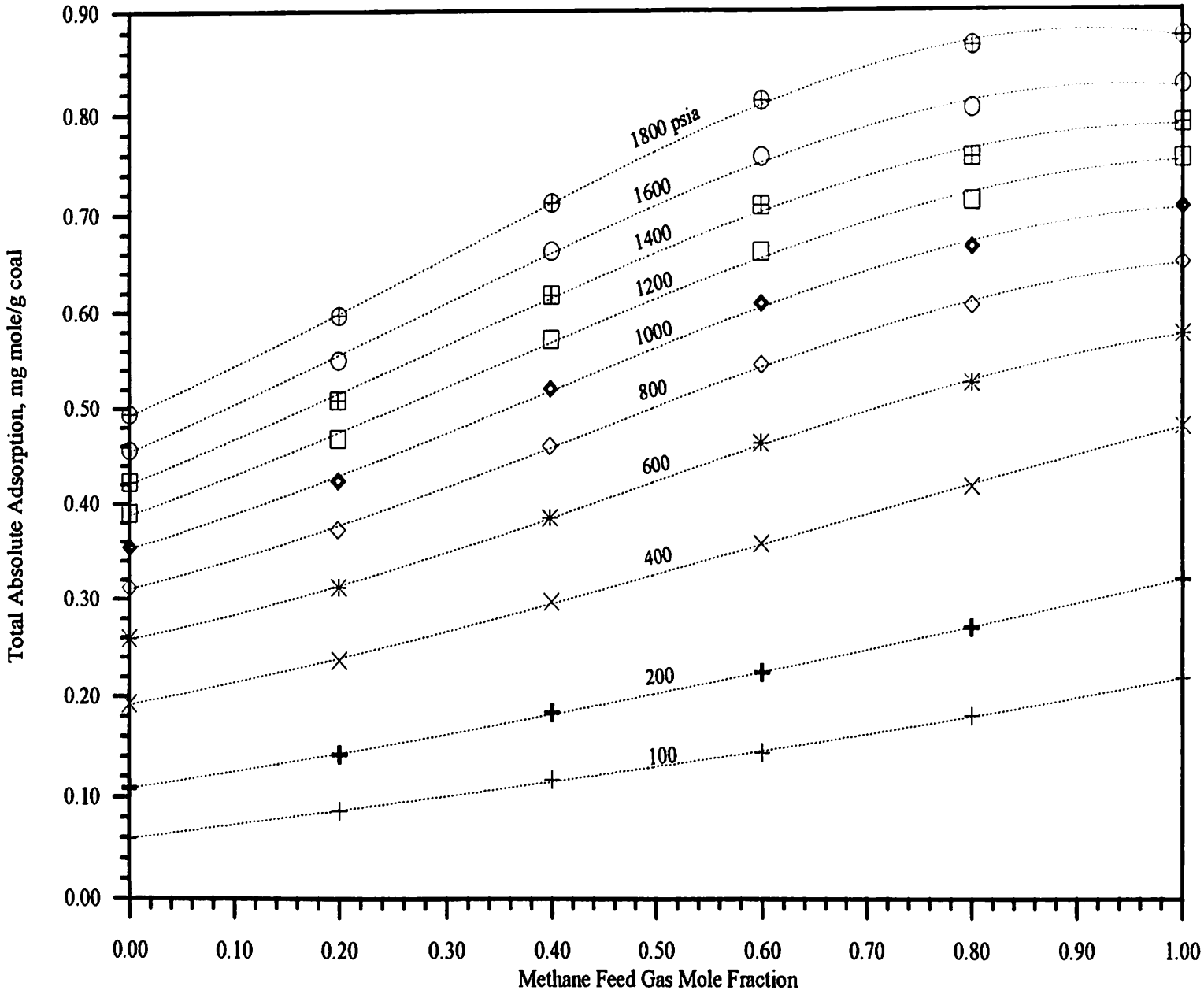

Figure 13. Effect of Feed Gas Composition on Total Absolute Adsorption for Methane-Nitrogen Mixtures

uniformly to the pure component isotherm.

The total, methane and nitrogen adsorption data are shown as a function of methane feed gas mole fraction in Figures 13 through 15. For total adsorption (Figure 13), the lower pressure isobars are linear while at higher pressures they become slightly non-linear. This indicates that the two components are competing for the same adsorption sites at higher pressures. From Figures 14 and 15, methane and nitrogen are shown to be competing for the same adsorption sites. A deviation from ideal behavior (straight isobar) in either direction indicates that one component is displacing the other component from the coal surface. The non-linearity of the data indicates that the components are competing. As the methane composition increases in Figure 14, methane adsorption increases non-linearly with a corresponding non-linear decrease in nitrogen adsorption as seen in Figure 15. The methane appears to be preferentially adsorbed over the nitrogen throughout the methane composition range (20/80, 40/60, 60/40, 80/20) with the maximum nitrogen displacement occurring at higher pressures. The rapid drop in nitrogen adsorption (Figure 15) as low amounts of methane are added to the mixture show that (at the higher pressures, where competitive adsorption occurs) the methane efficiently displaces the nitrogen (adsorbing preferentially with respect to nitrogen).

The component exhibiting positive deviations (from straight isobar) is the component being preferentially adsorbed, while negative deviations indicate the least adsorbed component. Figure 16 yields additional proof that the methane and nitrogen are competing for the same adsorption sites. The negative deviation of Figure 16 indicates that the methane is displacing the nitrogen component on the coal surface. As the methane composition increases, more of the nitrogen is displaced. Figure 16 also illustrates the effect of pressure on the x and y.

Figure 16 illustrates that the extended Loading Ratio Correlation (LRC) is inadequate in describing the adsorption behavior of the interested gases on this

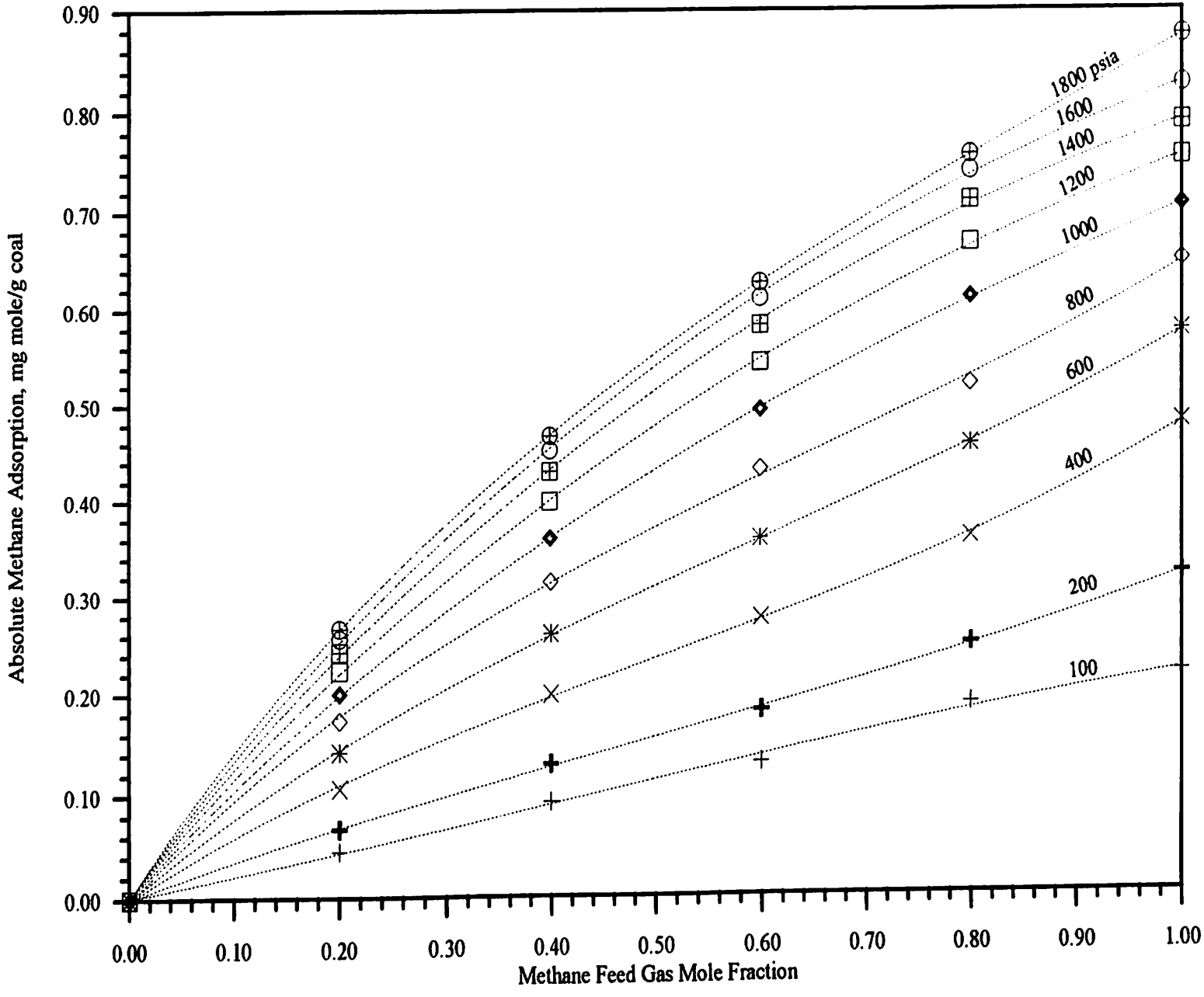

Figure 14. Effect of Feed Gas Composition on Absolute Adsorption for Methane from Methane-Nitrogen Mixtures

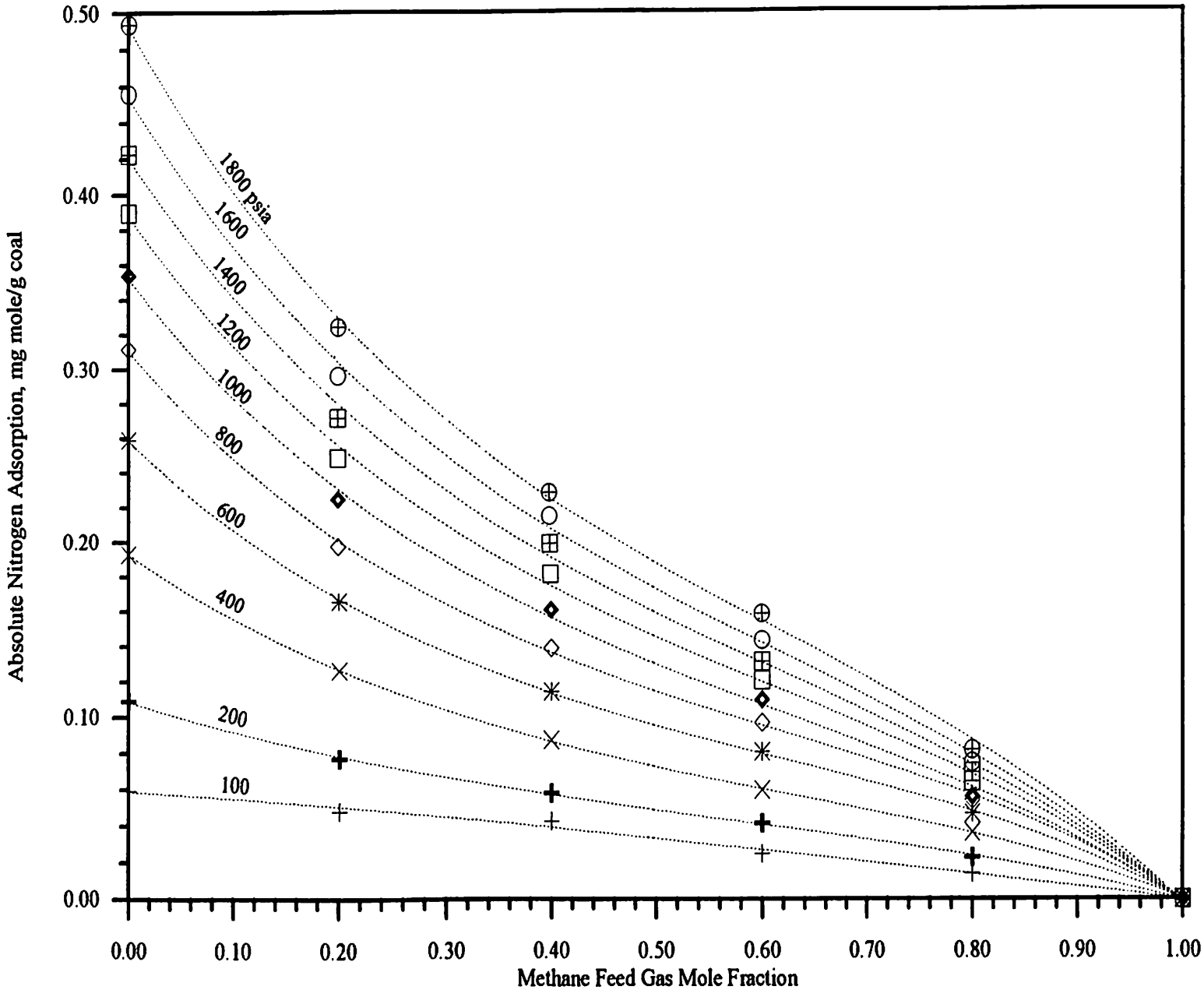

Figure 15. Effect of Feed Gas Composition on Absolute Adsorption for Nitrogen from Methane-Nitrogen Mixtures

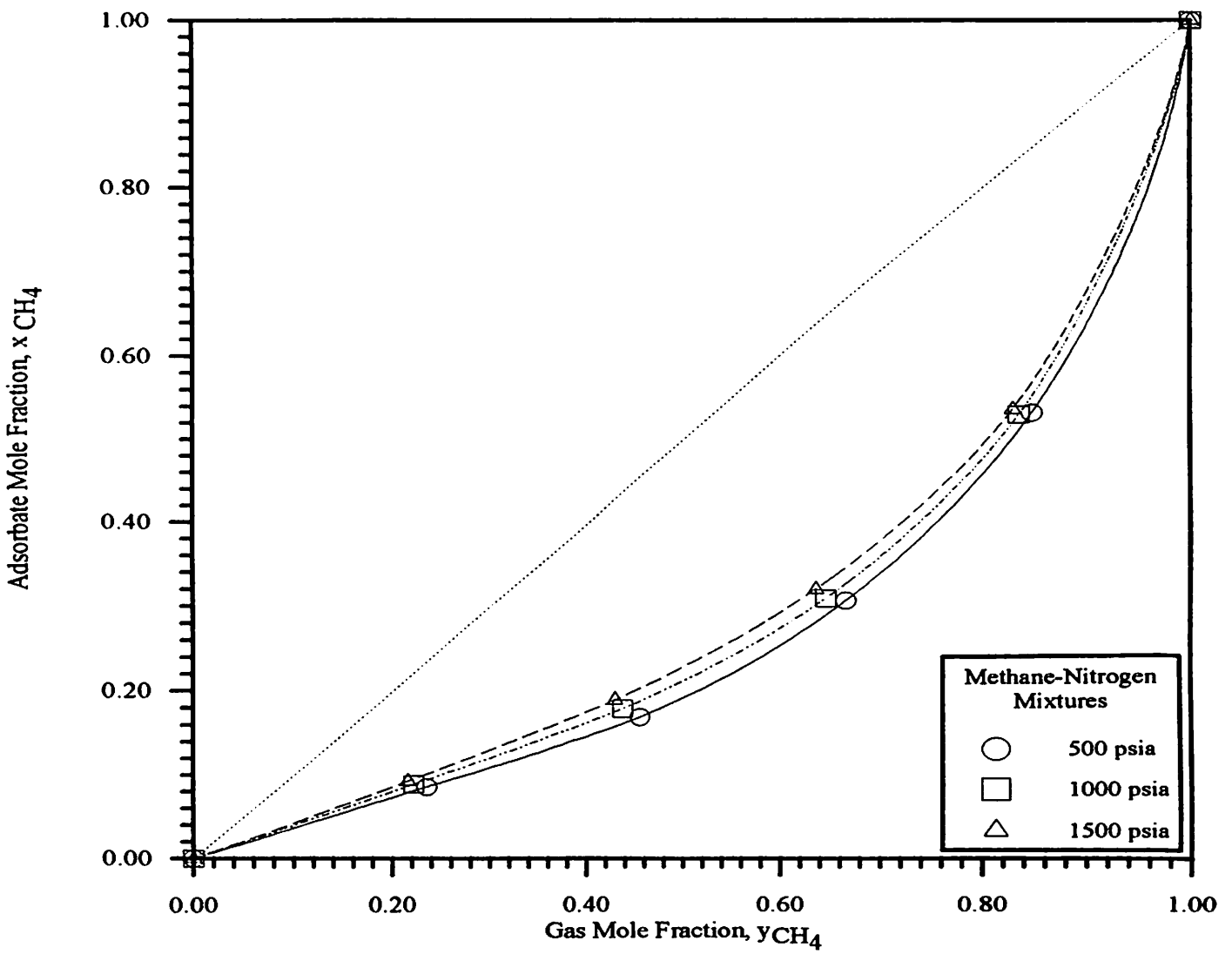

Figure 16. Phase Compositions for Adsorption of Methane-Nitrogen Mixtures on Wet Fruitland Coal

substrate. Equation III-8 may be rearranged, by noting that $x_1/x_2 = \omega_1/\omega_2$, to yield

$$\left[\frac{y_1}{1-y_1}\right] = \left[\frac{L_2 B_2}{L_1 B_1}\right]\left[\frac{x_1}{1-x_1}\right] \qquad \text{(VI-1)}$$

where y_i, x_i, ω_i, L_i, and B_i are the gas phase composition, adsorbate composition, amount adsorbed and Loading Ratio Correlation constants for component i. Thus, the LRC expression predicts x_i-y_i relations that are independent of pressure. This is not consistent with the data in Figure 16, where a slight but discernible pressure dependence is evident.

Methane-Carbon Dioxide Mixture Adsorption

Methane/carbon dioxide mixture adsorption data are shown in Figures 17 to 23. Measurements were made for binary methane/carbon dioxide injection gas molar compositions of 20/80, 40/60, 60/40 and 80/20. The experimental data are included in Tables XLV through XLVIII of Appendix C. Figure 17 shows the total adsorption as a function of pressure including the pure methane and carbon dioxide isotherms. As seen with the methane/nitrogen mixture, the adsorption capacity increases as more carbon dioxide is added to the mixture. Figure 18 illustrates absolute methane adsorption as a function of pressure, and similar data for carbon dioxide appear in Figure 19.

Total, methane and carbon dioxide data are shown as a function of methane feed gas composition in Figures 20 through 22. While each isotherm is slightly non-linear, the magnitude of the non-linearity is less than the non-linearity of the corresponding methane/nitrogen figures. This can be interpreted as that while methane and carbon dioxide compete for the same adsorption sites, the carbon dioxide does not dominate the methane as seen with methane displacing the

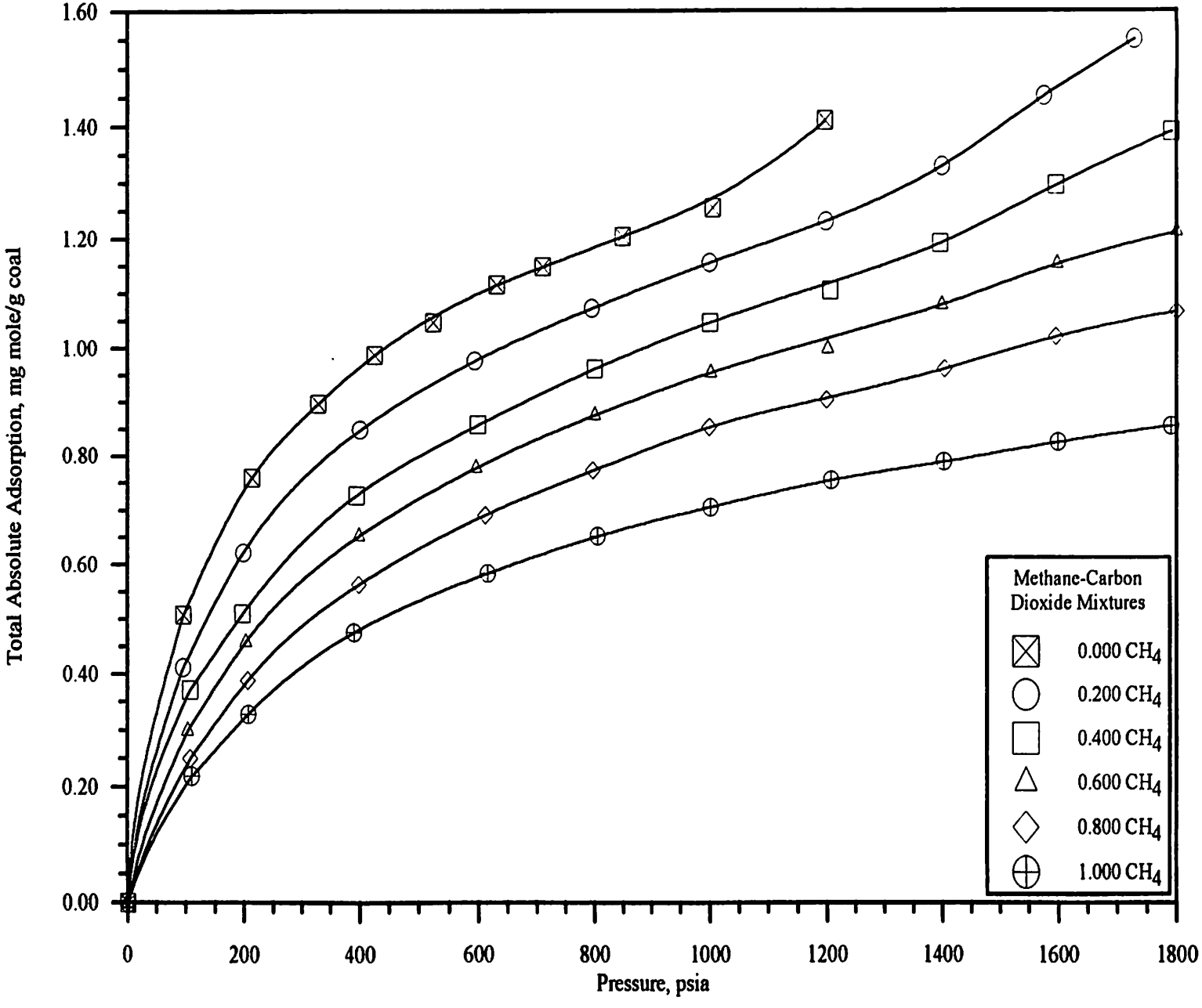

Figure 17. Total Absolute Adsorption for Methane-Carbon Dioxide Mixtures at 115 °F on Wet Fruitland Coal

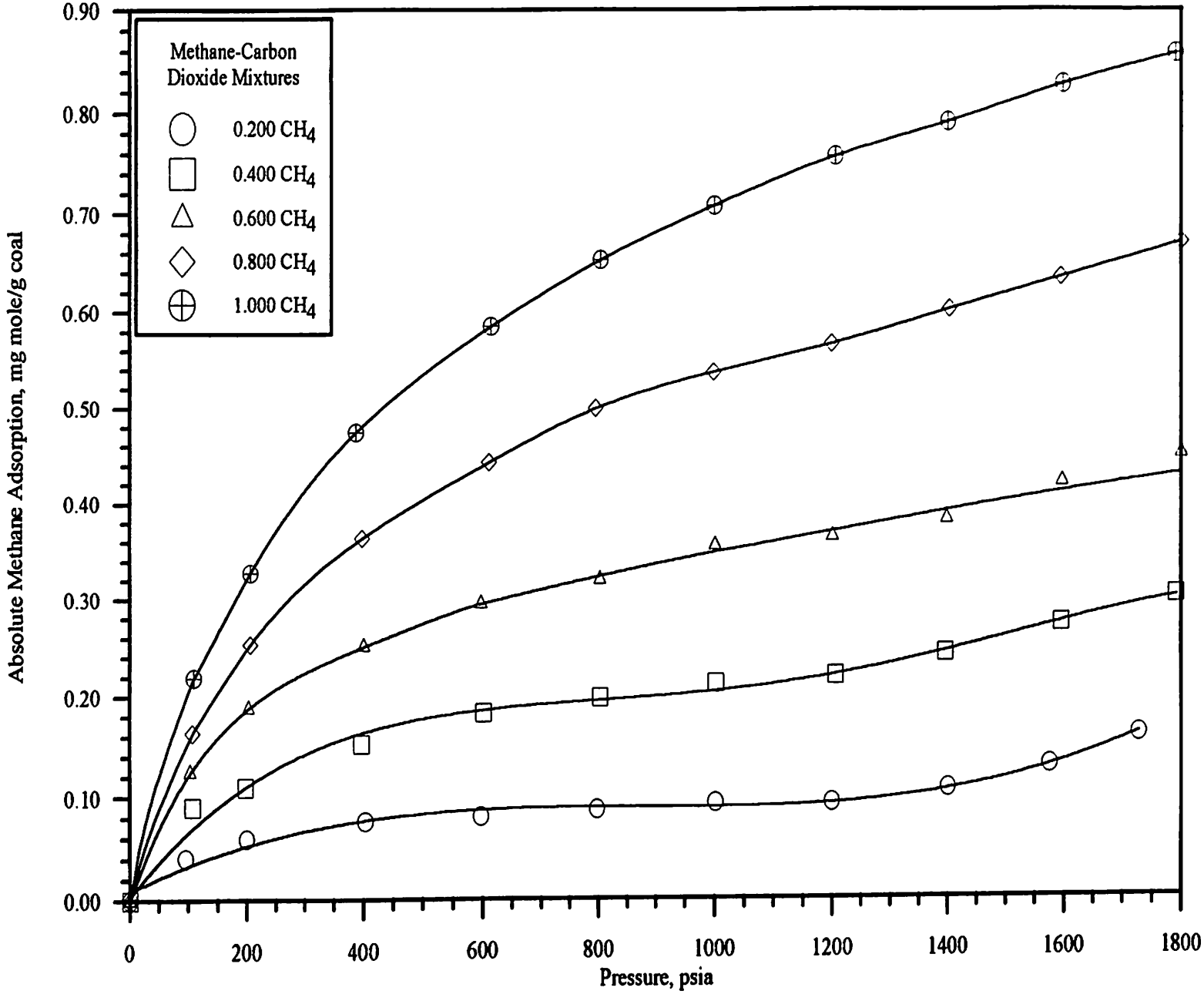

Figure 18. Absolute Adsorption of Methane from Methane-Carbon Dioxide Mixtures at 115 °F on Wet Fruitland Coal

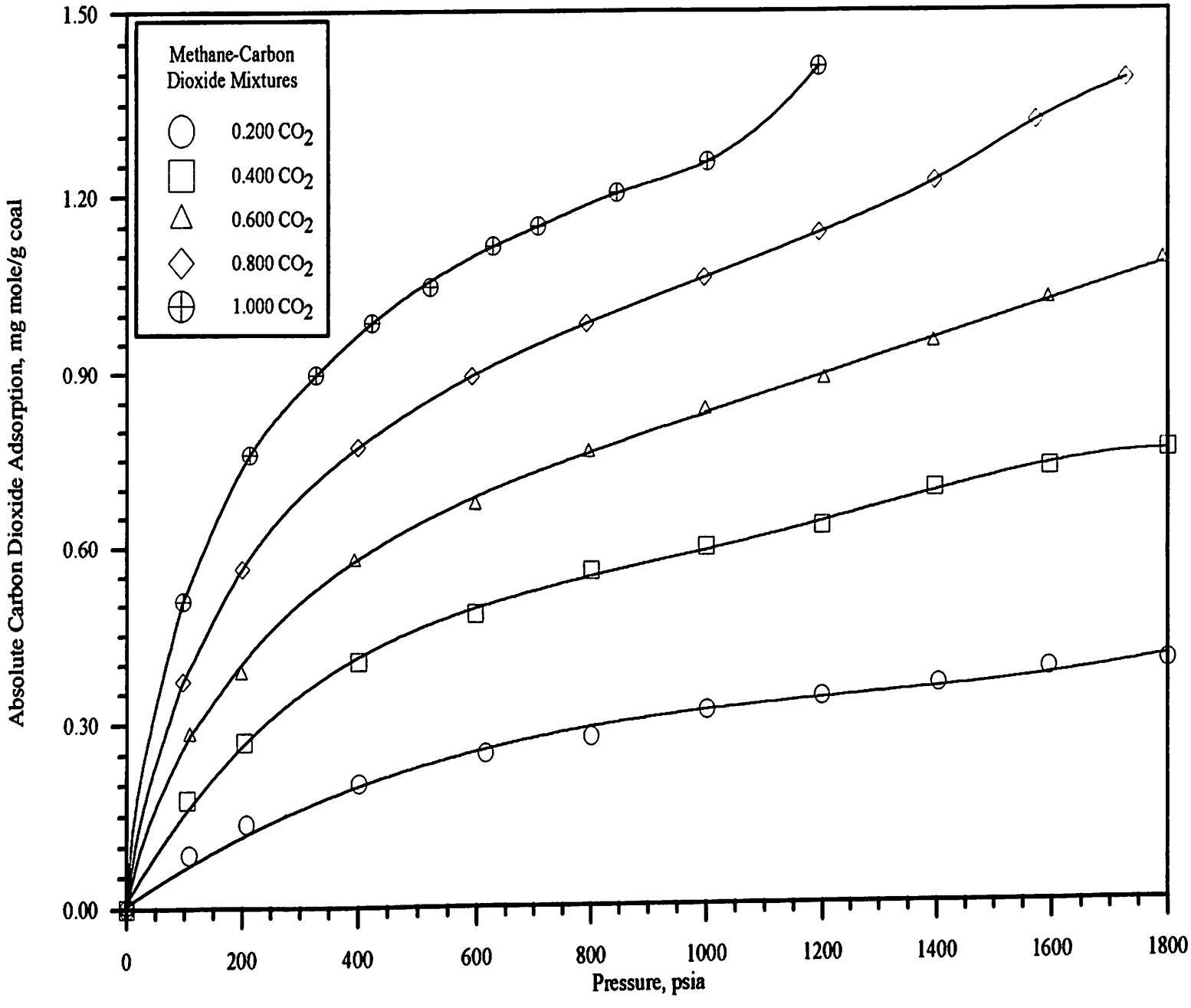

Figure 19. Absolute Adsorption of Carbon Dioxide from Methane-Carbon Dioxide Mixtures at 115 °F on Wet Fruitland Coal

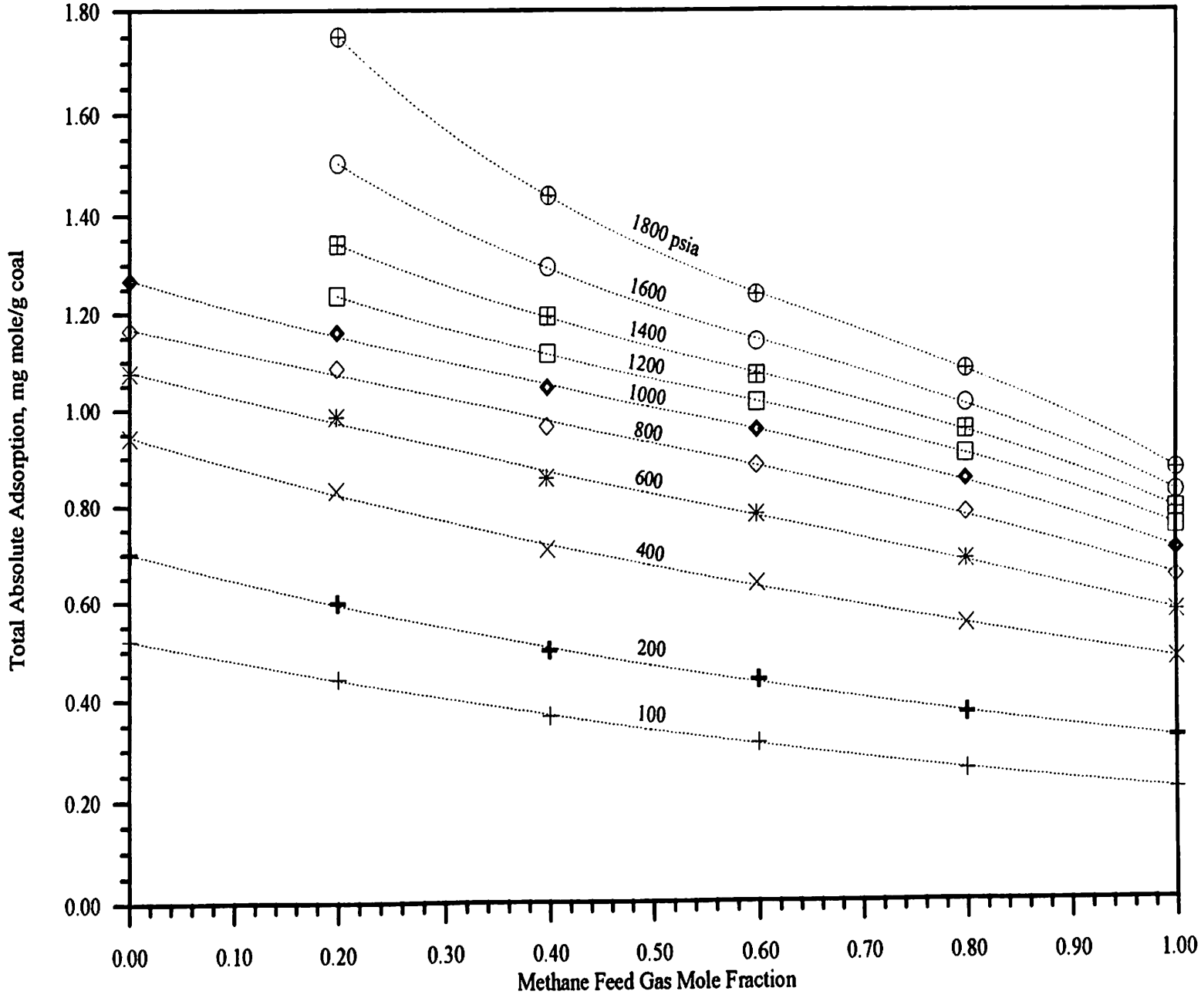

Figure 20. Effect of Feed Gas Composition on Total Absolute Adsorption for Methane-Carbon Dioxide Mixtures

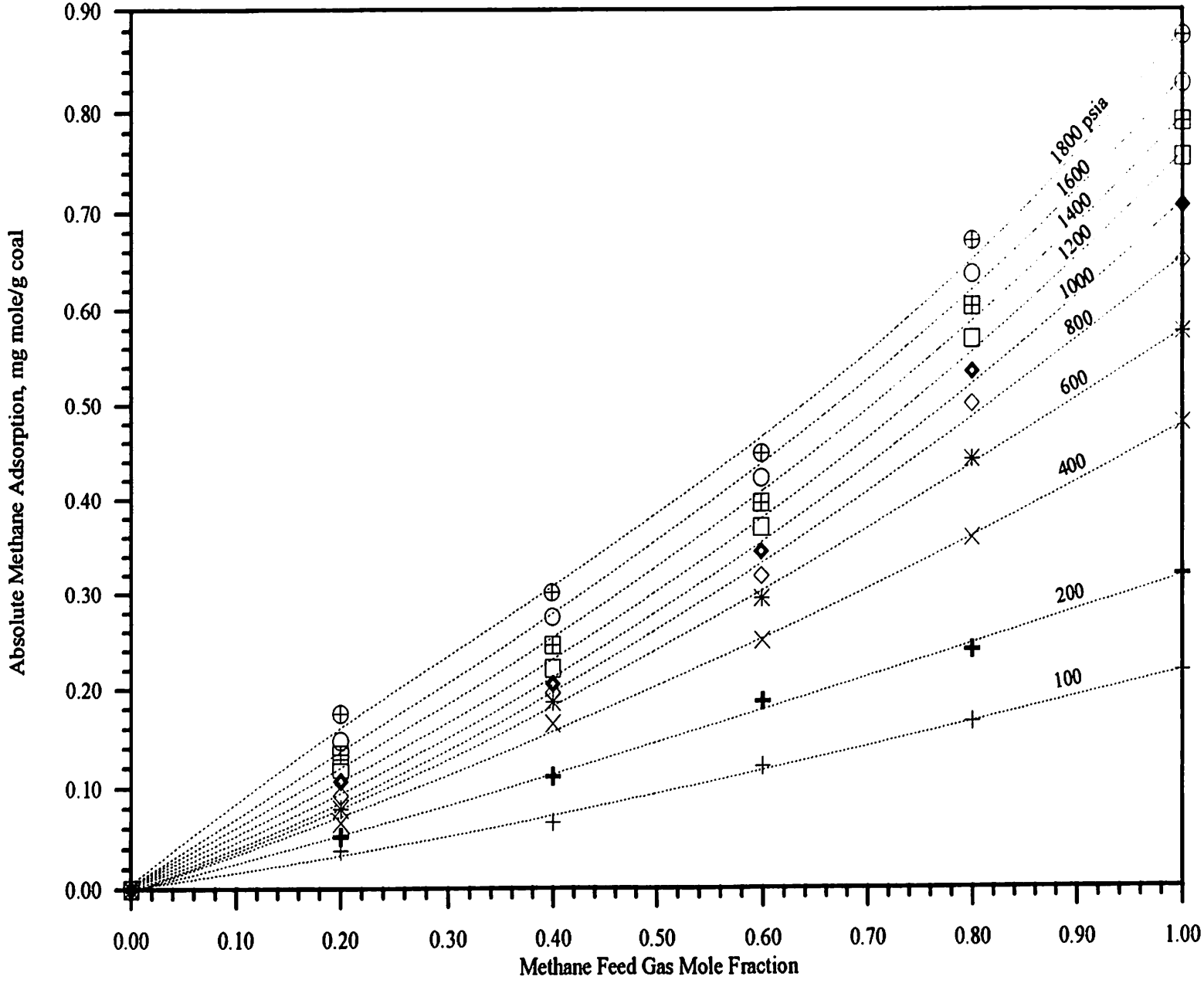

Figure 21. Effect of Feed Gas Composition on Absolute Adsorption for Methane from Methane-Carbon Dioxide Mixtures

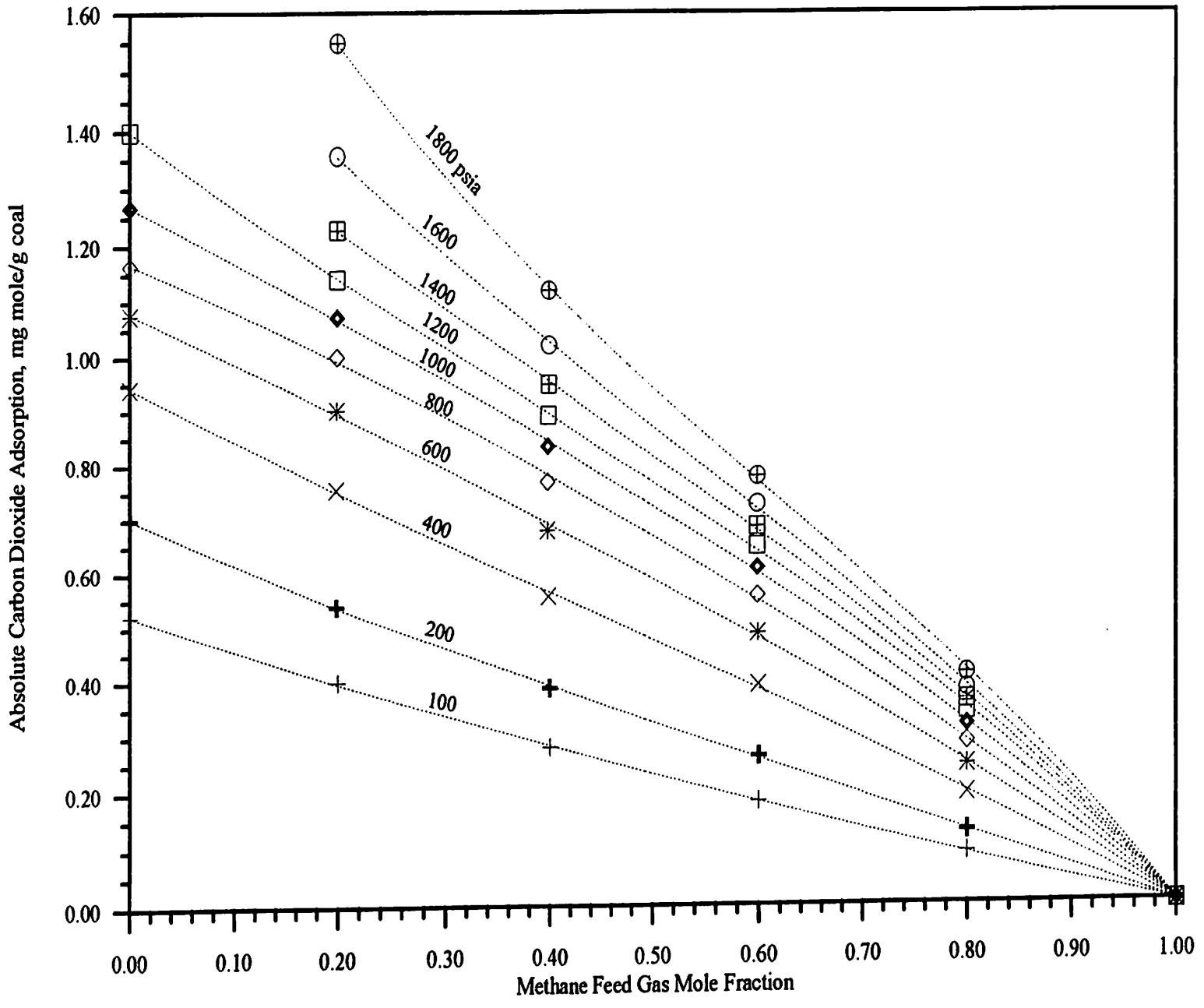

Figure 22. Effect of Feed Gas Composition on Absolute Adsorption for Carbon Dioxide from Methane-Carbon Dioxide Mixtures

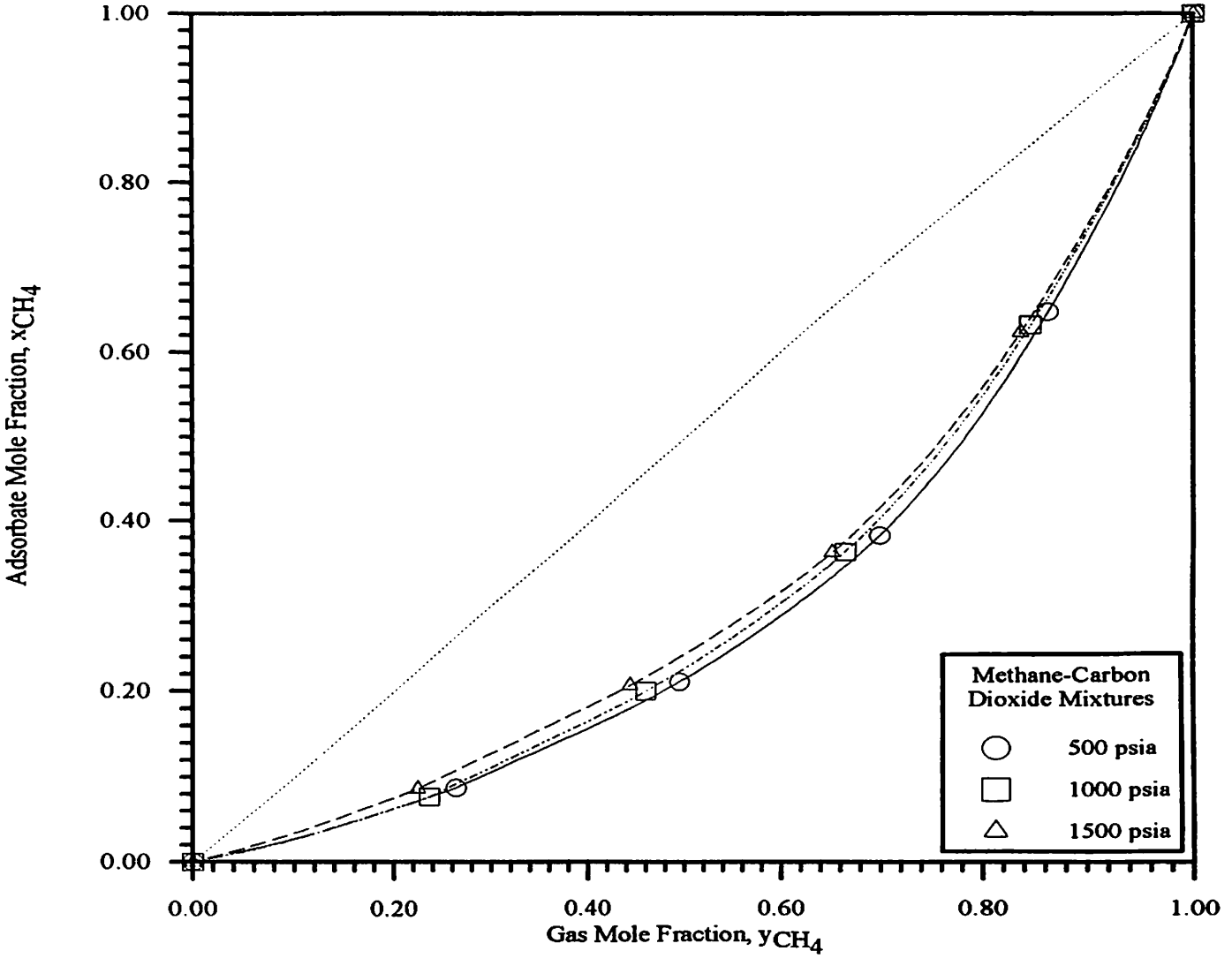

Figure 23. Phase Compositions for Adsorption of Methane-Carbon Dioxide Mixtures on Wet Fruitland Coal

nitrogen molecules in the methane/nitrogen mixtures. This is shown in Figure 23. The non-linear data is an indication that the components are competing for the same adsorption sites. The methane/carbon dioxide x-y plot, Figure 23, indicates that the carbon dioxide is displacing the methane component from the substrate surface. Figure 23 also shows a slight pressure dependence, again demonstrating the inadequacies of the loading ratio correlation.

Figure 23 further proves that the methane and carbon dioxide are competing for the same adsorption sites. Negative deviation of Figure 23 indicates that the methane is being displaced by the preferentially-adsorbed carbon dioxide component. A small concentration of carbon dioxide in the gas phase displaces a significant amount of methane from the surface. As the methane composition decreases, less of the methane is displaced.

These figures indicate that the two components are competing for the same adsorption sites with the coal surface, showing a tendency to adsorb more of the carbon dioxide molecules than the competing methane molecules. In addition, carbon dioxide displaces the most methane at high pressures and high methane compositions.

Nitrogen-Carbon Dioxide Mixture Adsorption

Binary mixture measurements were made for nitrogen/carbon dioxide injection gas molar compositions of 20/80, 40/60, 60/40, 70/30 and 80/20. An additional 70/30 mixture was tested (compared to the other mixtures) to confirm the behavior of the 60/40 and 80/20 mixtures. The mixture information is shown in Figures 24 to 30 with the experimental data tabulated in Appendix C (Tables XLIX through LIII). The order of the figures is the same as with previous mixtures. In Figure 26, the tenth datum point of the 80/20 (80% CO_2) mixture is suspect. The same datum point in Figures 24 and 25 are consistent with the surrounding data,

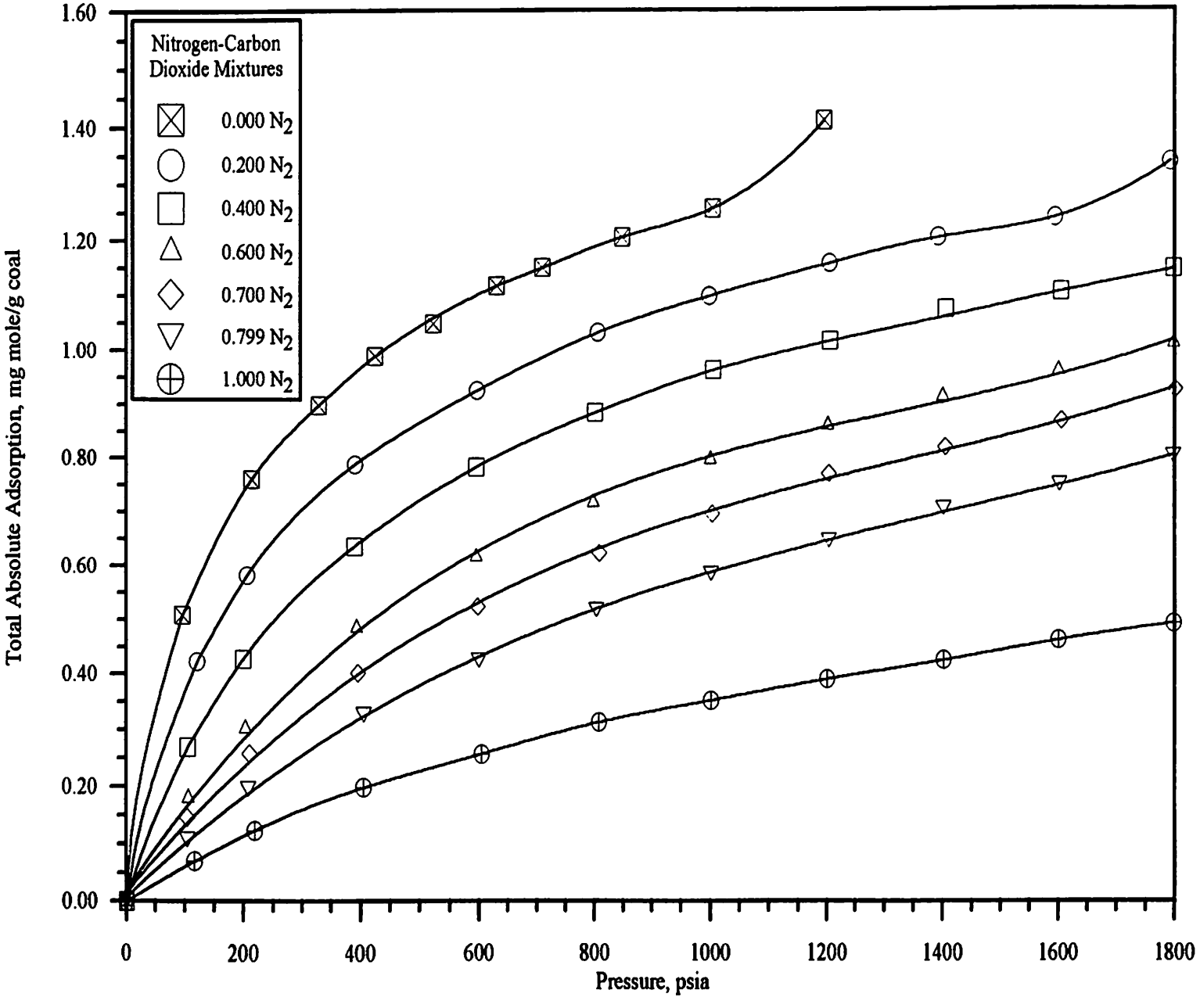

Figure 24. Total Absolute Adsorption for Nitrogen-Carbon Dioxide Mixtures at 115 °F on Wet Fruitland Coal

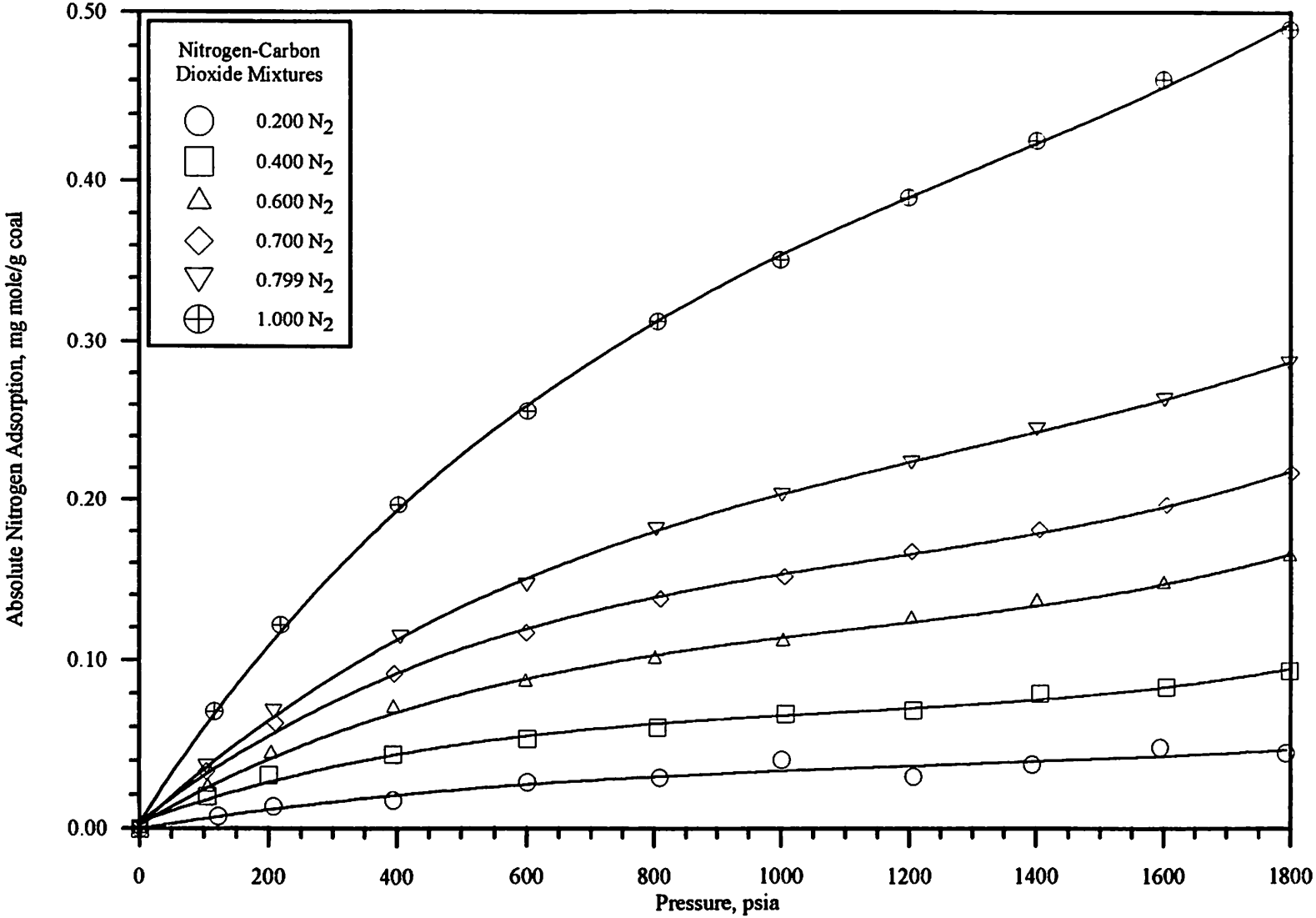

Figure 25. Absolute Adsorption of Nitrogen from Nitrogen-Carbon Doxide Mixtures at 115 °F on Wet Fruitland Coal

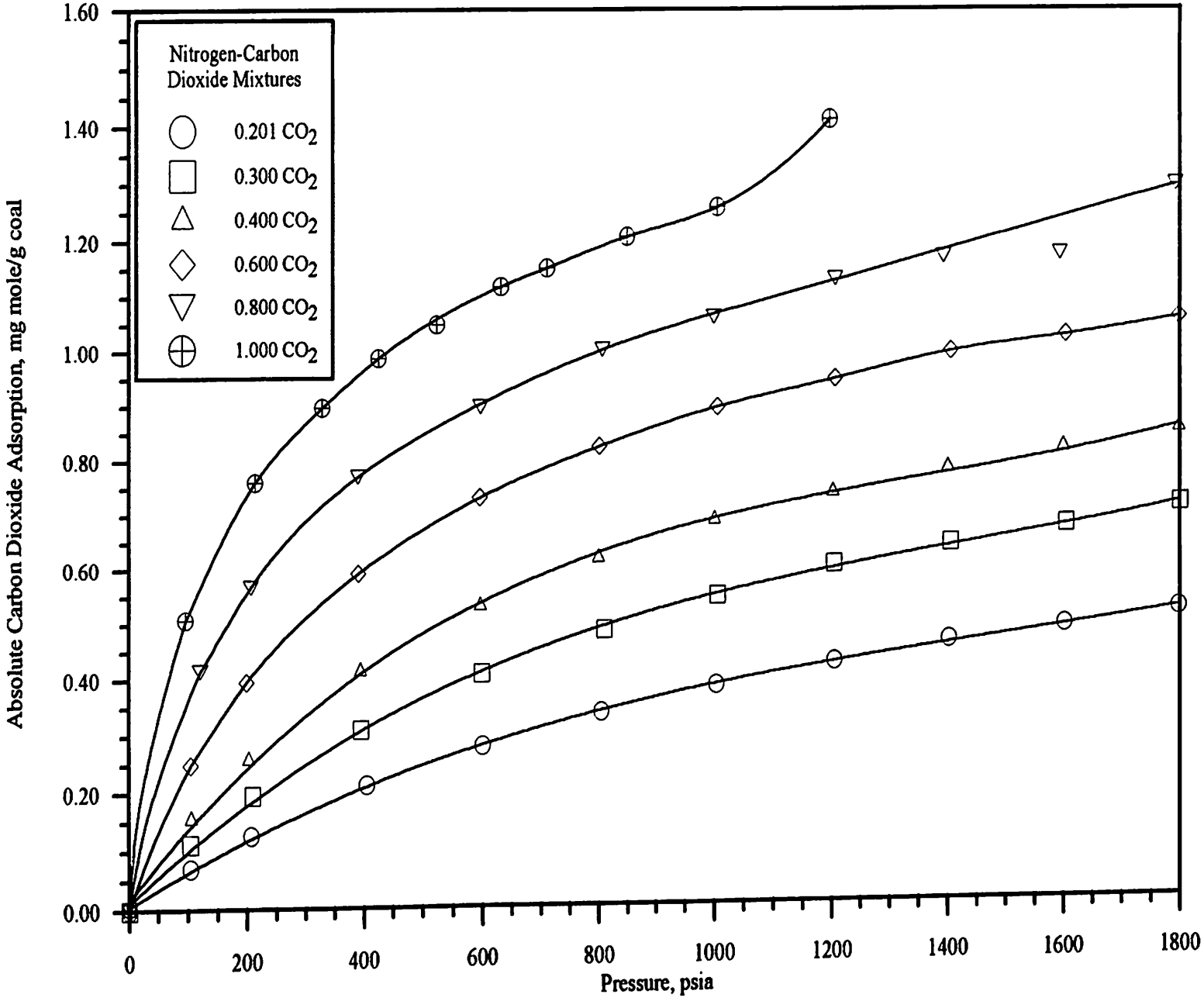

Figure 26. Absolute Adsorption of Carbon Dioxide from Nitrogen-Carbon Dioxide Mixtures at 115 °F on Wet Fruitland Coal

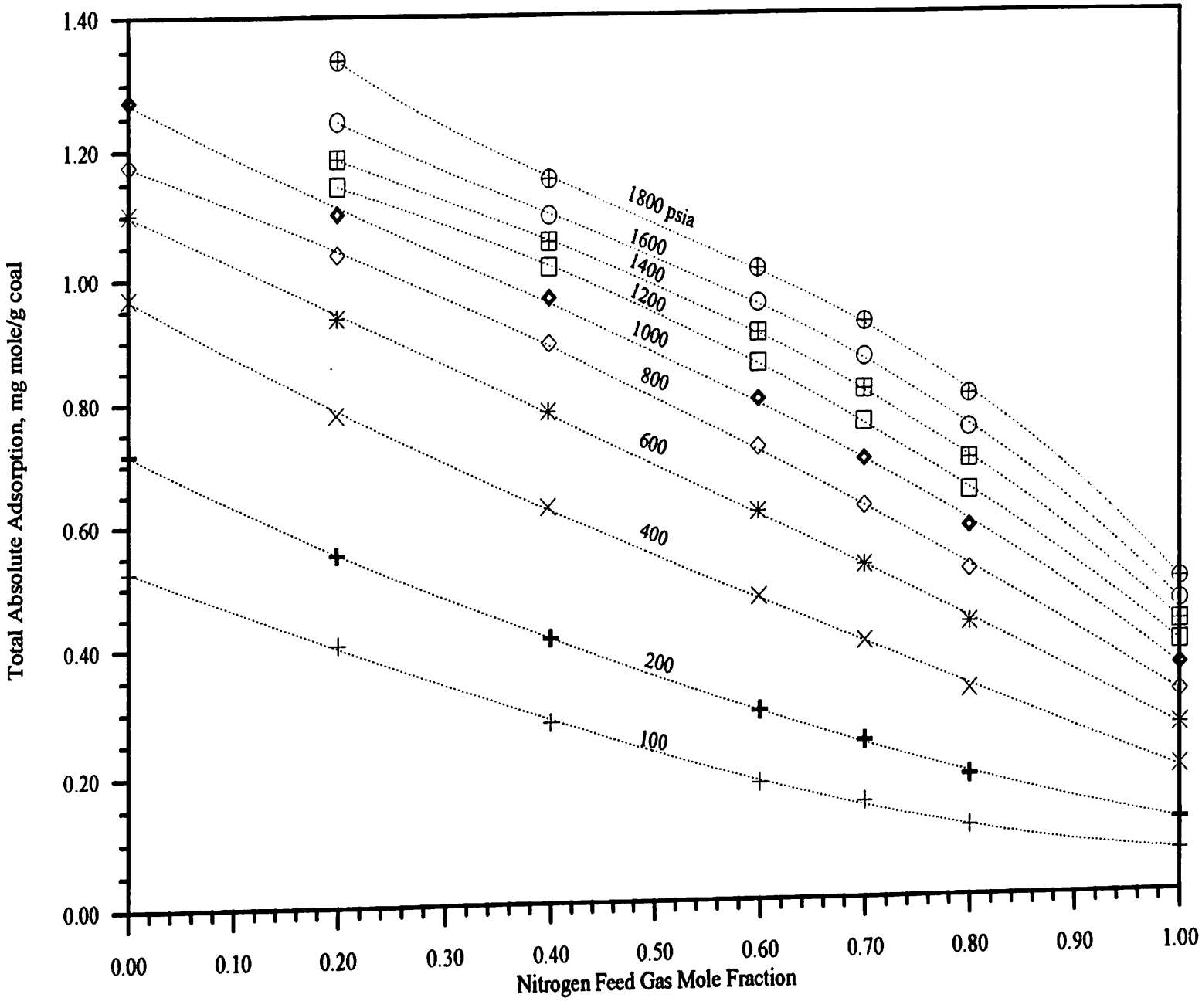

Figure 27. Effect of Feed Gas Composition on Total Absolute Adsorption for Nitrogen-Carbon Dioxide Mixtures

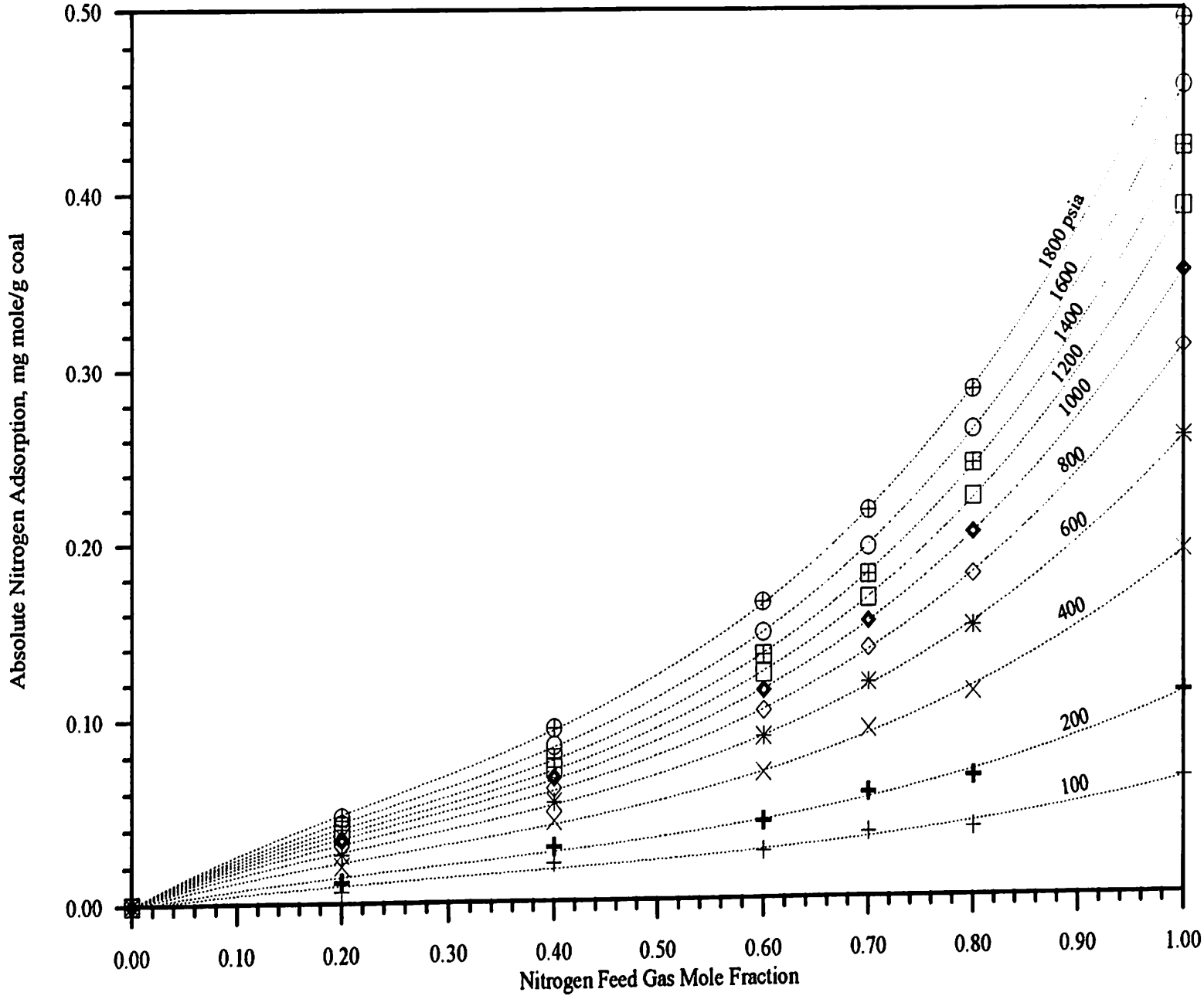

Figure 28. Effect of Feed Gas Composition on Absolute Adsorption for Nitrogen from Nitrogen-Carbon Dioxide Mixtures

indicating that the suspect datum point (Figure 26) is an inadequacy of the software graphing package to fit that point. The 80/20 mixture of Figure 26 is showing some of the multimolecular (Type II) adsorption (as seen with the 100% CO_2 isotherm).

The non-linear adsorption data (Figures 27-29) are a good indication that the components are competing for the same adsorption sites. The negative deviation of the nitrogen data (Figure 28) indicate that the nitrogen is being displaced by the carbon dioxide molecules. As seen with methane-nitrogen mixture adsorption (Figure 15), the rapid drop in nitrogen adsorption as low amounts of carbon dioxide are added to the mixture show that (at higher pressures, where competitive adsorption occurs) the carbon dioxide efficiently displaces the nitrogen, adsorbing preferentially with respect to nitrogen. The carbon dioxide component displays positive deviations as seen in Figure 29. The equilibrium x-y plot in Figure 30 further proves that the carbon dioxide molecules are displacing the nitrogen from the coal surface as illustrated by the negative deviation. Small amounts of carbon dioxide added to the mixture are displacing significant numbers of nitrogen molecules. Figure 30 again show an effect of pressure on the x-y relation illustrating the inadequacies of the LRC.

Figure 31 shows an adsorbate mole fraction as a function of gas mole fraction for all three binary mixtures. Each mixture is shown relative to component one (the lighter component), as indicated. The negative deviations indicates competition between components for the same coal surface adsorption sites. The deviation is a measure of how much of the lower-adsorbing component is displaced by the preferentially-adsorbing component. The methane/carbon dioxide mixtures show the least deviation, indicating that the carbon dioxide molecules displaces fewer methane molecules from the coal surface than occurs at low gas compositions of the heavier component in the other two mixtures. The methane/nitrogen mixture values are similar to the methane/carbon dioxide mixture except at higher gas phase

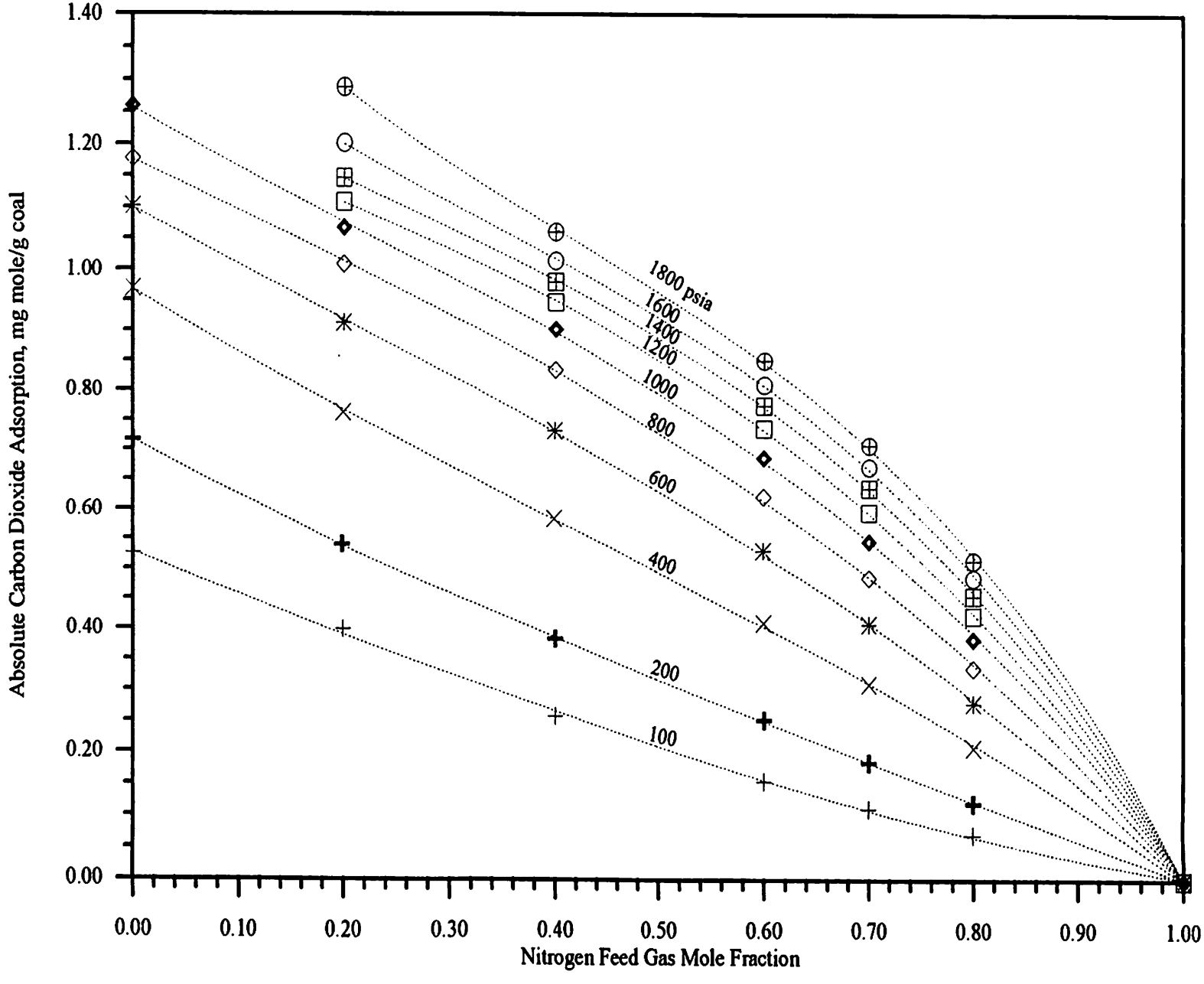

Figure 29. Effect of Feed Gas Composition on Absolute Adsorption for Carbon Dioxide from Nitrogen-Carbon Dioxide Mixtures

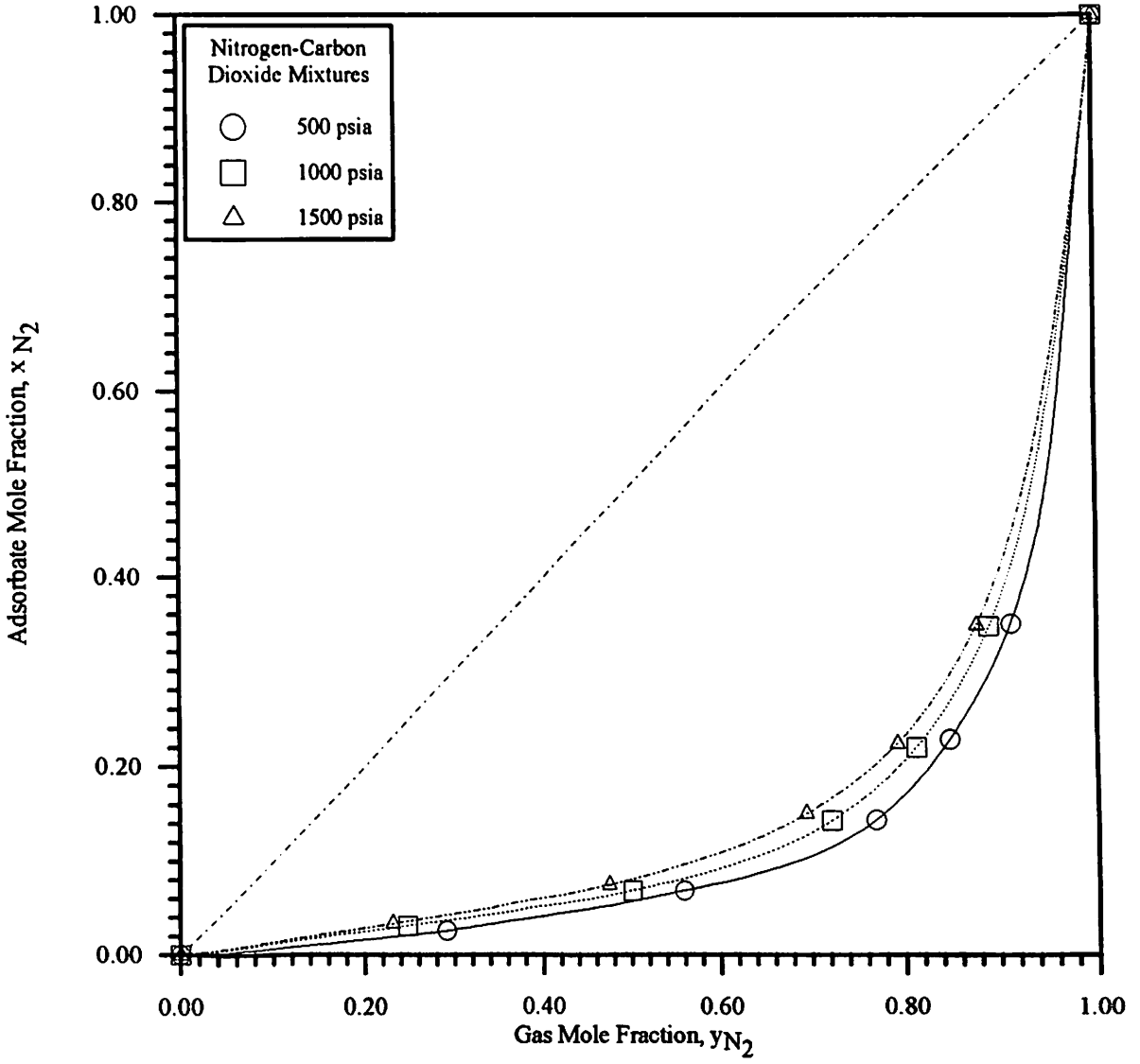

Figure 30. Phase Compositions for Adsorption of Nitrogen-Carbon Dioxide Mixtures on Wet Fruitland Coal

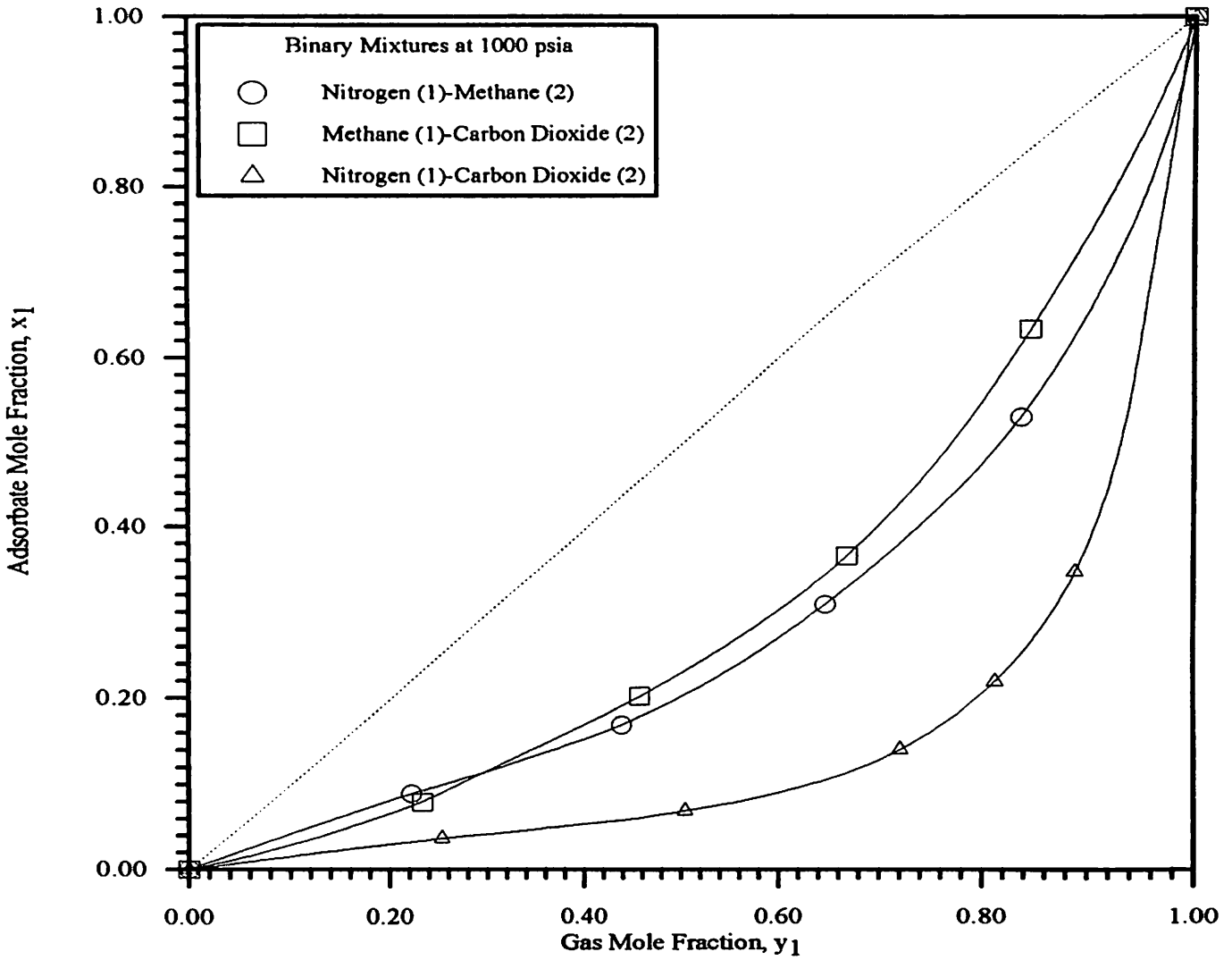

Figure 31. Phase Compositions for Adsorption of Binary Mixtures on Wet Fruitland Coal at 1,000 psia

compositions where more of the methane is displaced. The greatest competition comes from the nitrogen/carbon dioxide mixture as indicated by significantly larger deviations. Small amounts of carbon dioxide added to the mixture displace significantly more of the nitrogen from the surface. This behavior was anticipated since the pure nitrogen and pure carbon dioxide sorption capacity differed by four fold (refer to Figure 9).

In looking at Figure 31, nitrogen does a much less adequate job of displacing methane from the coal surface than does carbon dioxide. Small amounts of carbon dioxide displace considerably larger amounts of methane than the nitrogen. A mixture of nitrogen and carbon dioxide (high in carbon dioxide composition) may prove to be economically better than injecting pure carbon dioxide.

Figure 32 shows the amount of methane adsorbed as a function of the composition of the injected gas in the equilibrium gas phase for nitrogen and carbon dioxide at three pressures (500, 1000, and 1800 psia). This illustrates the relative displacement efficiency of carbon dioxide and nitrogen. At each isobar, the amount of methane adsorbed on the coal surface is lower for carbon dioxide than nitrogen, meaning that more of the methane is being displaced from the coal surface (remaining in the gas phase).

Previous Experimental Data

Figures 33 through 49 compare the current work with experimental data collected by Amoco Production Company [4]. The Amoco data was re-processed with the software developed for the current work, yielding a direct heads-up comparison. That is, any differences in auxiliary input information (e.g., compressibility factors, adsorbed phase density) are removed from the comparisons. After re-processing the Amoco data, the pure components showed differences from Amoco's original data analysis of less than one percent, while the mixture deviations (low and mid range

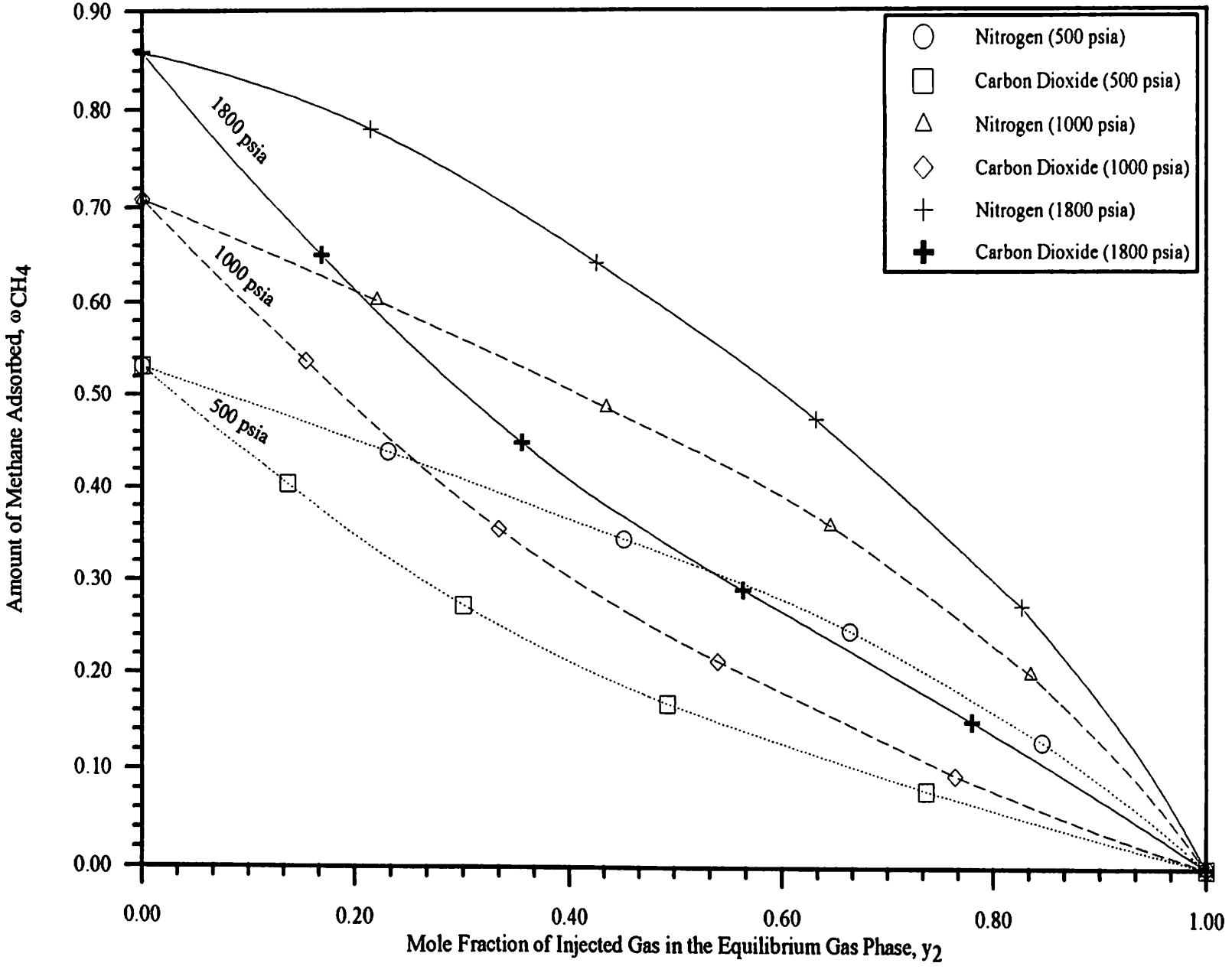

Figure 32. Displacement Efficiency of Carbon Dioxide and Nitrogen

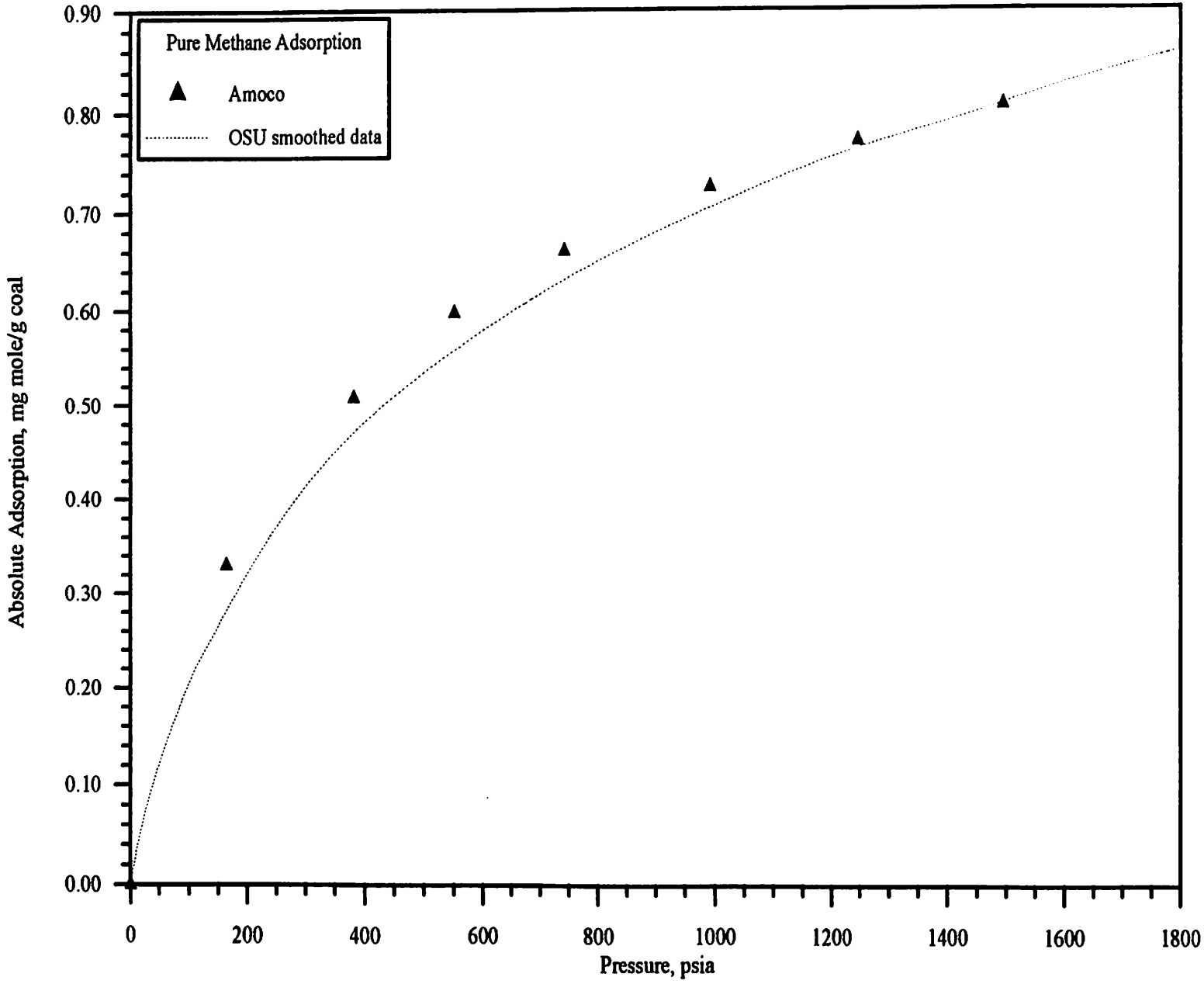

Figure 33. Comparison of Pure Methane Adsorption Data from OSU and Amoco

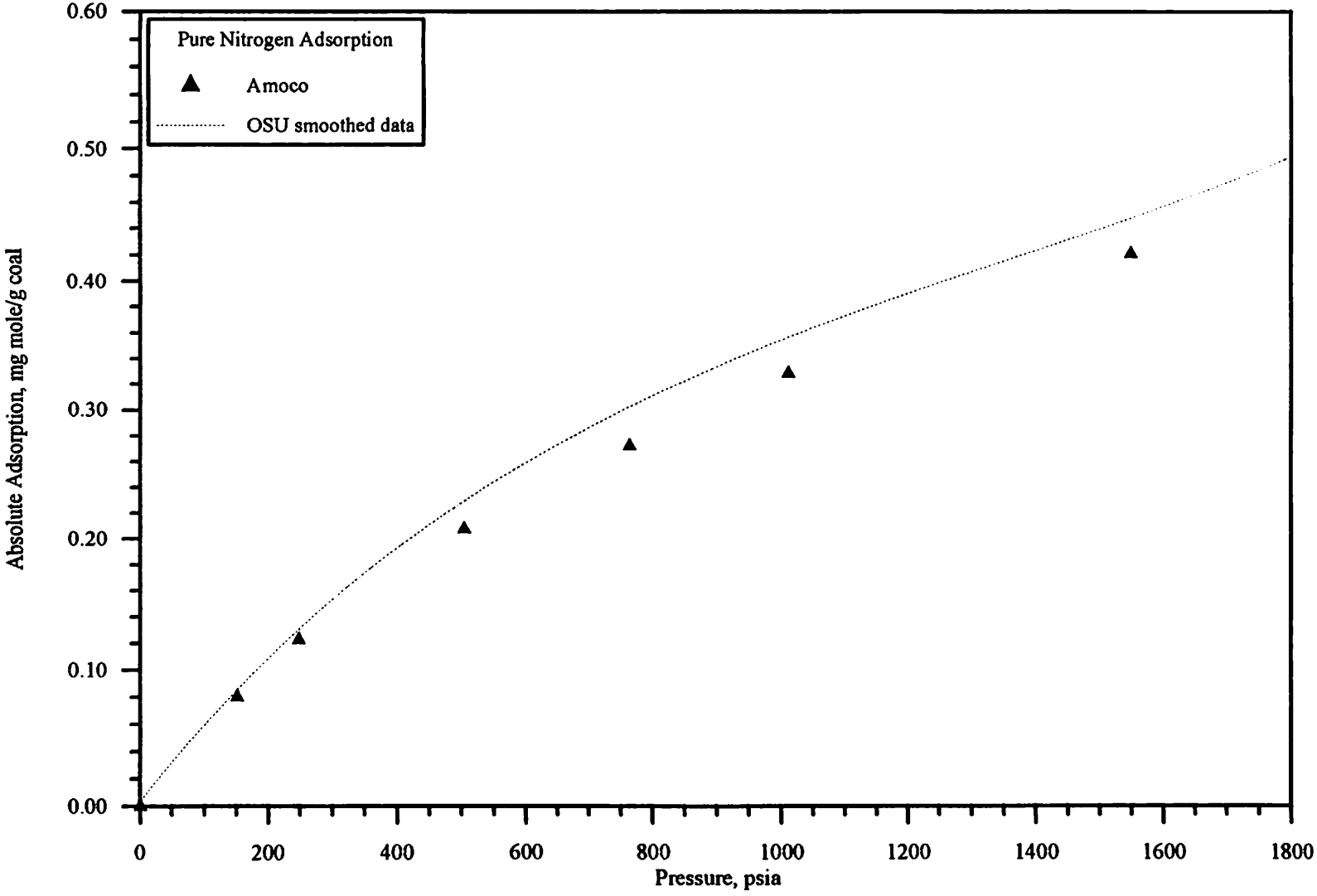

Figure 34. Comparison of Pure Nitrogen Adsorption Data from OSU and Amoco

pressures) ranged from one to two percent, with a maximum of six percent occurring at higher pressures (within experimental uncertainty). The Amoco data are represented as solid, bold symbols with the dashed lines representing the smoothed data of the current work.

Figure 33 illustrates pure methane adsorption. The current work differs from the Amoco data by a maximum of twelve percent at low pressures, while agreeing within one percent at high pressures. For nitrogen (Figure 34), the current work differs slightly (within one percent) from that measured by Amoco at low pressures, while differences at higher pressures approach six percent. Carbon dioxide adsorption is shown in Figure 35. The current work and that of Amoco differ by less than one percent to 600 psia, while higher pressures (800 psia) differ by two percent.

Methane/nitrogen mixtures data are compared in Figures 36 through 49. Amoco performed measurements for 12/88, 14/86, 19/81, 20/80 and 80/20 mixtures. Figure 36 illustrates the total adsorption as a function of pressure. The 20/80 mixture of the current work differs from that of Amoco by ten percent, while the 80/20 mixtures are in good agreement (three percent). The Amoco 19/81 mixture is very consistent with the 20/80 mixture of the current work. The Amoco 14/86 mixture shows adsorption of as much or more (at higher pressures) than the 19/81 mixture (which raises questions regarding the Amoco data).

Figure 37 illustrates the methane adsorption as a function of pressure. At 20/80, the data differ by as much as eight percent, at 80/20, differences are less than nine percent. The Amoco 19/81 mixture data fall almost exactly on the 20/80 mixture of the current work.

For nitrogen adsorption as a function of pressure (Figure 38), the 20/80 (20% CH_4) data are consistent with Amoco, while the 80/20 (80% CH_4) mixtures differs by as much as forty percent. Amoco's 12/88, 14/86, 19/81 and 20/80 mixture data may be suspect, since the data show the lower nitrogen compositions adsorbing more

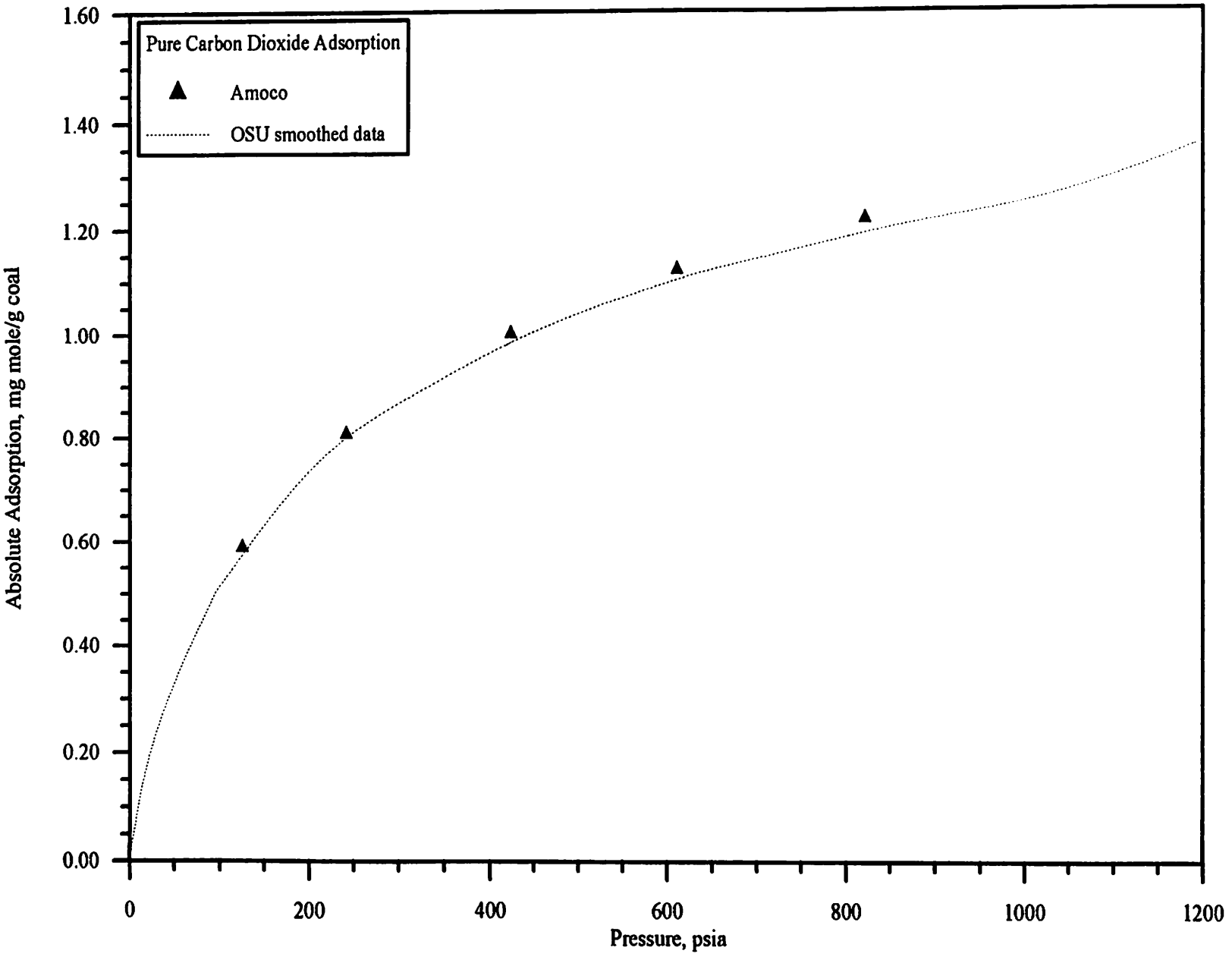

Figure 35. Comparison of Pure Carbon Dioxide Adsorption Data from OSU and Amoco

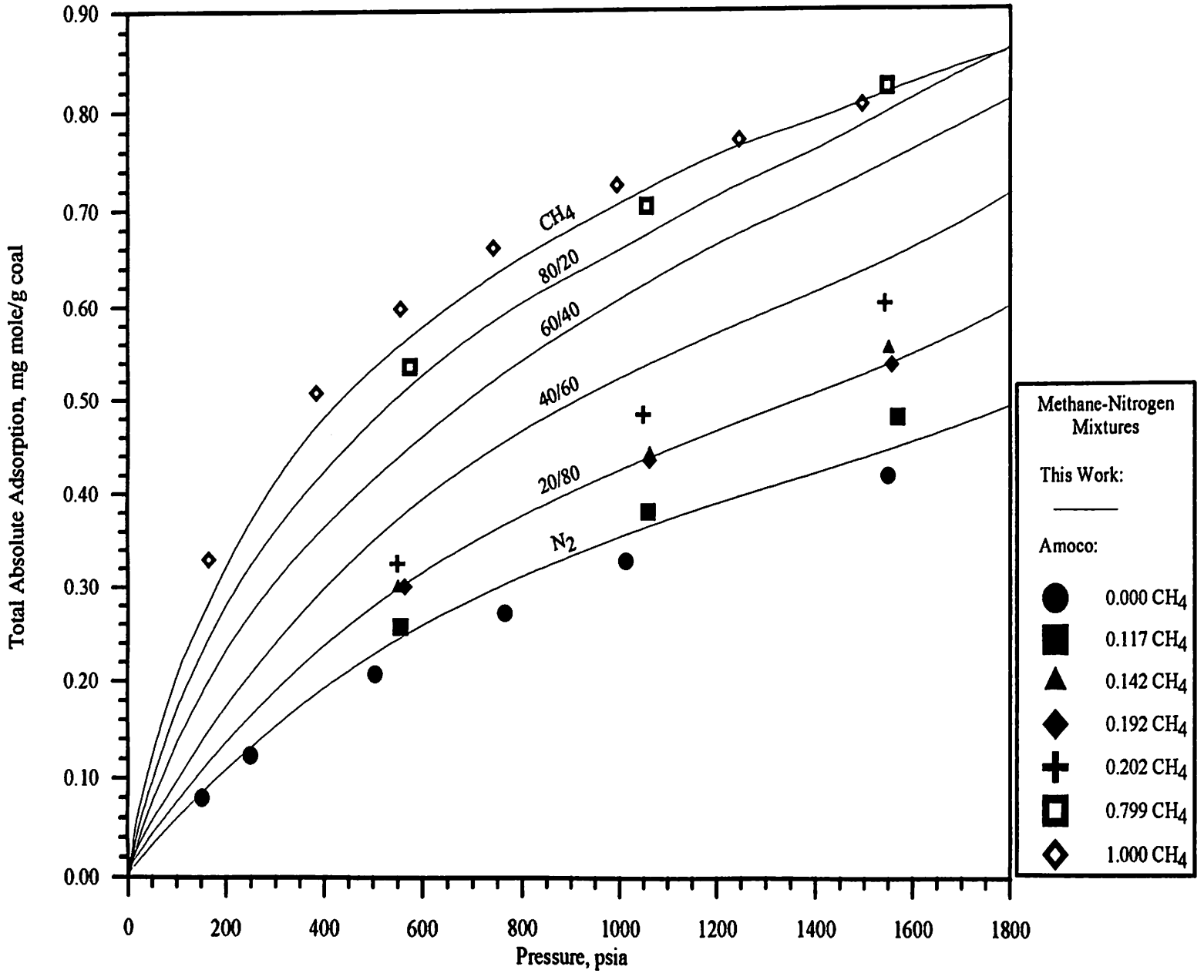

Figure 36. Comparison of Total Absolute Adsorption Data for Methane-Nitrogen Mixtures from OSU and Amoco

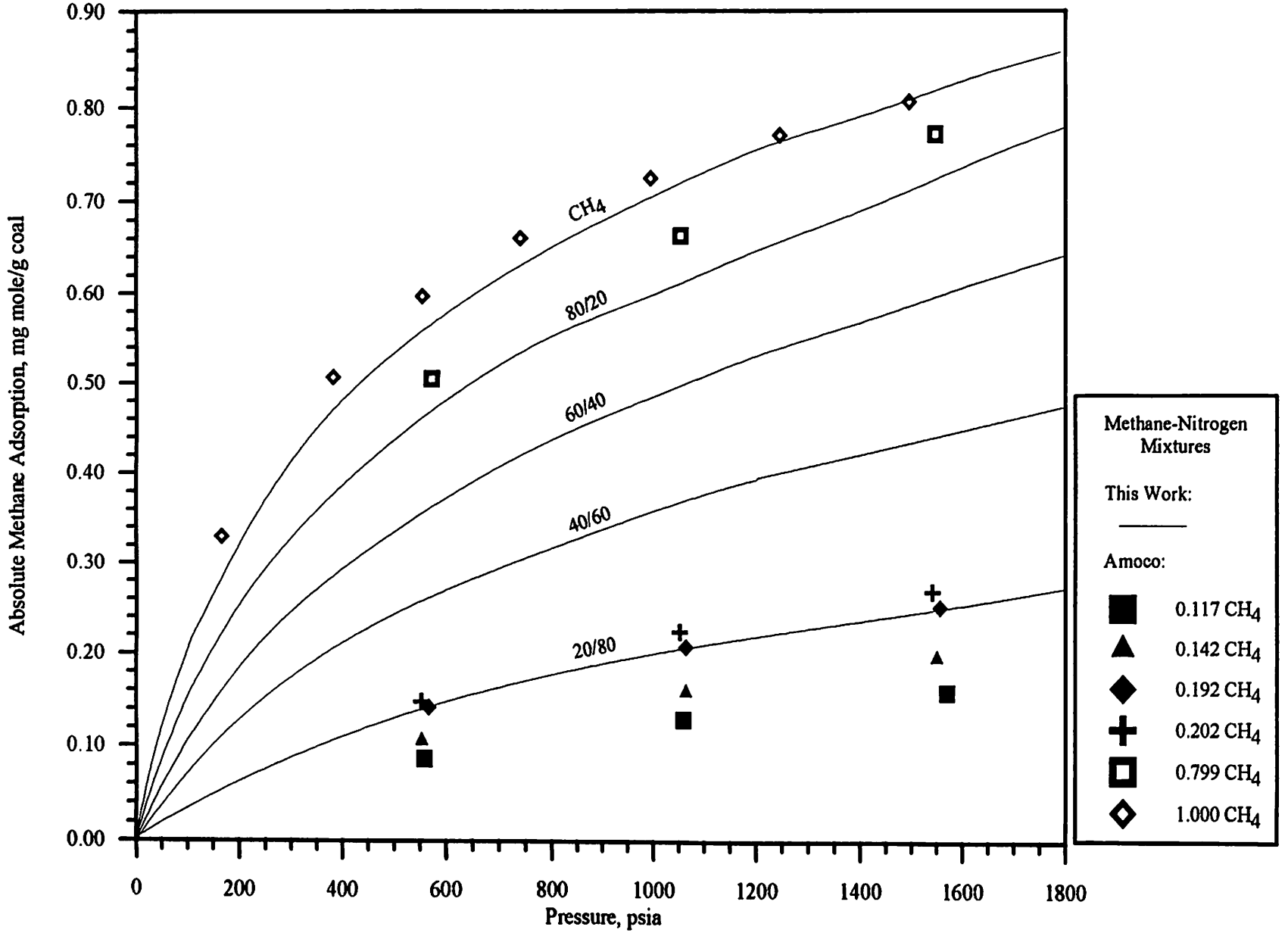

Figure 37. Comparison of Methane Adsorption Data from Methane-Nitrogen Mixtures from OSU and Amoco

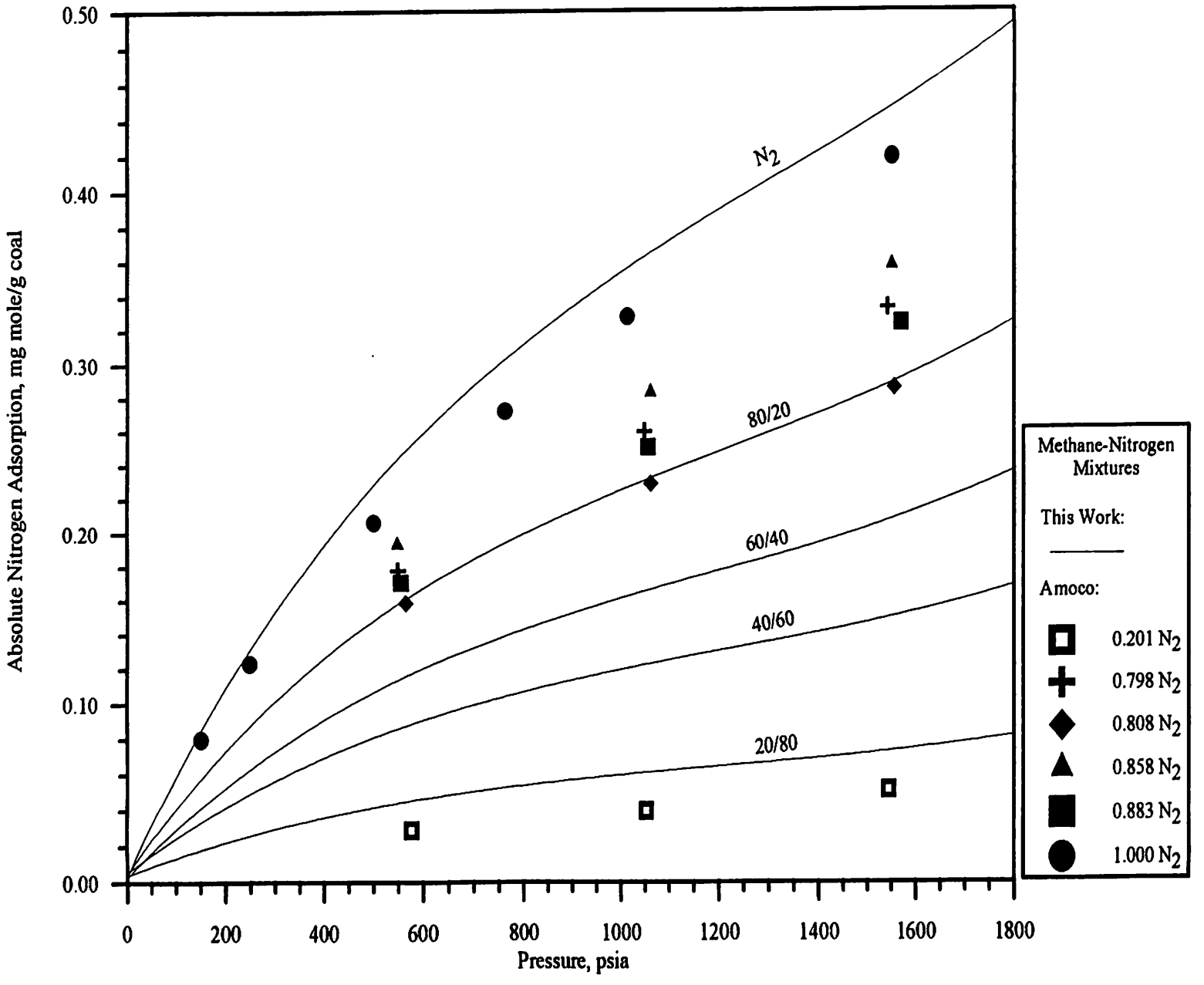

Figure 38. Comparison of Nitrogen Adsorption Data from Methane-Nitrogen Mixtures from OSU and Amoco

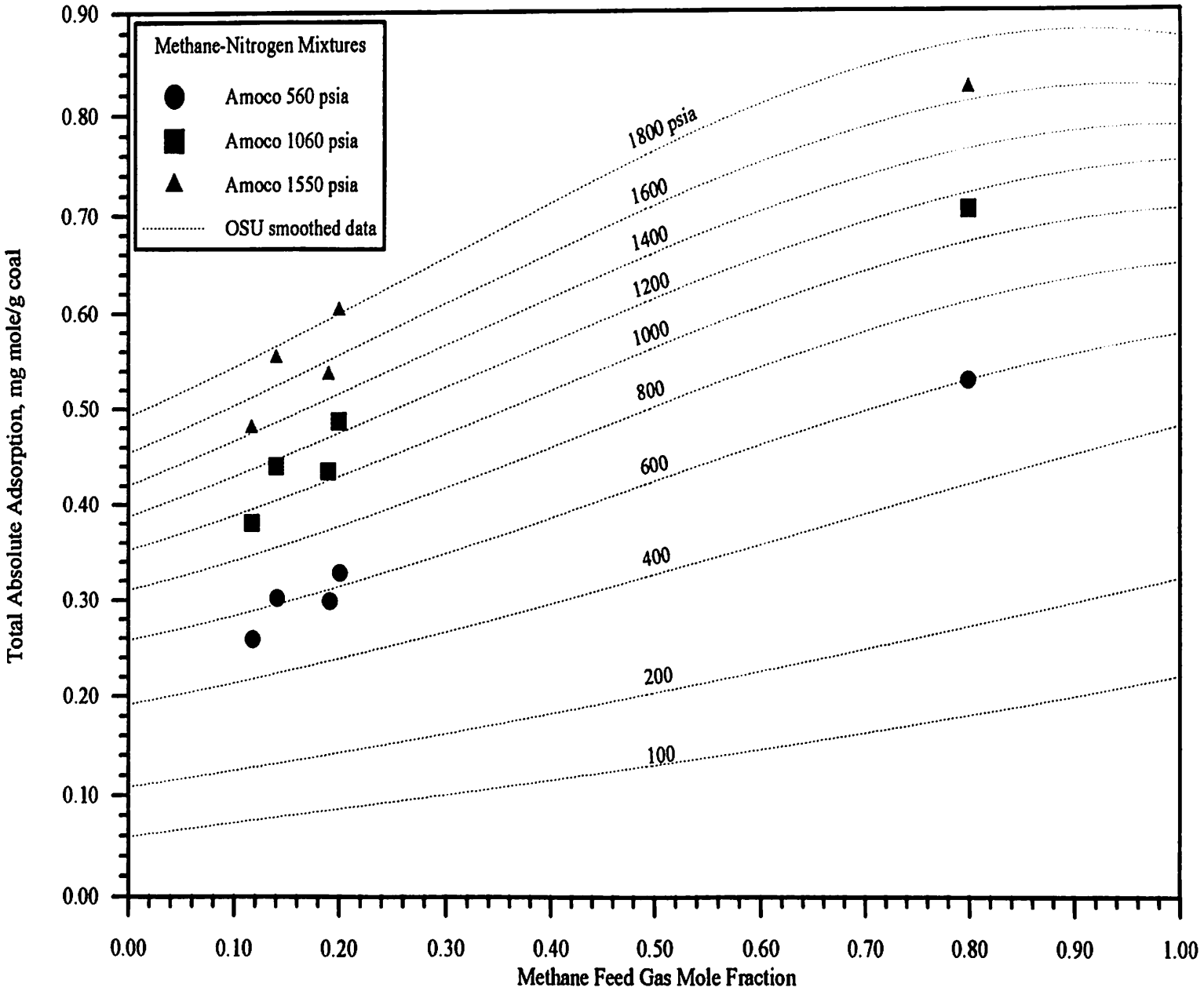

Figure 39. Comparison of Total Adsorption Data from Methane-Nitrogen Mixtures from OSU and Amoco

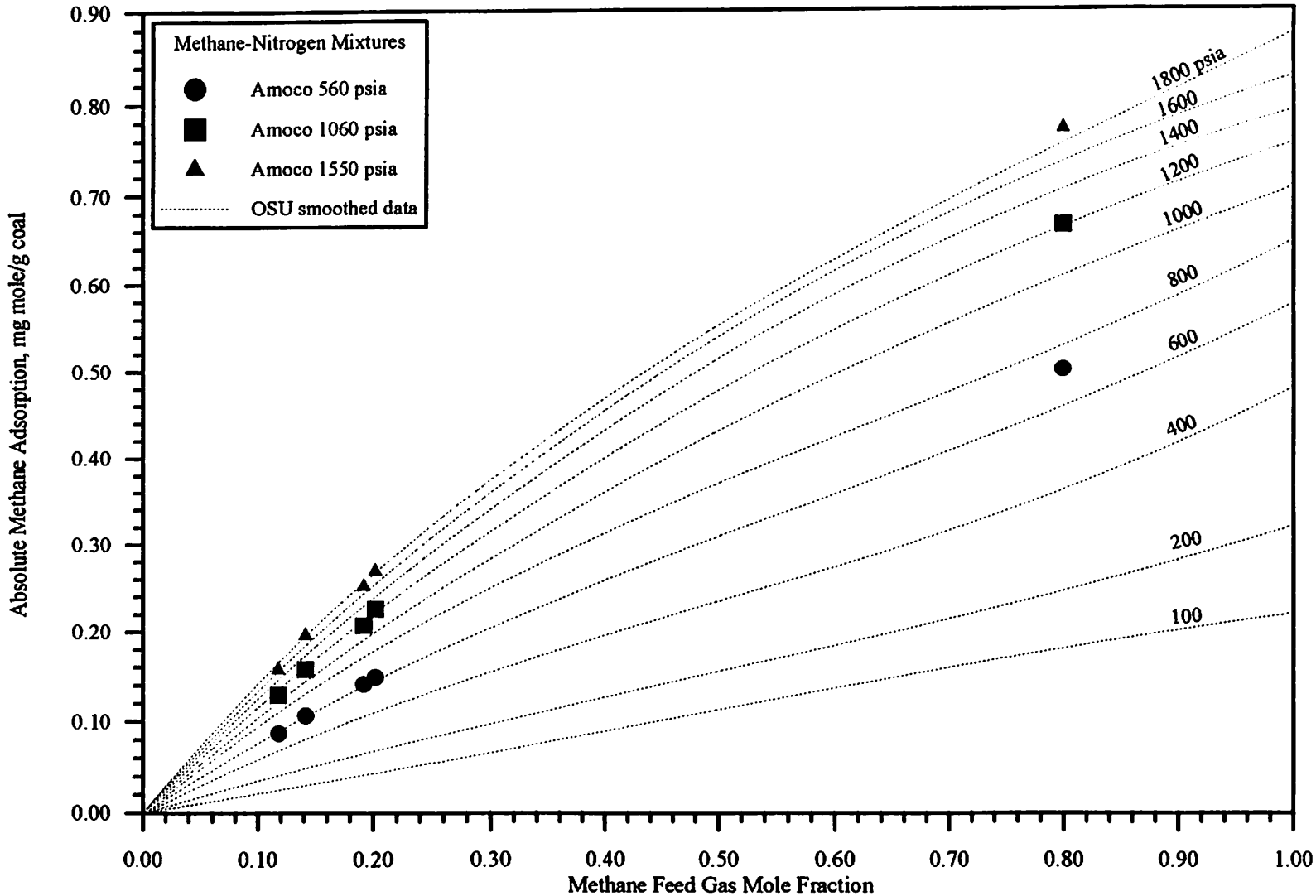

Figure 40. Comparison of Methane Adsorption Data from Methane-Nitrogen Mixtures from OSU and Amoco

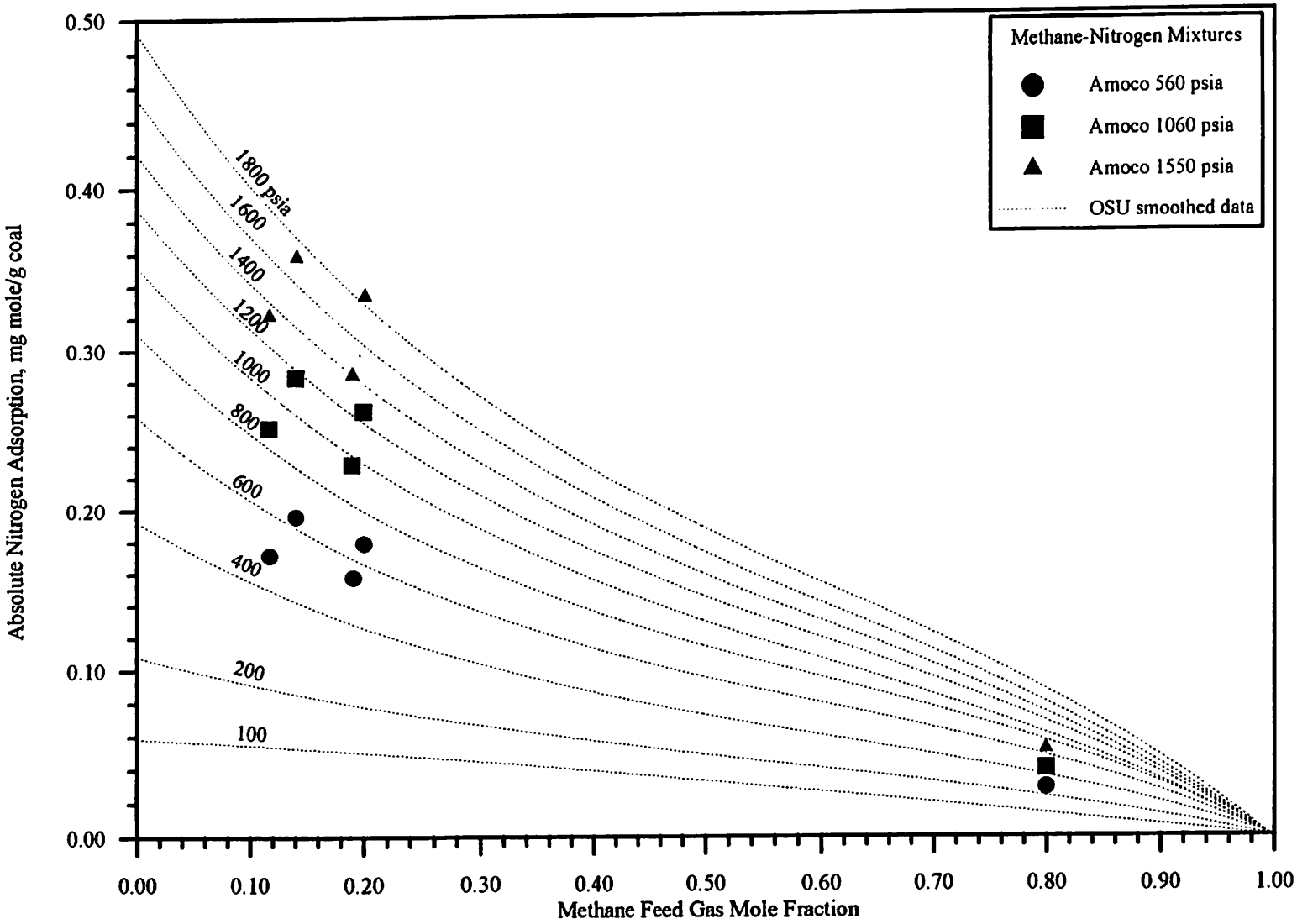

Figure 41. Comparison of Nitrogen Adsorption Data from Methane-Nitrogen Mixtures from OSU and Amoco

than the higher compositions. This verifies the trend seen in Figure 36 with the 14/86 mixture.

The Amoco methane/nitrogen mixtures in Figures 39 through 41, show the amount adsorbed (total and individual adsorption) as a function of the methane feed gas composition. The Amoco data are at pressures of around 560, 1060 and 1550 psia. The low and medium pressure data are in qualitative agreement with the current work. The high pressure points differ by as much as 300 psia from the current work. The low methane composition data points exhibit "oscillatory" behavior in some instances (Figures 39 and 41).

The methane adsorption as a function of methane mole fraction is shown in Figure 40. The Amoco data appear smoother here than in Figure 39, but all data points are shifted to higher pressures (as much as 300 psia) from the present data. Nitrogen adsorption in Figure 41 is in disagreement with the current work. The trend, as seen with other isobars, is again apparent with the nitrogen adsorption data fluctuating at low methane feed gas mole fractions.

Figure 42 shows the adsorbate mole fraction as a function of feed gas mole fraction for the methane/nitrogen mixtures at 1000 psia. The two Amoco data sets are very consistent at high methane compositions, while showing a significant difference at the lower methane composition.

Methane/carbon dioxide mixture data are compared Figures 43 through 49. Amoco performed measurements for compositions of 48/52 and 92/8. Figure 43 illustrates the total adsorption as a function of pressure. The 48/52 Amoco mixture data are consistent with current work at low pressures, with larger differences occurring at high pressures. The 92/8 mixture data differs significantly throughout the pressure range.

Figure 44 illustrates methane adsorption as a function of pressure. The 48/52 mixture data are consistent with the current work. The 92/8 mixture of

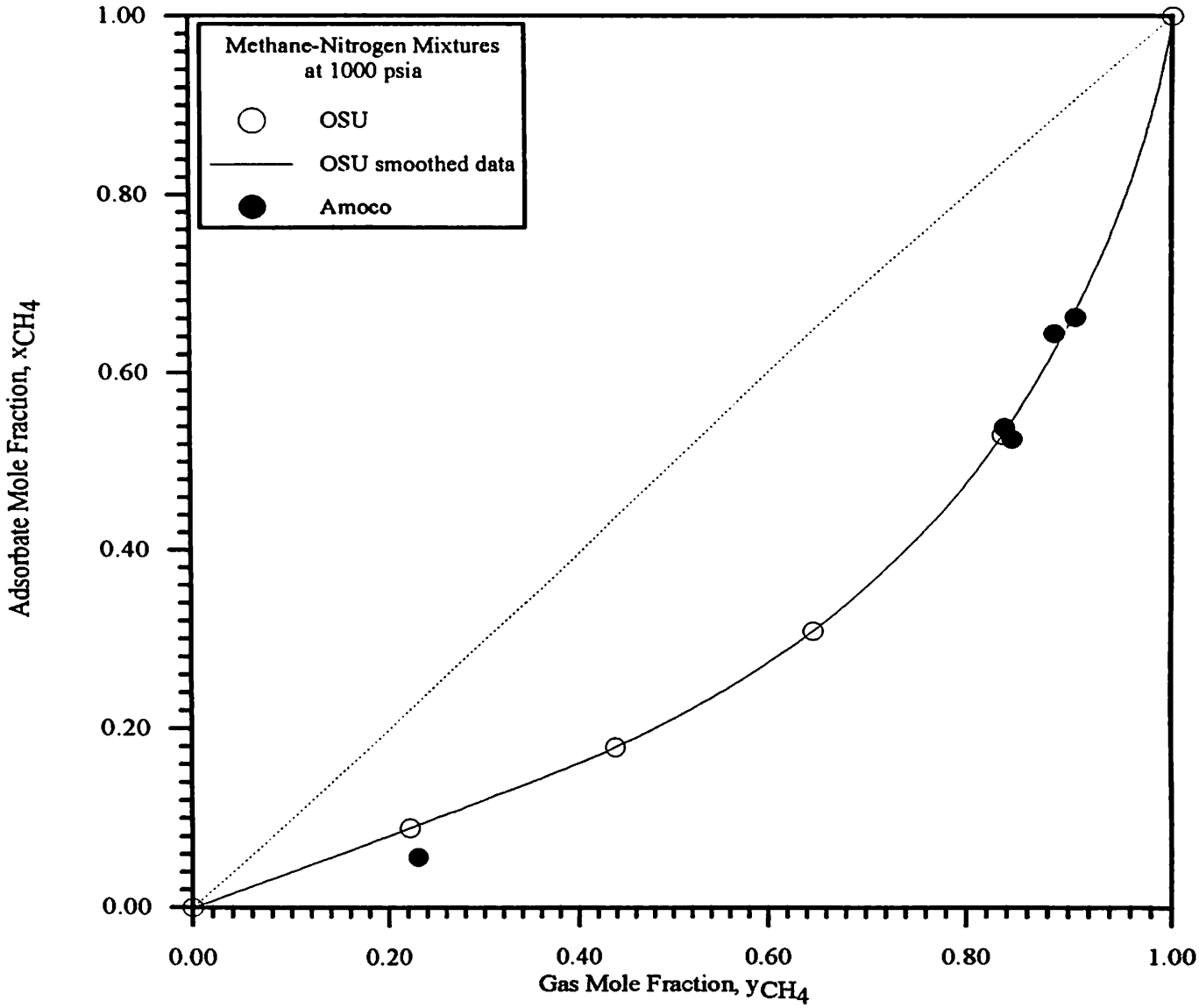

Figure 42. Comparison of Adsorption Data from Methane-Nitrogen Mixtures from OSU and Amoco

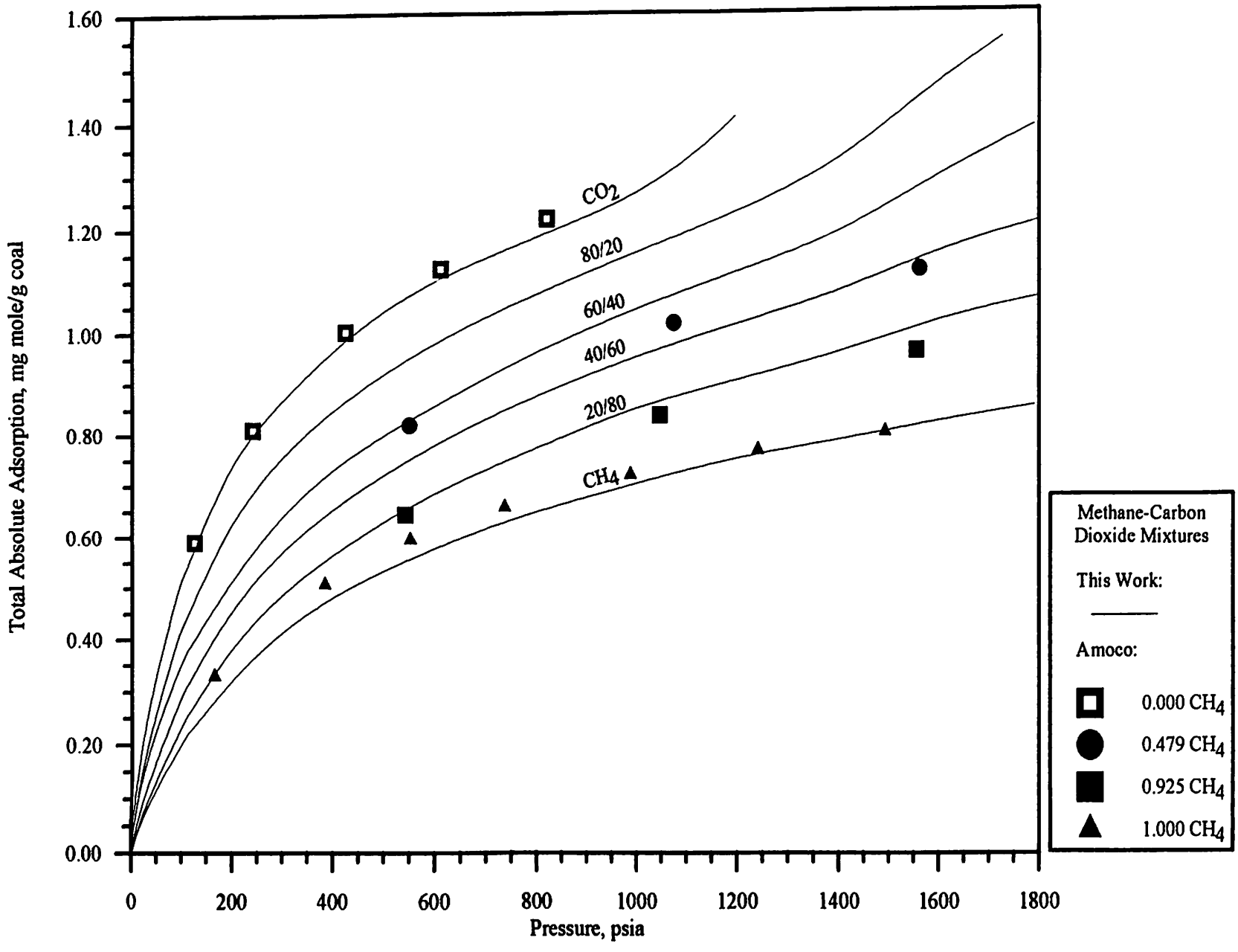

Figure 43. Comparison of Total Adsorption Data from Methane-Carbon Dioxide Mixtures from OSU and Amoco

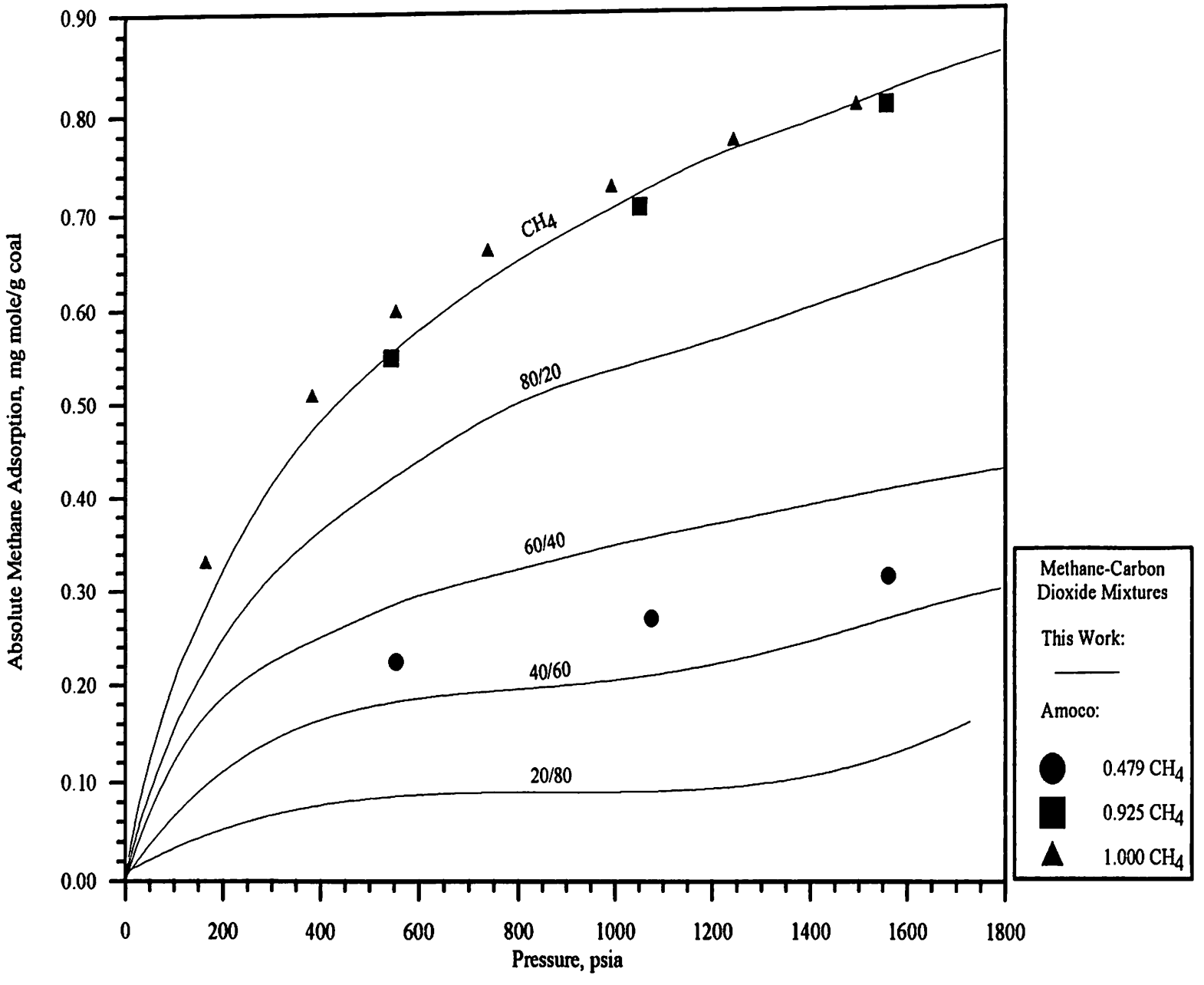

Figure 44. Comparison of Methane Adsorption Data from Methane-Carbon Dioxide Mixtures from OSU and Amoco

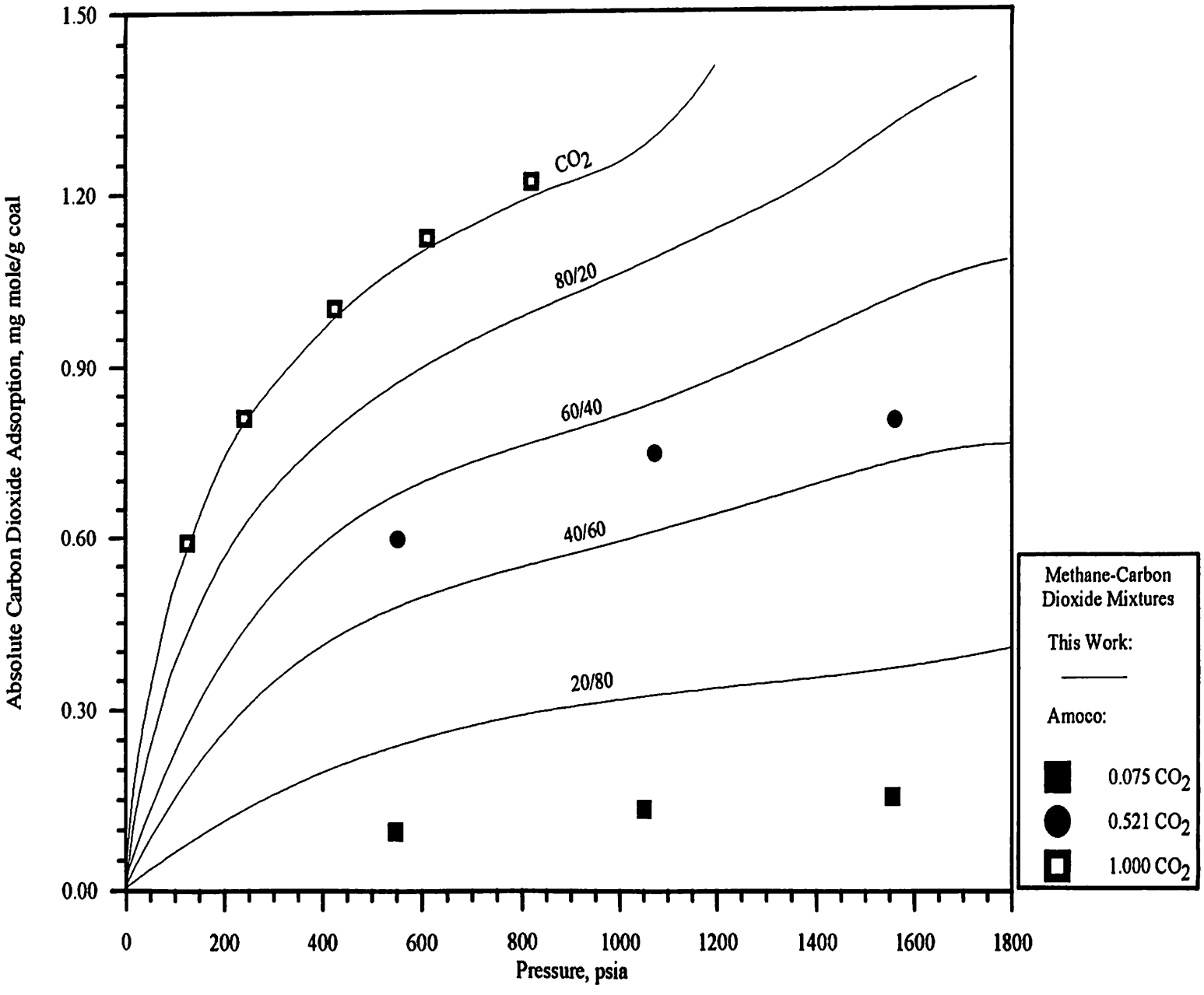

Figure 45. Comparison of Carbon Dioxide Adsorption Data from Methane-Carbon Dioxide Mixtures from OSU and Amoco

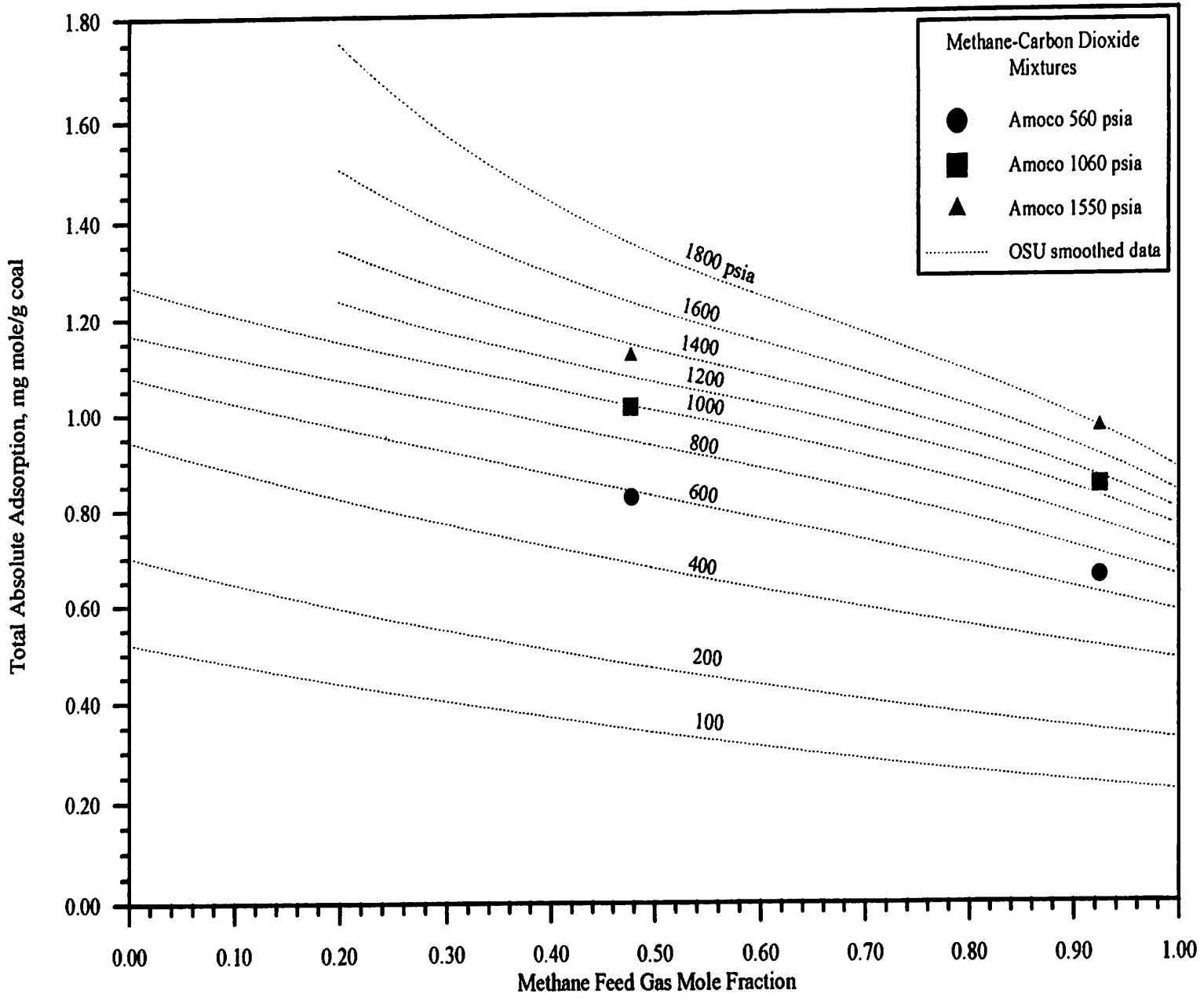

Figure 46. Comparison of Total Adsorption Data from Methane-Carbon Dioxide Mixtures from OSU and Amoco

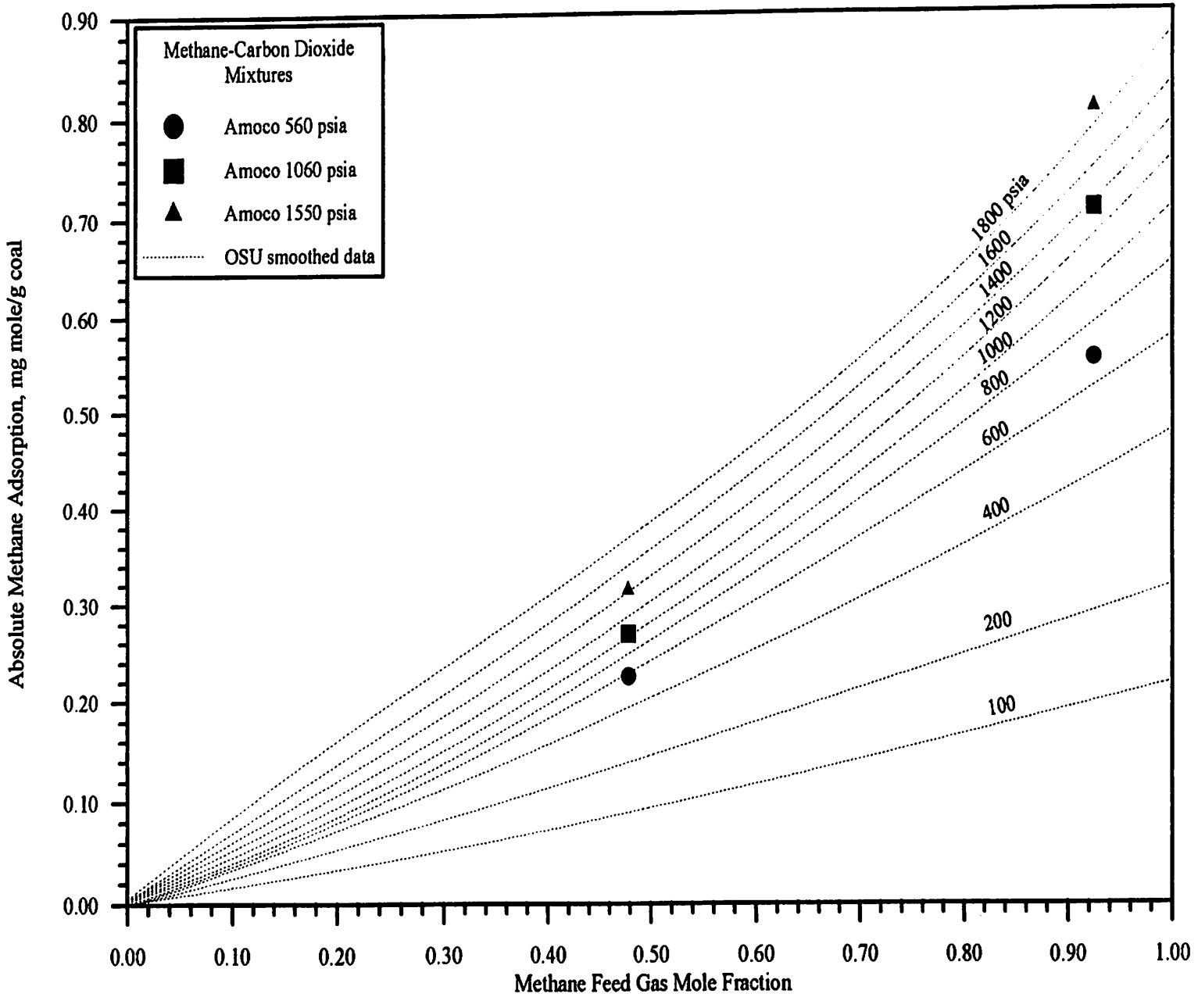

Figure 47. Comparison of Methane Adsorption Data from Methane-Carbon Dioxide Mixtures from OSU and Amoco

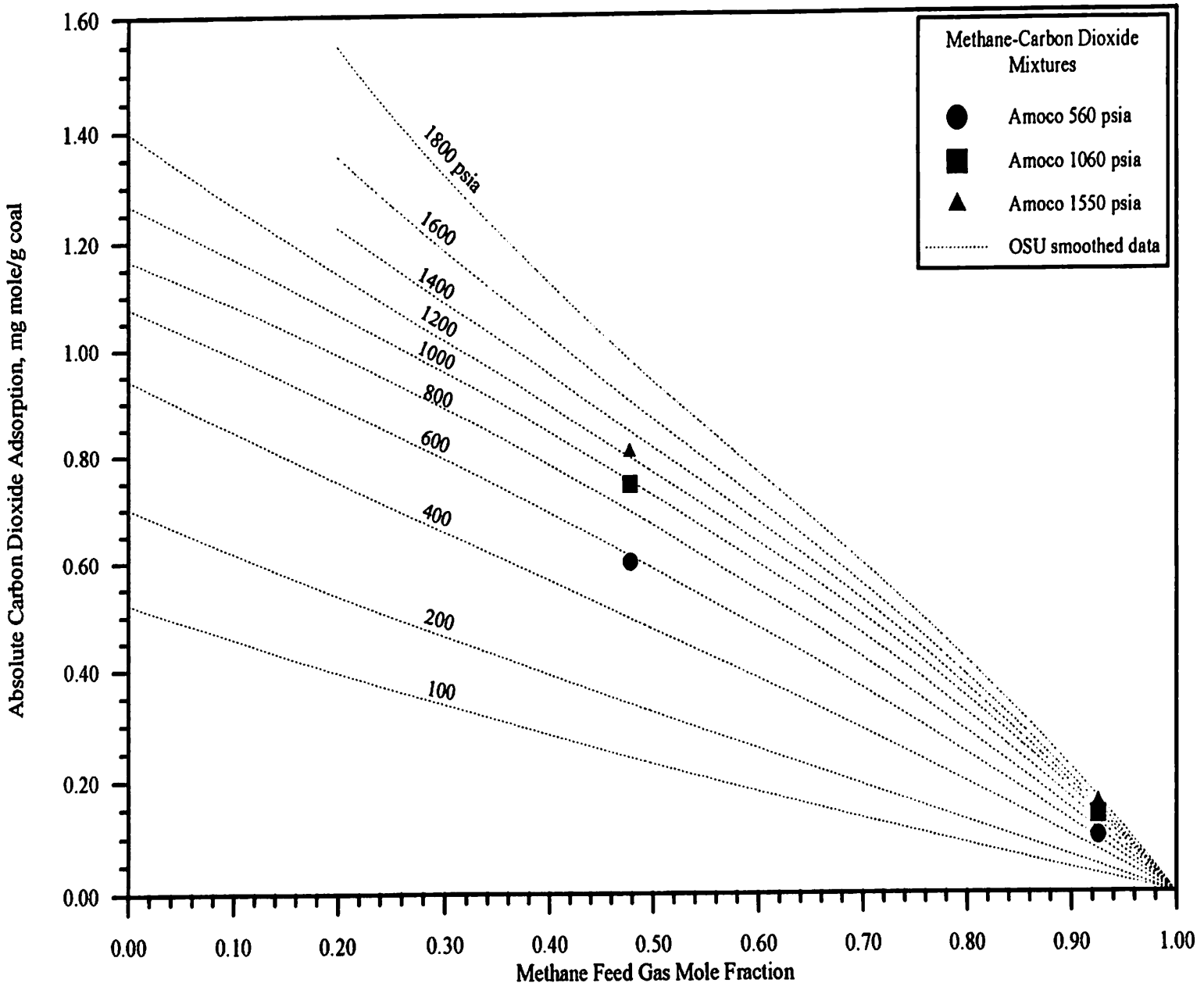

Figure 48. Comparison of Carbon Dioxide Adsorption Data from Methane-Carbon Dioxide Mixtures from OSU and Amoco

Amoco is suspect because the adsorption curve extends over the pure methane isotherm, suggesting that more adsorption is occurring with a 92/8 mixture than with pure methane. For carbon dioxide adsorption as a function of pressure (Figure 45), the two studies (8/92 and 52/48 mixtures) agree well.

Absolute adsorption (total and individual adsorption) as a function of methane feed gas composition are shown in Figures 46 through 48. For the total adsorption (Figure 46), the two data sets are offset by as much as 300 psia at both compositions. For methane adsorption, the Amoco studies are similar to current work but differ by up to 300 psia. For carbon dioxide adsorption (Figure 48), the values are less by up to 300 psia.

Figure 49 shows the adsorbate composition as a function of feed gas mole fraction. Amoco data are in good agreement with the current work with both compositions falling on top of the smoothed data line.

Adsorption Results on an Organic Coal Basis

In addition to organic material, all coals contain inorganic constituents which are commonly referred to as mineral matter [27]. The mineral matter acts as an inert diluent with respect to gas adsorption [27]. This means that the mineral matter does not contribute to gas adsorption, but instead the gas adsorption takes place on the organic material, with the mineral matter causing a reduction in the gas content. This illustrates the importance of coal purity in determining the adsorption capacity. The gas content will be greater for coals with lower mineral matter content.

A quantitative measure of the mineral matter content can be obtained from the proximate analysis using the Parr expression [27]. A detailed discussion appears in Appendix E describing the Parr equation and how the organic coal content is determined. The mineral matter content of the current work was determined to be 75.7 percent, as compared to 82.0 percent for Amoco (see calculations in Appendix

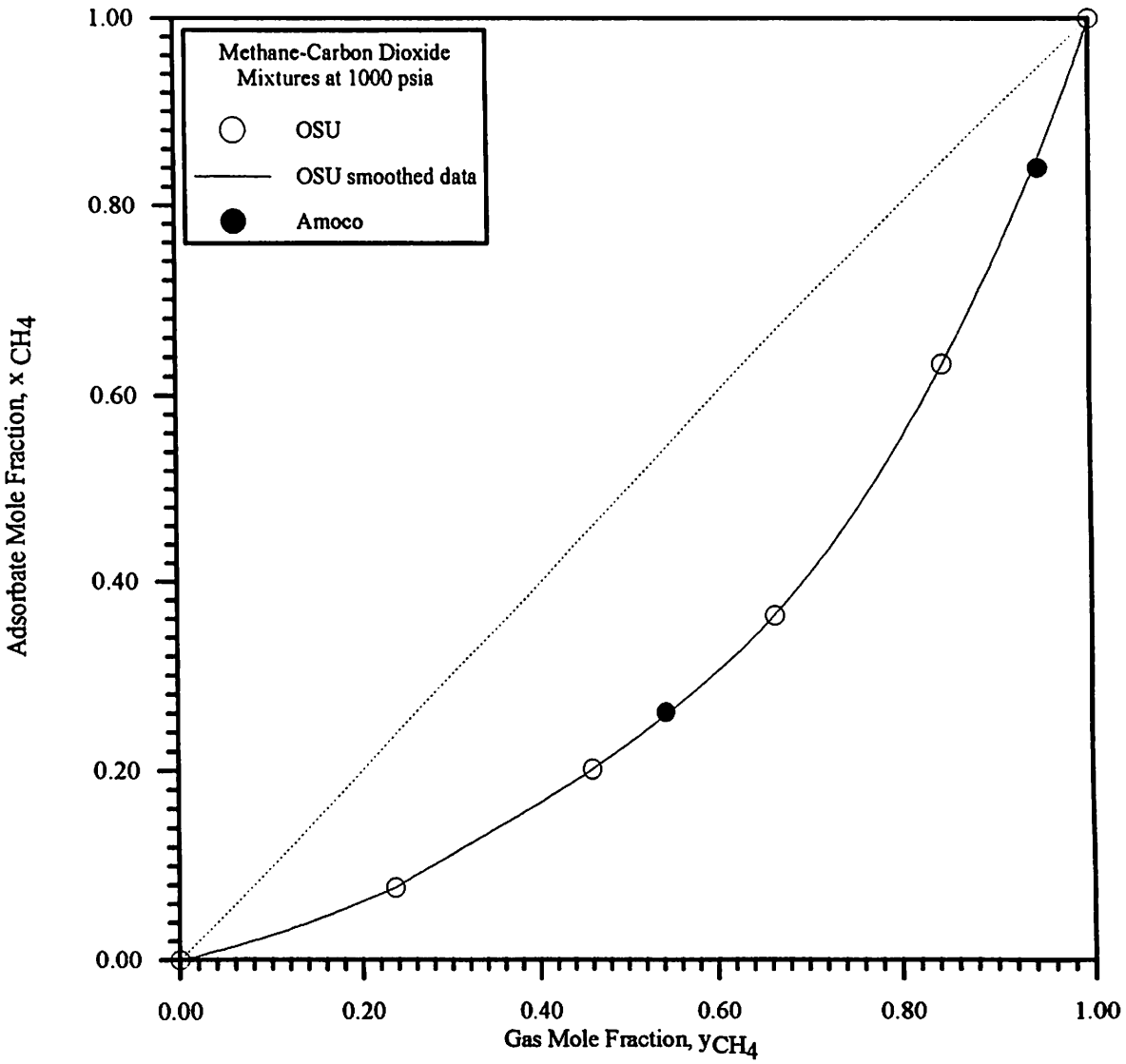

Figure 49. Comparison of Adsorption Data from Methane-Carbon Dioxide Mixtures from OSU and Amoco

E). The adsorption results are expressed relative to a unit mass of organic coal.

If adsorption is expressed on an organic coal basis, the values of ω will increase in magnitude. Amoco data will increase to a lesser extent than the OSU values. Figures illustrating the amount adsorbed on an organic coal basis are located in Appendix E (Figures 85-99).

For pure methane (Figure 85), the differences between the current work and Amoco increase from five percent at low pressures to ten percent at high pressures. The nitrogen (Figure 86) data differ from Amoco by 13 percent (low-to-high pressures). Carbon dioxide differs by six-to-seven percent through 1200 psia.

Figure 88 illustrates total adsorption for methane-nitrogen mixtures. The 80/20 mixture differ by six percent at higher pressures. The 20/80 isotherm differs from Amoco by less than nine percent. The methane adsorption data (20/80 and 80/20) in Figure 89 are very consistent with Amoco data. Nitrogen adsorption data (Figure 90) are inconsistent with Amoco differing by thirty percent (20/80) and ten percent (80/20), respectively. The low methane composition isotherms of Amoco (Figure 91) continue to exhibit the oscillatory behavior previously mentioned. The high methane composition isotherm (80/20) are below the current work by as much as 150 psia (as seen in Figures 91, 92, and 93).

Figure 94 show methane-carbon dioxide adsorption for the current work and Amoco. The 48/52 (Amoco) isotherm is inconsistent with the current work. The 92/8 mixture is consistent with current work. Figure 95 illustrates methane adsorption. Both Amoco mixtures are consistent with current work. The carbon dioxide adsorption data (Figure 96) are in agreement with the current work for both mixtures. Figure 97 shows the total adsorption as a function of methane feed gas composition. The high methane composition mixture (92/8) is consistent with the current work. The 48/52 mixture differs by as much as 300 psia. The same is true for methane and carbon dioxide adsorption in Figure 98 and 99 (92/8 isotherm in

good agreement, 48/52 isotherm inconsistent with current work).

Discussion

Pure methane and nitrogen illustrate Type I monolayer adsorption throughout the current work with all replicate experimental data falling within the experimental uncertainty. Carbon Dioxide shows Type I adsorption through 1200 psia, with multimolecular adsorption (Type II) occurring at higher pressures.

For methane/nitrogen mixture adsorption, the mixtures are very consistent and fall uniformly between the pure nitrogen and methane limits. The 80/20 mixture approaches the pure methane isotherm indicating that competition is occurring between components. The competitive idea is confirmed by looking at Figure 15. The rapid drop in nitrogen adsorption with small amounts of injected methane confirm that the methane is being preferentially adsorbed with respect to nitrogen.

For methane/carbon dioxide mixture adsorption, the trends are similar as seen with the methane/nitrogen mixture. The competition between components is confirmed by Figure 21 where the carbon dioxide is preferentially adsorbed over the methane.

In nitrogen/carbon dioxide mixture adsorption, the trends are as described above with the carbon dioxide molecules being preferentially adsorbed with respect to the nitrogen (as seen in Figure 28).

Figure 32 best illustrates the conclusion by showing the displacement efficiency of carbon dioxide and nitrogen for removing methane from the coal surface. At all three pressures (500, 1000 and 1800 psia), carbon dioxide does a better job than nitrogen of displacing methane from the surface. For carbon dioxide, less methane is adsorbed to the coal surface with more remaining in the gas phase (displaced from the surface). While nitrogen efficiently removes methane from the

coal surface, the carbon dioxide molecules are preferentially adsorbed appearing to do a better job of displacing methane.

In comparing OSU and Amoco pure component adsorption data, the pure methane data agree, with the largest differences occurring at mid-range pressures. Nitrogen comparisons show small differences at low pressures propagating into larger differences at higher pressures. The carbon dioxide data sets are very consistent with differences being within the experimental uncertainty.

For mixture comparisons, the methane/nitrogen mixtures are very consistent with the 20/80 mixture (as seen in Figures 37 and 38). There is disagreement with the remaining methane/nitrogen mixtures. The Amoco data are suspect because of the "oscillatory" behavior of the low methane composition mixtures (Figure 38). For methane/carbon dioxide mixtures, the 48/52 mixture agrees with current work (Figure 44 and 45). The 92/8 mixture is in disagreement with the current work and is suspect because the mixture is shown to adsorb more than the pure component (Figure 44).

In expressing the adsorption on an organic coal basis, the pure components were significantly worse. The mixtures showed slight improvements. The figures which showed the greatest improvement were those as a function of feed gas composition. The isobars of the current work were in closer agreement with Amoco than when plotted as a function of organic and inorganic (neglecting mineral matter content) coal.

TABLE I

ADSORPTION OF METHANE (OSU16) ON WET FRUITLAND COAL AT 115 °F

Pressure, psia	Absolute Adsorption, mg mole/g coal
95.4	0.193
203.0	0.318
401.1	0.477
604.4	0.584
802.6	0.658
1002.0	0.711
1201.4	0.762
1401.8	0.799
1598.3	0.838
1798.9	0.869

TABLE II

ADSORPTION OF METHANE (OSU23) ON WET FRUITLAND COAL AT 115 °F

Pressure, psia	Absolute Adsorption, mg mole/g coal
110.5	0.219
207.1	0.328
390.5	0.476
618.6	0.586
807.9	0.654
1004.3	0.709
1208.6	0.758
1402.9	0.792
1599.3	0.828
1790.7	0.858

TABLE III

ADSORPTION OF NITROGEN (OSU17) ON WET FRUITLAND COAL AT 115 °F

Pressure, psia	Absolute Adsorption, mg mole/g coal
115.5	0.0688
207.7	0.111
405.1	0.190
601.2	0.256
801.2	0.309
1000.4	0.358
1199.6	0.399
1400.0	0.439
1599.1	0.475
1795.4	0.506

TABLE IV

ADSORPTION OF NITROGEN (OSU19) ON WET FRUITLAND COAL AT 115 °F

Pressure, psia	Absolute Adsorption, mg mole/g coal
116.7	0.0692
218.3	0.122
404.7	0.197
604.9	0.257
808.7	0.313
1001.8	0.352
1201.2	0.390
1402.3	0.425
1600.0	0.461
1798.7	0.490

TABLE V

ADSORPTION OF NITROGEN (OSU20) ON WET FRUITLAND COAL AT 115 °F

Pressure, psia	Absolute Adsorption, mg mole/g coal
124.0	0.0768
211.0	0.115
404.2	0.190
622.5	0.255
808.3	0.298
1006.6	0.345
1204.4	0.384
1399.5	0.416
1606.4	0.453
1795.8	0.481

TABLE VI

ADSORPTION OF CARBON DIOXIDE (OSU24) ON WET FRUITLAND COAL AT 115 °F

Pressure, psia	Absolute Adsorption, mg mole/g coal
91.7	0.482
211.2	0.781
404.3	0.984
616.8	1.12
800.2	1.21
1008.6	1.30
1193.1	1.36
1375.7	1.73
1592.1	4.62
1751.8	4.97

TABLE VII

ADSORPTION OF CARBON DIOXIDE (OSU25)
ON WET FRUITLAND COAL AT 115 °F

Pressure, psia	Absolute Adsorption, mg mole/g coal
101.7	0.512
208.9	0.731
326.5	0.868
425.1	0.948
522.5	1.02
630.4	1.08
733.5	1.13
814.8	1.16
911.6	1.21
1063.6	1.29
1205.3	1.31
1371.5	1.68
1529.5	4.33
1691.5	5.35

TABLE VIII

ADSORPTION OF CARBON DIOXIDE (OSU26)
ON WET FRUITLAND COAL AT 115 °F

Pressure, psia	Absolute Adsorption, mg mole/g coal
96.7	0.508
214.9	0.761
330.6	0.899
427.5	0.989
527.1	1.05
635.1	1.12
712.7	1.15
851.0	1.21
1008.1	1.26
1198.6	1.41
1295.3	1.55
1488.8	3.79
1800.8	5.05

TABLE IX

ADSORPTION OF METHANE-NITROGEN MIXTURE (0.200 METHANE)
ON WET FRUITLAND COAL AT 115 °F

Pressure, psia	Gas Phase Mole Fraction, y_1	Absolute Methane Adsorption, mg mole/g coal	Absolute Nitrogen Adsorption, mg mole/g coal
125.2	0.139	0.0445	0.0533
214.1	0.144	0.0697	0.0819
397.9	0.151	0.110	0.126
599.1	0.157	0.147	0.165
807.0	0.161	0.176	0.199
1010.8	0.165	0.200	0.226
1207.1	0.167	0.222	0.249
1406.4	0.170	0.238	0.272
1601.8	0.172	0.255	0.301
1801.0	0.173	0.272	0.323

TABLE X

ADSORPTION OF METHANE-NITROGEN MIXTURE (0.400 METHANE)
ON WET FRUITLAND COAL AT 115 °F

Pressure, psia	Gas Phase Mole Fraction, y_1	Absolute Methane Adsorption, mg mole/g coal	Absolute Nitrogen Adsorption, mg mole/g coal
152.1	0.312	0.103	0.0453
248.7	0.320	0.151	0.0653
603.3	0.342	0.272	0.120
802.0	0.349	0.319	0.141
1001.0	0.354	0.359	0.161
1203.7	0.358	0.395	0.177
1394.7	0.361	0.424	0.197
1601.6	0.364	0.452	0.214
1795.0	0.367	0.474	0.235

TABLE XI

ADSORPTION OF METHANE-NITROGEN MIXTURE (0.600 METHANE) ON WET FRUITLAND COAL AT 115 °F

Pressure, psia	Gas Phase Mole Fraction, y_1	Absolute Methane Adsorption, mg mole/g coal	Absolute Nitrogen Adsorption, mg mole/g coal
102.7	0.524	0.109	0.0301
213.9	0.530	0.194	0.0482
400.5	0.543	0.294	0.0704
600.8	0.551	0.374	0.0874
802.8	0.557	0.440	0.104
1002.0	0.563	0.488	0.120
1201.3	0.566	0.533	0.132
1399.0	0.569	0.569	0.142
1601.8	0.572	0.608	0.154
1796.0	0.574	0.642	0.167

TABLE XII

ADSORPTION OF METHANE-NITROGEN MIXTURE (0.800 METHANE) ON WET FRUITLAND COAL AT 115 °F

Pressure, psia	Gas Phase Mole Fraction, y_1	Absolute Methane Adsorption, mg mole/g coal	Absolute Nitrogen Adsorption, mg mole/g coal
104.2	0.747	0.159	0.0170
199.4	0.755	0.252	0.0262
403.0	0.764	0.388	0.0372
597.7	0.770	0.481	0.0447
806.8	0.774	0.555	0.0506
1007.3	0.779	0.602	0.0597
1201.7	0.781	0.648	0.0664
1402.3	0.783	0.691	0.0703
1601.6	0.784	0.738	0.0753
1800.0	0.785	0.781	0.0806

TABLE XIII

ADSORPTION OF METHANE-CARBON DIOXIDE MIXTURE (0.200 METHANE) ON WET FRUITLAND COAL AT 115 °F

Pressure, psia	Gas Phase Mole Fraction, y_1	Absolute Methane Adsorption, mg mole/g coal	Absolute Carbon Dioxide Adsorption, mg mole/g coal
96.1	0.334	0.0410	0.371
199.7	0.301	0.0594	0.563
403.0	0.270	0.0762	0.774
597.7	0.256	0.0811	0.898
798.2	0.244	0.0879	0.988
1003.2	0.236	0.0942	1.06
1199.6	0.231	0.0942	1.14
1400.7	0.226	0.107	1.22
1575.3	0.221	0.130	1.32
1728.1	0.217	0.161	1.39

TABLE XIV

ADSORPTION OF METHANE-CARBON DIOXIDE MIXTURE (0.400 METHANE) ON WET FRUITLAND COAL AT 115 °F

Pressure, psia	Gas Phase Mole Fraction, y_1	Absolute Methane Adsorption, mg mole/g coal	Absolute Carbon Dioxide Adsorption, mg mole/g coal
107.5	0.568	0.0905	0.281
197.8	0.537	0.110	0.383
396.4	0.508	0.152	0.577
603.0	0.480	0.184	0.676
803.8	0.469	0.198	0.767
1003.6	0.459	0.213	0.837
1206.9	0.451	0.220	0.888
1397.4	0.445	0.244	0.951
1595.6	0.439	0.274	1.02
1791.3	0.435	0.303	1.09

TABLE XV

ADSORPTION OF METHANE-CARBON DIOXIDE MIXTURE (0.600 METHANE) ON WET FRUITLAND COAL AT 115 °F

Pressure, psia	Gas Phase Mole Fraction, y_1	Absolute Methane Adsorption, mg mole/g coal	Absolute Carbon Dioxide Adsorption, mg mole/g coal
104.1	0.764	0.125	0.175
202.7	0.733	0.188	0.270
400.7	0.709	0.251	0.403
599.4	0.688	0.296	0.485
804.6	0.678	0.320	0.559
1005.1	0.665	0.356	0.601
1202.9	0.657	0.365	0.636
1399.6	0.655	0.382	0.699
1598.1	0.648	0.421	0.736
1800.3	0.643	0.450	0.765

TABLE XVI

ADSORPTION OF METHANE-CARBON DIOXIDE MIXTURE (0.800 METHANE) ON WET FRUITLAND COAL AT 115 °F

Pressure, psia	Gas Phase Mole Fraction, y_1	Absolute Methane Adsorption, mg mole/g coal	Absolute Carbon Dioxide Adsorption, mg mole/g coal
107.8	0.903	0.164	0.0863
206.6	0.886	0.254	0.135
400.5	0.868	0.365	0.200
615.3	0.856	0.445	0.249
800.8	0.846	0.502	0.275
1002.4	0.845	0.538	0.318
1200.7	0.840	0.567	0.340
1404.8	0.836	0.603	0.362
1596.3	0.834	0.636	0.387
1800.5	0.831	0.672	0.398

TABLE XVII

ADSORPTION OF NITROGEN-CARBON DIOXIDE MIXTURE (0.200 NITROGEN) ON WET FRUITLAND COAL AT 115 °F

Pressure, psia	Gas Phase Mole Fraction, y_1	Absolute Nitrogen Adsorption, mg mole/g coal	Absolute Carbon Dioxide Adsorption, mg mole/g coal
121.4	0.393	0.00723	0.415
207.0	0.350	0.0131	0.568
393.4	0.306	0.0166	0.772
601.2	0.276	0.0272	0.899
809.3	0.260	0.0301	1.00
1002.2	0.247	0.0408	1.06
1206.7	0.242	0.0308	1.13
1393.6	0.234	0.0380	1.17
1594.6	0.227	0.0479	1.17
1792.1	0.226	0.0446	1.29

TABLE XVIII

ADSORPTION OF NITROGEN-CARBON DIOXIDE MIXTURE (0.400 NITROGEN) ON WET FRUITLAND COAL AT 115 °F

Pressure, psia	Gas Phase Mole Fraction, y_1	Absolute Nitrogen Adsorption, mg mole/g coal	Absolute Carbon Dioxide Adsorption, mg mole/g coal
105.1	0.671	0.0191	0.249
199.5	0.627	0.0314	0.396
393.4	0.576	0.0437	0.594
600.9	0.542	0.0529	0.733
805.6	0.518	0.0600	0.827
1008.1	0.501	0.0682	0.894
1207.2	0.488	0.0703	0.944
1406.6	0.477	0.0803	0.993
1604.6	0.469	0.0841	1.02
1798.7	0.462	0.0938	1.05

TABLE XIX

ADSORPTION OF NITROGEN-CARBON DIOXIDE MIXTURE (0.600 NITROGEN) ON WET FRUITLAND COAL AT 115 °F

Pressure, psia	Gas Phase Mole Fraction, y_1	Absolute Nitrogen Adsorption, mg mole/g coal	Absolute Carbon Dioxide Adsorption, mg mole/g coal
105.9	0.852	0.0242	0.155
203.0	0.818	0.0440	0.258
394.7	0.781	0.0714	0.413
598.2	0.756	0.0870	0.531
801.7	0.736	0.101	0.617
1003.4	0.721	0.112	0.685
1203.8	0.708	0.125	0.734
1401.5	0.698	0.136	0.777
1600.4	0.689	0.147	0.813
1798.3	0.682	0.164	0.844

TABLE XX

ADSORPTION OF NITROGEN-CARBON DIOXIDE MIXTURE (0.700 NITROGEN) ON WET FRUITLAND COAL AT 115 °F

Pressure, psia	Gas Phase Mole Fraction, y_1	Absolute Nitrogen Adsorption, mg mole/g coal	Absolute Carbon Dioxide Adsorption, mg mole/g coal
104.5	0.908	0.0336	0.112
209.8	0.882	0.0622	0.195
395.7	0.856	0.0920	0.310
599.5	0.837	0.117	0.407
810.6	0.823	0.138	0.486
1007.6	0.812	0.152	0.545
1205.0	0.804	0.168	0.602
1405.4	0.795	0.181	0.637
1605.5	0.788	0.196	0.670
1801.0	0.782	0.216	0.707

TABLE XXI

ADSORPTION OF NITROGEN-CARBON DIOXIDE MIXTURE (0.799 NITROGEN) ON WET FRUITLAND COAL AT 115 °F

Pressure, psia	Gas Phase Mole Fraction, y_1	Absolute Nitrogen Adsorption, mg mole/g coal	Absolute Carbon Dioxide Adsorption, mg mole/g coal
104.7	0.948	0.0367	0.0701
207.3	0.934	0.0694	0.126
405.1	0.917	0.114	0.212
600.6	0.905	0.147	0.278
804.9	0.896	0.182	0.336
1004.8	0.888	0.204	0.382
1205.2	0.882	0.224	0.422
1402.6	0.877	0.245	0.459
1601.9	0.872	0.263	0.485
1797.9	0.868	0.286	0.513

CHAPTER VII

ANALYSIS OF EXPERIMENTAL ERRORS

The method used to estimate the errors in the adsorption experiments is based on the theory of multivariate error propagation [28]. This method of error propagation describes the manner in which errors in experimentally measured variables are propagated into errors in any quantity calculated based upon the experimental variables. To determine the uncertainty or error associated with each quantity, the desired quantity is expressed as an analytical function of the measured variables. In error propagation calculations, the uncertainty in each measured variable is expressed in terms of its standard deviation, σ. The uncertainty expressions assumes that the input variables are uncorrelated and the response of the calculated quantity to the measured variables are expressed as a Taylor series truncated after the linear term [28].

For a result, R, calculated from a set of input data (x_1, x_2, ..., x_N), the uncertainty in R is expressed as [28]

$$\sigma_R^2 = \sum_{i=1}^{N} \left[\left(\frac{\partial R}{\partial x_i} \right)^2 \sigma_{x_i}^2 \right] \qquad \text{(VII-1)}$$

where the summation is carried out over all input variables, x_i. Equation VII-1 indicates that the uncertainty in a measured variable (R) is dependent on product of the rate of change in R with respect to each experimentally measured variable (x_i) and the uncertainty in the measured variable. The major difficulty in error

estimation is assigning realistic estimates to the measured variable uncertainties. In the present work, these estimates were based on previous experience [29,15] with similar equipment and on replicate experiments.

Experimental Uncertainties in Pure Component Adsorption

The following uncertainty expressions were derived from the governing equations discussed in the Experimental Procedure chapter. The adsorption uncertainties ($\sigma_{n_{ads}}$) are composed of two contributions: the amount of gas injected from the positive displacement pump ($\sigma_{n_{inj}}$), and the amount of unadsorbed gas in the cell ($\sigma_{n_{unads}}$). Thus, the overall uncertainty in the amount adsorbed is composed of two terms —the uncertainty in the amount injected, and the uncertainty in the amount of gas remaining in the cell at equilibrium.

$$\sigma^2_{n_{ads}} = \sigma^2_{n_{inj}} + \sigma^2_{n_{unads}} \tag{VII-2}$$

During an experiment, multiple gas injections are made from the positive displacement injection pump into the equilibrium cell. The amount of gas contained in the injection pump can be written as the total pump volume times the density of the gas as determined from the pump conditions (pressure and temperature). The amount of gas injected can be written as

$$n_{inj} = \sum_j \left[\rho_{p_i} V_{p_i} - \rho_{p_f} V_{p_f} \right]_j \tag{VII-3}$$

where $(\rho_{p_i})_j$ and $(\rho_{p_f})_j$ are the gas densities at the initial and final pump conditions for the jth injection, and $(V_{p_i})_j$ and $(V_{p_f})_j$ are the initial and final pump volumes in

the injection pump for the jth injection. The uncertainty in the amount injected becomes

$$\sigma^2_{n_{inj}} = \sum_j \left[\left(V^2_{p_i} + V^2_{p_f} \right) \sigma^2_{\rho_p} + 2\rho^2_p \sigma^2_{V_p} \right]_j \qquad \text{(VII-4)}$$

The above expression assumes that the gas injections are done by keeping the initial and final pump conditions (pressure and temperature) equal for a given injection. The following assumptions are then valid.

$$\rho_{p_f} = \rho_{p_i} = \rho_p \qquad \text{(VII-5)}$$

$$\sigma_{\rho_{p_f}} = \sigma_{\rho_{p_i}} = \sigma_\rho \qquad \text{(VII-6)}$$

$$\sigma_{V_{p_f}} = \sigma_{V_{p_i}} = \sigma_{V_p} \qquad \text{(VII-7)}$$

However, the above injection uncertainty expression (Equation VII-4) yields errors in excess of 50 percent. Errors of this magnitude were clearly not observed experimentally, with deviations within replicate experiments not exceeding several percent. The coefficient, $(V^2_{p_i} + V^2_{p_f})$, for the uncertainty in the pump density overwhelms all other contributions. This arose from the presence of dead volume in the injection pump (V_p, includes the volume of tubing, valves, and "dead" volume in the pump, composed of clearance at the end of the piston and between the piston and the cylinder wall). Tests showed that the dead volume was approximately 140 cc. A more realistic expression for the injection uncertainties results if the value of n_{inj} is calculated as

$$n_{inj} = \sum_j \left[\rho_p \left(V_{p_f} - V_{p_i} \right) \right]_j = \sum_j \left(\rho_p \Delta V_{inj} \right)_j \qquad \text{(VII-8)}$$

Thus,

$$\sigma^2_{n_{inj}} = (\Delta V)^2 \sigma^2_{\rho_p} + 2\rho_p^2 \sigma^2_{V_p} \qquad \text{(VII-9)}$$

where ΔV is the gas volume injected by the positive displacement pump. This expression removes the dead volume from the injection volume uncertainties. The proper accounting for dead volume effects on the injection uncertainty expression is unresolved at the time of this writing, and will require further investigation.

The uncertainty in the amount of gas remaining in the void volume (free space) in the equilibrium cell is a function of the cell section gas density (ρ_c) and the void volume in the cell (V_{void}) as shown in Equation V-3. The uncertainty expression is given as

$$\sigma^2_{n_{unads}} = \rho_c^2 \sigma^2_{V_{void}} + V^2_{void} \sigma^2_{\rho_c} \qquad \text{(VII-10)}$$

From the governing equations, the void volume is the difference between the unadsorbed gas void volume (V_{He}) as determined by the helium calibration, and the volume occupied by the adsorbed phase (V_{ads}) as shown Governing Equations section of Chapter V. The uncertainty expression, based on $V_{void} = V_{He} - V_{ads}$, is given as

$$\sigma^2_{V_{void}} = \sigma^2_{V_{He}} + \sigma^2_{V_{ads}} \qquad \text{(VII-11)}$$

The uncertainty in the adsorbed volume, based on $V_{ads} = n_{ads}\, \nu_{ads}$, involves the adsorbed phase specific volume (ν_{ads}) and the moles adsorbed (n_{ads}).

$$\sigma^2_{V_{ads}} = n^2_{ads} \sigma^2_{\nu_{ads}} + \nu^2_{ads} \sigma^2_{n_{ads}} \qquad \text{(VII-12)}$$

The uncertainty in the helium calibration will include the amount of helium injected (n_{He}) from the positive displacement injection pump and the helium gas density at the cell conditions (ρ_{He}).

$$\sigma^2_{V_{He}} = \left[\frac{1}{\rho_{He}}\right]^2 \sigma^2_{n_{He}} + \left[\frac{n_{He}}{\rho^2_{He}}\right]^2 \sigma^2_{\rho_{He}} \qquad \text{(VII-13)}$$

Combining Equations VII-11 and VII-12 into VII-10 yields

$$\sigma^2_{V_{void}} = \sigma^2_{V_{He}} + n^2_{ads}\,\sigma^2_{v_{ads}} + v^2_{ads}\sigma^2_{n_{ads}} \qquad \text{(VII-14)}$$

Substituting Equations VII-9, VII-10 and VII-14 into VII-2, based on Equation V-1, yields the expression for the uncertainty in the amount adsorbed.

$$\sigma^2_{n_{ads}} = \left\{\sum_j \left[(\Delta V)^2 \sigma^2_{\rho_p} + 2\rho^2_p \sigma^2_{V_p}\right]_j + \rho^2_g \sigma^2_{V_{He}} + \rho^2_g\, n^2_{ads}\, \sigma^2_{v_{ads}} + V^2_{void}\, \sigma^2_{\rho_g}\right\} / \left[1 - \rho^2_g v^2_{ads}\right] \qquad \text{(VII-15)}$$

The term in the denominator of Equation VII-15, $\left[1-\rho^2_g v^2_{ads}\right]$, is very nearly unity and neglected in the uncertainty calculations. The pure component experimental uncertainty expression is simplified to the following.

$$\sigma^2_{n_{ads}} = \sum_j \left[(\Delta V)^2 \sigma^2_{\rho_p} + 2\rho^2_p \sigma^2_{V_p}\right]_j + \rho^2_g \sigma^2_{V_{He}} + \rho^2_g\, n^2_{ads}\, \sigma^2_{v_{ads}} + V^2_{void}\, \sigma^2_{\rho_g} \qquad \text{(VII-16)}$$

Equation VII-16 represents the total uncertainty associated with the pure component adsorption value. The bracketed term represents uncertainties associated with the pump injection with the remaining three terms being related to uncertainties in the amount of unadsorbed free gas in the cell. The pump section

uncertainties are associated with pump gas density and pump volume errors. The uncertainties from the cell section come from errors in the helium void volume, the moles adsorbed, the cell gas density and the adsorbed phase molar volume.

The Error Analysis Appendix of the Supplementary Material contains an investigation of each individual contribution to the overall uncertainties [40]. Figures containing information in various forms illustrate the errors in the pump and cell section measurements and how these errors contribute to the overall adsorption uncertainty. The results of the error analysis can identify which term contributes the most to uncertainties in the experimental results. Once identified, the experimental apparatus and/or procedure can be designed or modified to minimize these errors.

The percentage uncertainties in the amounts adsorbed in the pure component (methane, nitrogen, carbon dioxide) experiments range from one to three percent over the complete pressure range. Although the magnitudes differ slightly, the general trends are the same. The largest contribution comes from the unadsorbed gas calculations; the injection uncertainties contribute very little to the overall uncertainty. Of the factors contributing to the unadsorbed gas uncertainty, the dominate terms are from uncertainties in the adsorbed phase molar volume and void volume measurements, which make up approximately 80 percent of the pure component overall adsorption uncertainties. The overall pure component experimental uncertainties are illustrated in Figures 50, 51 and 52 as error bars indicating the error associated with each experimental measurement.

Experimental Uncertainties in Binary Mixture Adsorption

The uncertainty expressions for the adsorption of multicomponent gas mixtures are a little more complex because a material balance is written for each component. The resulting expressions are generalized forms of the pure gas equations developed earlier. The uncertainty expression for mixtures include the

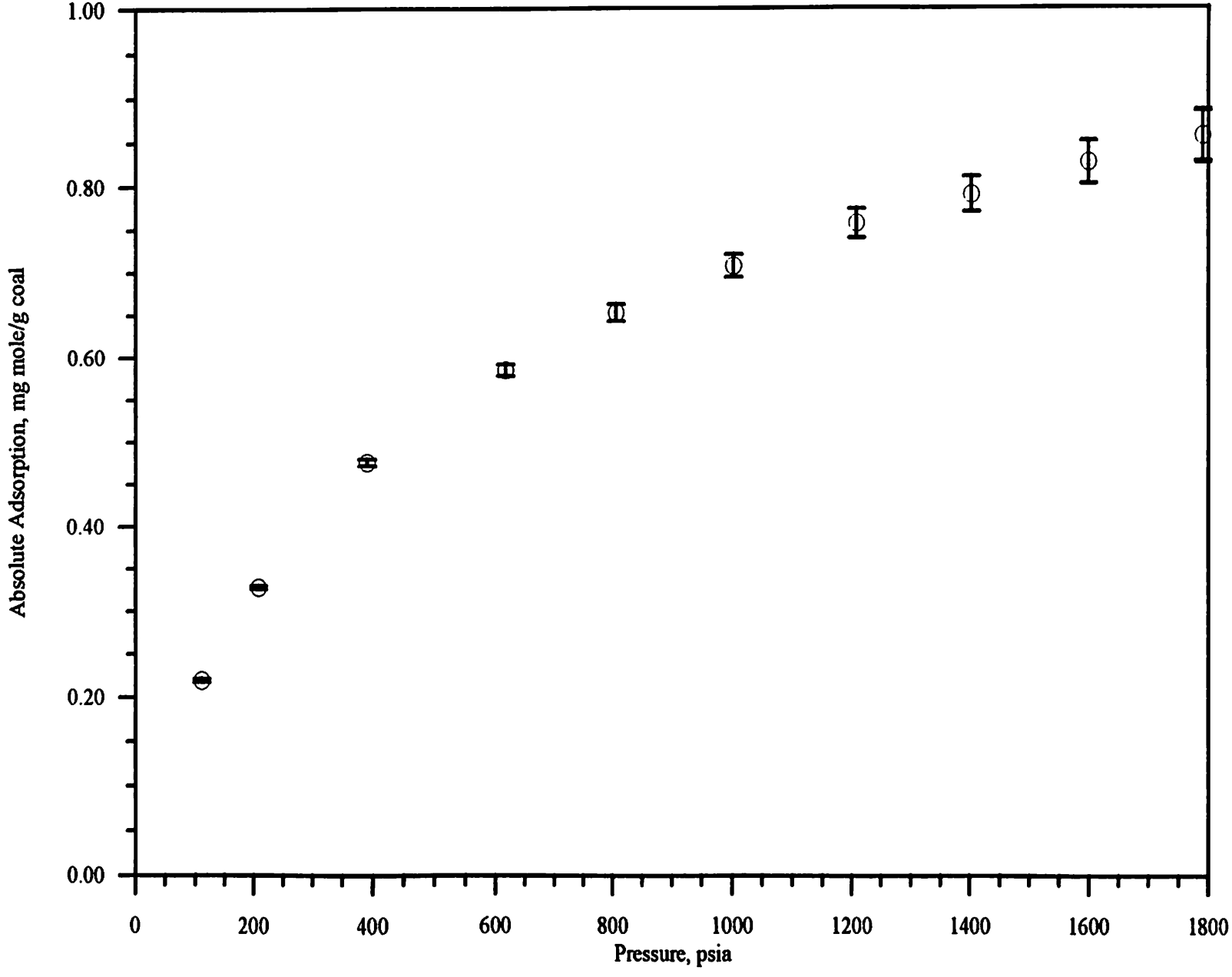

Figure 50. Uncertainties Associated with Pure Methane Adsorption Isotherm

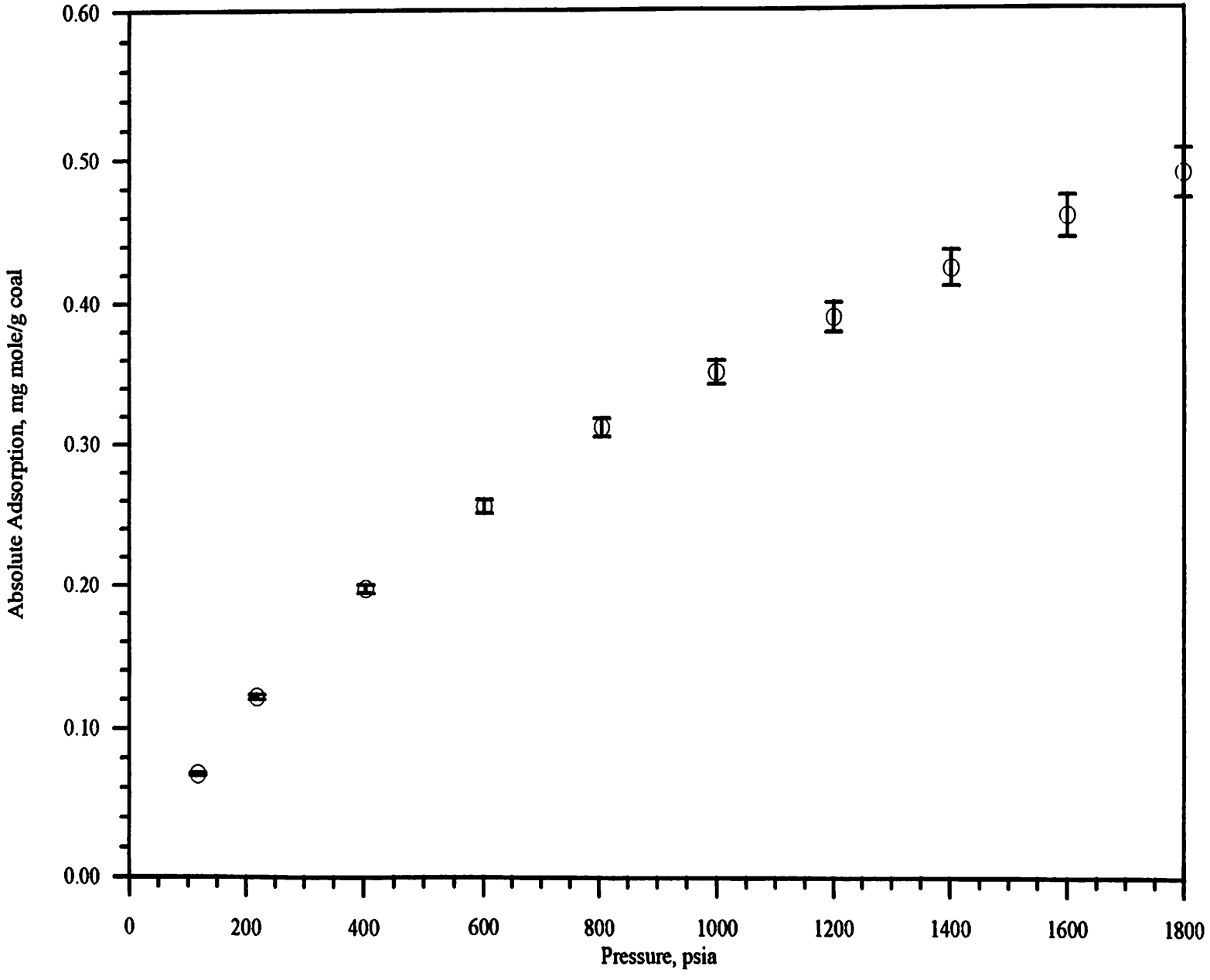

Figure 51. Uncertainties Associated with Pure Nitrogen Adsorption Isotherm

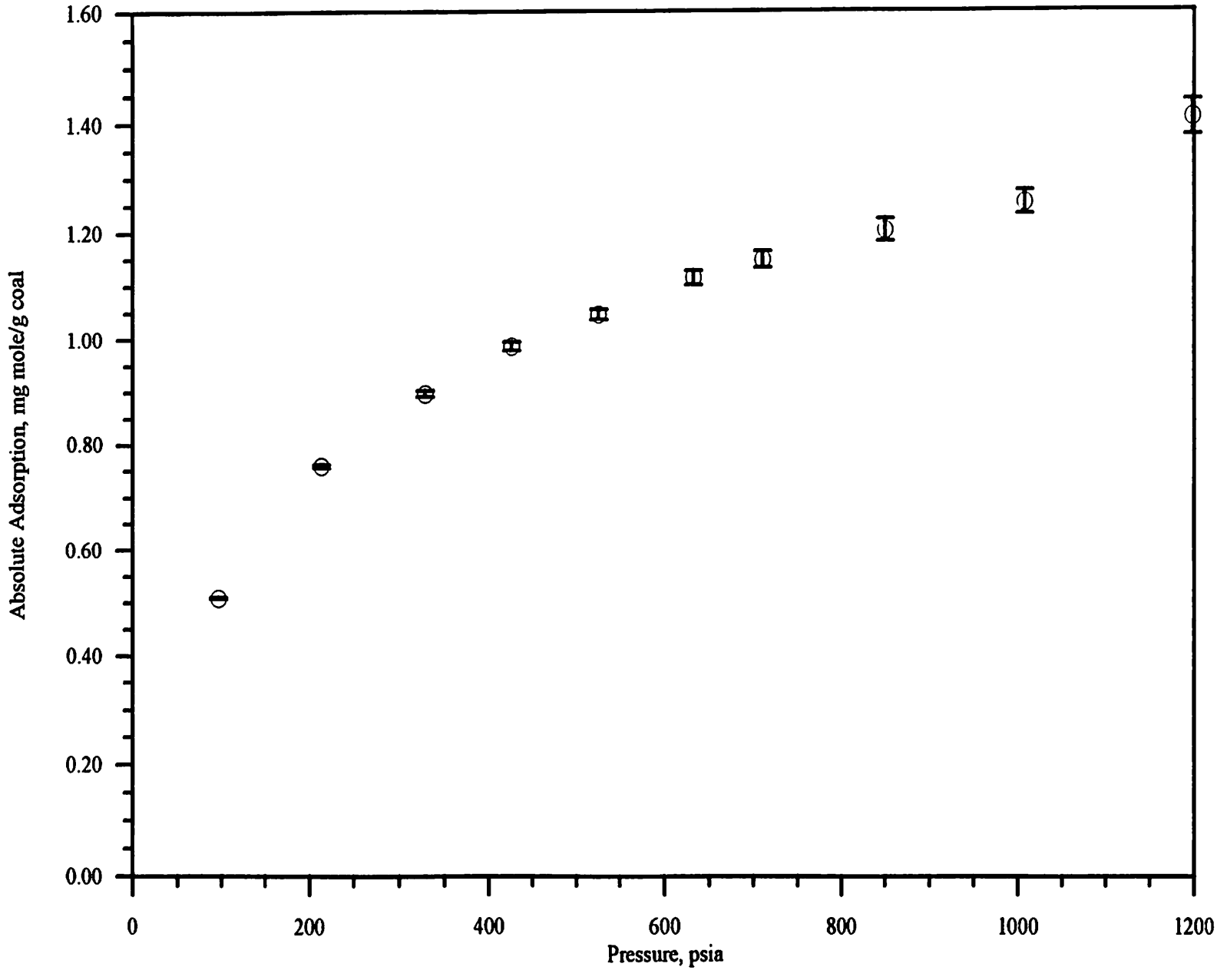

Figure 52. Uncertainties Associated with Pure Carbon Dioxide Adsorption Isotherm

gas composition of component k in the pump and cell sections, represented as z_k and y_k, respectively. Uncertainties associated with the gas compositions contribute to the overall uncertainty. The compositional uncertainties are represented as σ_{z_k} and σ_{y_k}. Equation VII-17 describes the uncertainties propagated in experimental gas mixture adsorption results based on Equation V-4.

$$\sigma^2_{n_{ads\,k}} = z_k^2\left\{\sum_j\left[(\Delta V)^2\sigma^2_{\rho_p} + 2\rho_p^2\sigma^2_{V_p}\right]_j\right\} + \left\{\sum_j\left[\rho_p\left(V_{p_i} - V_{p_f}\right)\right]_j\right\}^2\sigma^2_{z_k}$$
$$+ (y_k\rho_g)^2\left[\sigma^2_{V_{He}} + n^2_{ads}\,\sigma^2_{v_{ads}} + v^2_{ads}\sigma^2_{n_{ads}}\right] + (y_k\,V_{void})^2\sigma^2_{\rho_g} + (\rho_g\,V_{void})^2\sigma^2_{y_k} \qquad \text{(VII-17)}$$

The uncertainty expression for binary mixtures includes the above-mentioned pure component contributions with the addition of the compositional uncertainties for both the pump and cell gases. The pump section injection uncertainties come from three sources: uncertainties in the pump volume, the pump density and the pump section composition. The cell section unadsorbed gas uncertainties are composed of five terms with the addition of the cell section composition uncertainty to the previously-discussed pure component contributions. (A detailed discussion can be found in the Error Analysis Appendix of the Supplementary Material illustrating each individual contribution and how it affects the overall uncertainty.)

Three binary mixtures are given as examples in the Supplementary Material: 20/80 methane/nitrogen mixture, 40/60 methane/carbon dioxide mixture, 80/20 nitrogen/carbon dioxide mixture. Figures similar to those shown for the pure components are presented for each mixture. Information obtained in these figures can be used to determine which are the dominating terms and help in minimizing the overall experimental error.

For the pure components, the overall uncertainty increases from around one to three percent over the pressure range of interest. For mixtures, the overall

uncertainty increases from around one-to-four percent (depending on the mixture) to a high of around seven percent. Although the magnitudes change, the general trends are similar to those seen with the pure components. The injection errors contribute little to the overall error with the unadsorbed free gas errors being the major contributor. For mixtures, the magnitude of the injection error term is twice that of the pure examples and can be explained by the addition of the (dominating) pump section compositional uncertainty term. The unadsorbed cell section uncertainty terms are the major contributor to the overall uncertainty. While the pump and cell section compositional uncertainties contribute significantly to the overall error, the adsorbed phase molar volume and void volume contributions dominate for the methane/nitrogen mixture. The overall uncertainty is represented in Figure 53 by error bars for both the methane and nitrogen components. The error for methane range from 0.5 to 1.4 percent while those for nitrogen range from 1.4 to 5.0 percent. The larger nitrogen uncertainties (relative to methane) are explained by the fact that there is a much higher concentration of nitrogen in the gas phase relative to methane (20/80 mixture). These uncertainties result in large errors in the calculated amount of nitrogen in the gas phase and, consequently, in the calculated amount of nitrogen adsorbed.

The methane/carbon dioxide example is a 40/60 composition. The general trends are similar to the methane/nitrogen mixture. The uncertainty in the methane, ranging from 0.9 to 4.0 percent, is over three times that for carbon dioxide, increasing from 0.4 to 1.4 percent. The void volume and adsorbed phase molar volume errors contribute the most to the overall uncertainty. The error bars are shown in Figure 54.

The 80/20 nitrogen/carbon dioxide mixture trends are similar to previous mixtures. The nitrogen errors range from 3.3 to 5.2 percent with the carbon dioxide errors ranging from 0.4 to 0.55 percent. The unadsorbed gas errors contribute the

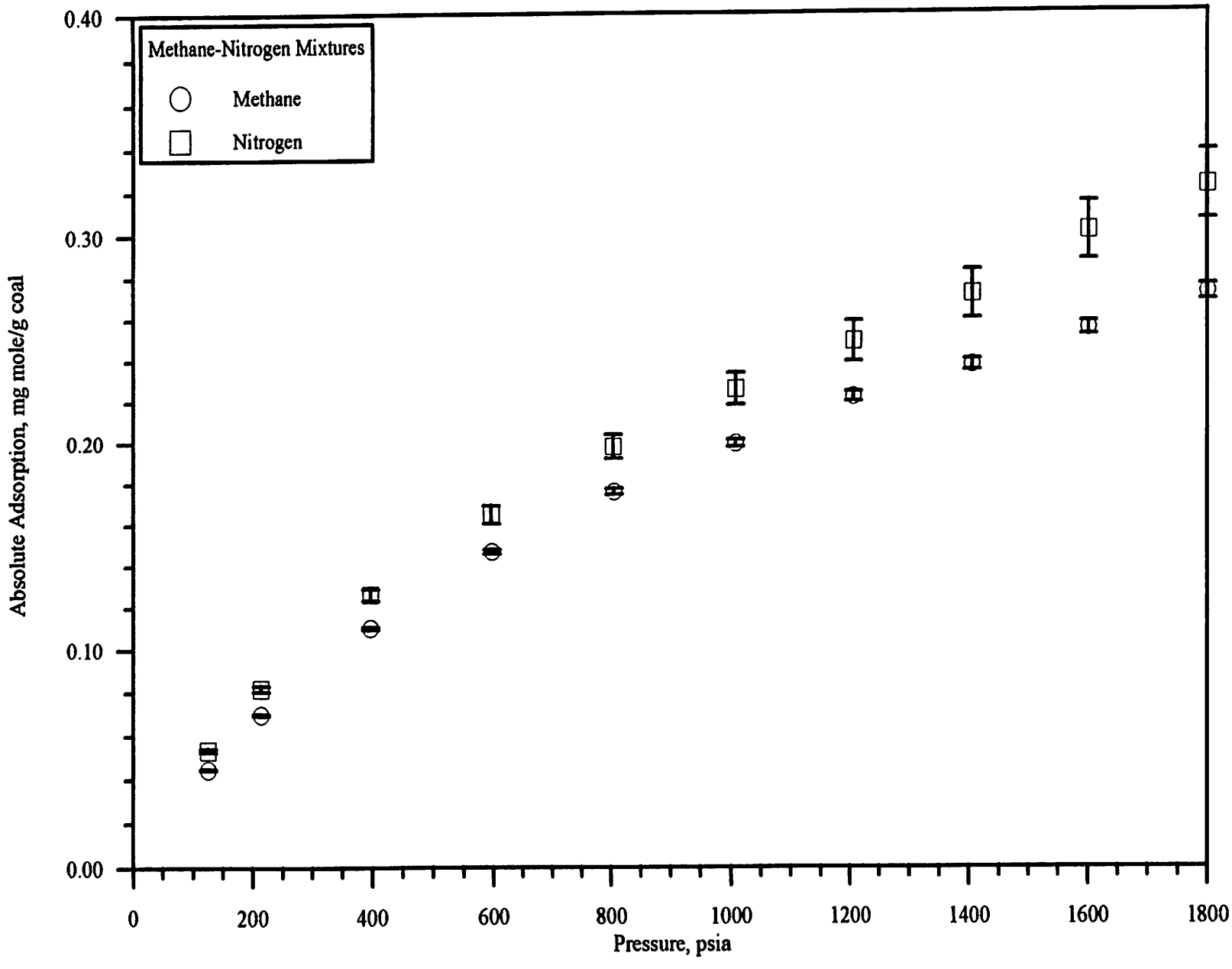

Figure 53. Uncertainties Associated with Methane-Nitrogen Mixture (0.20,0.80) Adsorption Isotherm

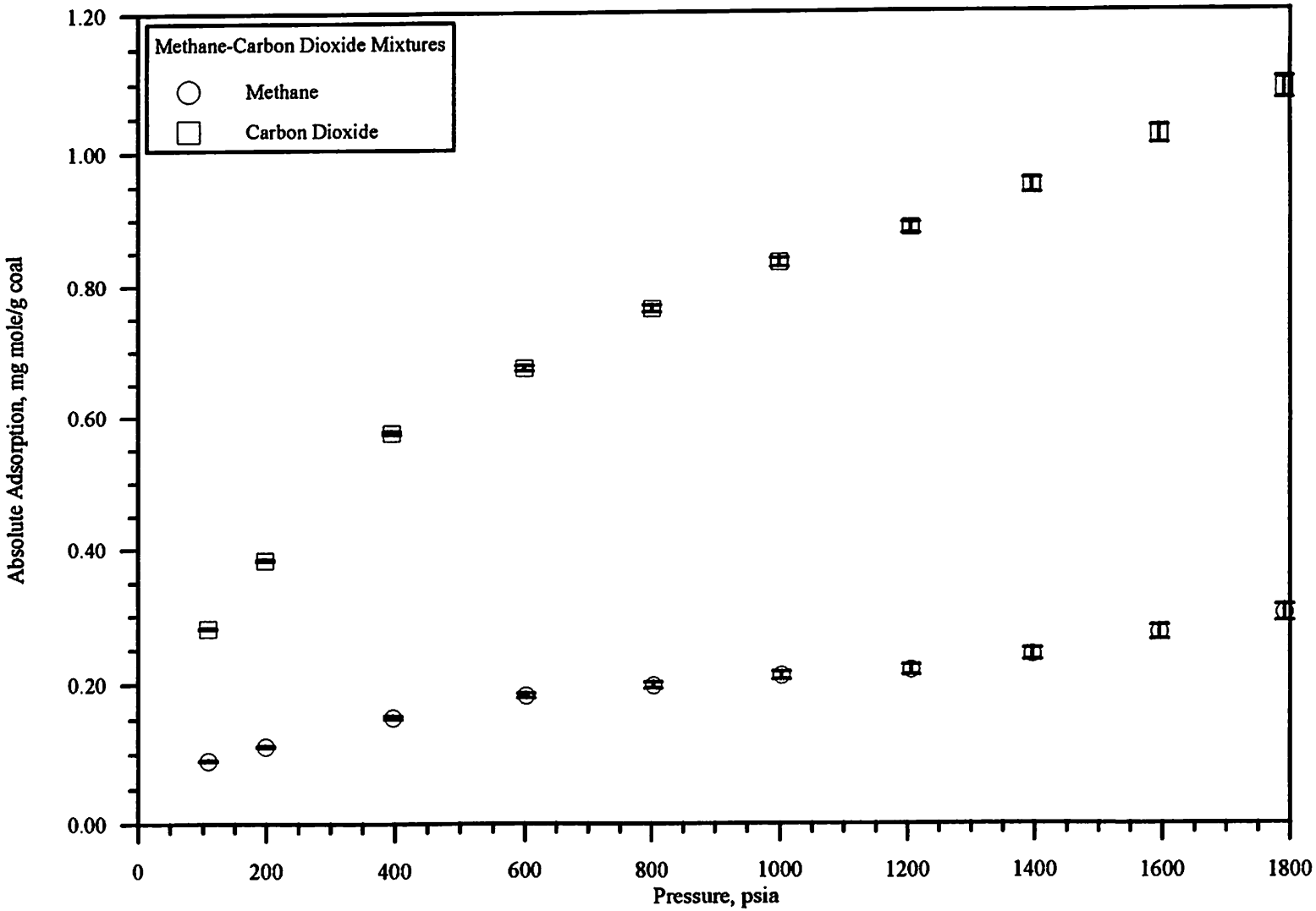

Figure 54. Uncertainties Associated with Methane-Carbon Dioxide Mixture (0.40,0.60) Adsorption Isotherm

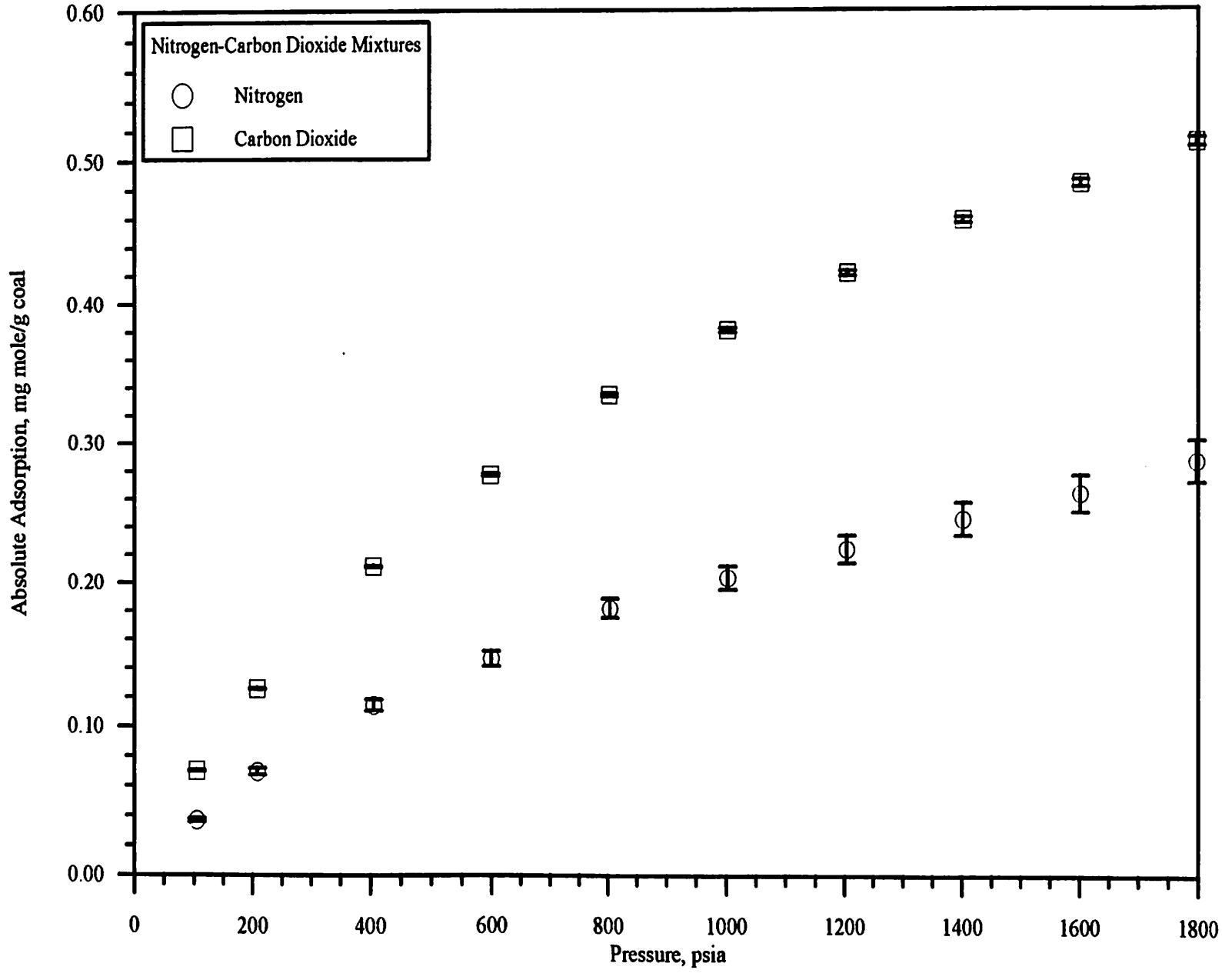

Figure 55. Uncertainties Associated with Nitrogen-Carbon Dioxide Mixture (0.80,0.20) Adsorption Isotherm

most while the pump injection errors contributing more than with the pure examples but considerably less than the unadsorbed gas uncertainties. The void volume term is again the dominate contributor to the overall uncertainty. The uncertainties are illustrated in Figure 55.

One of the major considerations in multivariate error propagation is assigning realistic estimates to the uncertainties in the measured variables. The estimates for the uncertainties in the measured variables were based on experience [29,15] with similar experimental apparatus. The uncertainties are tabulated in Table XXII. The measured variable estimates are conservative (that is, they would tend to err on the high side), and they should provide a realistic account of the experimental uncertainties.

TABLE XXII

ESTIMATES FOR MEASURED VARIABLE UNCERTAINTIES

Measured Variable	Symbol	Uncertainty Estimate
temperature	σ_T	0.1 K
pressure	σ_P	0.2 psi
displacement pump volume	σ_{V_p}	0.02 cc
pure component density	$\sigma_{\rho pure}$	$0.001*\rho$
mixture density	$\sigma_{\rho mix}$	$0.002*\rho$
adsorbed phase molar volume	$\sigma_{v_{ads}}$	$0.15*v_{ads}$
Helium injection	$\sigma_{V_{He}}$	$0.003*V_{void}$
pump gas composition	σ_{z_k}	0.002
cell gas composition	σ_{y_k}	0.002

Discussion

The error analysis for volumetrically measuring the adsorption of pure and multicomponent gases on a wet coal substrate indicates that the expected error for

the pure components will range between one and three percent over the complete pressure range. For binary mixtures, the individual component errors will range from one to seven percent. The major contributors were associated with the adsorbed phase molar volume, void volume, injection pump dead volume and compositional terms.

The overall error can be minimized by reducing the equilibrium cell void volume, by obtaining better estimates for the adsorbed phase molar volume (and, perhaps, by reduction in the injection pump dead volume). For binary mixture measurements, improvements in the accuracy of the feed gas synthesis and analysis of the equilibrium cell gas composition in addition to the above mentioned pure component suggestions will be needed to reduce the overall uncertainty.

More detailed discussion of the error propagation for the adsorption experiments appear in an earlier publication [28]. This progress report from Oklahoma State University to Amoco contains example applications of error propagation equations for the particular gases being tested. Additional discussion and examples are located in the Supplementary Material describing contributions to the overall uncertainty associated with the pure component and binary mixture adsorption experiment [40].

CHAPTER VIII

DATA CORRELATION

The data correlation described here is used to develop and test mathematical models which describe the adsorption behavior of gases on coal at conditions of interest. The resulting models will provide improved computational tools for designing optimum strategies for coalbed methane production.

The pure component adsorption data were fit to three models; a simple Langmuir isotherm, a Loading Ratio Correlation and the Asymptotic Behavior Correlation [15]. The models were fit using a regression program developed by Dr. K. A. M. Gasem [15]. As discussed in the experimental error analysis, the experimental uncertainties associated with the adsorption measurements increase as a function of pressure. This requires that weighted regressions be employed, assigning different emphases to the various data points. The weighting factors were taken as the uncertainties obtained from the error analysis program from equations described in the error analysis of this report. Root mean square error (RMS), average absolute percent deviation (AAPD) and weighted root mean square error (WRMS) statistical information was generated for each correlation model. This statistical output is used as the basis for comparing model correlations.

Simple Langmuir Model for Pure Components

The specific form of the Langmuir isotherm used in the data regressions was presented in the Literature Review (Equation III-1). The Langmuir is a two constant (L,B) model which expresses the amount adsorbed on the coal surface per unit mass

of adsorbent as a function of pressure. Optimum values for the model constants were determined for each pure component.

Optimum Langmuir model constant values for each pure component adsorption isotherm are tabulated in Table XXIII. The model constants for various replicate isotherm measurements for a specific substance are in good agreement. The AAPD for the data typically range from 1.2 to 2.4 percent.

Loading Ratio Correlation for Pure Components

The Loading Ratio Correlation (LRC) is a three constant correlation [36] (L,B,η) as seen in Equation III-8 (for mixtures). The specific form of the LRC (pure components) used to correlate the experimental adsorption data is seen in Equation VIII-1. Results of the weighted regressions are shown in Table XXIV.

$$\omega = \left[\frac{LBP^{\eta}}{1+BP^{\eta}}\right] \qquad \text{(VIII-1)}$$

The pressure is raised to a power η. When η equals one, the LRC expression reduces to the simple Langmuir model. When regressing the data for all pure substance, the optimum values of η for methane, nitrogen and carbon dioxide was 0.84, 0.88 and 0.81, respectively. To establish a model of equivalent form for all components, regressions were performed on all pure substances simultaneously, specifying a common value for the model constant (η). The optimum value for η was determined by calculating the total sum of squares as a function of η, as seen in Figure 56. The total sum of squares will be a minimum at the optimum value for η. The sum of squares for each component is shown in Figure 56. Regression results were relatively insensitive to the value of η, with the optimum value lying between 0.86 to 0.88. A value of 0.87 was used as the optimum common value for η.

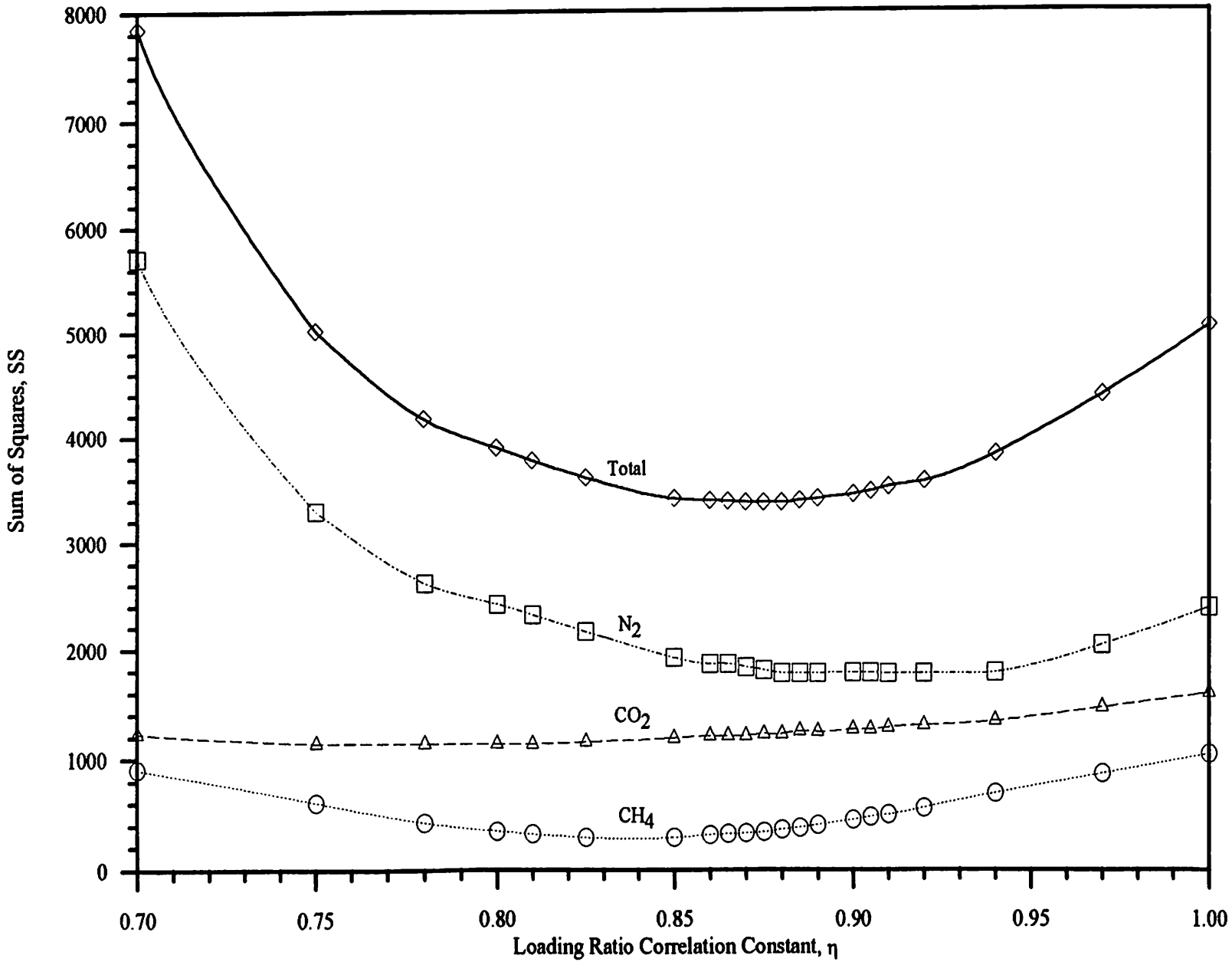

Figure 56. Determination of Optimium Value for the Loading Ratio Correlation Exponent, η

Statistics and model constants for the Loading Ratio Correlation with the η fixed at 0.87 are tabulated in Table XXV. The AAPD's range from 0.50 to 1.2, well within the expected experimental uncertainties in the data.

The simplification of the LRC made by fixing the model constant (η) is justified by the fact that changes in the regressed statistical results are within the predicted experimental uncertainty as discussed below. The Loading Ratio Correlation can be simplified to the following.

$$\omega = \left[\frac{LBP^{0.87}}{1 + BP^{0.87}} \right] \qquad \text{(VIII-2)}$$

In comparing the data for the fixed and optimized exponent (η) cases, as tabulated in Tables XXIV and XXV, the methane errors (RMS, AAPD, WRMS) increase by as much as three fold. This was expected since the optimum value (regressing only methane data) for η (0.84) is smaller than the fixed value (0.87). Still, the majority of the differences are within the predicted experimental uncertainty. In addition, the LRC with the fixed exponent is expected to predict the experimental data at low and mid-range pressures but under-predict at higher pressures. This is seen in Figure 57 where the exponent (η) is regressed for each run, as compared to Figure 58 where the exponent is fixed at 0.87. Figure 59 (η = 0.87) shows the percent deviation between the experimental data and model prediction as a function of pressure for both pure methane isotherms. Figures showing percent deviation as a function of pressure for all pure components are separate, individually fit isotherms. The Loading Ratio Correlation deviates by one percent at low and mid-range pressures increasing to two percent at high pressures.

For nitrogen, the statistics are very similar for both the regressed and fixed values for η. This was expected since the fixed and optimum value for η are similar.

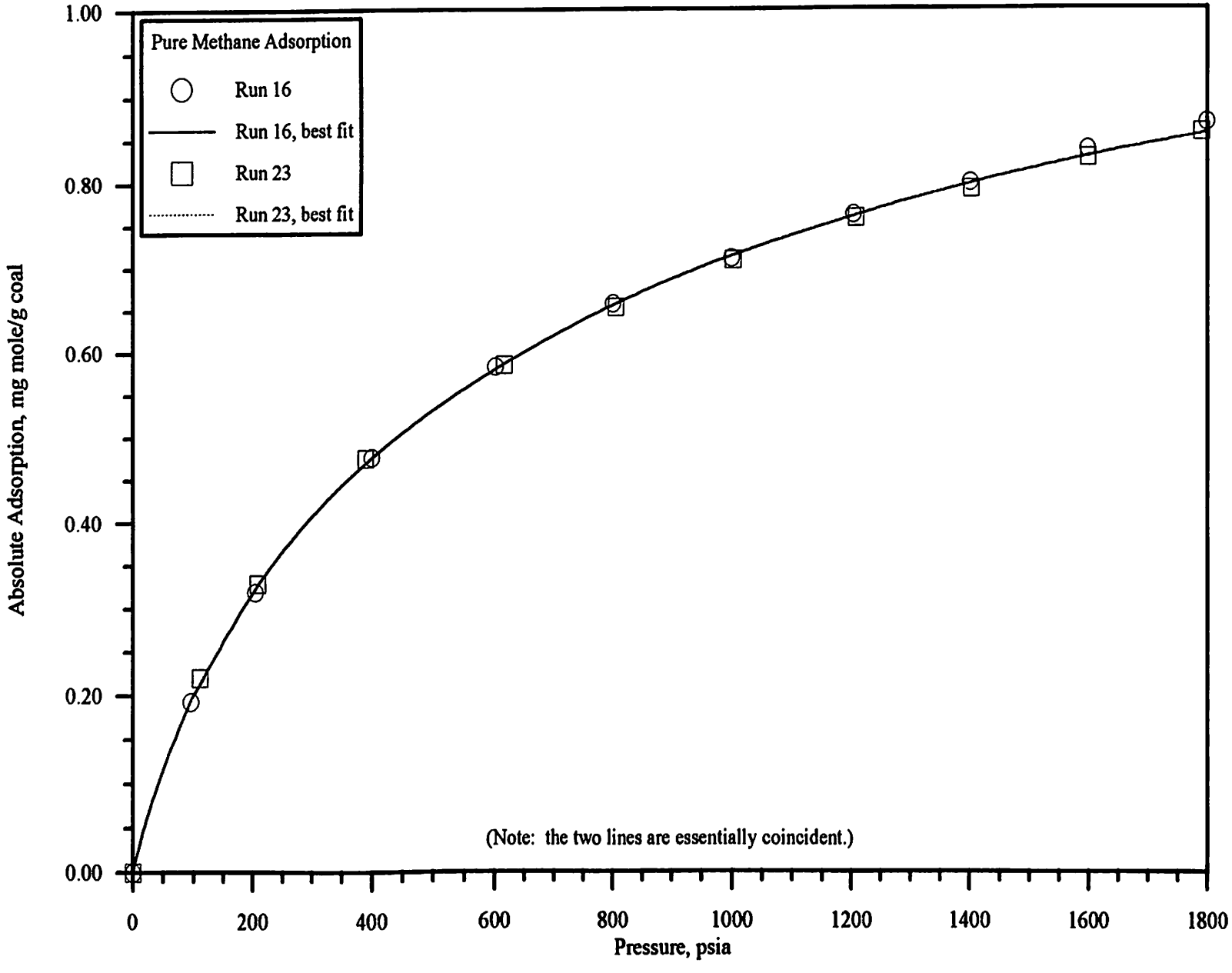

Figure 57. Absolute Adsorption of Methane at 115 °F on Wet Fruitland Coal using a Loading Ratio Correlation

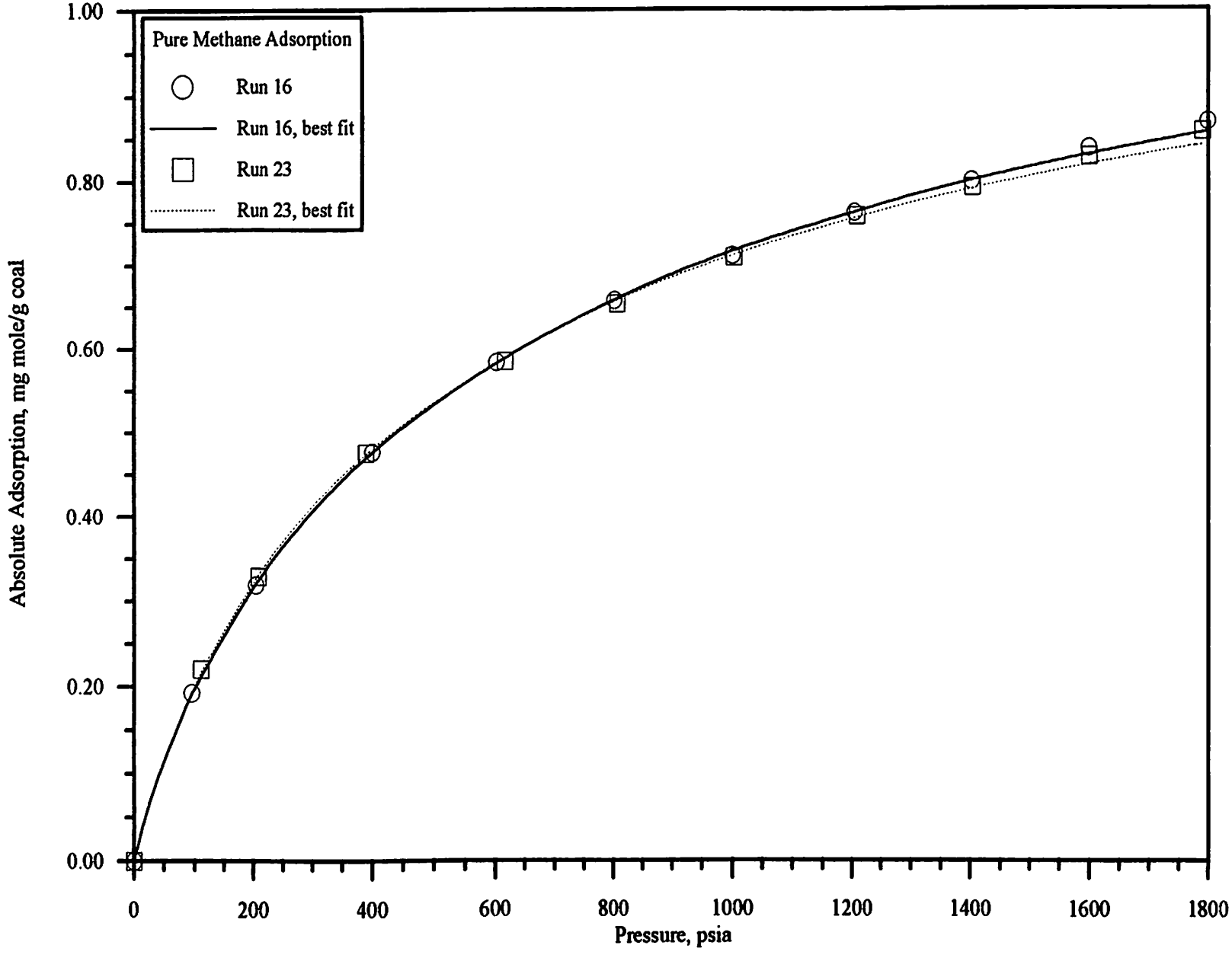

Figure 58. Absolute Adsorption of Methane at 115 °F on Wet Fruitland Coal using a Loading Ratio Correlation ($\eta = 0.87$)

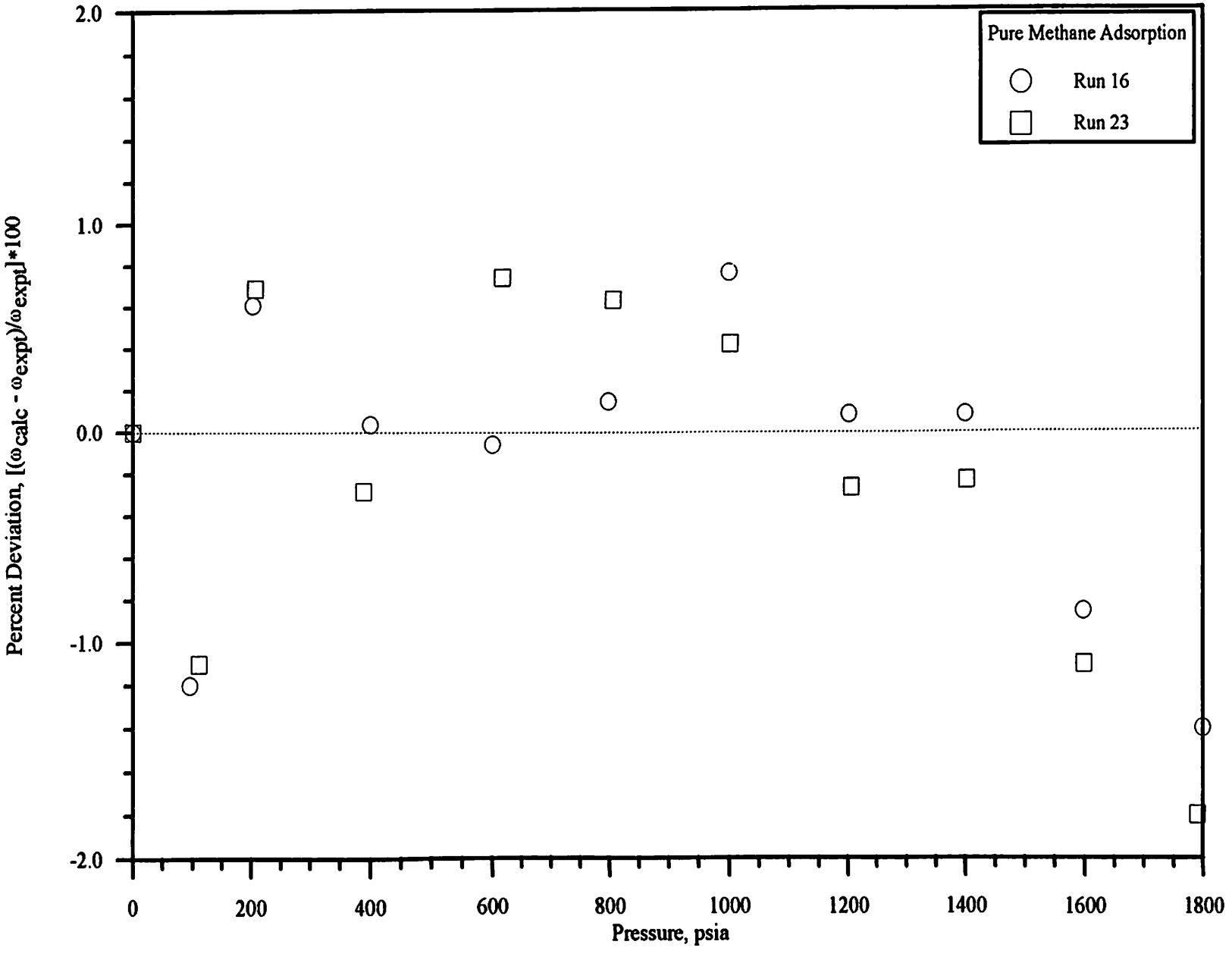

Figure 59. Deviations of Loading Ratio Correlation Prediction from Pure Methane Adsorption Data ($\eta = 0.87$)

The behavior of the LRC for nitrogen is illustrated in Figures 60 and 61. The model seems to adequately predict the middle and high pressures with deviations not exceeding 1.5 percent (as seen in Figure 62). The model appears to have more difficulty at low pressures, where the largest errors appear. The second datum point of Run 19 is suspect. (This point was deleted from the calculations and probably incorrect; it showed a seven percent deviation.)

Figures 63 and 64 present the behavior of pure carbon dioxide. The errors (AAPD) in the model double when fixing the exponent but are still within the experimental uncertainty. The trends are similar to methane and nitrogen in that the model under-predicts at low and high pressures and slightly over-predicts at middle pressures (as shown in Figure 65).

Asymptotic Correlation Model for Pure Components

The third correlation tested is the Asymptotic Behavior Correlation [15], which contains five model constants and is shown in Equation VIII-3

$$\omega = \left\{ C_1^{C_4} - C_1^{C_4} \left[\frac{1 - C_2^{\left(\frac{C_5 - P}{C_5}\right)^{C_3}}}{1 - C_2} \right] \right\}^{(1/C_4)} \qquad \text{(VIII-3)}$$

Tests on this model were include because it has shown impressive abilities to represent a variety of thermophysical properties [15,29]. The regressions were conducted by fixing three model constants (C_1, C_2, C_5) and regressing the remaining two (C_3, C_4). The constants (C_1, C_5) were fixed from the experimental data [15]. C_1 was defined as the pure component adsorption occurring at the maximum measured pressure, C_5 [15]. Model constants C_3 and C_4 are exponents which are specific to a given component. The model constants are tabulated in Table XXVI. The AAPD

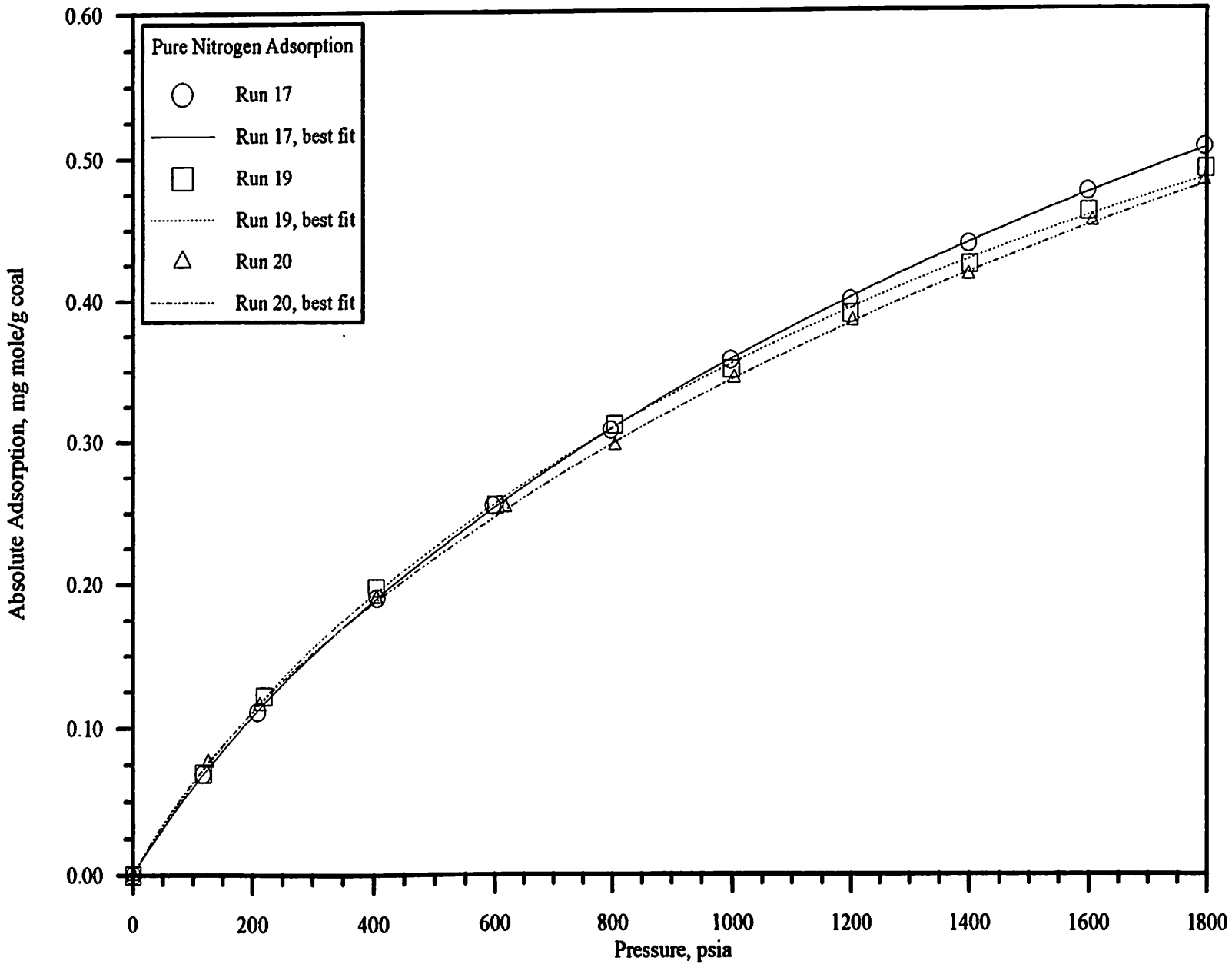

Figure 60. Absolute Adsorption of Nitrogen at 115 °F on Wet Fruitland Coal using a Loading Ratio Correlation

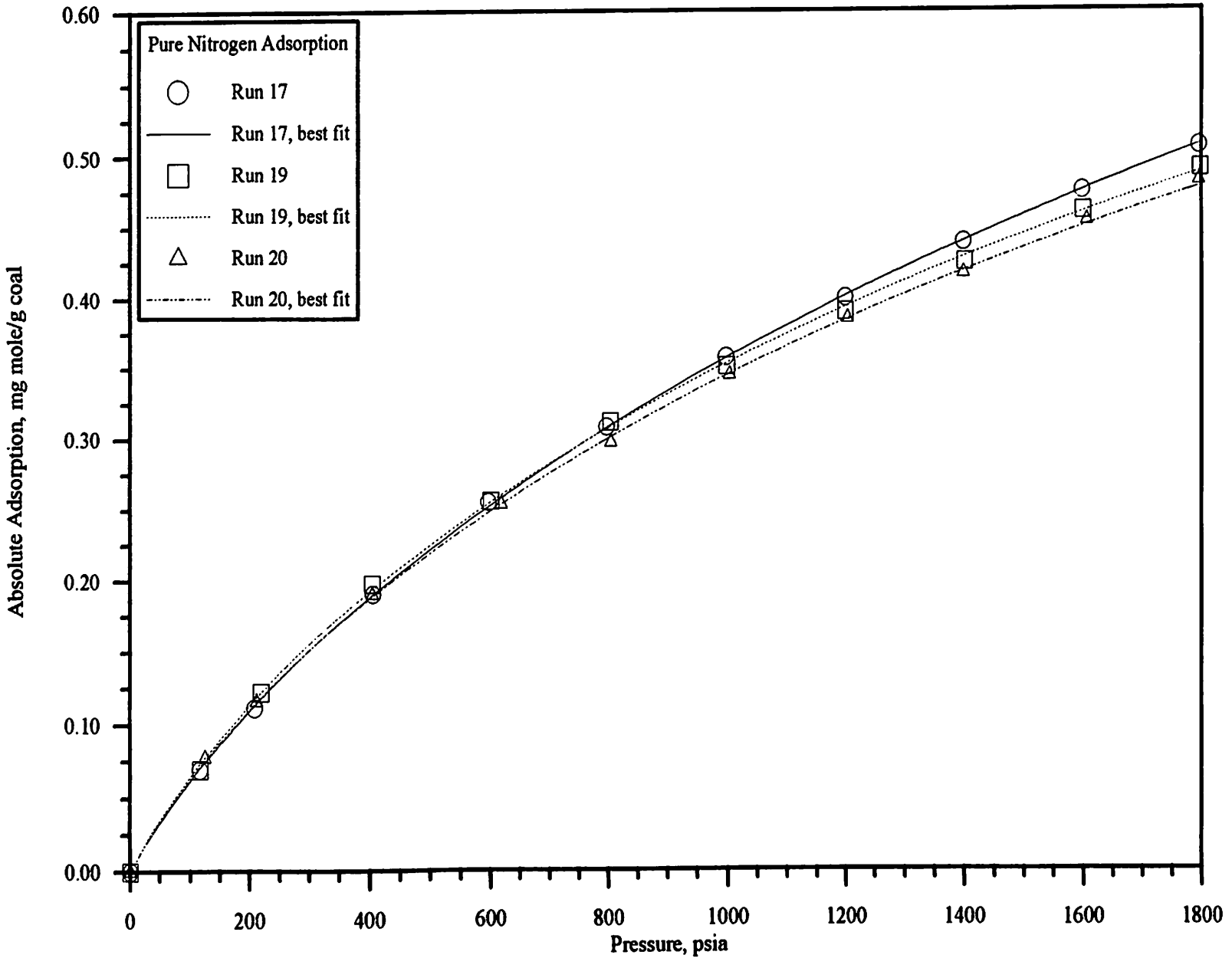

Figure 61. Absolute Adsorption of Nitrogen at 115 °F on Wet Fruitland Coal using a Loading Ratio Correlation ($\eta = 0.87$)

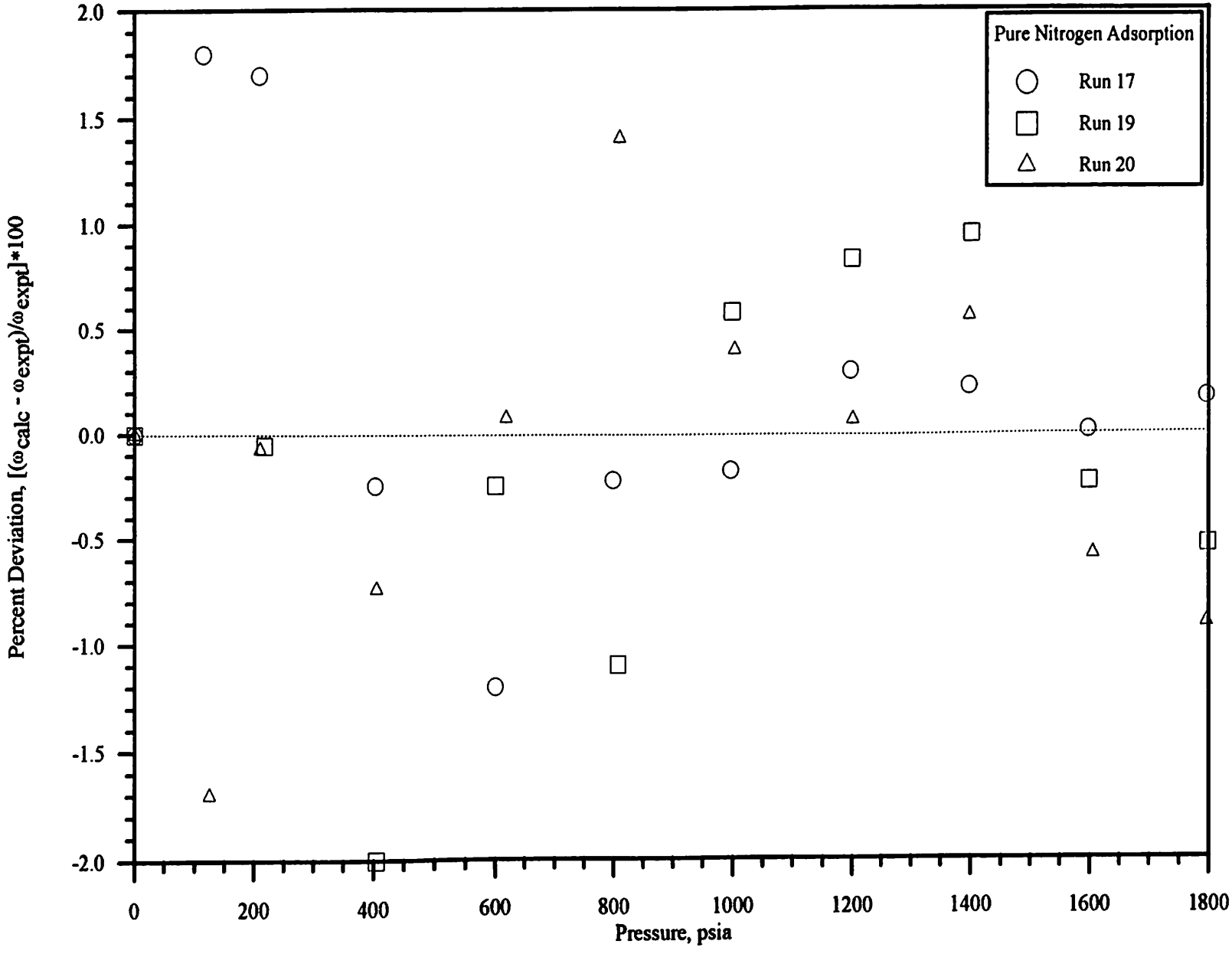

Figure 62. Deviations of Loading Ratio Correlation Prediction from Pure Nitrogen Adsorption Data ($\eta = 0.87$)

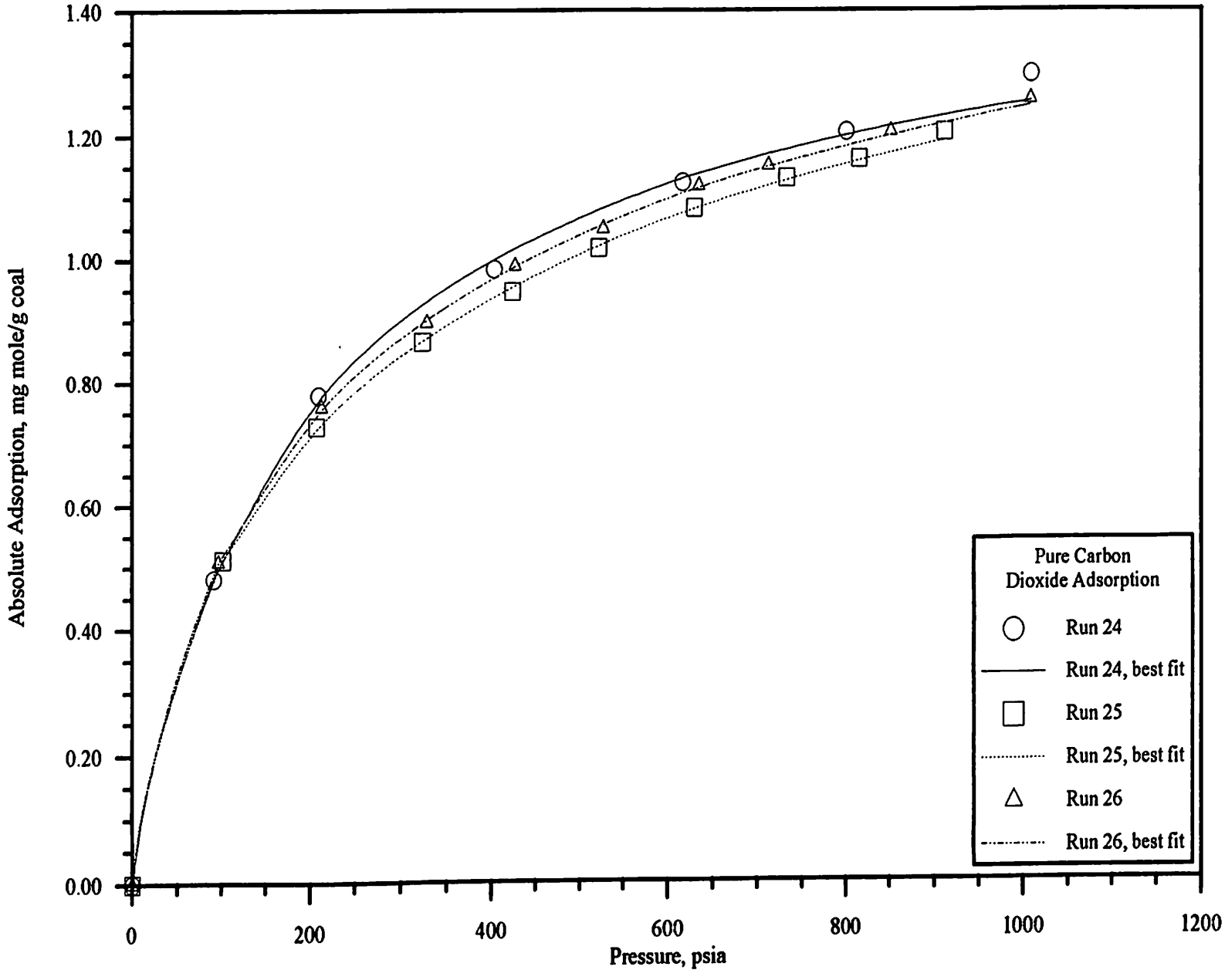

Figure 63. Absolute Adsorption of Carbon Dioxide at 115 °F on Wet Fruitland Coal using a Loading Ratio Correlation

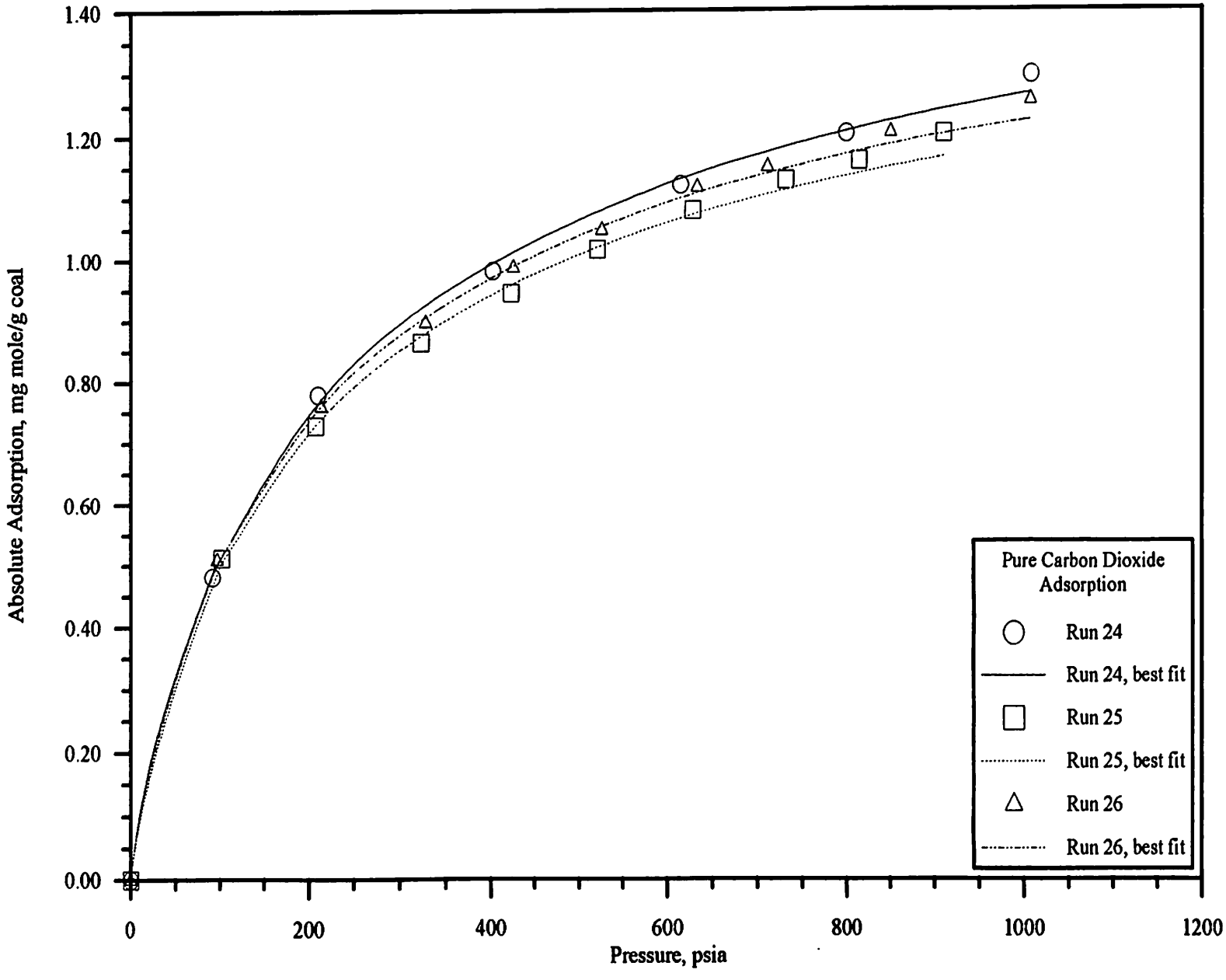

Figure 64. Absolute Adsorption of Carbon Dioxide at 115 °F on Wet Fruitland Coal using a Loading Ratio Correlation ($\eta = 0.87$)

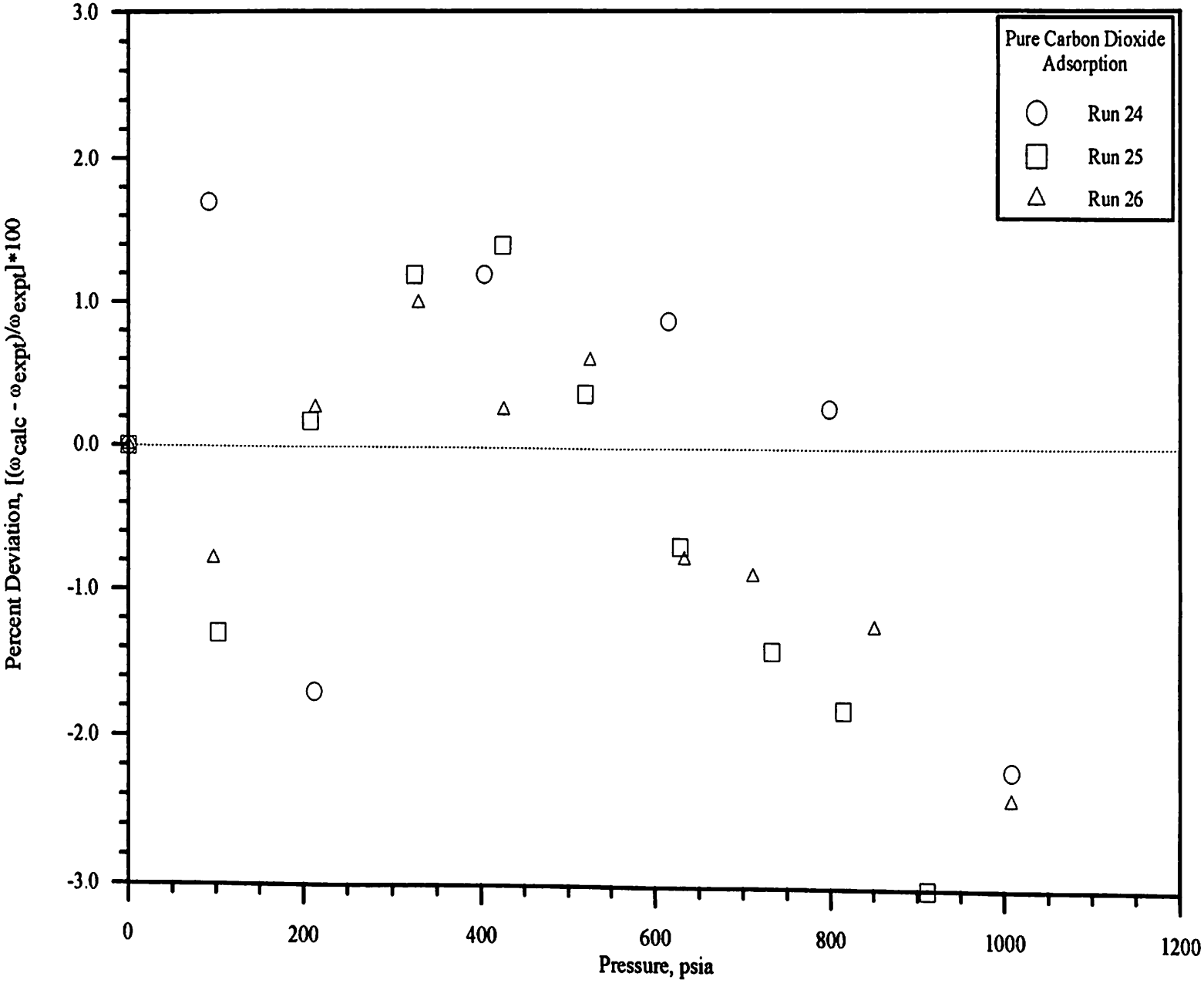

Figure 65. Deviations of Loading Ratio Correlation Predictions from Pure Carbon Dioxide Adsorption Data ($\eta = 0.87$)

values range from 0.72 to 2.1 percent.

The three pure component adsorption isotherm models (Langmuir, Loading Ratio Correlation, Asymptotic) are compared and statistical results tabulated in Table XXVII. Regressions were conducted using cumulative data for each pure component. For the LRC, two constants were regressed while fixing the exponent. Three constants of the asymptotic function were fixed while regressing the two exponential constants. For methane, the LRC out-performs the asymptotic function and simple Langmuir, with the AAPD being 0.7, 1.3 and 2.5, respectively. Nitrogen results for the LRC and asymptotic models are almost identical with the simple Langmuir appearing only slightly better. For carbon dioxide, the Loading Ratio Correlation is better than the simple Langmuir and Asymptotic models with the AAPD being 1.7, 2.2 and 2.0, respectively. For pure components, the asymptotic correlation out-performs the simple Langmuir. For all pure component adsorption data, the Loading Ratio Correlation model provides the best fit to the experimental data. The simple Langmuir model provides the worst fit, as expected, since the model uses only two constants. The LRC is significantly easier to apply than the asymptotic function which requires five model constants. Loading Ratio Correlation applications were made even easier by fixing the exponent and regressing the other two constants.

The trends seen with the pure components are all similar. The LRC under-predicts the data at low and high pressures while over-predicting in the mid-range, with errors being less than two percent.

The Loading Ratio Correlation constants optimized with cumulative pure component experimental data were used to predict the binary mixture behavior, as described below. The LRC constants used for the mixture calculations are tabulated in Table XXVIII. The LRC did the best job of fitting the pure component data, and thus, was the only model used for binary mixture correlations.

Loading Ratio Correlation for Binary Mixtures

The binary mixture adsorption data are presented in Figures 66 to 77. The symbols represent the experimentally measured data while the model predictions are shown as lines. Figure 66 shows methane adsorption for a methane/nitrogen mixture as a function of pressure, including the pure component data. The percentage deviations in the predicted methane adsorption from methane/nitrogen mixtures are illustrated in Figure 67. Deviations in the model approach 16 percent at low pressures and low methane mole fractions (0.20), but decrease to two percent at high methane compositions (0.80), as seen in Figure 67. Figure 68 shows the nitrogen adsorption from methane/nitrogen mixtures. Figure 69 shows the percent deviation for the nitrogen adsorption. The model deviates by 10-30 percent for the 20/80 and 40/60 compositions. Model deviations are reduced to 10-20 percent for the 60/40 and 80/20 mixtures. For methane/nitrogen mixtures, the extended Loading Ratio Correlation is reasonable in predicting the methane adsorption behavior, but is less adequate for nitrogen.

Similar figures are presented for methane/carbon dioxide mixtures. Figure 70 presents methane adsorption as a function of pressure. The model has difficulty at low and high pressures as seen in Figures 70 and 71. The low-methane mixture (20/80) deviates by 40 percent at low and high pressures. For carbon dioxide adsorption, the model does a better job of predicting the low pressure behavior as seen in Figures 72 and 73. The model has difficulty in predicting the high pressures as more carbon dioxide is added to the mixture. Model deviations approach 30 percent at low and high pressures. The model generally predicts within five percent at mid-range pressures. The model obviously cannot predict the high-pressure multilayer adsorption illustrated by the Type II adsorption isotherm (as seen in Figure 72). A deviation plot for carbon dioxide is illustrated in Figure 73. The low

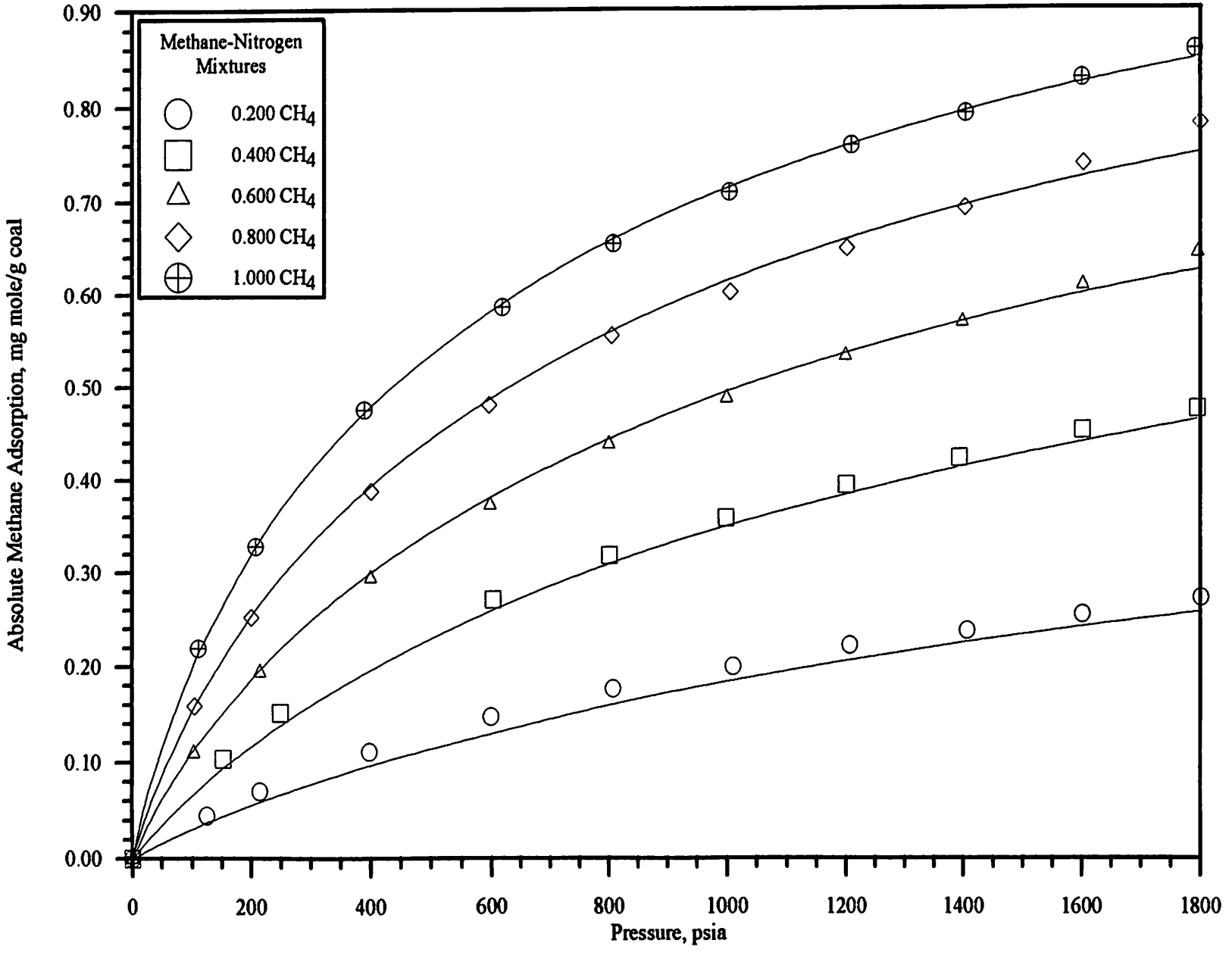

Figure 66. Loading Ratio Correlation Description of Methane-Nitrogen Mixtures: Methane Adsorption

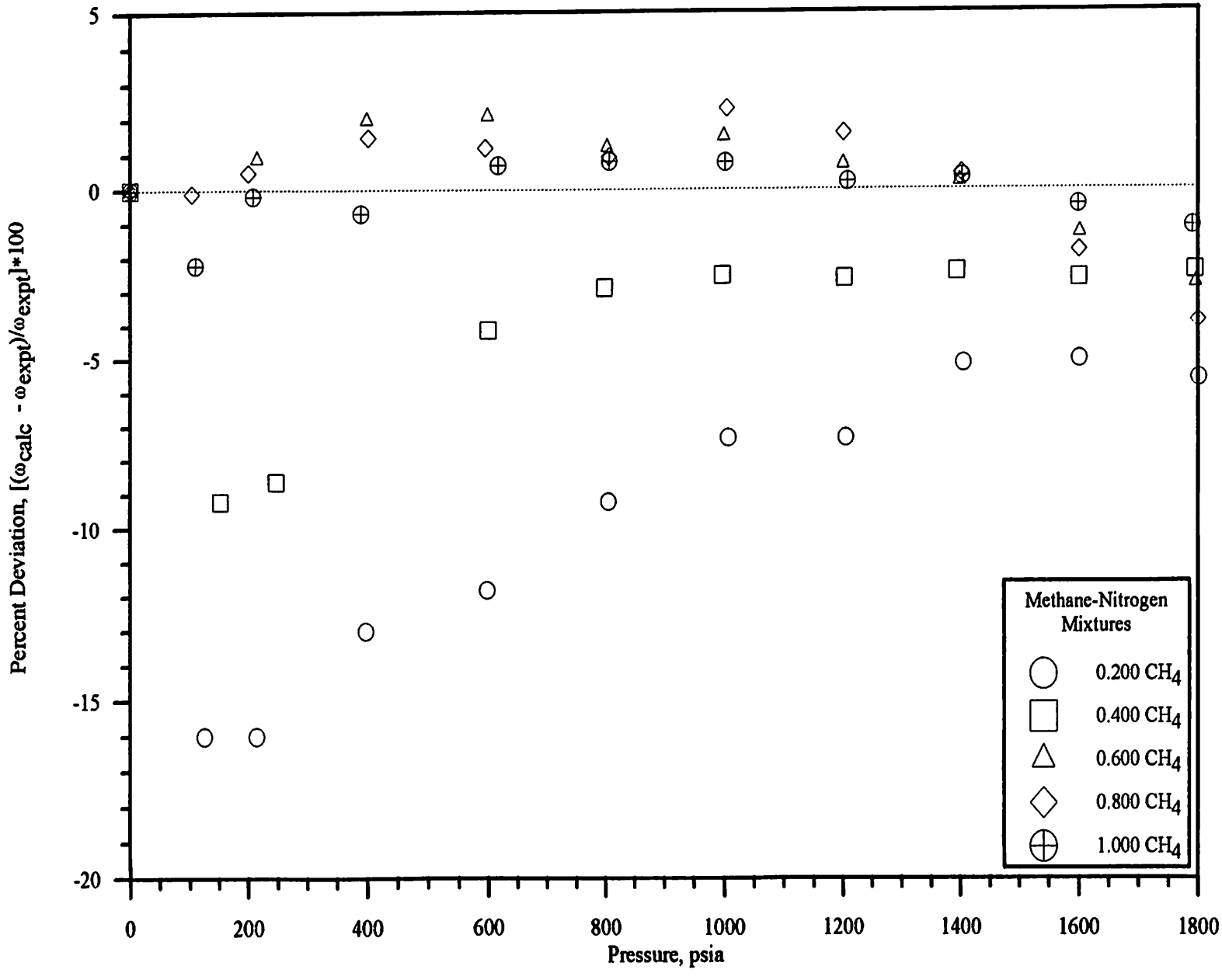

Figure 67. Deviations of Loading Ratio Correlation Predictions from Methane-Nitrogen Mixtures: Methane Adsorption

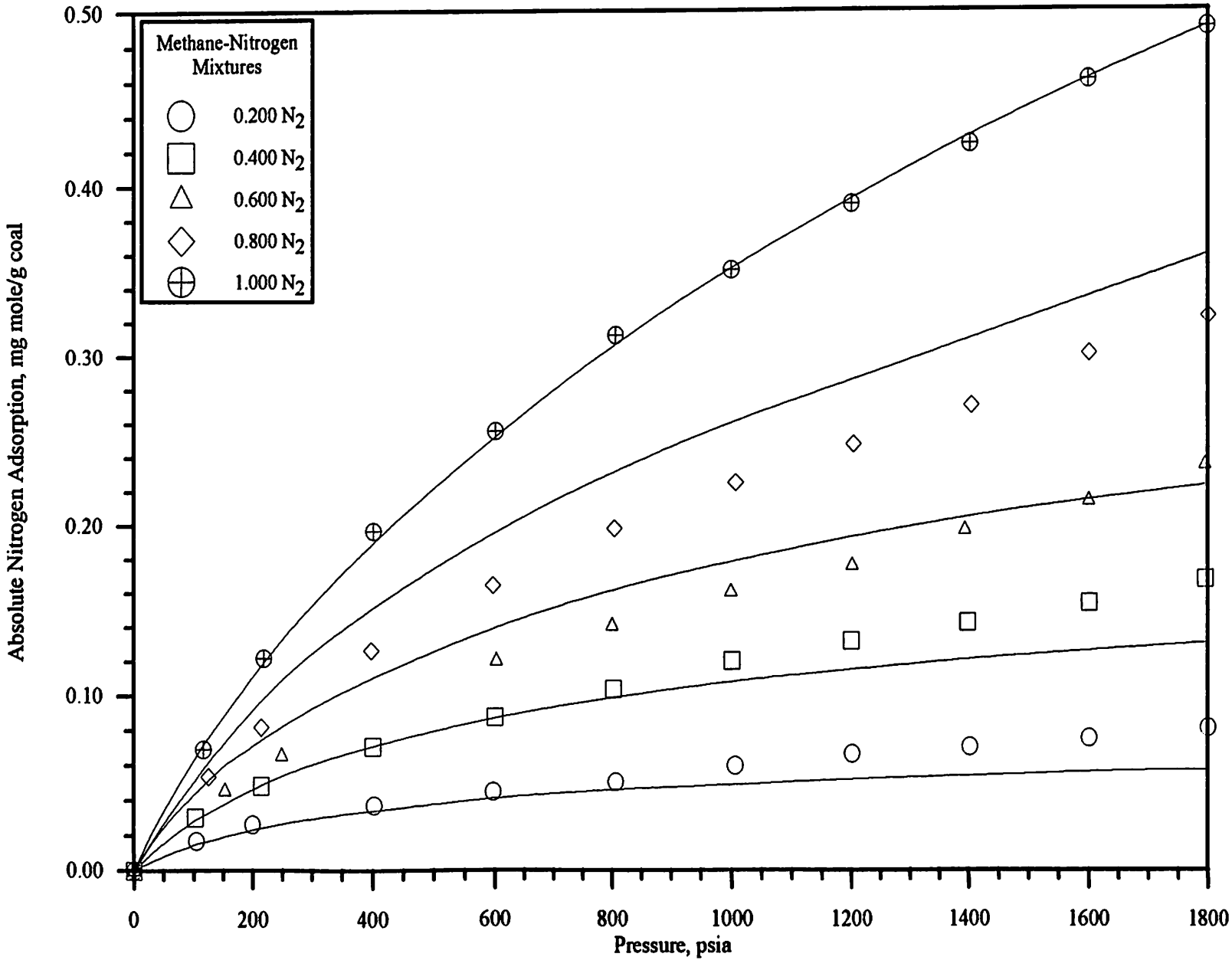

Figure 68. Loading Ratio Correlation Description of Methane-Nitrogen Mixtures: Nitrogen Adsorption

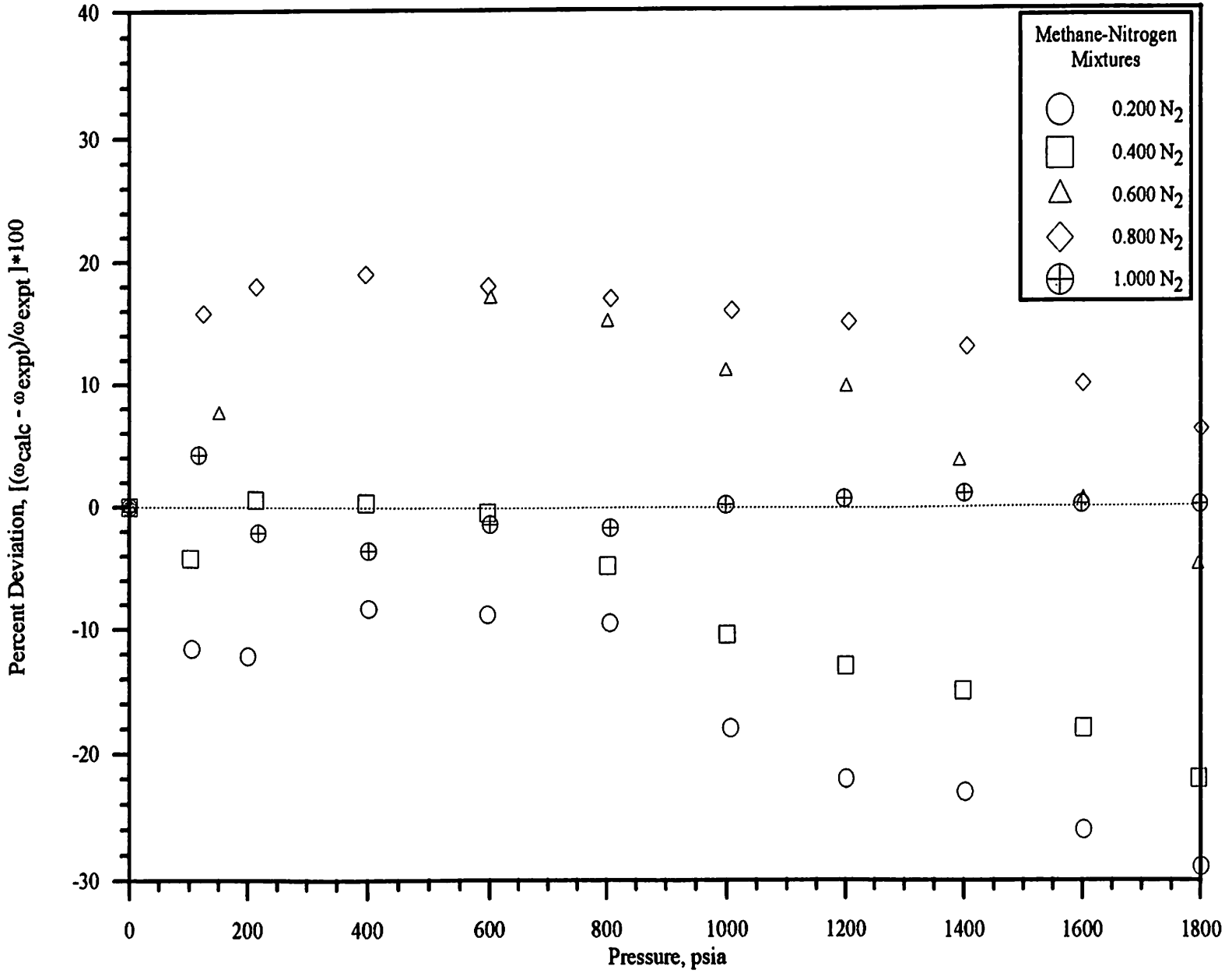

Figure 69. Deviations of Loading Ratio Correlation Prediction from Methane-Nitrogen Mixtures : Nitrogen Adsorption

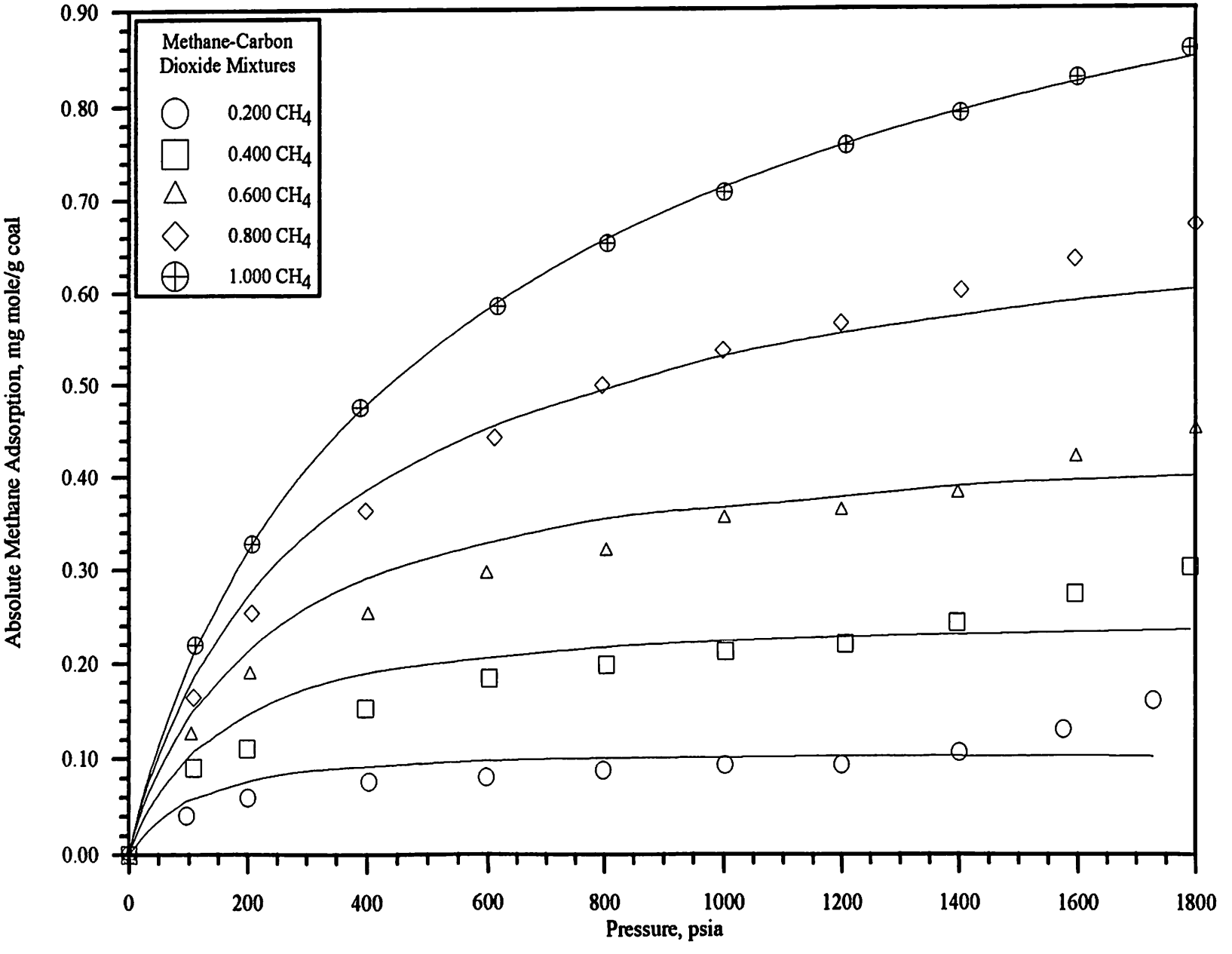

Figure 70. Loading Ratio Correlation Description of Methane-Carbon Dioxide Mixtures: Methane Adsorption

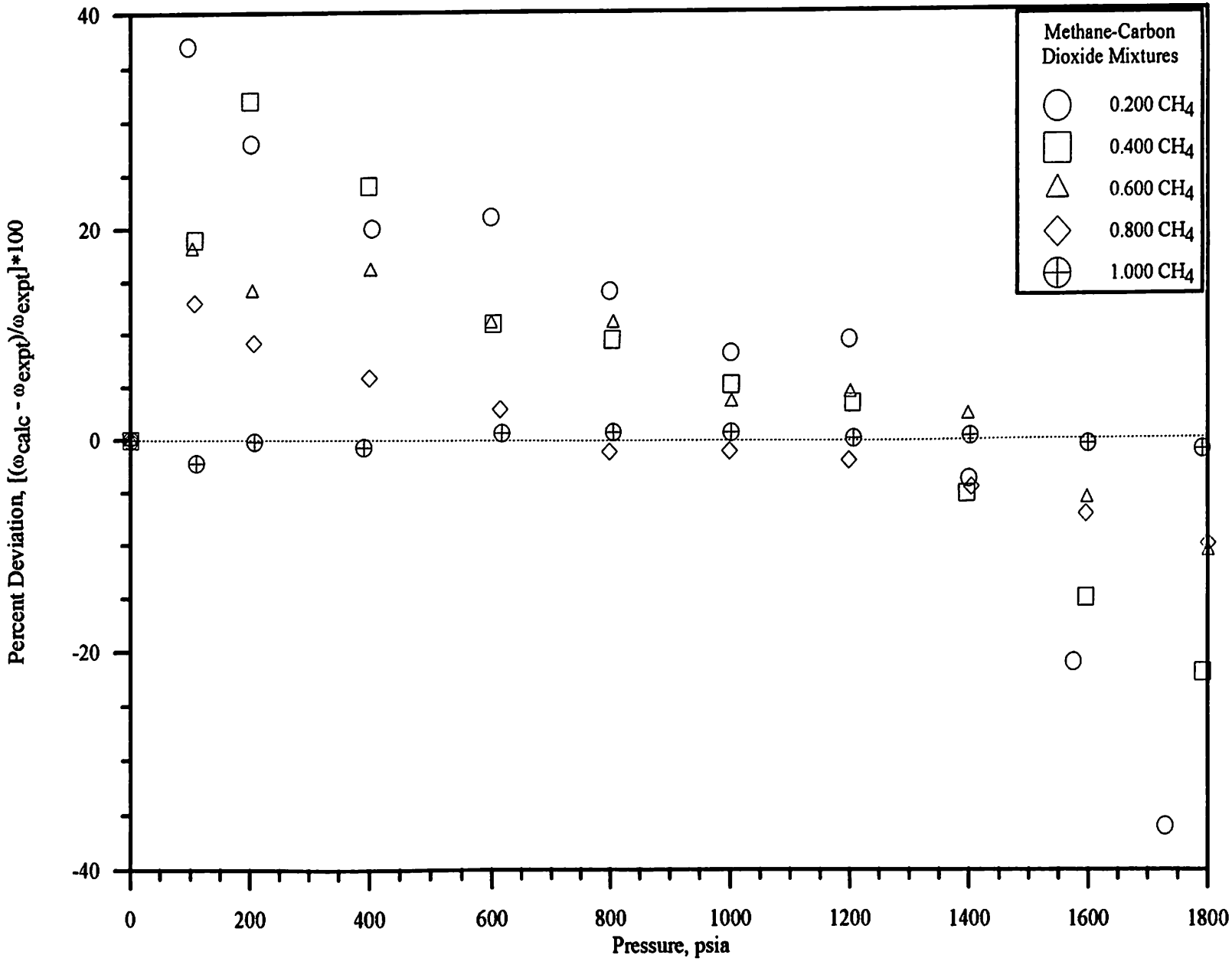

Figure 71. Deviations of Loading Ratio Correlation Prediction from Methane-Carbon Dioxide Mixtures: Methane Adsorption

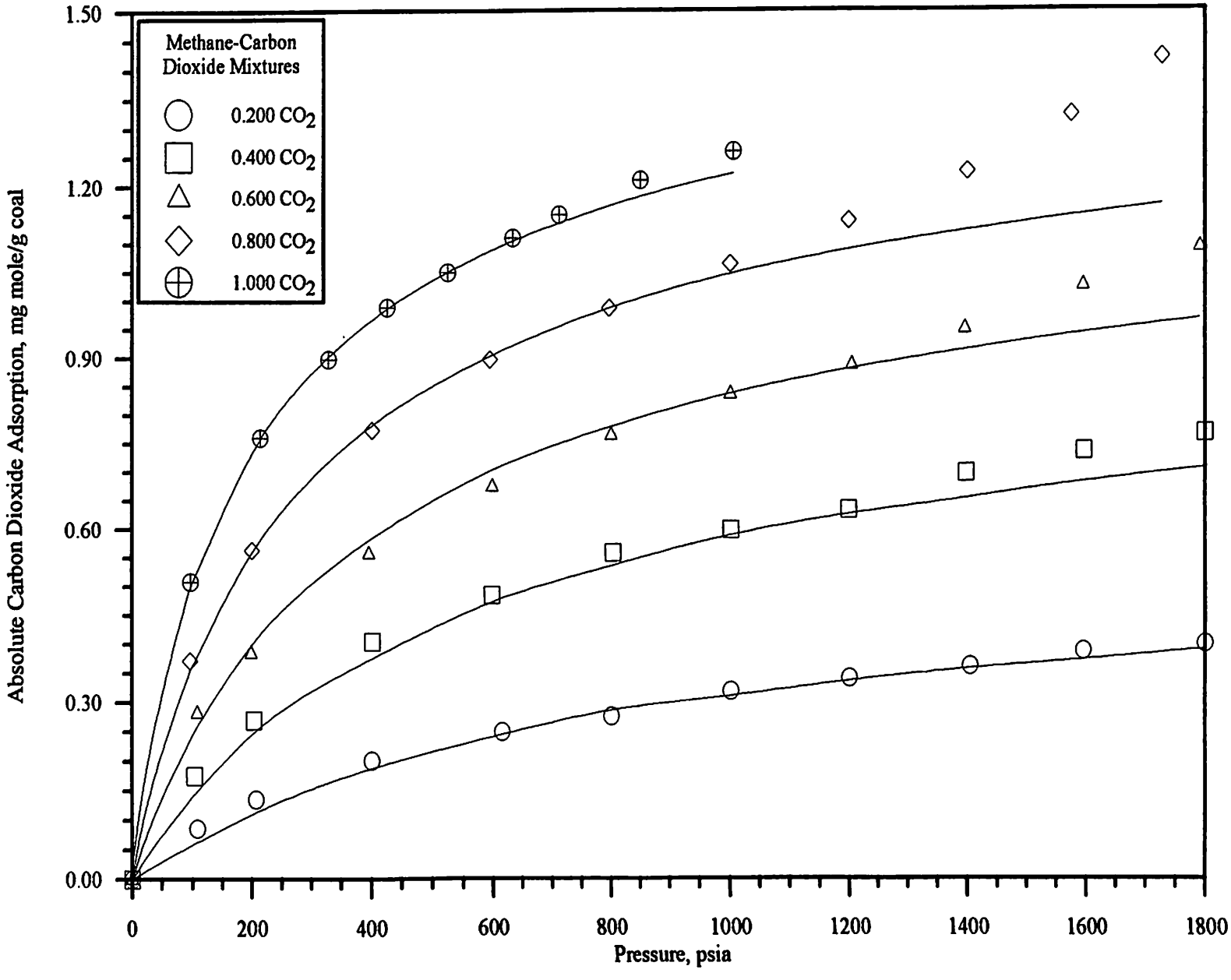

Figure 72. Loading Ratio Correlation Description of Methane-Carbon Dioxide Mixtures: Carbon Dioxide Adsorption

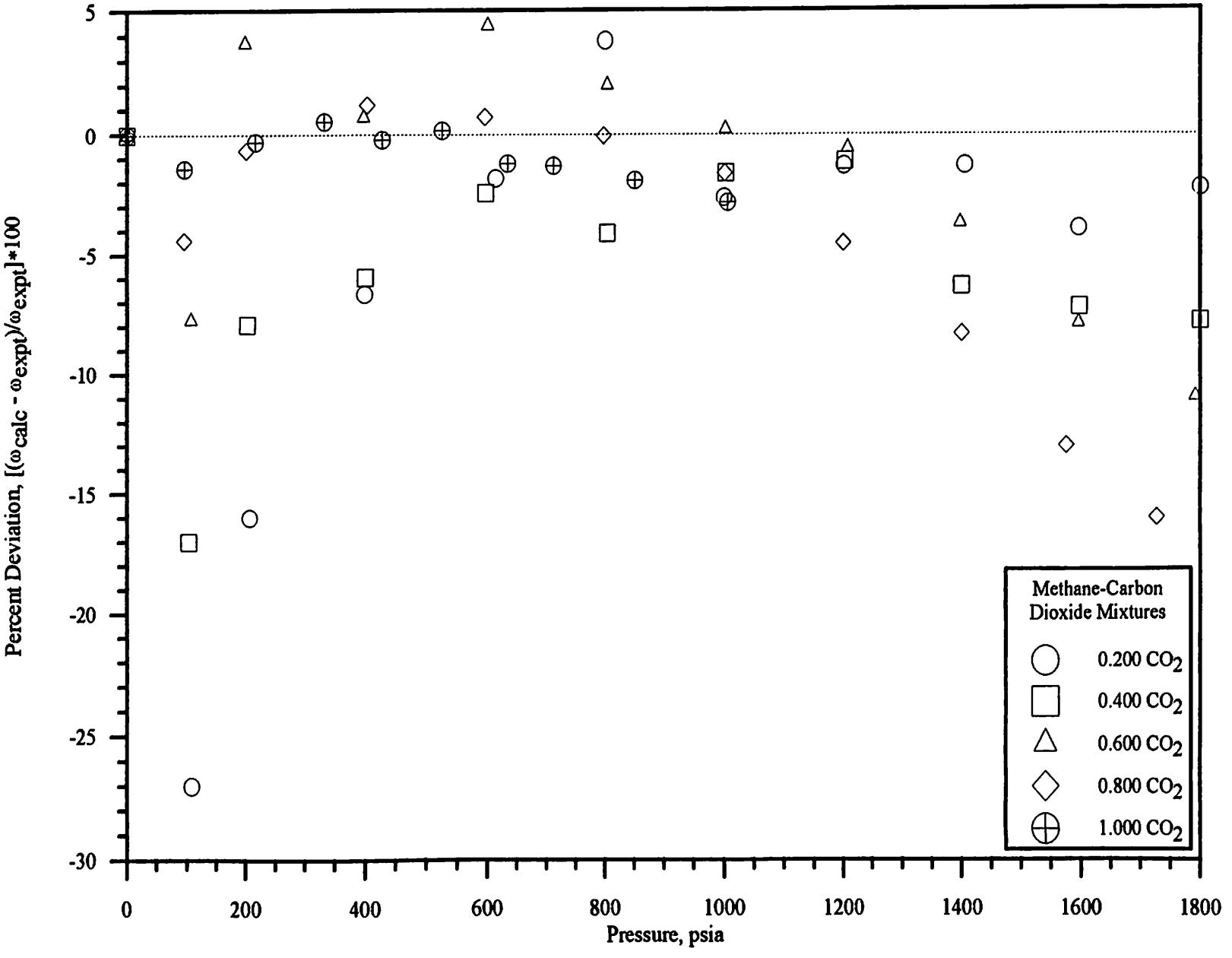

Figure 73. Deviations of Loading Ratio Correlation Prediction from Methane-Carbon Dioxide Mixtures: Carbon Dioxide Adsorption

and high pressure trends are similar to those described with earlier components. Model deviations (less than 1000 psi where the model should be applied) are consistent with the behavior mentioned previously, where methane is displaced preferentially by carbon dioxide. This shows up as over-predictions of methane adsorption by the simple model.

Figures 74 to 77 provide information for nitrogen/carbon dioxide mixtures. Figure 74 presents nitrogen adsorption as a function of pressure. The model can be seen to significantly misrepresent the experimental data, specifically at lower pressures. A deviation plot for nitrogen is seen in Figure 75 with deviations of 120 percent. A partial explanation for the large error is because so very little nitrogen is adsorbed. The model has difficulty, especially at low and mid-range pressures. Figure 76 illustrates carbon dioxide adsorption. The model appears to better predict the data than seen with nitrogen (Figure 74). The deviations (Figure 77) are less, but the model still has a difficult time at low pressures with deviations approaching 50 percent.

Discussion

The simple Langmuir is easily applied because of the two model constants, but is inadequate in describing even the pure component behavior. The simple Langmuir might be better served to be applied to low pressures. The Asymptotic Behavior Correlation provides a satisfactory fit to pure component data, but it is difficult to apply because of the five model constants.

The Loading Ratio Correlation does an excellent job of fitting pure component data; deviations are less than two percent. Binary mixture predictions are substantially worse (compared to pure components) as seen by the statistics tabulated in Table XXIX for binary mixtures. For mixtures, the model does a better job of predicting the adsorption behavior of the more highly adsorbed component.

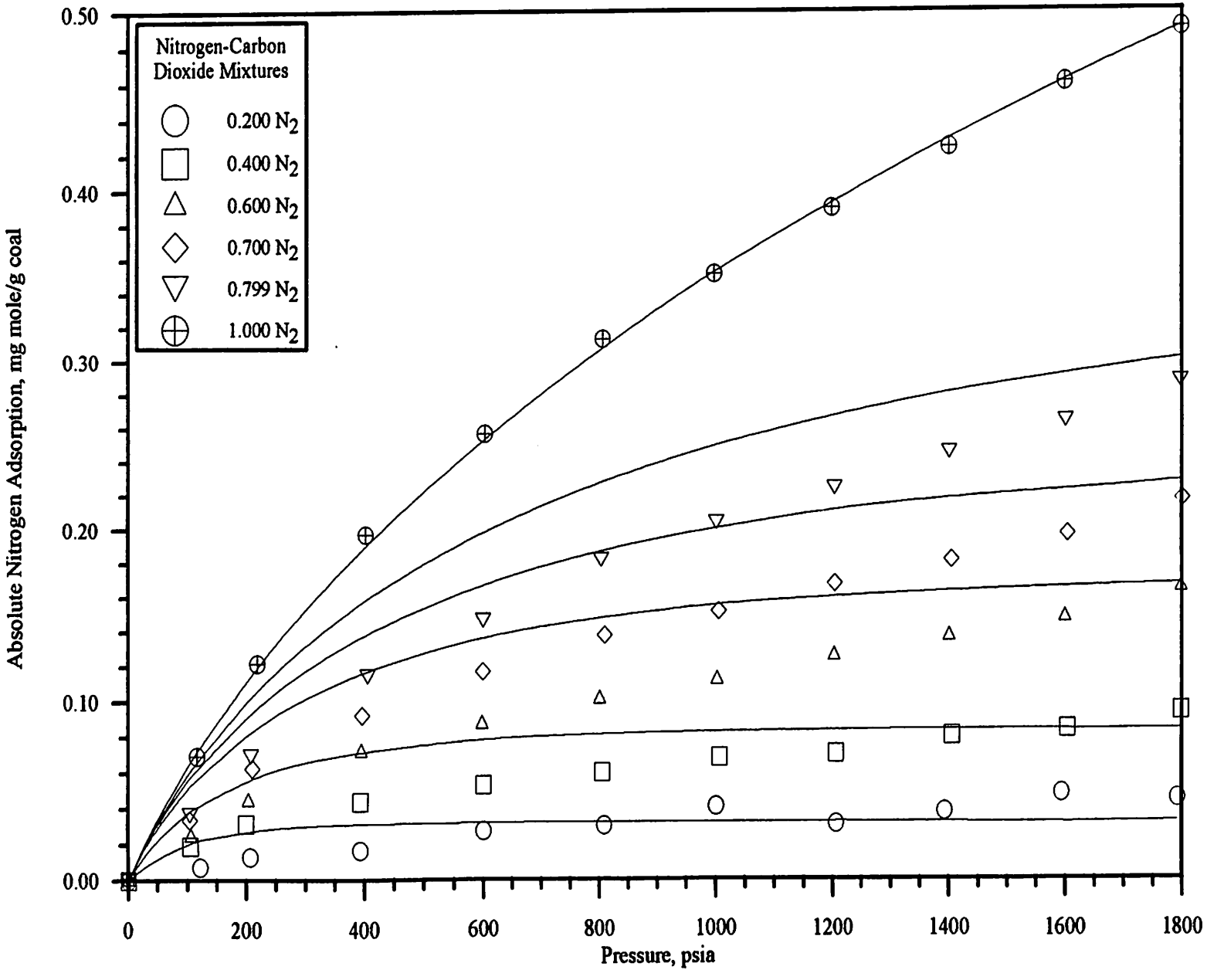

Figure 74. Loading Ratio Correlation Description of Nitrogen-Carbon Dioxide Mixtures: Nitrogen Adsorption

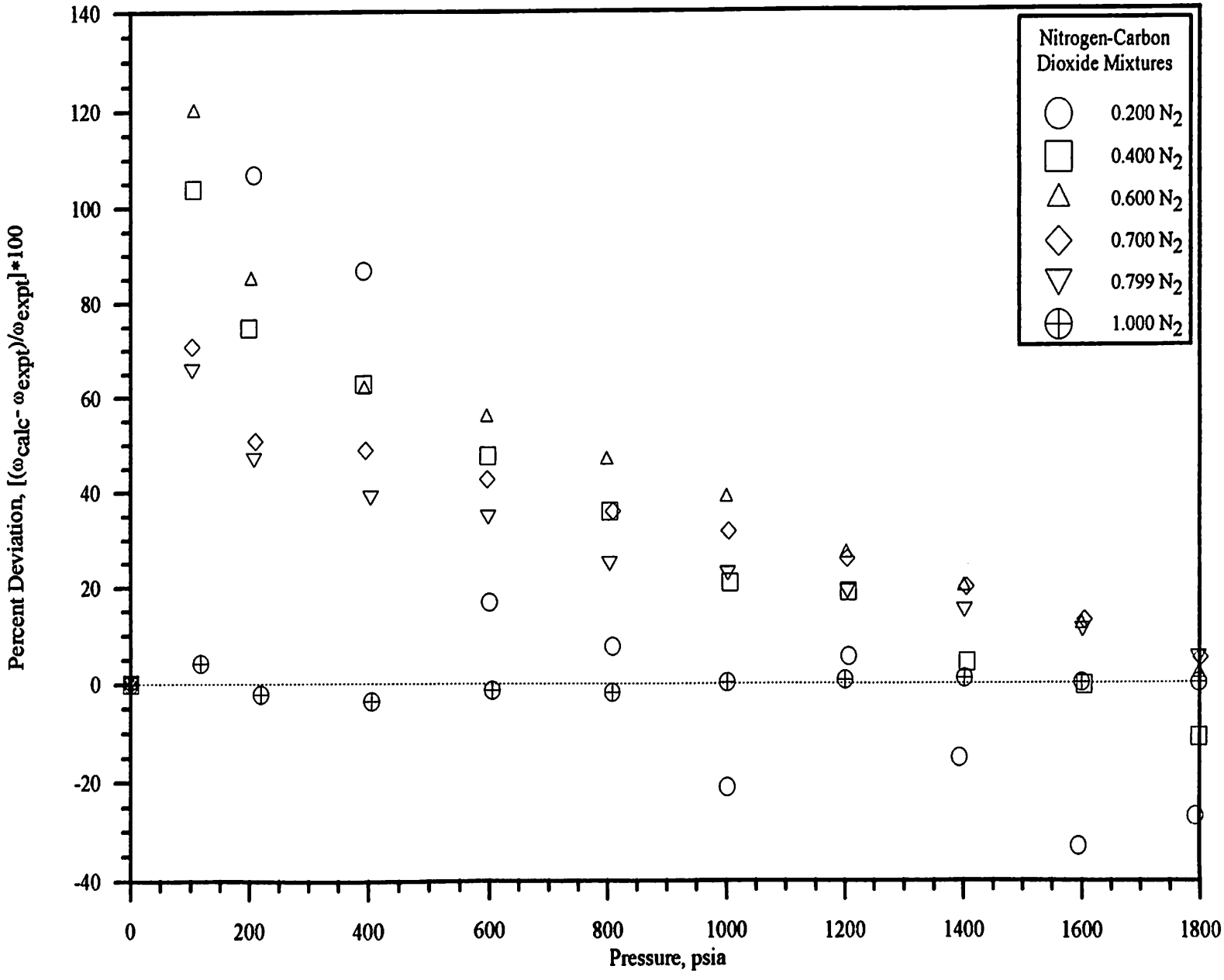

Figure 75. Deviations of Loading Ratio Correlation Prediction from Nitrogen-Carbon Dioxide Mixtures: Nitrogen Adsorption

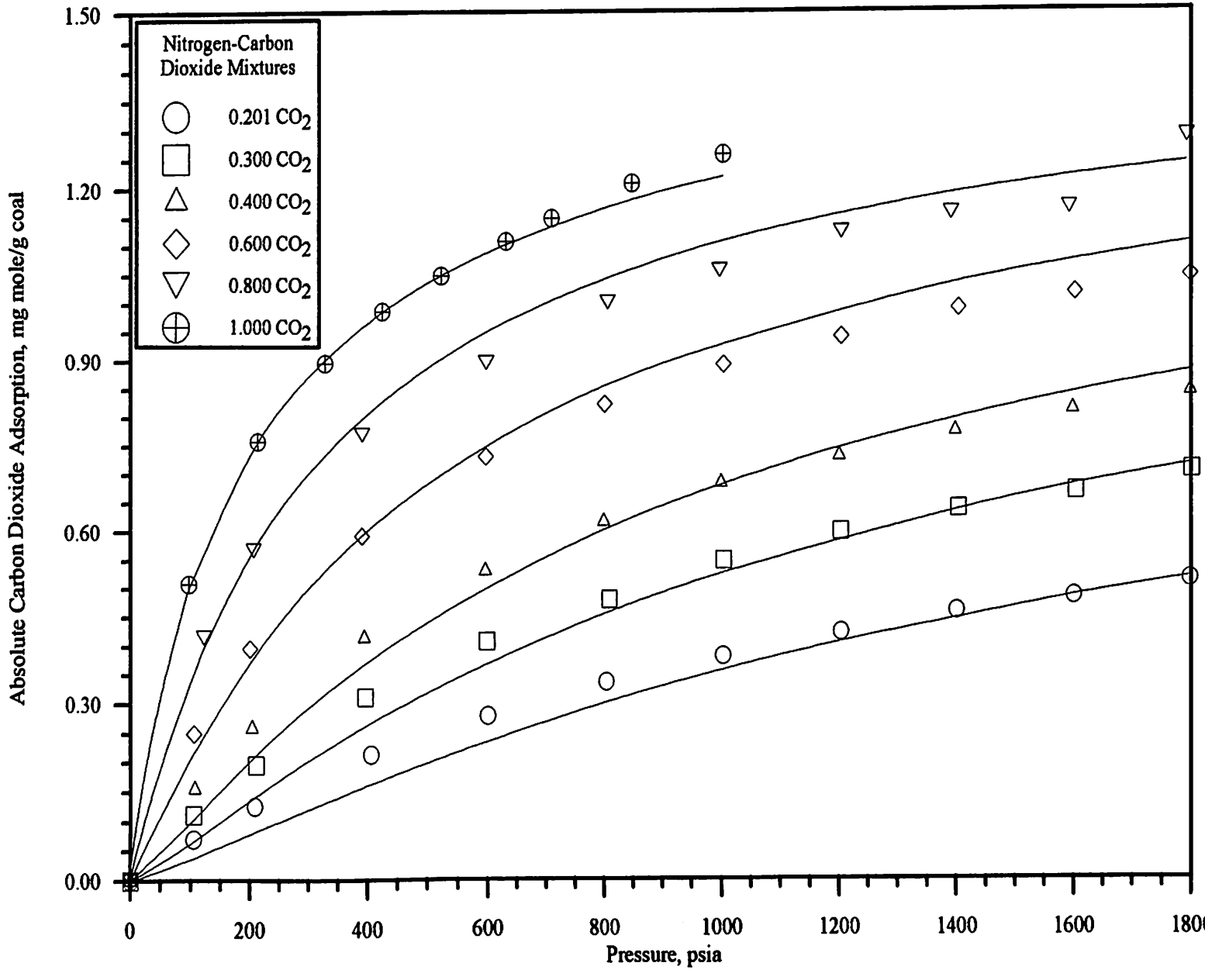

Figure 76. Loading Ratio Correlation Description of Nitrogen-Carbon Dioxide Mixtures: Carbon Dioxide Adsorption

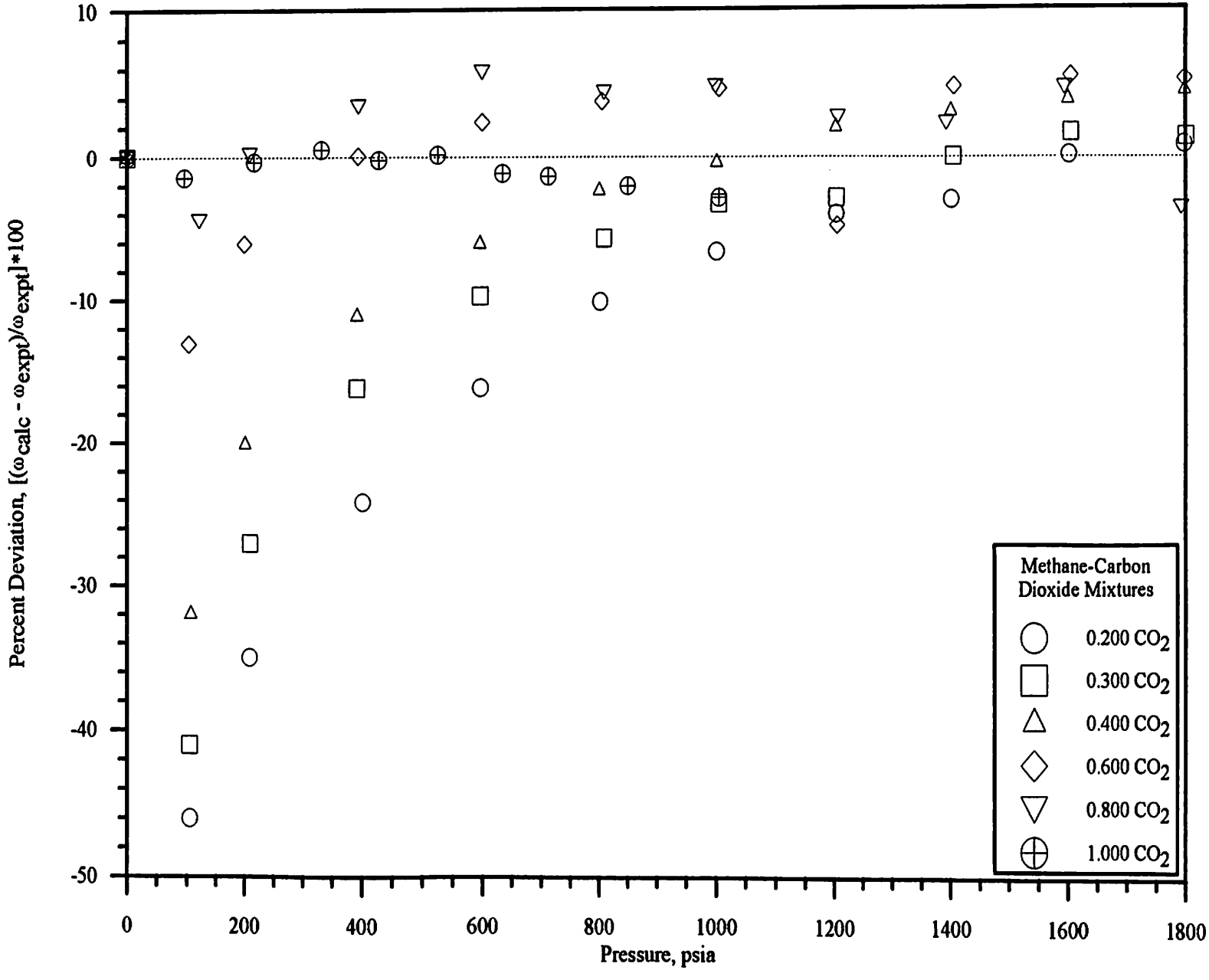

Figure 77. Deviations of Loading Ratio Correlation Prediction from Methane-Carbon Dioxide Mixtures: Carbon Dioxide Adsorption

For the component which adsorbs less, the model is less adequate in describing the behavior, significantly over-predicting at low and mid-range pressures. In comparing the AAPD for methane and nitrogen for the methane/nitrogen mixture, the AAPD values are 2.8 and 7.4, respectively. For the methane/carbon dioxide mixture, the AAPD values are 7.8 and 3.7. For the nitrogen\carbon dioxide mixture, the AAPD for nitrogen and carbon dioxide is 23 and 5.8, respectively.

TABLE XXIII

SIMPLE LANGMUIR MODEL FOR INDIVIDUAL PURE COMPONENT ADSORPTION ISOTHERMS

Component	Isotherm Identification	L, mg mole/g coal	B, $psia^{-1}$	RMSE	AAPD	WRMS
CH_4	OSU16	1.035	0.002226	0.017	2.1	1.5
CH_4	OSU23	1.004	0.002397	0.019	2.2	1.5
N_2	OSU17	0.9340	0.0006332	0.004	1.5	1.2
N_2	OSU19	0.8243	0.0007669	0.005	1.5	1.2
N_2	OSU20	0.8067	0.0007642	0.007	2.4	1.5
CO_2	OSU24	1.474	0.005277	0.024	1.2	1.1
CO_2	OSU25	1.369	0.005625	0.026	2.0	1.4
CO_2	OSU26	1.406	0.005673	0.026	1.8	1.3

TABLE XXIV

LOADING RATIO CORRELATION FOR INDIVIDUAL
PURE COMPONENT ADSORPTION ISOTHERMS

Component	Isotherm Identification	L, mg mole/g coal	B, $psia^{-1}$	η	RMSE	AAPD	WRMS
CH_4	OSU16	1.266	0.003785	0.846	0.003	0.4	0.6
CH_4	OSU23	1.239	0.004259	0.833	0.003	0.4	0.6
N_2	OSU17	1.224	0.0008284	0.900	0.001	0.3	0.6
N_2	OSU19	0.9936	0.0009969	0.915	0.003	1.1	1.0
N_2	OSU20	1.277	0.001134	0.837	0.001	0.4	0.6
CO_2	OSU24	1.545	0.006651	0.936	0.018	1.1	1.1
CO_2	OSU25	1.782	0.01373	0.732	0.005	0.4	0.6
CO_2	OSU26	1.712	0.01156	0.788	0.004	0.3	0.5

TABLE XXV

LOADING RATIO CORRELATION ($\eta = 0.87$) FOR INDIVIDUAL
PURE COMPONENT ADSORPTION ISOTHERMS

Component	Isotherm Identification	L, mg mole/g coal	B, $psia^{-1}$	η	RMSE	AAPD	WRMS
CH_4	OSU16	1.216	0.003511	0.87	0.005	0.5	0.7
CH_4	OSU23	1.170	0.003801	0.87	0.006	0.7	0.8
N_2	OSU17	1.369	0.0008663	0.87	0.001	0.5	0.7
N_2	OSU19	1.139	0.001104	0.87	0.003	1.2	1.1
N_2	OSU20	1.124	0.001086	0.87	0.002	0.6	0.8
CO_2	OSU24	1.640	0.008353	0.87	0.014	1.1	1.1
CO_2	OSU25	1.513	0.008997	0.87	0.016	1.1	1.1
CO_2	OSU26	1.561	0.008949	0.87	0.012	0.8	0.9

TABLE XXVI

ASYMPTOTIC FUNCTION MODEL CONSTANTS FOR INDIVIDUAL PURE COMPONENT ADSORPTION ISOTHERMS

Component	Isotherm Identification	C_1 mgmol/g coal	C_2	C_3	C_4	C_5 psia	RMSE	AAPD	WRMS
CH_4	OSU16	0.87	11.5	0.854	1.43	1800	0.008	1.0	1.0
CH_4	OSU23	0.87	11.5	0.746	1.58	1800	0.008	1.1	1.0
N_2	OSU17	0.50	11.5	0.638	1.13	1800	0.005	0.7	0.8
N_2	OSU19	0.50	11.5	0.589	1.20	1800	0.004	1.4	1.2
N_2	OSU20	0.50	11.5	0.510	1.29	1800	0.004	0.9	0.9
CO_2	OSU24	1.5	11.5	0.731	1.81	1300	0.016	2.1	1.6
CO_2	OSU25	1.5	11.5	0.362	2.52	1300	0.011	1.5	1.4
CO_2	OSU26	1.5	11.5	0.417	2.45	1300	0.013	1.6	1.5

TABLE XXVII

CUMULATIVE PURE COMPONENT ADSORPTION MODEL STATISTICS

Component	Model	L, mg mol/g coal	B, $psia^{-1}$	η	C_1 mg mol/g coal	C_2	C_3	C_4	C_5, $psia^{-1}$	RMSE	AAPD	WRMS
CH_4	Simple Langmuir	1.019	0.002311	—	—	—	—	—	—	0.022	2.5	1.6
CH_4	Loading Ratio	1.191	0.003663	0.87	—	—	—	—	—	0.022	0.7	0.8
CH_4	Asymptotic	—	—	—	0.87	11.5	0.800	1.50	1800	0.010	1.3	1.1
N_2	Simple Langmuir	0.8550	0.000721	—	—	—	—	—	—	0.022	2.1	1.4
N_2	Loading Ratio	1.204	0.001041	0.87	—	—	—	—	—	0.022	1.7	1.3
N_2	Asymptotic	—	—	—	0.50	11.5	0.579	1.21	1800	0.007	1.6	1.3
CO_2	Simple Langmuir	1.416	0.005525	—	—	—	—	—	—	0.022	2.2	1.5
CO_2	Loading Ratio	1.557	0.008886	0.87	—	—	—	—	—	0.022	1.7	1.3
CO_2	Asymptotic	—	—	—	1.50	11.5	0.503	2.26	1200	0.050	2.0	1.8

TABLE XXVIII

LOADING RATIO CORRELATION CONSTANTS USED WITH BINARY MIXTURES

Component	L, mg mole/g coal	B, $psia^{-1}$	Constant η
CH_4	1.191	0.003663	0.87
N_2	1.204	0.001041	0.87
CO_2	1.557	0.008886	0.87

TABLE XXIX

LOADING RATIO CORRELATION STATISTICS FOR BINARY MIXTURES

Mixture	Component	RMSE	AAPD	WRMS
CH_4-N_2	CH_4	0.010	2.8	1.7
	N_2	0.015	7.4	2.7
CH_4-CO_2	CH_4	0.023	7.8	2.8
	CO_2	0.046	3.7	1.9
N_2-CO_2	N_2	0.024	23	4.8
	CO_2	0.031	5.8	2.4

CHAPTER IX

CONCLUSIONS AND RECOMMENDATIONS

Conclusions

The following conclusions were made concerning the adsorption of pure methane, nitrogen, carbon dioxide and their binary mixtures on a wet Fruitland coal at 115°F and pressures to 1800 psia.

(1) Experimental data on adsorption of pure methane, nitrogen, carbon dioxide and their binary mixtures were determined on Fruitland coal with uncertainties of one to three percent for pure components and two to seven percent for components in the binary mixture.

(2) These data provide an improved basis for design and optimization of production methods for enhanced the recovery of coalbed methane.

(3) The type of adsorption observed for pure methane, nitrogen and methane/nitrogen mixtures is monomolecular, monolayer adsorption, classified as Type I adsorption.

(4) The type of adsorption observed for pure carbon dioxide and carbon dioxide mixtures is monomolecular at lower pressures with possible multilayer adsorption occurring at higher pressures.

(5) The multicomponent gas adsorption data indicate that different gas species are competing for the same sorption sites, as illustrated by the non-linearity (non-ideality) of the adsorption versus composition relation. The competing components theory is confirmed by the non-ideal behavior exhibited in the

adsorbate mole fraction as a function of gas phase mole fraction ($x_{adsorbate}$ versus y_{gas}) relations.

(6) Carbon dioxide has been shown to displace methane from the coal surface better than nitrogen (greater displacement efficiency).

(7) The Loading Ratio Correlation adequately describes the pure component adsorption behavior of methane and nitrogen (AAPD's of 0.7-1.7 %). It also describes pure carbon dioxide behavior at pressures below 1000 psia (AAPD of 1.7 %). The model cannot describe the high pressure adsorption behavior of carbon dioxide, which appears to be other than Type I adsorption.

(8) The extended Loading Ratio Correlation provides a useful qualitative description of mixture behavior. However, in a quantitative sense, errors (AAPD) ranged from 3 to 23 %.

(9) Use of a Loading Ratio Correlation constant of $\eta = 0.87$ is justified (for the systems here) by the fact that the model describes the pure components within their predicted experimental uncertainties.

(10) Trends in the Loading Ratio Correlation appear similar for each pure component and binary mixture. The model tends to under-predict at low and high pressures and over-predict at mid-range pressures. This suggests an inherent characteristic model limitation.

(11) The simple Langmuir model is easily applied and adequate for describing pure component adsorption for the current work (AAPD's of 2.5 %).

(12) The Asymptotic Behavior Correlation adequately describes the pure component adsorption (AAPD's of 1.3 %). However, it is more difficult to apply than the Langmuir model or Loading Ratio Correlation because it requires five model constants.

(13) At high pressures, the volume occupied by the adsorbed phase is large enough to yield a significant difference (15 %) between the Gibbs and

absolute adsorption values. The adsorbed phase volume cannot be neglected.

(14) Error propagation analysis identified the major factors contributing to the overall adsorption uncertainty. Reductions in the overall uncertainty can be accomplished by reducing the cell section void volume, reducing the injection pump dead volume, improving estimates for the adsorbed phase molar volume and designing better methods for synthesizing and analyzing gas mixtures.

(15) The experimental data are consistent with the literature contention that the adsorption capacity of the coal is independent of the moisture content as long as the moisture is maintained above the equilibrium moisture content.

(16) The experimental data are consistent with the literature contention that the adsorption strength is a function of the boiling points at atmospheric pressure. The higher the boiling point for a pure component gas, the greater will be the sorption capacity of the gas.

Recommendations

Within the course of collecting the experimental data, a number of refinements became apparent which could reduce the overall experimental uncertainty and minimize equipment malfunctions, yielding faster, better results. A few important recommendations appear below.

(1) Obtain better estimates for the adsorbed phase volume. The majority of the experimental uncertainty is the result of uncertainties in the adsorbed phase volume estimates. Haydel and Kobayashi have presented an expression for the adsorbed phase volume which is a function of pressure and temperature and could yield more realistic estimates of the adsorbed phase volume. The current work neglected any temperature influence.

(2) Minimize the void volume within the equilibrium cell-section to reduce the experimental uncertainties. In the present design, this is the second largest contributor to the overall uncertainty. Reductions in void volume will decrease the overall experimental uncertainty, and could be accomplished by using a different circulation pump (magnetically stirred) design.

(3) Reduce the dead volume in the positive displacement injection pump. New pump designs have the pump packing attached to the plunger, minimizing the injection pump dead volume.

(4) Replace the magnetic circulation pump with a pump which requires less maintenance. A different design which may serve this purpose has been described Drake, Dunbar and Smith.

(5) Minimize the number of fittings in the system. The most time-consuming problem was tracing high pressure leaks. The majority of the time, leak

were not large enough to be detected by the helium leak detector and required that the system be monitored over an extended period of time.

(6) Modify the pressure and/or temperature conditions in the pump section to minimize uncertainties in the gas compressibility factors. For example, methane at the temperature and pressure of interest has uncertainties in the compressibility factor approaching 0.3 %. Cell-section conditions are fixed by the field conditions of interest, but the pump-section conditions can be changed to minimize the uncertainties. The change could require only that the injection pump pressure and/or temperature be changed to values where the compressibility factors are more accurately known (i.e., less sensitive to pressure/temperature fluctuations).

(7) Utilize improved models for representing compressibility factors. A one percent change in compressibility factor (for mixtures) propagates into a ten percent difference in the calculated adsorption.

(8) Collect experimental data at different temperatures. Only one isotherm was of interest for the current work. Repeat similar tests at additional temperatures (80-150°F). This additional information will help define adsorption (of these gases on this adsorbent) as a function of temperature.

(9) Collect data at more mixture compositions, and higher pressures in order to further define physical adsorption on wet Fruitland coal and to confirm the results (trends) seen with other mixtures.

(10) Test more adsorption models and improve existing models. The existing models (e.g., Loading Ratio Correlation) does an adequate job for pure component behavior, but when extended to mixtures, the correlations fail. The extended Loading Ratio Correlation is not adequate to describing (a) the Type II adsorption (high pressures) occurring with the CH_4-CO_2 and N_2-CO_2 mixtures, (b) adsorption of the least-adsorbed component, and (c) the low

and high pressure adsorption behavior of both pure components and mixtures.

REFERENCES

1. Adamson, A. W., "Physical Chemistry of Surfaces," John Wiley and Sons, New York (1982).

2. Angus, S., K. M. de Reuck, and B. Armstrong, "International Thermodynamic Tables of the Fluid State Carbon Dioxide," International Union of Pure and Applied Chemistry, Pergamon Press, New York (1977).

3. Angus, S., K. M. de Reuck, and B. Armstrong, "International Thermodynamic Tables of the Fluid State-6 Nitrogen," International Union of Pure and Applied Chemistry, Pergamon Press, New York (1977).

4. Arri, L. E., D. Yee, W. D. Morgan, and M. W. Jeansome, *Modeling Coalbed Methane Production with Binary Gas Sorption*, SPE Report 24363, May 1992.

5. Baughman, G. L., "Synthetic Fuels Data Handbook," Cameron Engineers, Inc., Denver, Colorado (1978).

6. Castellan, G. W., "Physical Chemistry," Addison-Wesley Publishing Company, Reading, Massachusetts (1983).

7. David, D. J., "Gas Chromatographic Detectors," John Wiley and Sons, New York (1974).

8. De Boer, J. H., "The Dynamical Character of Adsorption," Second Edition, Oxford University Press, Ely House, London (1968).

9. DeGance, A. E., *Multicomponent High Pressure Adsorption Equilibria on Carbon Substrates*, Amoco Production Company, Report 90319ART0008, November 1990.

10. Dillard, D. D., M. Waxman, and R. L. Robinson, Jr., *Volumetric Data and Virial Coefficients for Helium, Krypton, and Helium-Krypton Mixtures*, Jour. Chem. Eng. Data, Vol. 23, No. 4, 269-274, October 1978.

11. Drake, B. D., M. T. Dunbar, and R. L. Smith, Jr., *An Easy to Construct, Economical, Safe, High-pressure Magnetic Pump for Pressures to 140 MPa Suitable for Circulation of Supercritical Fluids*, American Institute of Physics, Vol. 61, No. 9, Sept. 1990.

12. Dymond, J. H., and E. B. Smith, "The Virial Coefficients of Pure Gases and Mixtures," Clarendon Press, Oxford (1980).

13. Ettre, L. S., and Zlatkis, A., "The Practice of Gas Chromatography," Interscience Publishers, New York (1967).

14. Felder, R. M., and R. W. Rousseau, "Elementary Principles of Chemical Processes," John Wiley and Sons, New York (1986).

15. Gasem, Khaled M., Personal Communication, Oklahoma State University, (1991-1993).

16. Gilmer, H. B., and R. Kobayashi, *The Study of Gas-Solid Equilibrium at High Pressures by Gas-Chromatography: Part I. Ethane, Propane, and n-Butane at Essentially Infinite Dilutions in the Methane-Silica Gel System*, A.I.Ch.E. Journal, Vol. 10, No. 6, 797-803

17. Goodwin, R. D., "The Thermophysical Properties of Methane, from 90 to 500 K at Pressures to 700 Bar," National Bureau of Standards Technical Note 653, Department of Commerce (1974).

18. Haney, R. D., and H. Bliss, *Compressibilities of Nitrogen-Carbon Dioxide Mixtures*, Ind. Eng. Chem Fund., Vol. 36, No. 11, 989-993, November 1944.

19. Haydel, J. J., and R. Kobayashi, *Adsorption Equilibria in the Methane-Propane-Silica Gel System at High Pressures*, Ind. Eng. Chem. Fund., Vol. 6, No. 4, 546-554, November 1967.

20. Holste, J. C., et. al., "Properties of CO_2 Mixtures with N_2 and with CH_4," Gas Processors Association and Gas Research Institute, Research Report RR-122, Tulsa, Oklahoma (1989).

21. Keyes, F. G., and H. G. Burks, *The Equation of State for Binary Mixtures of Methane and Nitrogen*, Ind. Eng. Chem., Vol. 50, 1100-1106, April 1928.

22. McCarty, R. D., "Thermophysical Properties of Helium-4 from 2 to 1500 K with Pressures to 1000 Atmospheres," National Bureau of Standards Technical Note 631, Department of Commerce (1972).

23. McNair, H. M., and Bonelli, E. J., "Basic Gas Chromatography," Varian Aerograph, Walnut Creek, California (1969).

24. Myers, A. L., and J. M. Prausnitz, *Thermodynamics of Mixed-Gas Adsorption*, A.I.Ch.E. Journal, Vol. 11, No. 1, 121-129, January 1965.

25. Payne, H. K., G. A. Sturdevant, and T. W. Leland, *Improved Two-Dimensional Equation of State to Predict Adsorption of Pure and Mixed Hydrocarbons*, Ind. Eng. Chem. Fund., Vol. 7, No. 3, 363-374, August 1968.

26. Reamer, H. H., R. H. Olds, B. H. Sage, and W. N. Lacey, *Phase Equilibria in Hydrocarbon Systems*, Ind. Eng. Chem., Vol. 36, No. 2, January 1944.

27. Rightmire, C. T., G. E. Eddy, and J. N. Kerr, "Coalbed Methane Resources of the United States," American Association of Petroleum Geologists, Tulsa, Oklahoma (1984).

28. Robinson, R. L., Jr., *Adsorption Studies for Optimum Production of Coalbed Methane*, Progress Report to Amoco Production Company, (1992).

29. Robinson, R. L., Jr., Personal Comunication, Oklahoma State University, (1991-1993).

30. Ross, S., and J. P. Oliver, "On Physical Adsorption," Interscience Publishers, John Wiley and Sons, New York (1964).

31. Sandler, S. I., "Chemical and Engineering Thermodynamics," John Wiley and Sons, New York (1989).

32. Shoemaker, D. P., et. al., "Experiments in Physical Chemistry," McGraw-Hill Book Company, New York (1981).

33. Smith, J. M., and H. C. van Ness, "Introduction to Chemical Engineering Thermodynamics," McGraw-Hill Book Company, New York, (1987).

34. Tsederberg, N. V., V. N. Popov, and N. A. Morozova, "Thermodynamic and Thermophysical Properties of Helium," Wiener Bindery Ltd., Jerusaleum (1971).

35. Van Ness, H. C., *Adsorption of Gases on Solids*, Ind. Eng. Chem. Fund., Vol. 8, No. 3, 464-473, August 1969.

36. Wojciechowski, B. W., and C. C. Hsu, W. Can. J. Chem. Eng., 1985, Vol. 63, 789.

37. Yang, R. T., "Gas Separation by Adsorption Processes," Butterworths, Boston, (1987).

38. Young, D. M., and A. D. Crowell, "Physical Adsorption of Gases," Butterworths, Washington D.C. (1962).

39. Younglove, B. A., "Thermophysical Properties of Fluids. I. Argon, Ethylene, Parahydrogen, Nitrogen, Nitrogen Trifluoride, and Oxygen," Journal of Physical and Chemical Reference Data, Vol. 11, No. 1, 1-162 to 1-255, 1982.

40. Hall, F. E., Adsorption Experiment Supplementary Material, School of Chemical Engineering, Oklahoma State University, (1993).

41. Zhou, C., Ph.D. Dissertation, Oklahoma State University, in preparation (1993).

42. Grapher for Windows, Golden Software, Inc., (1993).

43. ElectroChem, OLI Systems, Inc., Morris Plains, NY, (1991).

APPENDICES

APPENDIX A

GAS COMPRESSIBILITY FACTORS

APPENDIX A

GAS COMPRESSIBILITY FACTORS

The accuracies of the compressibility factors used in the pure component and mixture calculations are critical to the adsorption computations. In mixture adsorption experiments, a one percent error in compressibility factor can propagate into a ten percent error in the adsorption values. An accurate compressibility factor is necessary for proper processing of experimental data.

Helium is used to perform the void volume test which determines the gas volume (V_{void}) within the recirculation loop of the cell section. This gas phase volume is extremely important to all calculations as discussed in the error analysis. All void volume tests were performed over a pressure range of 100-1000 psia (150 psia intervals). The compressibility factors for helium were calculated from a virial infinite-series expansion [33] written as a function of pressure (atms) and truncated after the linear term as in Equation A-1. Compressibility factor data were obtained from National Bureau of Standards Technical Note 631 for helium, [22].

$$Z_{He} = 1 + B(T)\, P_{atm} \qquad \text{(A-1)}$$

$$B(T) = 0.001471 - 4.779\text{E-}6\, T_K + 4.920\text{E-}9\, T^2_K \qquad \text{(A-2)}$$

Second virial coefficient data as a function of temperature was obtained from the above reference and fit to a second order polynomial describing the virial coefficient as a function of temperature. The data were fit at four isotherms (250,

300, 350, 400 K) using a least-squares method. The temperatures of experimental interest are 96.6°F (309.3 K) and 115.0°F (319.3 K) for the pump and cell sections, respectively. Equation A-2 describes the second virial coefficient as a function of temperature.

The calculated second virial coefficients and compressibility factors were compared to and agreed with literature (within 0.2 percent) [10]. The above functions were used to calculate the compressibility factor for the four isotherms and compared to experimental data with the residuals shown in Figure 78. Data (300 and 350 K) were obtained from the National Bureau of Standard Technical Note 631 and (313.15, 323.15 K) from "Thermodynamic and Thermophysical Properties of Helium" [22]. The latter reference was used because the isotherms (313.15, 323.15 K) were closer to the pump and cell section temperatures (309.3 and 319.3 K). As seen in Figure 78, the truncated virial expansion does an excellent job of predicting the correct compressibility factor for helium, with a residual not exceeding 0.04 percent throughout the pressure range (100-1000 psia) of interest.

Pure methane compressibility factors were calculated from an equation by Jacobsen and Stewart documented in the International (IUPAC) Thermodynamic Tables for methane [17]. The equation is complex (32 constants) with the ability to cover the temperature from the triple point to over 400 K and pressures to 400 bar (5800 psi). The expression is given as

$$
\begin{aligned}
Z = 1 &+ \omega(N_1 + N_2\tau^{0.5} + N_3\tau + N_4\tau^2 + N_5\tau^3) + \omega^2(N_6 + N_7\tau + N_8\tau^2 + N_9\tau^3) \\
&+ \omega^3(N_{10} + N_{11}\tau + N_{12}\tau^2) + \omega^4(N_{13}\tau) + \omega^5(N_{14}\tau^2 + N_{15}\tau^3) + \omega^6(N_{16}\tau^2) \\
&+ \omega^7(N_{17}\tau^2 + N_{18}\tau^3) + \omega^8(N_{19}\tau^3) + \omega^2 e^{\alpha\omega^2}[(N_{20}\tau^3 + N_{21}\tau^4) \\
&+ \omega^2(N_{22}\tau^3 + N_{23}\tau^5) + \omega^4(N_{24}\tau^3 + N_{25}\tau^4) + \omega^6(N_{26}\tau^3 + N_{27}\tau^5) \\
&+ \omega^8(N_{28}\tau^3 + N_{29}\tau^4) + \omega^{10}(N_{30}\tau^3 + N_{31}\tau^4 + N_{32}\tau^5)]
\end{aligned}
\qquad \text{(A-3)}
$$

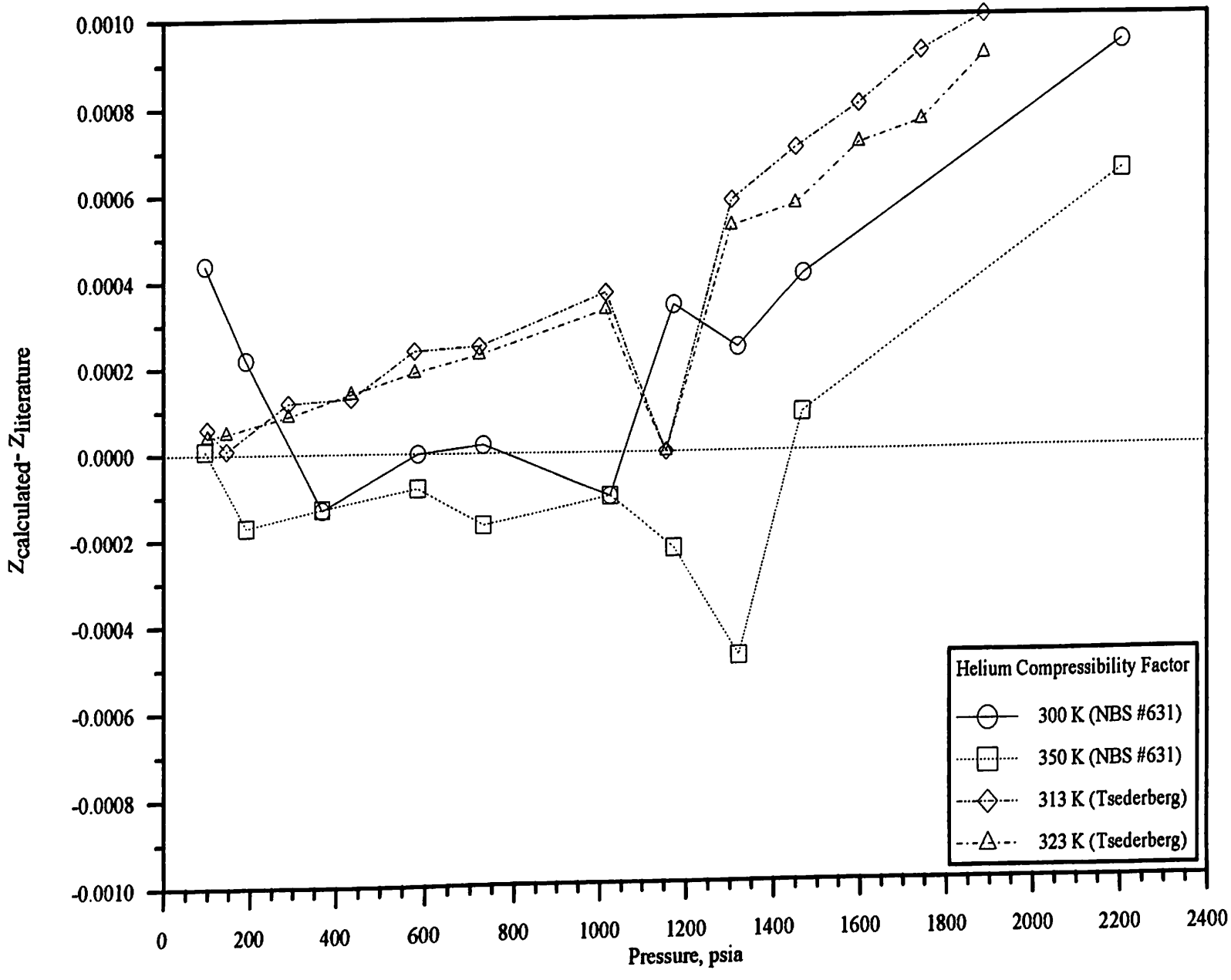

Figure 78. Helium Compressibility Factor Comparison of Calculated Values with Literature

where $\omega = \rho/\rho_c$, $\tau = T_c/T$, $\rho = 0.101095$ mole/cc and $T_c = 190.555$ K. The model constants (N_{ij}) and physical constants are tabulated in Section 3 (Table G) of the IUPAC tables for methane, and Table XXX at the end of this appendix. Figure 79 illustrates deviations in compressibility factor. The program does an excellent job of predicting the methane compressibility factor as seen by the residuals not exceeding 0.01 percent throughout the operating pressure range.

The nitrogen compressibility factor expression is identical in form to that used with methane except for the constants. The model constants and physical properties constants in Equation A-3 are listed in Section 3 (Table D) of the IUPAC tables and Table XXXI.

The compressibility factor program used to calculate the nitrogen Z-factor was compared to experimental data obtained from the IUPAC tables [2]. The literature data are for two isotherms at 310 and 320 K which are very close to the pump/cell section operating temperatures. The literature compressibility factor data are consistent with the calculated compressibility factor values through 2200 psia as seen in Figure 80. The residuals show that all generated compressibility factors compare within 0.004 percent of the documented literature values.

The compressibility factor expression for carbon dioxide is shown in Equation A-4. The analytical equation-of-state is documented in the International Union of Pure and Applied Chemistry (IUPAC) reference [2]. The σ term is defined as the reduced density, $\sigma = \rho/\rho_c$, where ρ_c is 0.01063 moles/cc. The T_c/T term is represented as τ with a critical (T_c) temperature of 304.21 K. The equation-of-state constants (b_{ij}) are tabulated in Table XXXII, or Section 3 (Table G) of the IUPAC tables [2].

$$Z_{CO_2} = 1 + \sigma \left[\sum_{i=0}^{9} \sum_{j=0}^{Ji} b_{ij} (\tau - 1)^j (\sigma - 1)^i\right] \qquad \text{(A-4)}$$

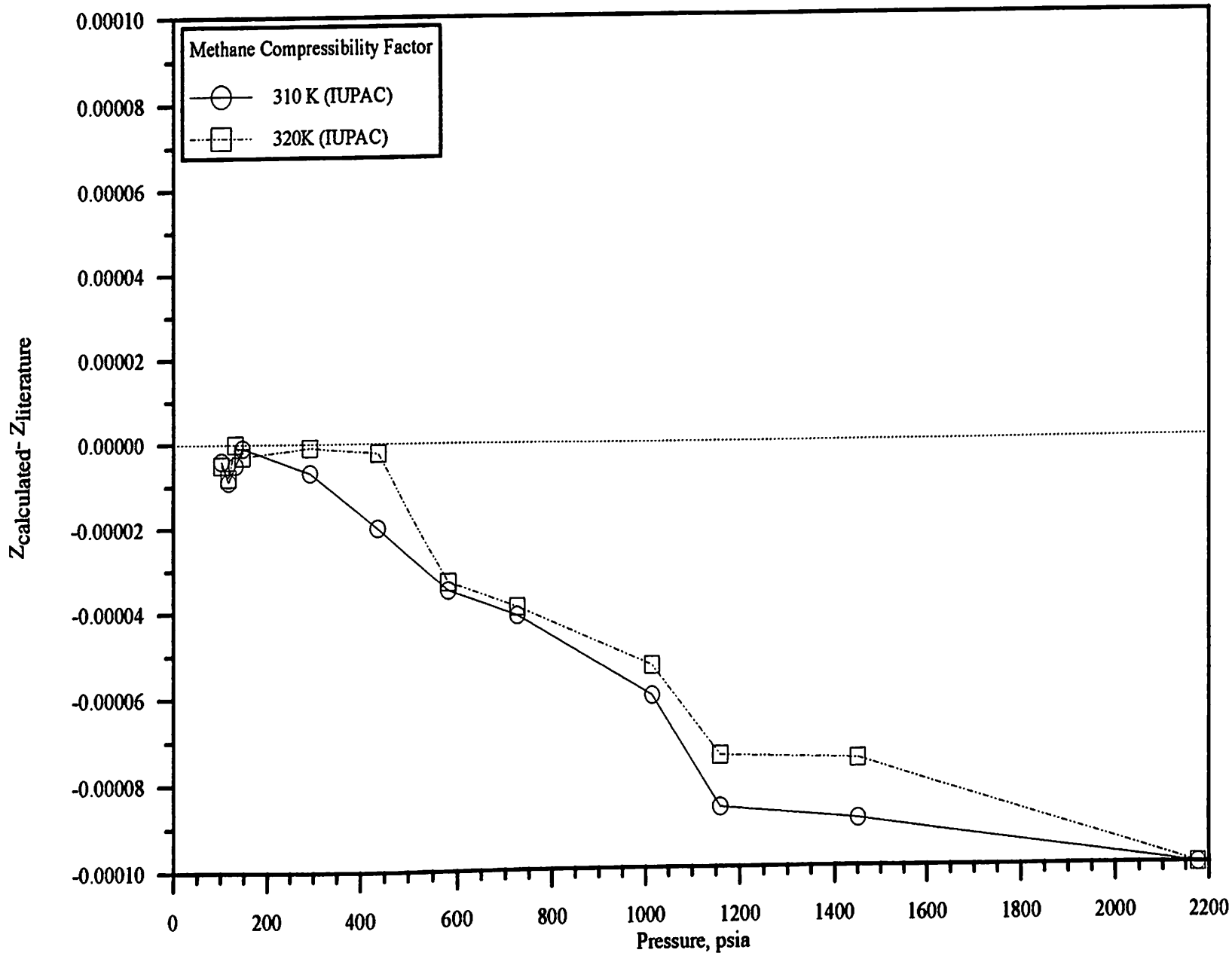

Figure 79. Methane Compressibility Factor Comparison of Calculated Values with Literature

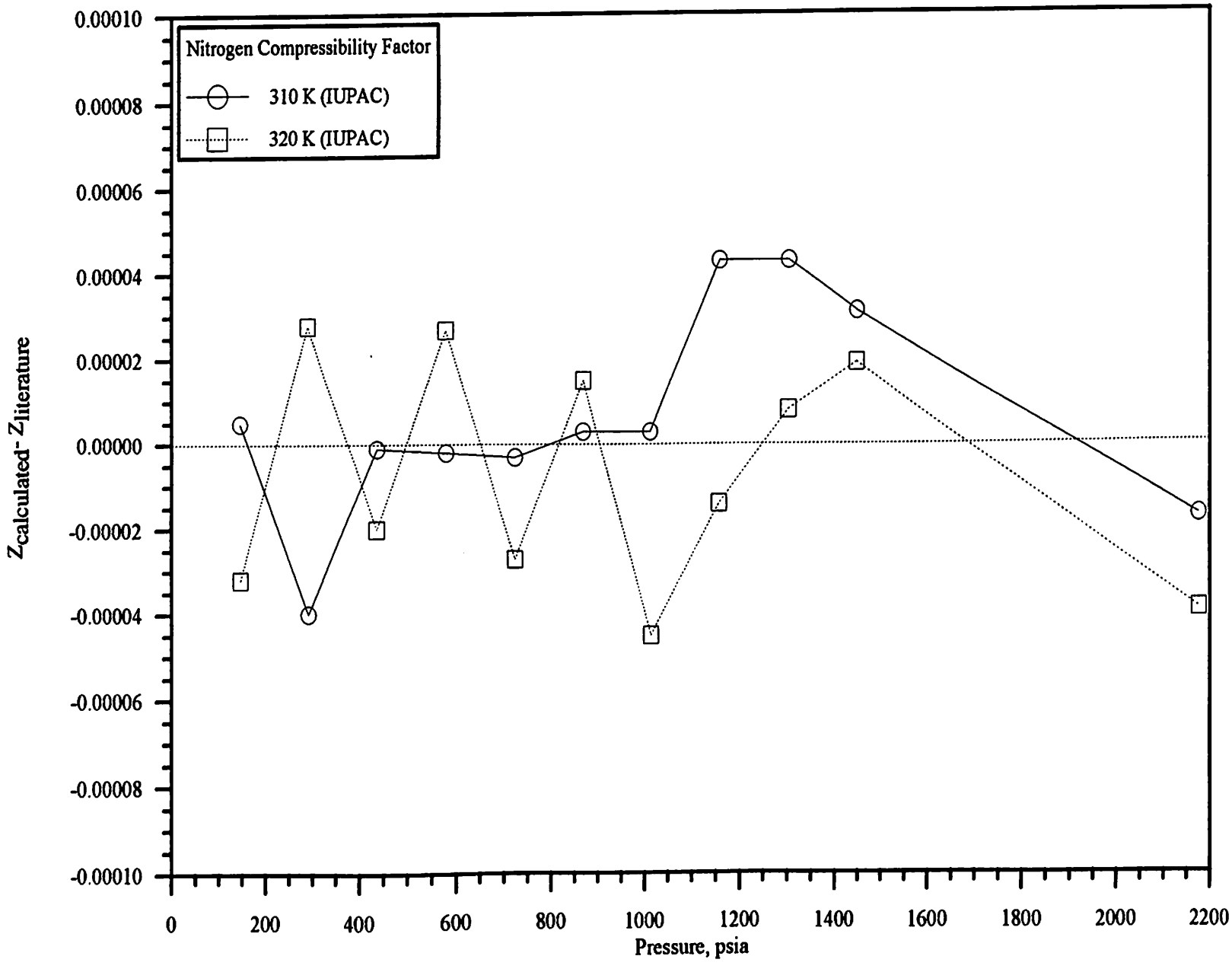

Figure 80. Nitrogen Compressibility Factor Comparison of Calculated Values with Literature

The calculated compressibility factors were again compared to experimental data tabulated in the IUPAC tables (310 and 320 K) for carbon dioxide. Residuals illustrated in Figure 81 show deviations from the literature not exceeding 0.004 percent for pressures to 2200 psia.

The gas mixture adsorption calculations are extremely sensitive to the compressibility factors. Experimental data obtained from the literature was used in the Redlich-Kwong equation-of-state (RK EOS) to calculate mixture compressibility factors. Pure component data, at the specific temperatures and pressures, were used to determine the pure-substance RK EOS model constants. Binary experimental literature data over selected temperature and pressure ranges were used to determine optimum interaction parameters in the RK EOS. With the RK EOS model constants and binary interaction parameters known, the Redlich-Kwong equation-of-state was used to determine the compressibility factors for the gas mixtures. The RK EOS is a typical cubic equation-of-state composed of an attractive (att) and repulsive (rep) contribution and shown below [33].

$$P = \left[\frac{RT}{V-b_{mix}}\right]_{att} - \left[\frac{a_{mix}}{T^{0.5}V(V-b_{mix})}\right]_{rep} \qquad \text{(A-5)}$$

$$a_{mix} = \sum_i \sum_j y_i y_j \left[a_i a_j\right]^{0.5}\left(1-C_{ij}\right) \qquad \text{(A-6)}$$

$$b_{mix} = \sum_i y_i b_i \qquad \text{(A-7)}$$

The RK EOS model constants, a_k and b_k, are determined from pure component experimental data. For mixtures, mixing rules accounting for the differences in the

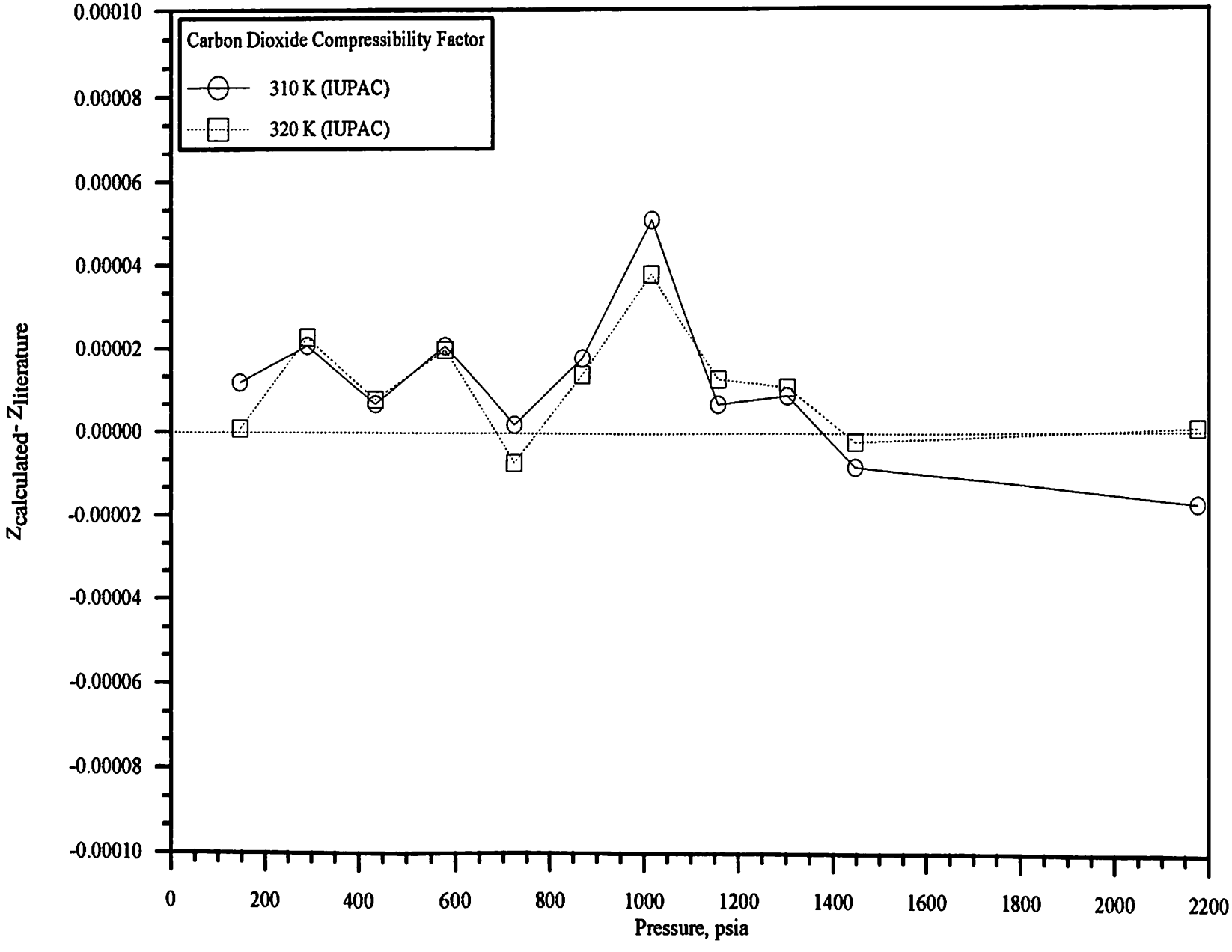

Figure 81. Carbon Dioxide Compressibility Factor Comparison of Calculated Values with Literature

molecules must be used, as shown in Equations A-6 and A-7. The binary interaction parameter, C_{ij}, becomes important in the calculations, and values were optimized from experimental literature data obtained under conditions near those of the adsorption experiments.

For the methane/nitrogen mixture, experimental literature data were obtained from Keyes and Burks, [21]. The data were at a temperature of 323.15 K (122°F) over a pressure range of 500-2100 psia. These conditions are close to the adsorption experiment conditions. The optimum binary interaction parameter for the methane/nitrogen mixture under these conditions was determined to be 0.0859. The tabulated literature data in Tables I through III of the Keyes-Burks article were compared to the calculated compressibility factors and residuals are shown in Figure 82 for the three literature mixtures. All deviations for the 0.4331/0.5669 and 0.7953/0.2047 mixtures are within 0.1 percent of the literature values. These two mixtures show similar trends (comparable differences from calculated values) throughout the pressure range of interest. The 0.8037/0.1963 mixture is within 0.5 percent of the literature with the maximum difference occurring at 1900 psia. Two mixtures (80/20 and 81/19) are similar in composition but differ significantly from the calculated compressibility factor (suggesting the 80/20 mixture data are suspect).

The same procedure was used for methane/carbon dioxide, with the literature data being from Reamer, Olds, Sage and Lacey, [26]. The literature data were at 310.93K (100°F) over a pressure range of 150-1800 psia. The optimum interaction parameter was 0.1032, and used to compare with the literature. The four compositions of Reamer (et. al.) were compared to the calculated compressibility factors with the differences shown in Figure 83. Three of the mixtures (40/60, 60/40, 85/15) shown differences of within 0.5 percent, with the 20/80 mixture differing by 1.2 percent at higher pressures. Holste and Hall [20], tabulates

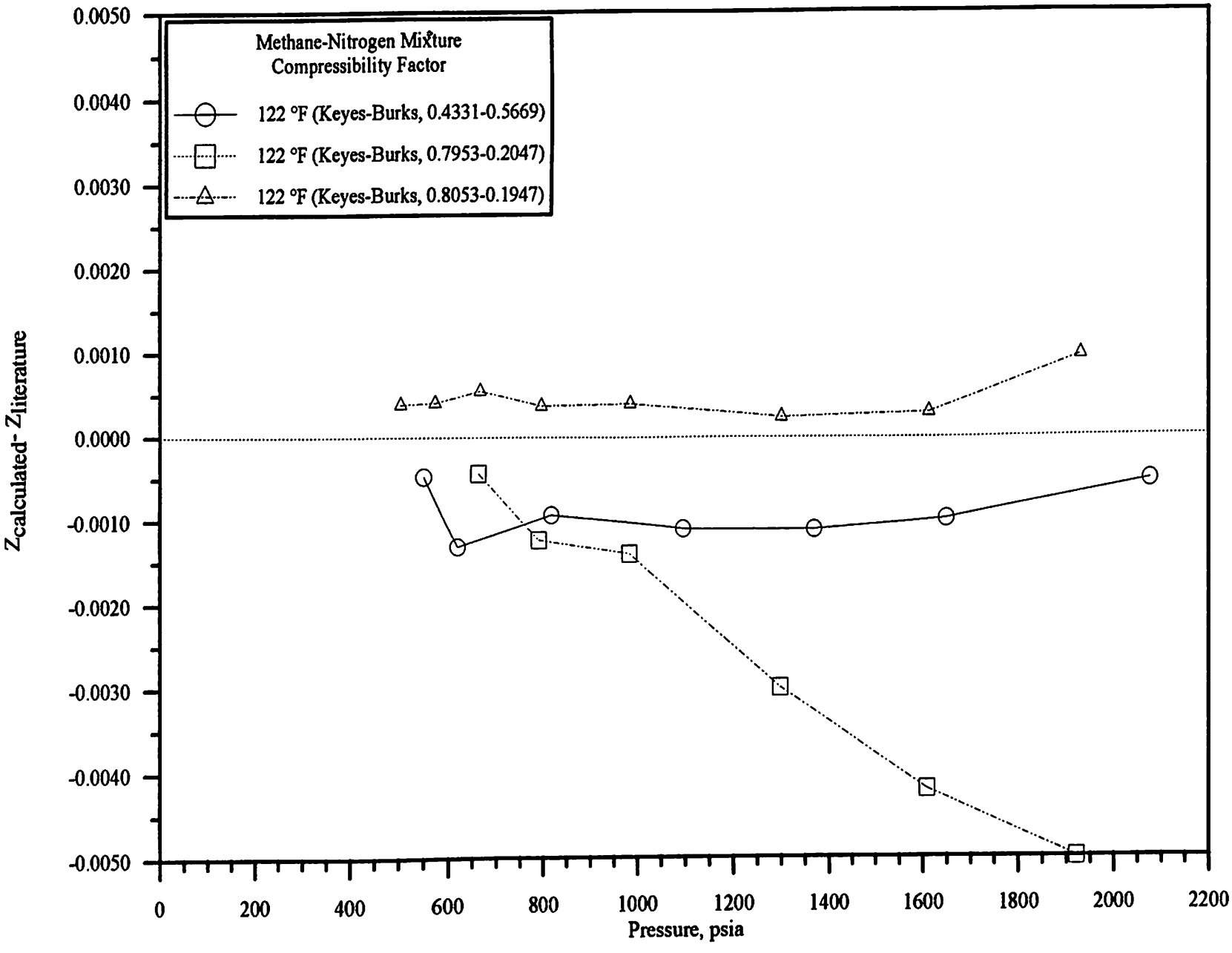

Figure 82. Compressibility Factor for Methane-Nitrogen Mixtures Comparison of Calculated Values with Literature

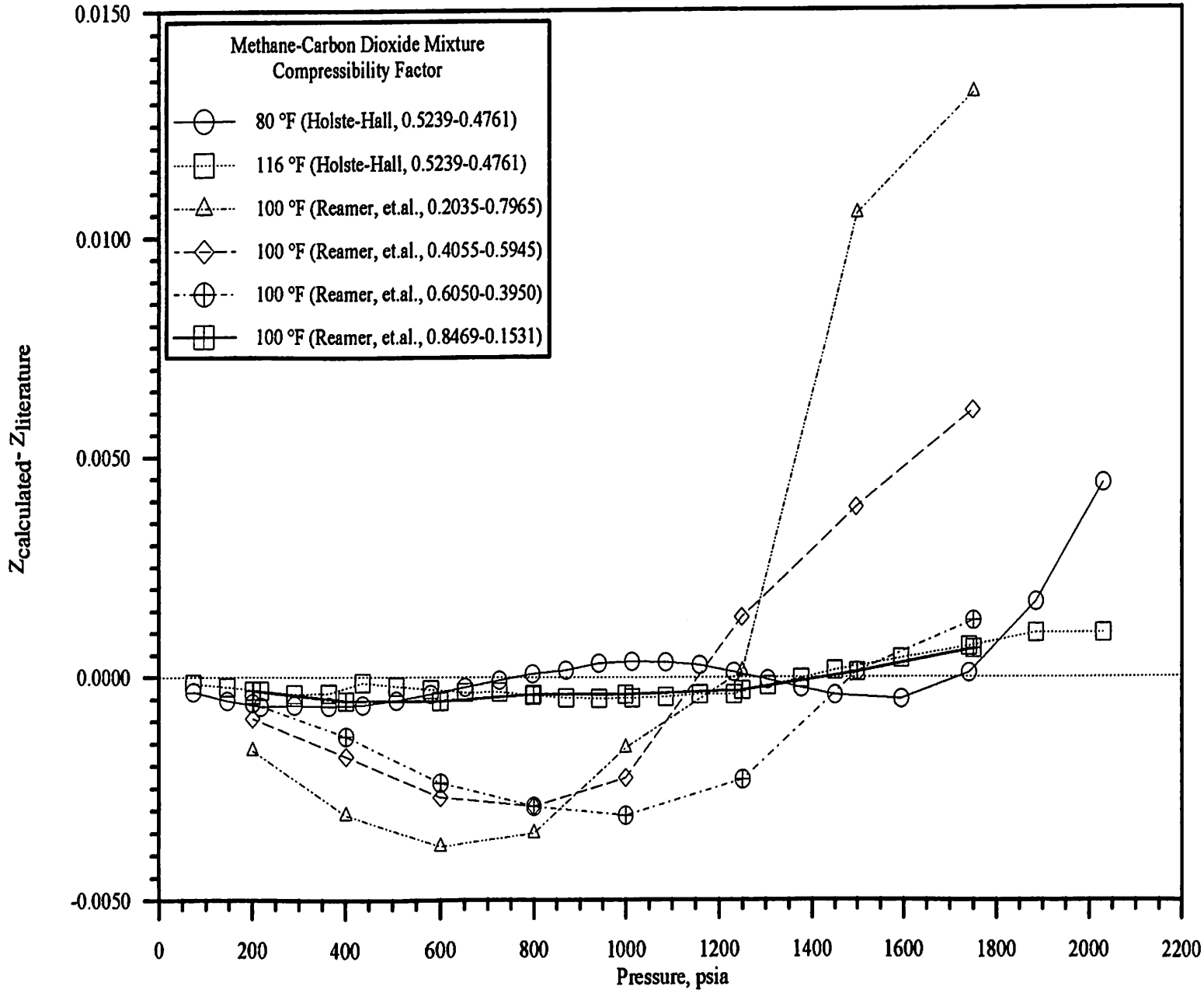

Figure 83. Compressibility Factor for Methane-Carbon Dioxide Mixtures Comparison of Calculated Values with Literature

compressibility factors at two temperatures (80.33, 116.33°F) over a 50-2000 psia pressure range. Although their data are limited to one mixture composition (0.5329-0.4761), the data were used to compare compressibility factors. Deviations in compressibility factor for the 80°F isotherm are within 0.15 percent through 1800 psia. Deviations for the 116°F isotherm are within 0.1 percent to 2000 psia.

Experimental data from Haney and Bliss, [18], were used to calculate an interaction parameter of -0.0537 for the nitrogen/carbon dioxide mixtures. The data were collected over a pressure range of 400-1900 psia at a temperature of 323.15 K. The Haney and Bliss data are very consistent with the calculated compressibility factors with the differences within 0.1 percent (as seen in Figure 84). Data by Holste and Hall [20] were used to compare compressibility factors. Literature data (four different experiments at 80°F) presented by Holste and Hall consists of only one composition (0.5530,0.4470) at one temperature (80.33°F), extending between 15-2500 psia. The 80°F (Holste-Hall) data are consistent with the current work within 0.1 % through 1800 psia.

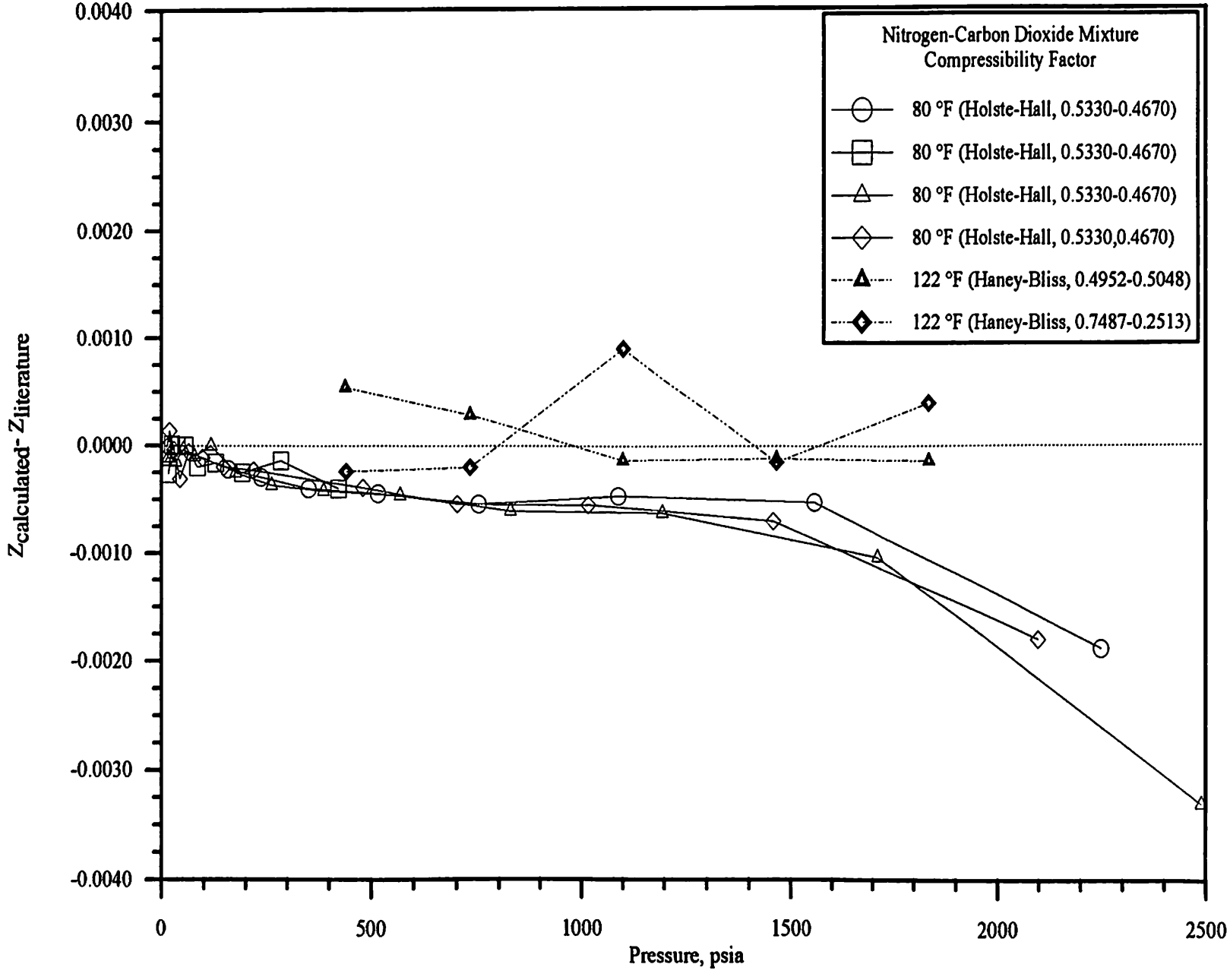

Figure 84. Compressibility Factor for Nitrogen-Carbon Dioxide Mixtures Comparison of Calculated Values with Literature

TABLE XXX

NUMERICAL COEFFICIENT (N_i) VALUES USED IN EQUATION A-3 FOR METHANE

Model Constant, N_i	Constant Value
1	-0.133485595546
2	2.57395483665
3	-4.21259560708
4	1.21838193459
5	-0.567664713645
6	0.141357820610
7	0.218272994555
8	-1.67854271263
9	11.9046702802
10	-0.055049624997
11	0.222991427494
12	0.989983917221
13	0.0895580146022
14	-0.408865640150
15	1.35937683339
16	0.147116126108
17	-0.0135078041807
18	0.214314159875
19	-0.0359787643676
20	-9.19269130423
21	1.36468925696
22	-11.669982483
23	0.485346197864
24	-3.3840871158
25	0.16922194059
26	-1.51553322986
27	-0.0806250313879
28	-0.0369326536783
29	0.0528555059265
30	-0.0478198692008
31	-0.00692834320138
32	-0.00057222052999
α	-0.98113911

TABLE XXXI

NUMERICAL COEFFICIENT (N_i) VALUES USED IN EQUATION A-3 FOR NITROGEN

Model Constant, N_i	Constant Value
1	0.185927462121
2	1.30155934655
3	-2.64054394027
4	0.292709245322
5	-0.287482987766
6	0.161225592835
7	-0.135129830972
8	0.0000137262707287
9	13.6860808703
10	0.00128973300860
11	0.315240491447
12	-0.548670430729
13	0.0744966916902
14	-0.151712926147
15	-0.728119881405
16	0.112790673192
17	-0.0187922799332
18	0.0460360632178
19	-0.00251321896106
20	-12.5428246147
21	-0.722843603762
22	-9.07779852949
23	0.333590008958
24	-2.10175282174
25	-0.244752749620
26	-0.611651799016
27	-0.0244254052253
28	-0.0230295508018
29	0.0157620487302
30	-0.0126428070667
31	-0.00146576723582
32	0.0000915063203408
α	-0.70371896

TABLE XXXII

NUMERICAL CONSTANT VALUES USED IN
EQUATION A-4 FOR CARBON DIOXIDE

	j = 0	j = 1	j = 2	j = 3	j = 4	j = 5	j = 7
i = 0	-0.725854437	-1.68332974	0.259587221	0.376945574	-0.670755370	-0.871456126	-0.149156928
i = 1	0.447869183	1.26050691	5.96957049	15.4645885	19.4449475	8.64880497	0.0
i = 2	-0.172011999	-1.83458178	-4.61487677	-3.82121926	3.60171349	4.92265552	0.0
i = 3	0.00446304911	-1.76300541	-11.1436705	-27.8215446	-27.1685720	-6.42177872	0.0
i = 4	0.255491571	2.37414246	7.50925141	6.61133318	-2.42663210	-2.57944032	0.0
i = 5	0.594667298	1.16974683	7.43706410	15.0646731	9.57496845	0.0	0.0
i = 6	-0.147960010	-1.69233071	-4.68219937	-3.13517448	0.0	0.0	0.0
i = 7	0.0136710441	-0.100492330	-1.63653806	-1.87082988	0.0	0.0	0.0
i = 8	0.0392284575	0.441503812	0.886741970	0.0	0.0	0.0	0.0
i = 9	-0.0119872097	-0.0846051949	0.0464564370	0.0	0.0	0.0	0.0

APPENDIX B

PURE COMPONENT EXPERIMENTAL ADSORPTION DATA

TABLE XXXIII

PURE METHANE ADSORPTION DATA (OSU16)

Void Volume, cc	Percent Moisture Content	Dry Coal Mass, g	Water Mass in Coal, g	Pump Temperature, °F	Cell Temperature, °F
72.7	11.9	61.9	7.98	96.7	115.0

Pump Pressure, psia	Pump Z factor	Injection Volume, cc	Initial Cell Pressure, psia	Final Cell Pressure, psia	Cell Z factor	Total gmoles gas injected	Total mgmoles gas in water	Absolute Adsorption mg mole/g coal
996.3	0.9041	9.98	3.0	95.4	0.9915	0.0300	0.0540	0.1926
996.3	0.9041	9.61	95.4	203.0	0.9819	0.0585	0.1125	0.3182
996.3	0.9041	16.46	203.0	401.1	0.9644	0.1071	0.2142	0.4773
996.3	0.9041	16.11	401.1	604.4	0.9470	0.1548	0.3109	0.5843
996.3	0.9041	15.48	604.4	802.6	0.9310	0.2005	0.3985	0.6579
996.3	0.9041	15.50	802.6	1002.0	0.9161	0.2464	0.4804	0.7111
996.3	0.9041	15.73	1002.0	1201.4	0.9029	0.2929	0.5567	0.7616
996.3	0.9041	15.77	1201.4	1401.8	0.8914	0.3395	0.6280	0.7991
996.3	0.9041	15.59	1401.8	1598.3	0.8820	0.3856	0.6933	0.8376
996.3	0.9041	15.77	1598.3	1798.9	0.8745	0.4322	0.7554	0.8690

TABLE XXXIV

PURE METHANE ADSORPTION DATA (OSU23)

Void Volume, cc	Percent Moisture Content	Dry Coal Mass, g	Water Mass in Coal, g	Pump Temperature, °F	Cell Temperature, °F
76.8	5.93	61.9	3.91	96.7	115.0

Pump Pressure, psia	Pump Z factor	Injection Volume, cc	Initial Cell Pressure, psia	Final Cell Pressure, psia	Cell Z factor	Total gmoles gas injected	Total mgmoles gas in water	Absolute Adsorption mg mole/g coal
996.5	0.9043	11.90	3.1	110.5	0.9902	0.0357	0.0305	0.2194
996.5	0.9043	8.91	110.5	207.1	0.9815	0.0621	0.0562	0.3281
996.5	0.9043	15.93	207.1	390.5	0.9653	0.1091	0.1023	0.4761
996.5	0.9043	18.79	390.5	618.6	0.9458	0.1647	0.1554	0.5862
996.5	0.9043	15.52	618.6	807.9	0.9305	0.2105	0.1962	0.6540
996.5	0.9043	16.14	807.9	1004.3	0.9160	0.2582	0.2357	0.7088
996.5	0.9043	16.95	1004.3	1208.6	0.9024	0.3083	0.2738	0.7578
996.5	0.9043	16.10	1208.6	1402.9	0.8913	0.3559	0.3077	0.7917
996.5	0.9043	16.41	1402.9	1599.3	0.8820	0.4044	0.3396	0.8280
996.5	0.9043	15.90	1599.3	1790.7	0.8747	0.4513	0.3686	0.8579

TABLE XXXV

PURE NITROGEN ADSORPTION DATA (OSU17)

Void Volume, cc	Percent Moisture Content	Dry Coal Mass, g	Water Mass in Coal, g	Pump Temperature, °F	Cell Temperature, °F
73.3	10.7	61.9	6.65	96.7	115.0

Pump Pressure, psia	Pump Z factor	Injection Volume, cc	Initial Cell Pressure, psia	Final Cell Pressure, psia	Cell Z factor	Total gmoles gas injected	Total mgmoles gas in water	Absolute Adsorption mg mole/g coal
996.3	1.002	9.65	2.7	115.5	0.9998	0.0262	0.0284	0.0688
996.3	1.002	7.54	115.5	207.7	0.9998	0.0463	0.0507	0.1111
996.3	1.002	15.82	207.7	405.1	1.000	0.0885	0.0974	0.1901
996.3	1.002	15.32	405.1	601.2	1.002	0.1294	0.1423	0.2561
996.3	1.002	15.20	601.2	801.2	1.004	0.1699	0.1866	0.3094
996.3	1.002	14.88	801.2	1000.4	1.006	0.2096	0.2294	0.3579
996.3	1.002	14.56	1000.4	1199.6	1.010	0.2484	0.2709	0.3994
996.3	1.002	14.40	1199.6	1400.0	1.014	0.2868	0.3114	0.4387
996.3	1.002	14.02	1400.0	1599.1	1.019	0.3242	0.3504	0.4748
996.3	1.002	13.49	1599.1	1795.4	1.025	0.3602	0.3878	0.5058

TABLE XXXVI

PURE NITROGEN ADSORPTION DATA (OSU19)

Void Volume, cc	Percent Moisture Content	Dry Coal Mass, g	Water Mass in Coal, g	Pump Temperature, °F	Cell Temperature, °F
75.0	9.72	61.9	5.19	96.7	115.0

Pump Pressure, psia	Pump Z factor	Injection Volume, cc	Initial Cell Pressure, psia	Final Cell Pressure, psia	Cell Z factor	Total gmoles gas injected	Total mgmoles gas in water	Absolute Adsorption mg mole/g coal
996.3	1.002	9.90	3.2	116.7	0.9998	0.0270	0.0224	0.06915
996.3	1.002	8.62	116.7	218.3	0.9998	0.0500	0.0416	0.1217
996.3	1.002	15.27	218.3	404.7	1.000	0.0907	0.0760	0.1974
996.3	1.002	15.80	404.7	604.9	1.002	0.1328	0.1118	0.2569
996.3	1.002	15.87	604.9	808.7	1.004	0.1752	0.1470	0.3132
996.3	1.002	14.56	808.7	1001.8	1.006	0.2140	0.1794	0.3516
996.3	1.002	14.84	1001.8	1201.2	1.010	0.2536	0.2118	0.3900
996.3	1.002	14.68	1201.2	1402.3	1.014	0.2927	0.2436	0.4245
996.3	1.002	14.25	1402.3	1600.0	1.019	0.3307	0.2739	0.4607
996.3	1.002	13.94	1600.0	1798.7	1.025	0.3679	0.3034	0.4904

TABLE XXXVII

PURE NITROGEN ADSORPTION DATA (OSU20)

Void Volume, cc	Percent Moisture Content	Dry Coal Mass, g	Water Mass in Coal, g	Pump Temperature, °F	Cell Temperature, °F
75.1	8.36	61.9	5.65	96.7	115.0

Pump Pressure, psia	Pump Z factor	Injection Volume, cc	Initial Cell Pressure, psia	Final Cell Pressure, psia	Cell Z factor	Total gmoles gas injected	Total mgmoles gas in water	Absolute Adsorption mg mole/g coal
996.6	1.003	10.71	2.1	124.0	0.9998	0.0289	0.0259	0.07683
996.6	1.003	7.24	124.0	211.0	0.9998	0.0482	0.0438	0.1154
996.6	1.003	15.76	211.0	404.2	1.000	0.0902	0.0826	0.1898
996.6	1.003	17.26	404.2	622.5	1.002	0.1362	0.1249	0.2546
996.6	1.003	14.32	622.5	808.3	1.004	0.1744	0.1599	0.2982
996.6	1.003	15.14	808.3	1006.6	1.006	0.2147	0.1960	0.3449
996.6	1.003	14.77	1006.6	1204.4	1.010	0.2541	0.2310	0.3845
996.6	1.003	14.23	1204.4	1399.5	1.014	0.2920	0.2644	0.4162
996.6	1.003	14.92	1399.5	1606.4	1.019	0.3317	0.2989	0.4531
996.6	1.003	13.31	1606.4	1795.8	1.025	0.3672	0.3296	0.4812

TABLE XXXVIII

PURE CARBON DIOXIDE ADSORPTION DATA (OSU24)

Void Volume, cc	Percent Moisture Content	Dry Coal Mass, g	Water Mass in Coal, g	Pump Temperature, °F	Cell Temperature, °F
76.9	5.82	61.9	3.83	96.7	115.0

Pump Pressure, psia	Pump Z factor	Injection Volume, cc	Initial Cell Pressure, psia	Final Cell Pressure, psia	Cell Z factor	Total gmoles gas injected	Total mgmoles gas in water	Absolute Adsorption mg mole/g coal
896.7	0.6403	12.87	2.6	91.7	0.9743	0.0488	0.4786	0.4816
896.7	0.6403	11.84	91.7	211.2	0.9396	0.0933	1.065	0.7810
896.7	0.6403	15.62	211.2	404.3	0.8802	0.1519	1.912	0.9845
896.7	0.6403	18.01	404.3	616.8	0.8084	0.2196	2.689	1.123
896.7	0.6403	17.81	616.8	800.2	0.7389	0.2864	3.230	1.206
896.7	0.6403	25.96	800.2	1008.6	0.6461	0.3839	3.712	1.299
896.7	0.6403	33.60	1008.6	1193.1	0.5422	0.5101	4.033	1.363
896.7	0.6403	65.04	1193.1	1375.7	0.4055	0.754	4.269	1.735
1200.7	0.2943	28.16	1375.7	1592.1	0.3550	1.062	4.460	4.621
907.9	0.6334	29.57	1592.1	1751.8	0.3448	1.176	4.550	4.973

TABLE XXXIX

PURE CARBON DIOXIDE ADSORPTION DATA (OSU25)

Void Volume, cc	Percent Moisture Content	Dry Coal Mass, g	Water Mass in Coal, g	Pump Temperature, °F	Cell Temperature, °F
77.4	5.71	61.9	3.37	96.7	115.0

Pump Pressure, psia	Pump Z factor	Injection Volume, cc	Initial Cell Pressure, psia	Final Cell Pressure, psia	Cell Z factor	Total gmoles gas injected	Total mgmoles gas in water	Absolute Adsorption mg mole/g coal
896.7	0.6403	13.93	3.1	101.7	0.9714	0.0529	0.4668	0.5122
896.7	0.6403	9.85	101.7	208.9	0.9403	0.0899	0.9294	0.7312
896.7	0.6403	9.56	208.9	326.5	0.9047	0.1258	1.398	0.8677
896.7	0.6403	7.92	326.5	425.1	0.8735	0.1555	1.758	0.9480
896.7	0.6403	8.17	425.1	522.5	0.8413	0.1862	2.083	1.019
896.7	0.6403	9.55	522.5	630.4	0.8035	0.2221	2.408	1.082
896.7	0.6403	9.81	630.4	733.5	0.7652	0.2589	2.685	1.131
896.7	0.6403	8.43	733.5	814.8	0.7329	0.2906	2.881	1.162
896.7	0.6403	11.32	814.8	911.6	0.6916	0.3332	3.088	1.205
896.7	0.6403	22.05	911.6	1063.6	0.6179	0.4160	3.364	1.291
896.7	0.6403	27.87	1063.6	1205.3	0.5343	0.5206	3.571	1.313
896.7	0.6403	60.69	1205.3	1371.5	0.4088	0.7485	3.758	1.682
910.5	0.6318	69.05	1371.5	1529.5	0.3603	1.015	3.889	4.335
910.0	0.6321	36.45	1529.5	1691.5	0.3481	1.156	3.984	5.347

TABLE XL

PURE CARBON DIOXIDE ADSORPTION DATA (OSU26)

Void Volume, cc	Percent Moisture Content	Dry Coal Mass, g	Water Mass in Coal, g	Pump Temperature, °F	Cell Temperature, °F
77.5	5.04	61.9	3.29	96.7	115.0

Pump Pressure, psia	Pump Z factor	Injection Volume, cc	Initial Cell Pressure, psia	Final Cell Pressure, psia	Cell Z factor	Total gmoles gas injected	Total mgmoles gas in water	Absolute Adsorption mg mole/g coal
896.7	0.6391	13.56	2.9	96.7	0.9729	0.0516	0.4327	0.5084
896.7	0.6391	11.03	96.7	214.9	0.9385	0.0931	0.9296	0.7615
896.7	0.6391	9.46	214.9	330.6	0.9034	0.1287	1.377	0.8992
896.7	0.6391	7.95	330.6	427.5	0.8727	0.1587	1.721	0.9890
896.7	0.6391	8.17	427.5	527.1	0.8397	0.1894	2.044	1.049
896.7	0.6391	9.64	527.1	635.1	0.8019	0.2257	2.359	1.118
896.7	0.6391	7.26	635.1	712.7	0.7731	0.2530	2.564	1.151
896.7	0.6391	14.50	712.7	851.0	0.7179	0.3076	2.885	1.206
896.7	0.6391	20.10	851.0	1008.1	0.6463	0.3833	3.186	1.257
896.7	0.6391	36.30	1008.1	1198.6	0.5387	0.5199	3.470	1.412
896.7	0.6391	28.95	1198.6	1295.3	0.4697	0.6289	3.584	1.547
906.8	0.6329	88.35	1295.3	1488.8	0.3641	0.9685	3.760	3.792
920.0	0.6246	62.41	1488.8	1800.8	0.3426	1.215	3.925	5.047

APPENDIX C

BINARY MIXTURE EXPERIMENTAL ADSORPTION DATA

TABLE XLI

METHANE-NITROGEN MIXTURE (0.200 METHANE) ADSORPTION DATA

Methane Feed Composition, z_1	Void Volume, cc	Percent Moisture Content	Dry Coal Mass, g	Water Mass in Coal, g	Pump Temperature, °F	Cell Temperature, °F
0.200	75.1	10.3	59.6	6.87	96.7	115.0

Pump Pressure, psia	Pump Z factor	Injection Volume, cc	Initial Cell Pressure, psia	Final Cell Pressure, psia	Cell Z factor	Total gmoles Gas Injected	Mgmoles Methane Dissolved in Water	Mgmoles Nitrogen Dissolved in Water	Gas Mole Fraction, y_1	Absolute Methane Adsorption, mg mole/g coal	Absolute Nitrogen Adsorption, mg mole/g coal
996.6	0.9944	11.00	2.9	125.2	0.9987	0.0303	0.0086	0.0275	0.1391	0.04455	0.05334
996.6	0.9944	7.59	125.2	214.1	0.9979	0.0508	0.0152	0.0464	0.1437	0.06974	0.08187
996.6	0.9944	15.11	214.1	397.9	0.9967	0.0915	0.0296	0.0844	0.1515	0.1103	0.1263
996.6	0.9944	16.11	397.9	599.1	0.9962	0.1350	0.0457	0.1245	0.1566	0.1473	0.1653
996.6	0.9944	16.22	599.1	807.0	0.9965	0.1788	0.0631	0.1645	0.1614	0.1763	0.1987
996.6	0.9944	15.58	807.0	1010.8	0.9975	0.2209	0.0802	0.2025	0.1650	0.1999	0.2261
996.6	0.9944	14.78	1010.8	1207.1	0.9994	0.2608	0.0964	0.2382	0.1672	0.2221	0.2489
996.6	0.9944	14.70	1207.1	1406.4	1.002	0.3005	0.1134	0.2732	0.1700	0.2376	0.2717
996.6	0.9944	14.40	1406.4	1601.8	1.005	0.3394	0.1298	0.3066	0.1720	0.2549	0.3015
996.6	0.9944	14.27	1601.8	1801.0	1.010	0.3779	0.1461	0.3401	0.1733	0.2721	0.3227

TABLE XLII

METHANE-NITROGEN MIXTURE (0.400 METHANE) ADSORPTION DATA

Methane Feed Composition, z_1	Void Volume, cc	Percent Moisture Content	Dry Coal Mass, g	Water Mass in Coal, g	Pump Temperature, °F	Cell Temperature, °F
0.400	75.1	10.3	59.6	6.87	96.7	115.0

Pump Pressure, psia	Pump Z factor	Injection Volume, cc	Initial Cell Pressure, psia	Final Cell Pressure, psia	Cell Z factor	Total gmoles Gas Injected	Mgmoles Methane Dissolved in Water	Mgmoles Nitrogen Dissolved in Water	Gas Mole Fraction, y_1	Absolute Methane Adsorption, mg mole/g coal	Absolute Nitrogen Adsorption, mg mole/g coal
996.6	0.9821	13.85	2.9	152.1	0.9966	0.0386	0.0233	0.0267	0.3117	0.1035	0.04530
996.6	0.9821	8.35	152.1	248.7	0.9946	0.0615	0.0389	0.0428	0.3204	0.1515	0.06530
996.6	0.9821	8.12	248.7	603.3	0.9884	0.1412	0.0984	0.0988	0.3418	0.2715	0.1201
996.6	0.9821	15.65	603.3	802.0	0.9861	0.1841	0.1316	0.1286	0.3486	0.3187	0.1408
996.6	0.9821	15.48	802.0	1001.0	0.9846	0.2266	0.1644	0.1577	0.3538	0.3594	0.1609
996.6	0.9821	15.47	1001.0	1203.7	0.9841	0.2690	0.1970	0.1866	0.3576	0.3955	0.1765
996.6	0.9821	14.48	1203.7	1394.7	0.9845	0.3088	0.2276	0.2130	0.3614	0.4240	0.1973
996.6	0.9821	15.36	1394.7	1601.6	0.9858	0.3509	0.2597	0.2411	0.3643	0.4523	0.2139
996.6	0.9821	14.19	1601.6	1795.0	0.9879	0.3898	0.2894	0.2666	0.3672	0.4742	0.2346

TABLE XLIII

METHANE-NITROGEN MIXTURE (0.600 METHANE) ADSORPTION DATA

Methane Feed Composition, z_1	Void Volume, cc	Percent Moisture Content	Dry Coal Mass, g	Water Mass in Coal, g	Pump Temperature, °F	Cell Temperature, °F
0.600	75. 1	10.3	59.6	6.87	96.7	115.0

Pump Pressure, psia	Pump Z factor	Injection Volume, cc	Initial Cell Pressure, psia	Final Cell Pressure, psia	Cell Z factor	Total gmoles Gas Injected	Mgmoles Methane Dissolved in Water	Mgmoles Nitrogen Dissolved in Water	Gas Mole Fraction, y_1	Absolute Methane Adsorption, mg mole/g coal	Absolute Nitrogen Adsorption, mg mole/g coal
996.6	0.9635	9.93	3.1	102.7	0.9958	0.0284	0.0264	0.0125	0.5238	0.1092	0.03008
996.6	0.9635	9.98	102.7	213.9	0.9915	0.0563	0.0551	0.0256	0.5305	0.1942	0.04825
996.6	0.9635	15.75	213.9	400.5	0.9844	0.1004	0.1035	0.0464	0.5428	0.2940	0.07045
996.6	0.9635	16.29	400.5	600.8	0.9777	0.1459	0.1543	0.0678	0.5510	0.3740	0.08737
996.6	0.9635	16.19	600.8	802.8	0.9718	0.1912	0.2040	0.0887	0.5573	0.4397	0.1039
996.6	0.9635	15.69	802.8	1002.0	0.9669	0.2351	0.2519	0.1086	0.5630	0.4882	0.1202
996.6	0.9635	15.52	1002.0	1201.3	0.9632	0.2785	0.2975	0.1283	0.5665	0.5329	0.1320
996.6	0.9635	15.17	1201.3	1399.0	0.9606	0.3210	0.3412	0.1474	0.5695	0.5692	0.1425
996.6	0.9635	15.50	1399.0	1601.8	0.9592	0.3643	0.3841	0.1668	0.5717	0.6081	0.1537
996.6	0.9635	14.70	1601.8	1796.0	0.9589	0.4055	0.4237	0.1850	0.5738	0.6426	0.1674

TABLE XLIV

METHANE-NITROGEN MIXTURE (0.800 METHANE) ADSORPTION DATA

Methane Feed Composition, z_1	Void Volume, cc	Percent Moisture Content	Dry Coal Mass, g	Water Mass in Coal, g	Pump Temperature, °F	Cell Temperature, °F
0.800	75.5	10.3	59.6	6.44	96.7	115.0

Pump Pressure, psia	Pump Z factor	Injection Volume, cc	Initial Cell Pressure, psia	Final Cell Pressure, psia	Cell Z factor	Total gmoles Gas Injected	Mgmoles Methane Dissolved in Water	Mgmoles Nitrogen Dissolved in Water	Gas Mole Fraction, y_1	Absolute Methane Adsorption, mg mole/g coal	Absolute Nitrogen Adsorption, mg mole/g coal
996.6	0.9391	10.61	2.9	104.2	0.9934	0.0310	0.0357	0.0063	0.7471	0.1587	0.01699
996.6	0.9391	8.71	104.2	199.4	0.9874	0.0560	0.0680	0.0117	0.7552	0.2522	0.02620
996.6	0.9391	17.30	199.4	403.0	0.9751	0.1056	0.1350	0.0227	0.7642	0.3885	0.03717
996.6	0.9391	15.94	403.0	597.7	0.9642	0.1513	0.1961	0.0328	0.7698	0.4812	0.04470
996.6	0.9391	16.79	597.7	806.8	0.9535	0.1994	0.2583	0.0432	0.7741	0.5555	0.05062
996.6	0.9391	15.88	806.8	1007.3	0.9443	0.2450	0.3153	0.0527	0.7788	0.6021	0.05969
996.6	0.9391	15.49	1007.3	1201.7	0.9367	0.2894	0.3673	0.0619	0.7814	0.6484	0.06644
996.6	0.9391	15.89	1201.7	1402.3	0.9303	0.3349	0.4179	0.0715	0.7830	0.6915	0.07031
996.6	0.9391	15.85	1402.3	1601.6	0.9253	0.3804	0.4653	0.0809	0.7842	0.7382	0.07527
996.6	0.9391	15.63	1601.6	1800.0	0.9218	0.4252	0.5100	0.0902	0.7853	0.7807	0.08063

TABLE XLV

METHANE-CARBON DIOXIDE MIXTURE (0.200 METHANE) ADSORPTION DATA

Methane Feed Composition, z_1	Void Volume, cc	Percent Moisture Content	Dry Coal Mass, g	Water Mass in Coal, g	Pump Temperature, °F	Cell Temperature, °F
0.200	76.0	8.90	59.6	5.82	96.6	115.0

Pump Pressure, psia	Pump Z factor	Injection Volume, cc	Initial Cell Pressure, psia	Final Cell Pressure, psia	Cell Z factor	Total gmoles Gas Injected	Mgmoles Methane Dissolved in Water	Mgmoles CO_2 Dissolved in Water	Gas Mole Fraction, y_1	Absolute Methane Adsorption, mg mole/g coal	Absolute CO_2 Adsorption, mg mole/g coal
996.5	0.7611	11.51	2.8	96.1	0.9811	0.0442	0.0134	0.5120	0.3341	0.04096	0.3714
996.5	0.7611	9.07	96.1	199.7	0.9590	0.0786	0.0250	1.093	0.3011	0.05940	0.5635
996.5	0.7611	15.65	199.7	403.0	0.9128	0.1379	0.0452	2.196	0.2705	0.07621	0.7742
996.5	0.7611	14.77	403.0	597.7	0.8661	0.1939	0.0630	3.150	0.2560	0.08107	0.8979
996.5	0.7611	16.26	597.7	798.2	0.8148	0.2555	0.0799	4.020	0.2444	0.08789	0.9878
996.5	0.7611	18.56	798.2	1003.2	0.7595	0.3259	0.0964	4.773	0.2360	0.09419	1.065
996.5	0.7611	20.34	1003.2	1199.6	0.7047	0.4030	0.1123	5.366	0.2311	0.09415	1.140
996.5	0.7611	24.58	1199.6	1400.7	0.6471	0.4962	0.1273	5.862	0.2257	0.1072	1.225
996.5	0.7611	24.75	1400.7	1575.3	0.5993	0.5900	0.1398	6.207	0.2215	0.1304	1.324
996.5	0.7611	23.14	1575.3	1728.1	0.5629	0.6777	0.1498	6.452	0.2174	0.1609	1.391

TABLE XLVI

METHANE-CARBON DIOXIDE MIXTURE (0.400 METHANE) ADSORPTION DATA

Methane Feed Composition, z_1	Void Volume, cc	Percent Moisture Content	Dry Coal Mass, g	Water Mass in Coal, g	Pump Temperature, °F	Cell Temperature, °F
0.400	76.2	8.87	59.6	5.80	96.6	115.0

Pump Pressure, psia	Pump Z factor	Injection Volume, cc	Initial Cell Pressure, psia	Final Cell Pressure, psia	Cell Z factor	Total gmoles Gas Injected	Mgmoles Methane Dissolved in Water	Mgmoles CO_2 Dissolved in Water	Gas Mole Fraction, y_1	Absolute Methane Adsorption, mg mole/g coal	Absolute CO_2 Adsorption, mg mole/g coal
996.5	0.8303	12.69	3.0	107.5	0.9837	0.0439	0.0253	0.3714	0.5684	0.09048	0.2813
996.5	0.8303	7.62	107.5	197.8	0.9690	0.0699	0.0437	0.7243	0.5371	0.1100	0.3830
996.5	0.8303	16.74	197.8	396.4	0.9356	0.1271	0.0815	1.498	0.5080	0.1521	0.5770
996.5	0.8303	16.43	396.4	603.0	0.8983	0.1831	0.1156	2.318	0.4803	0.1839	0.6762
996.5	0.8303	16.63	603.0	803.8	0.8623	0.2399	0.1482	3.036	0.4686	0.1985	0.7665
996.5	0.8303	17.43	803.8	1003.6	0.8261	0.2994	0.1787	3.695	0.4588	0.2128	0.8367
996.5	0.8303	18.69	1003.6	1206.9	0.7895	0.3631	0.2083	4.298	0.4508	0.2205	0.8878
996.5	0.8303	19.26	1206.9	1397.4	0.7565	0.4289	0.2350	4.799	0.4446	0.2436	0.9510
996.5	0.8303	21.39	1397.4	1595.6	0.7247	0.5019	0.2618	5.252	0.4395	0.2741	1.024
996.5	0.8303	21.82	1595.6	1791.3	0.6974	0.5763	0.2874	5.636	0.4354	0.3025	1.091

TABLE XLVII

METHANE-CARBON DIOXIDE MIXTURE (0.600 METHANE) ADSORPTION DATA

Methane Feed Composition, z_1	Void Volume, cc	Percent Moisture Content	Dry Coal Mass, g	Water Mass in Coal, g	Pump Temperature, °F	Cell Temperature, °F
0.600	76.2	8.87	59.6	5.80	96.6	115.0

Pump Pressure, psia	Pump Z factor	Injection Volume, cc	Initial Cell Pressure, psia	Final Cell Pressure, psia	Cell Z factor	Total gmoles Gas Injected	Mgmoles Methane Dissolved in Water	Mgmoles CO_2 Dissolved in Water	Gas Mole Fraction, y_1	Absolute Methane Adsorption, mg mole/g coal	Absolute CO_2 Adsorption, mg mole/g coal
996.5	0.8706	11.95	3.0	104.1	0.9874	0.0388	0.0328	0.1979	0.7638	0.1247	0.1749
996.5	0.8706	9.28	104.1	202.7	0.9747	0.0684	0.0605	0.4332	0.7326	0.1884	0.2696
996.5	0.8706	16.78	202.7	400.7	0.9490	0.1219	0.1130	0.9169	0.7089	0.2511	0.4030
996.5	0.8706	16.22	400.7	599.4	0.9225	0.1737	0.1604	1.439	0.6882	0.2959	0.4849
996.5	0.8706	16.91	599.4	804.6	0.8959	0.2277	0.2073	1.953	0.6777	0.3204	0.5595
996.5	0.8706	17.01	804.6	1005.1	0.8696	0.2820	0.2488	2.475	0.6646	0.3563	0.6005
996.5	0.8706	16.95	1005.1	1202.9	0.8454	0.3361	0.2885	2.947	0.6574	0.3647	0.6357
996.5	0.8706	18.03	1202.9	1399.6	0.8237	0.3936	0.3274	3.367	0.6464	0.3824	0.6994
996.5	0.8706	18.74	1399.6	1598.1	0.8030	0.4534	0.3631	3.797	0.6484	0.4206	0.7359
996.5	0.8706	19.20	1598.1	1800.3	0.7846	0.5147	0.3979	4.201	0.6434	0.4497	0.7653

TABLE XLVIII

METHANE-CARBON DIOXIDE MIXTURE (0.800 METHANE) ADSORPTION DATA

Methane Feed Composition, z_1	Void Volume, cc	Percent Moisture Content	Dry Coal Mass, g	Water Mass in Coal, g	Pump Temperature, °F	Cell Temperature, °F
0.800	76.2	8.62	59.6	5.80	96.7	115.0

Pump Pressure, psia	Pump Z factor	Injection Volume, cc	Initial Cell Pressure, psia	Final Cell Pressure, psia	Cell Z factor	Total gmoles Gas Injected	Mgmoles Methane Dissolved in Water	Mgmoles CO_2 Dissolved in Water	Gas Mole Fraction, y_1	Absolute Methane Adsorption, mg mole/g coal	Absolute CO_2 Adsorption, mg mole/g coal
996.5	0.8923	11.74	3.0	107.8	0.9888	0.0364	0.0400	0.0840	0.9035	0.1641	0.08629
996.5	0.8923	9.27	107.8	206.6	0.9782	0.0647	0.0740	0.1898	0.8859	0.2539	0.1351
996.5	0.8923	16.66	206.6	400.5	0.9575	0.1156	0.1364	0.4237	0.8677	0.3648	0.2003
996.5	0.8923	17.74	400.5	615.3	0.9352	0.1697	0.2001	0.7034	0.8557	0.4446	0.2492
996.5	0.8923	15.30	615.3	800.8	0.9162	0.2164	0.2508	0.9649	0.8465	0.5016	0.2751
996.5	0.8923	16.86	800.8	1002.4	0.8975	0.2679	0.3043	1.209	0.8449	0.5378	0.3184
996.5	0.8923	16.60	1002.4	1200.7	0.8800	0.3186	0.3527	1.477	0.8402	0.5668	0.3400
996.5	0.8923	17.58	1200.7	1404.8	0.8637	0.3722	0.3996	1.748	0.8364	0.6026	0.3618
996.5	0.8923	16.80	1404.8	1596.3	0.8504	0.4235	0.4414	1.989	0.8344	0.6357	0.3874
996.5	0.8923	17.87	1596.3	1800.5	0.8381	0.4780	0.4828	2.263	0.8308	0.6718	0.3980

TABLE XLIX

NITROGEN-CARBON DIOXIDE MIXTURE (0.200 NITROGEN) ADSORPTION DATA

Nitrogen Feed Composition, z_1	Void Volume, cc	Percent Moisture Content	Dry Coal Mass, g	Water Mass in Coal, g	Pump Temperature, °F	Cell Temperature, °F
0.200	76.9	7.85	59.6	5.07	96.5	115.0

Pump Pressure, psia	Pump Z factor	Injection Volume, cc	Initial Cell Pressure, psia	Final Cell Pressure, psia	Cell Z factor	Total gmoles Gas Injected	Mgmoles Nitrogen Dissolved in Water	Mgmoles CO_2 Dissolved in Water	Gas Mole Fraction, y_1	Absolute Nitrogen Adsorption, mg mole/g coal	Absolute CO_2 Adsorption, mg mole/g coal
996.3	0.8366	13.72	3.0	121.4	0.9825	0.0501	0.0090	0.5126	0.3929	0.00723	0.4155
996.3	0.8366	7.63	121.4	207.0	0.9674	0.0776	0.0137	0.9196	0.3505	0.01308	0.5684
996.3	0.8366	14.87	207.0	393.4	0.9320	0.1312	0.0228	1.789	0.3063	0.01664	0.7725
996.3	0.8366	16.16	393.4	601.2	0.8884	0.1895	0.0313	2.699	0.2756	0.02721	0.8993
996.3	0.8366	17.06	601.2	809.3	0.8434	0.2511	0.0397	3.484	0.2602	0.03014	1.003
996.3	0.8366	17.01	809.3	1002.2	0.7988	0.3124	0.0467	4.116	0.2473	0.04081	1.059
996.3	0.8366	19.67	1002.2	1206.7	0.7527	0.3833	0.0549	4.656	0.2416	0.03081	1.127
996.3	0.8366	20.22	1206.7	1393.6	0.7085	0.4563	0.0614	5.067	0.2345	0.03803	1.166
996.3	0.8366	23.97	1393.6	1594.6	0.6616	0.5427	0.0680	5.421	0.2274	0.04792	1.170
996.3	0.8366	25.94	1594.6	1792.1	0.6251	0.6363	0.0758	5.674	0.2262	0.04457	1.294

TABLE L

NITROGEN-CARBON DIOXIDE MIXTURE (0.400 NITROGEN) ADSORPTION DATA

Nitrogen Feed Composition, z_1	Void Volume, cc	Percent Moisture Content	Dry Coal Mass, g	Water Mass in Coal, g	Pump Temperature, °F	Cell Temperature, °F
0.400	72.9	13.7	59.2	9.41	96.5	115.0

Pump Pressure, psia	Pump Z factor	Injection Volume, cc	Initial Cell Pressure, psia	Final Cell Pressure, psia	Cell Z factor	Total gmoles Gas Injected	Mgmoles Nitrogen Dissolved in Water	Mgmoles CO_2 Dissolved in Water	Gas Mole Fraction, y_1	Absolute Nitrogen Adsorption, mg mole/g coal	Absolute CO_2 Adsorption, mg mole/g coal
996.7	0.9302	11.20	3.1	105.1	0.9927	0.0363	0.0247	0.4502	0.6713	0.01910	0.2494
996.7	0.9302	8.77	105.1	199.5	0.9842	0.0642	0.0437	0.9594	0.6273	0.03145	0.3957
996.7	0.9302	16.18	199.5	393.4	0.9642	0.1158	0.0785	2.099	0.5756	0.04373	0.5938
996.7	0.9302	16.44	393.4	600.9	0.9410	0.1681	0.1123	3.347	0.5420	0.05286	0.7331
996.7	0.9302	16.02	600.9	805.6	0.9170	0.2192	0.1432	4.539	0.5185	0.05998	0.8265
996.7	0.9302	16.11	805.6	1008.1	0.8930	0.2705	0.1723	5.644	0.5008	0.06821	0.8941
996.7	0.9302	16.09	1008.1	1207.2	0.8701	0.3218	0.2000	6.625	0.4880	0.07028	0.9442
996.7	0.9302	16.86	1207.2	1406.6	0.8479	0.3755	0.2269	7.506	0.4775	0.08034	0.9932
996.7	0.9302	16.91	1406.6	1604.6	0.8271	0.4294	0.2528	8.277	0.4687	0.08410	1.022
996.7	0.9302	64.77	1604.6	1798.7	0.8088	0.4840	0.2777	8.929	0.4616	0.09379	1.053

TABLE LI

NITROGEN-CARBON DIOXIDE MIXTURE (0.600 NITROGEN) ADSORPTION DATA

Nitrogen Feed Composition, z_1	Void Volume, cc	Percent Moisture Content	Dry Coal Mass, g	Water Mass in Coal, g	Pump Temperature, °F	Cell Temperature, °F
0.600	73.2	13.4	59. 2	9.18	96.5	115.0

Pump Pressure, psia	Pump Z factor	Injection Volume, cc	Initial Cell Pressure, psia	Final Cell Pressure, psia	Cell Z factor	Total gmoles Gas Injected	Mgmoles Nitrogen Dissolved in Water	Mgmoles CO_2 Dissolved in Water	Gas Mole Fraction, y_1	Absolute Nitrogen Adsorption, mg mole/g coal	Absolute CO_2 Adsorption, mg mole/g coal
996.7	0.9096	10.34	2.8	105.9	0.9968	0.0309	0.0308	0.2006	0.8517	0.02424	0.1553
996.7	0.9096	8.83	105.9	203.0	0.9927	0.0569	0.0563	0.4704	0.8177	0.04397	0.2579
996.7	0.9096	16.37	203.0	394.7	0.9837	0.1051	0.1034	1.084	0.7811	0.07139	0.4134
996.7	0.9096	16.38	394.7	598.2	0.9733	0.1533	0.1501	1.804	0.7557	0.08699	0.5314
996.7	0.9096	15.96	598.2	801.7	0.9627	0.2002	0.1939	2.565	0.7357	0.1009	0.6173
996.7	0.9096	15.66	801.7	1003.4	0.9525	0.2463	0.2356	3.318	0.7209	0.1115	0.6856
996.7	0.9096	15.48	1003.4	1203.8	0.9426	0.2918	0.2751	4.069	0.7077	0.1254	0.7342
996.7	0.9096	15.26	1203.8	1401.5	0.9338	0.3367	0.3131	4.775	0.6978	0.1361	0.7767
996.7	0.9096	15.33	1401.5	1600.4	0.9260	0.3818	0.3503	5.452	0.6895	0.1471	0.8128
996.7	0.9096	15.34	1600.4	1798.3	0.9192	0.4269	0.3863	6.092	0.6822	0.1640	0.8442

TABLE LII

NITROGEN-CARBON DIOXIDE MIXTURE (0.700 NITROGEN) ADSORPTION DATA

Nitrogen Feed Composition, z_1	Void Volume, cc	Percent Moisture Content	Dry Coal Mass, g	Water Mass in Coal, g	Pump Temperature, °F	Cell Temperature, °F
0.700	73.0	13.7	59.2	9.41	96.5	115.0

Pump Pressure, psia	Pump Z factor	Injection Volume, cc	Initial Cell Pressure, psia	Final Cell Pressure, psia	Cell Z factor	Total gmoles Gas Injected	Mgmoles Nitrogen Dissolved in Water	Mgmoles CO_2 Dissolved in Water	Gas Mole Fraction, y_1	Absolute Nitrogen Adsorption, mg mole/g coal	Absolute CO_2 Adsorption, mg mole/g coal
996.7	0.9854	9.80	3.0	104.5	0.9980	0.0285	0.0331	0.1259	0.9081	0.03365	0.1116
996.7	0.9854	9.38	104.5	209.8	0.9952	0.0553	0.0641	0.3243	0.8817	0.06216	0.1952
996.7	0.9854	15.51	209.8	395.7	0.9898	0.0995	0.1161	0.7377	0.8562	0.09201	0.3097
996.7	0.9854	16.35	395.7	599.5	0.9837	0.1461	0.1699	1.250	0.8374	0.1169	0.4067
996.7	0.9854	16.51	599.5	810.6	0.9775	0.1932	0.2230	1.821	0.8226	0.1379	0.4857
996.7	0.9854	15.09	810.6	1007.6	0.9722	0.2362	0.2706	2.368	0.8119	0.1516	0.5456
996.7	0.9854	15.11	1007.6	1205.0	0.9678	0.2793	0.3169	2.912	0.8038	0.1677	0.6016
996.7	0.9854	14.97	1205.0	1405.4	0.9634	0.3220	0.3617	3.493	0.7948	0.1812	0.6373
996.7	0.9854	14.90	1405.4	1605.5	0.9601	0.3645	0.4053	4.058	0.7876	0.1965	0.6702
996.7	0.9854	14.61	1605.5	1801.0	0.9580	0.4062	0.4472	4.580	0.7825	0.2165	0.7073

TABLE LIII

NITROGEN-CARBON DIOXIDE MIXTURE (0.799 NITROGEN) ADSORPTION DATA

Nitrogen Feed Composition, z_1	Void Volume, cc	Percent Moisture Content	Dry Coal Mass, g	Water Mass in Coal, g	Pump Temperature, °F	Cell Temperature, °F
0.799	72.6	14.0	59.2	9.68	96.5	115.0

Pump Pressure, psia	Pump Z factor	Injection Volume, cc	Initial Cell Pressure, psia	Final Cell Pressure, psia	Cell Z factor	Total gmoles Gas Injected	Mgmoles Nitrogen Dissolved in Water	Mgmoles CO_2 Dissolved in Water	Gas Mole Fraction, y_1	Absolute Nitrogen Adsorption, mg mole/g coal	Absolute CO_2 Adsorption, mg mole/g coal
996.7	0.9930	9.19	3.1	104.7	0.9988	0.0261	0.0356	0.0734	0.9481	0.03672	0.07011
996.7	0.9930	8.86	104.7	207.3	0.9973	0.0508	0.0690	0.1838	0.9342	0.06939	0.1257
996.7	0.9930	16.26	207.3	405.1	0.9944	0.0960	0.1306	0.4483	0.9175	0.1145	0.2119
996.7	0.9930	15.43	405.1	600.6	0.9916	0.1389	0.1885	0.7570	0.9055	0.1467	0.2781
996.7	0.9930	15.91	600.6	804.9	0.9891	0.1831	0.2466	1.112	0.8957	0.1820	0.3360
996.7	0.9930	15.08	804.9	1004.8	0.9872	0.2250	0.3013	1.478	0.8881	0.2038	0.3817
996.7	0.9930	14.91	1004.8	1205.2	0.9860	0.2665	0.3544	1.854	0.8820	0.2238	0.4219
996.7	0.9930	14.58	1205.2	1402.6	0.9857	0.3070	0.4053	2.224	0.8773	0.2451	0.4592
996.7	0.9930	14.36	1402.6	1601.9	0.9858	0.3469	0.4547	2.624	0.8720	0.2632	0.4845
996.7	0.9930	14.10	1601.9	1797.9	0.9870	0.3861	0.5023	3.001	0.8683	0.2862	0.5129

APPENDIX D

COAL SAMPLE ANALYSIS

APPENDIX D

COAL SAMPLE ANALYSIS

The coal used in this work was supplied by the Amoco Production Company, Research Center, in Tulsa, Oklahoma. The following coal analysis was completed by Amoco. The coal sample was identified as sample identification 11344-2 by Amoco and weighed 433.97 grams with approximately 18.8 percent water. The equilibrium moisture content of this sample is 2.203 weight percent water (as determined by proximate analysis) with a dry density of 1.446 grams per cc (as determined from the sample analysis). The X-ray Diffraction Mineral Percentages are: quartz—16 %, feldspar—1 %, calcite—trace, dolomite—1 %, kaolinite—1 %, illite—trace, organic coal—75.7 %, plagioclase feldspar—1 % and feldspar K—trace amounts. The Vitrinite analysis classifies the coal at a very mature maturation level with a medium volatile bituminous coal ranking. An analysis (proximate and ultimate) of the coal substrate is tabulated in Tables LIV and LV, respectively.

The proximate analysis is used to determine the moisture, volatile matter, ash and fixed carbon content of the coal but does not include testing for sulfur, phosphorous or any other constituents [27]. The equilibrium moisture content is the moisture that a coal sample can hold when in equilibrium with an atmosphere of 96-97 percent relative humidity [27]. Moisture content is determined by drying the sample at temperatures just above 100°C for one hour and determining the lost mass of the sample. Volatile matter of coal represents the products which are given off as vapors when the coal is heated. Volatile matter is determined from the amount of volatiles driven from a sample when heated to 950°C for seven minutes. Ash is

determined by weighing the residue remaining after heating the coal sample to redness in air, then finish heating to constant weight at a temperature between 700-750°C. Fixed carbon is the material remaining after determination of moisture, ash and volatile matter. The fixed carbon content is determined by difference from the moisture content, ash and volatile matter values [27].

Mineral matter analysis in coal is determined by heating the coal to ash and analyzing the ash. The chemical composition of the ash is expressed as oxides of aluminum, iron, calcium, magnesium, titanium, sodium and potassium. The lower mineral matter content, the better the coal quality.

The ultimate analysis of coal is used to determine the carbon, hydrogen, sulfur, nitrogen and ash content in the material as a whole and estimation of the oxygen content by difference [27].

Both the proximate and ultimate testing are done in accordance with procedures developed by the American Society for Testing and Materials (ASTM) [27].

TABLE LIV

PROXIMATE ANALYSIS, PERCENT MASS

Analysis	As Received	Moisture Free	Dry Ash Free
Total Moisture	2.203	—	—
Volatile Matter	19.76	20.20	25.39
Ash	20.00	20.45	—
Fixed Carbon	58.04	59.35	74.61
Heat Value, Btu/lbm	11 996.8	12 236.0	15 381.5

TABLE LV

ULTIMATE ANALYSIS, PERCENT MASS

Analysis	As Received	Moisture Free	Dry Ash Free
Hydrogen	4.18	4.27	5.37
Carbon	67.12	68.63	86.27
Nitrogen	1.54	1.57	1.97
Oxygen	0.87	0.89	1.12
Sulfur	4.10	4.19	5.27
Total Moisture	2.20	—	—
Ash	20.00	20.45	—

APPENDIX E

ADSORPTION RESULTS ON AN ORGANIC COAL BASIS

APPENDIX E

ADSORPTION RESULTS ON AN ORGANIC COAL BASIS

All coals contain inorganic and organic constituents. The inorganic constituents are called mineral matter [27]. The mineral matter acts as an inert diluent with respect to gas adsorption. The mineral matter does not contribute to the gas adsorption, but instead the gas adsorption takes place on the organic (pure) coal [27]. The mineral matter reduces the gas content providing no contribution to the gas adsorption. Coal with lower mineral matter contents have higher gas adsorption capacities.

A quantitative measure of the amount of mineral matter can be obtained from the proximate coal analysis (as seen in Appendix D) using the Parr expression [27]. The Parr equation determines the mineral matter using

$$y_{pure} = 1 - \left[1.08 A_{ash} + 0.55 S_{sulfur}\right] \qquad \text{D-1}$$

where y_{pure}, A_{ash} and S_{sulfur} are the mass fractions of pure (organic) coal, ash and sulfur (on a dry basis), respectively. The bracketed term in Equation D-1 is the mineral matter mass fraction.

Adsorption results from the current work were compared to Amoco data using an organic coal basis (as discussed in Chapter VI). The mass fraction of organic coal used in the current work was determined to be 75.7 percent, compared to 82.0 percent for Amoco [4]. The adsorption results are illustrated in Figures 85 through 99, with the discussion found in Chapter VI. As seen in Table LVI, current work differs from Amoco in the amount of ash and sulfur content —20.35 as compared to

16.35 percent, and 4.19 compared to 0.65 percent, respectively.

TABLE LVI

ORGANIC COAL CONTENT OF COAL SAMPLE

	Current Work, Mass Percent	Amoco [4], Mass Percent
Ash Content, A_{ash}	0.203	0.163
Sulfur Content, S_{sulfur}	0.0419	0.0065
Pure (Organic) Coal, y_{pure}	0.757	0.820

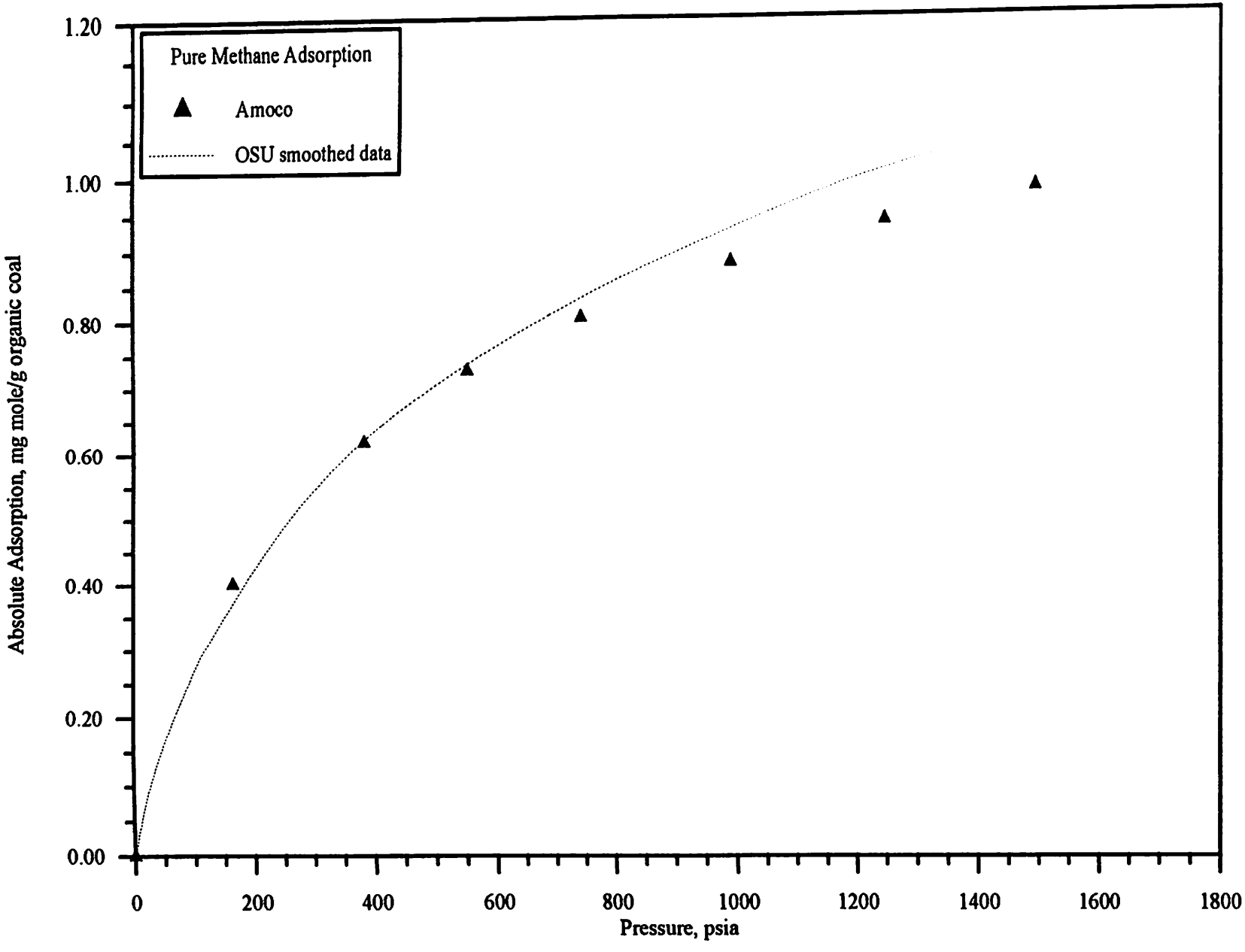

Figure 85. Comparison of Pure Methane Adsorption Data from OSU and Amoco (Organic Coal Basis)

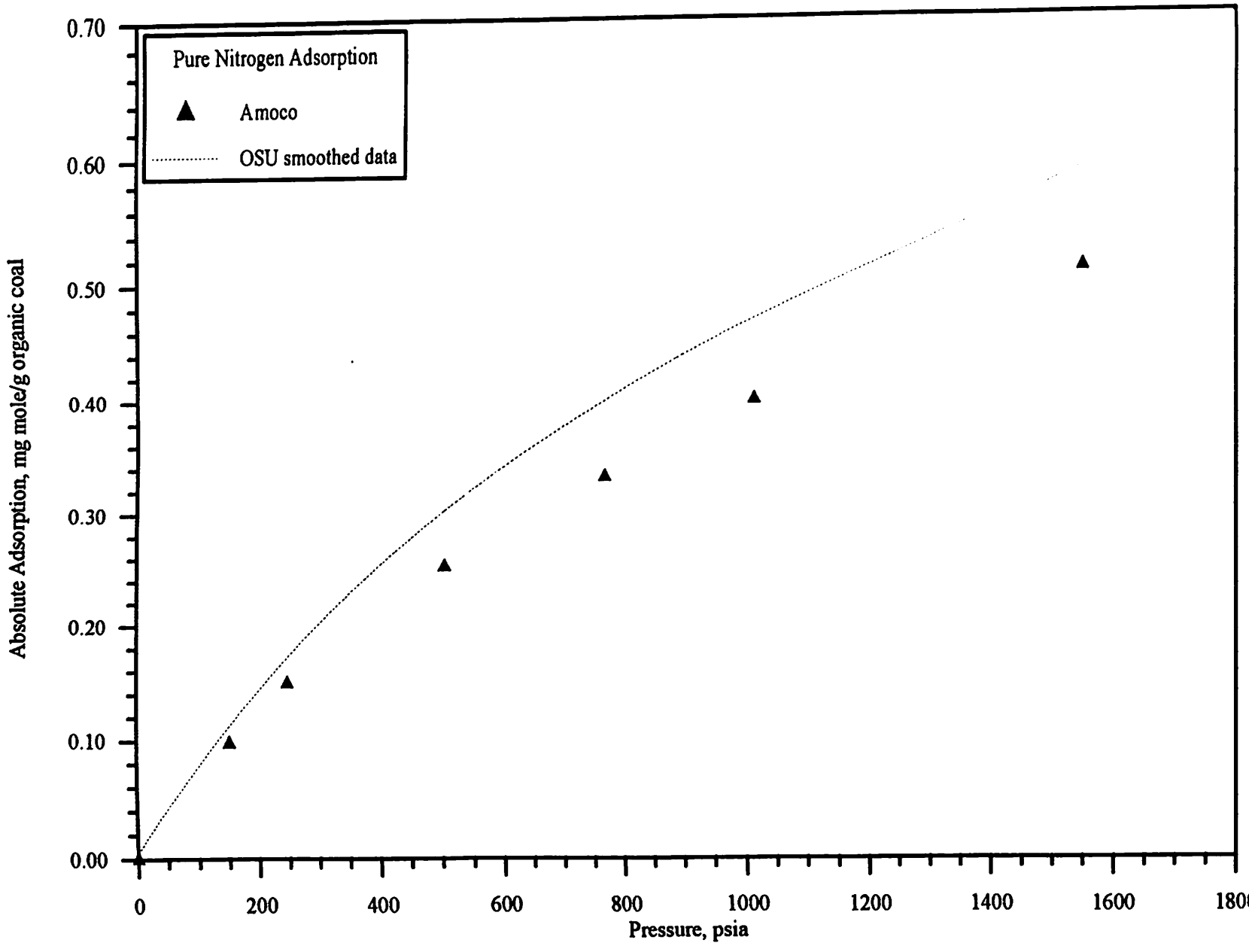

Figure 86. Comparison of Pure Nitrogen Adsorption Data from OSU and Amoco (Organic Coal Basis)

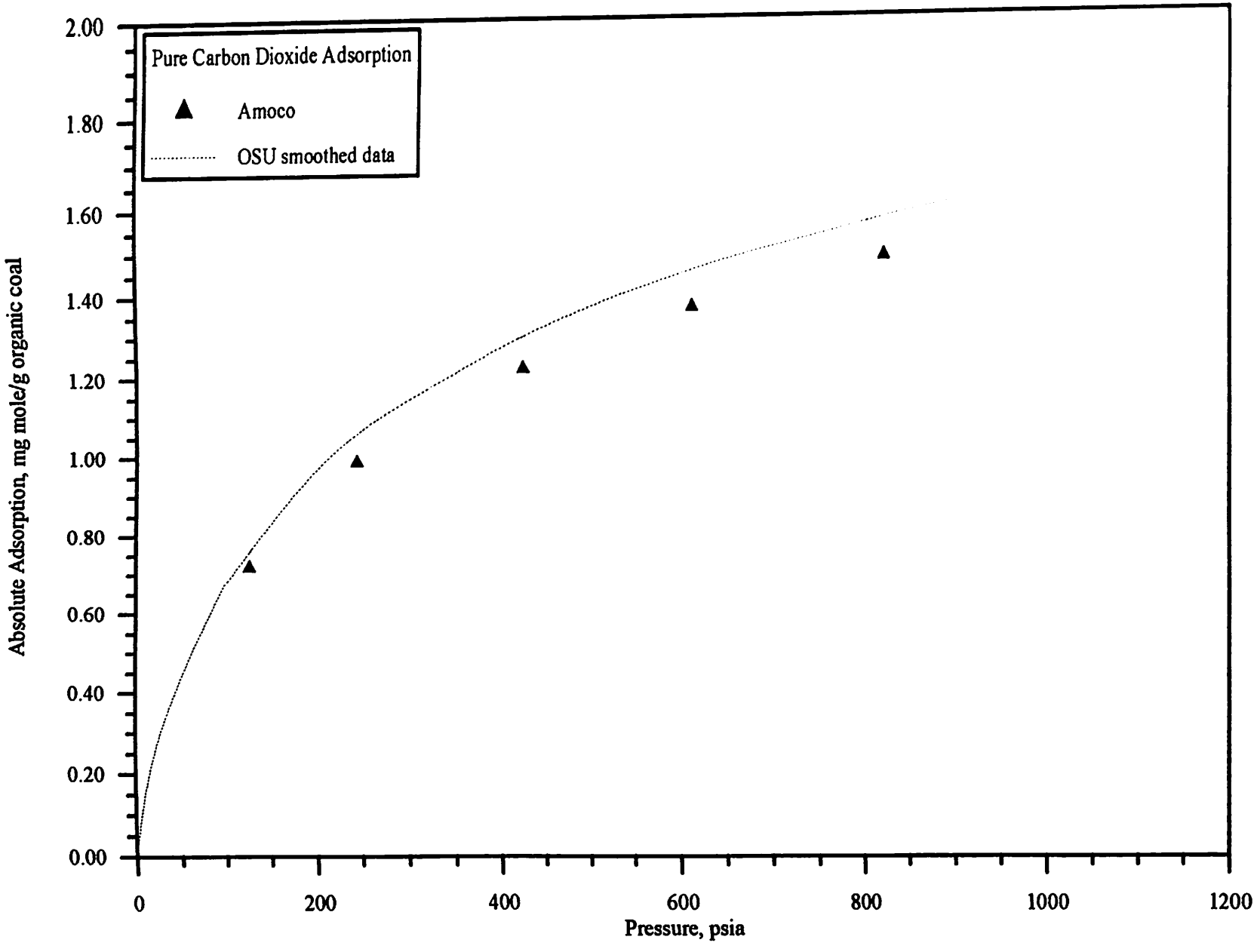

Figure 87. Comparison of Pure Carbon Dioxide Adsorption Data from OSU and Amoco (Organic Coal Basis)

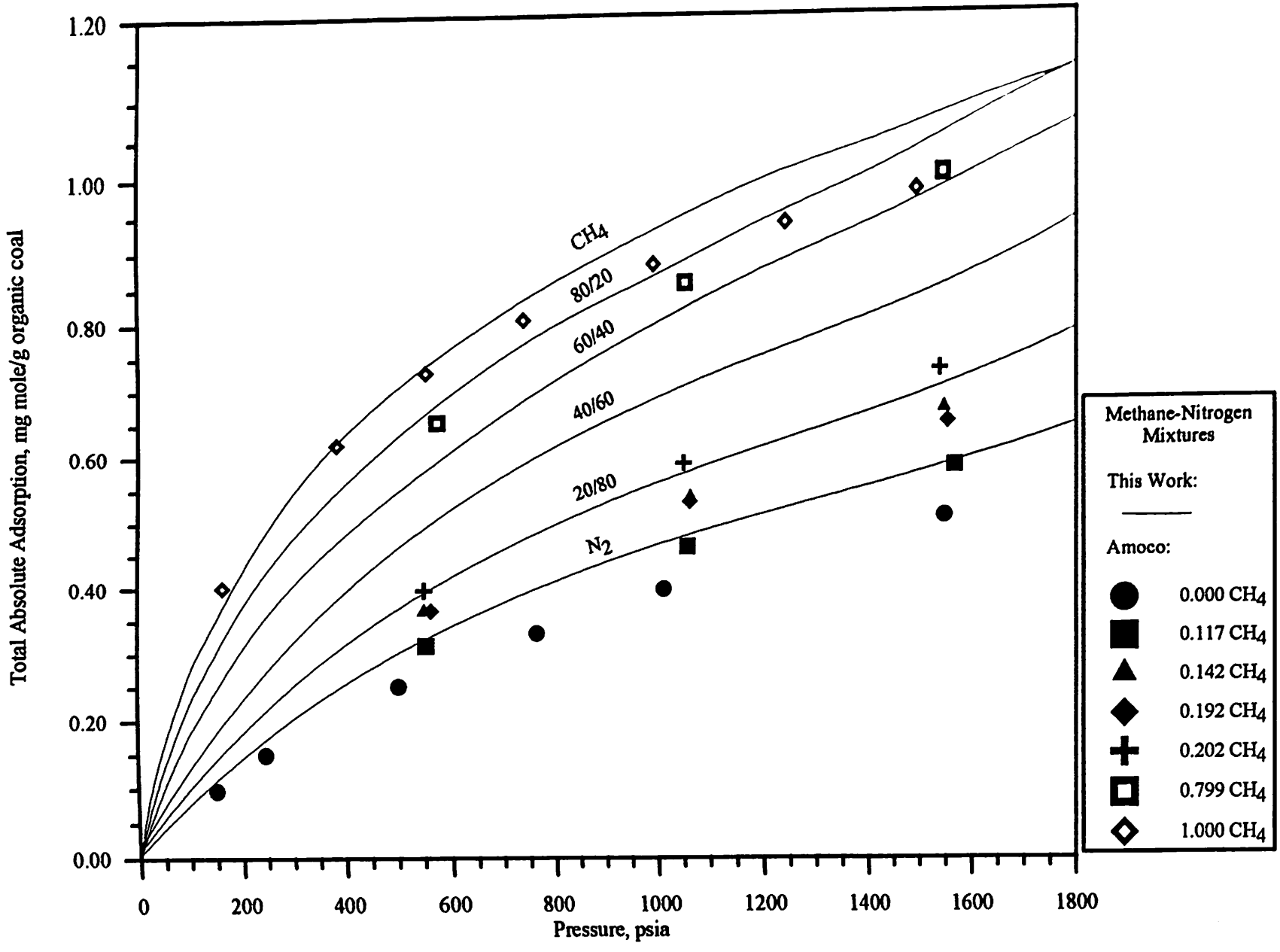

Figure 88. Comparison of Total Absolute Adsorption Data for Methane-Nitrogen Mixtures from OSU and Amoco (Organic Coal Basis)

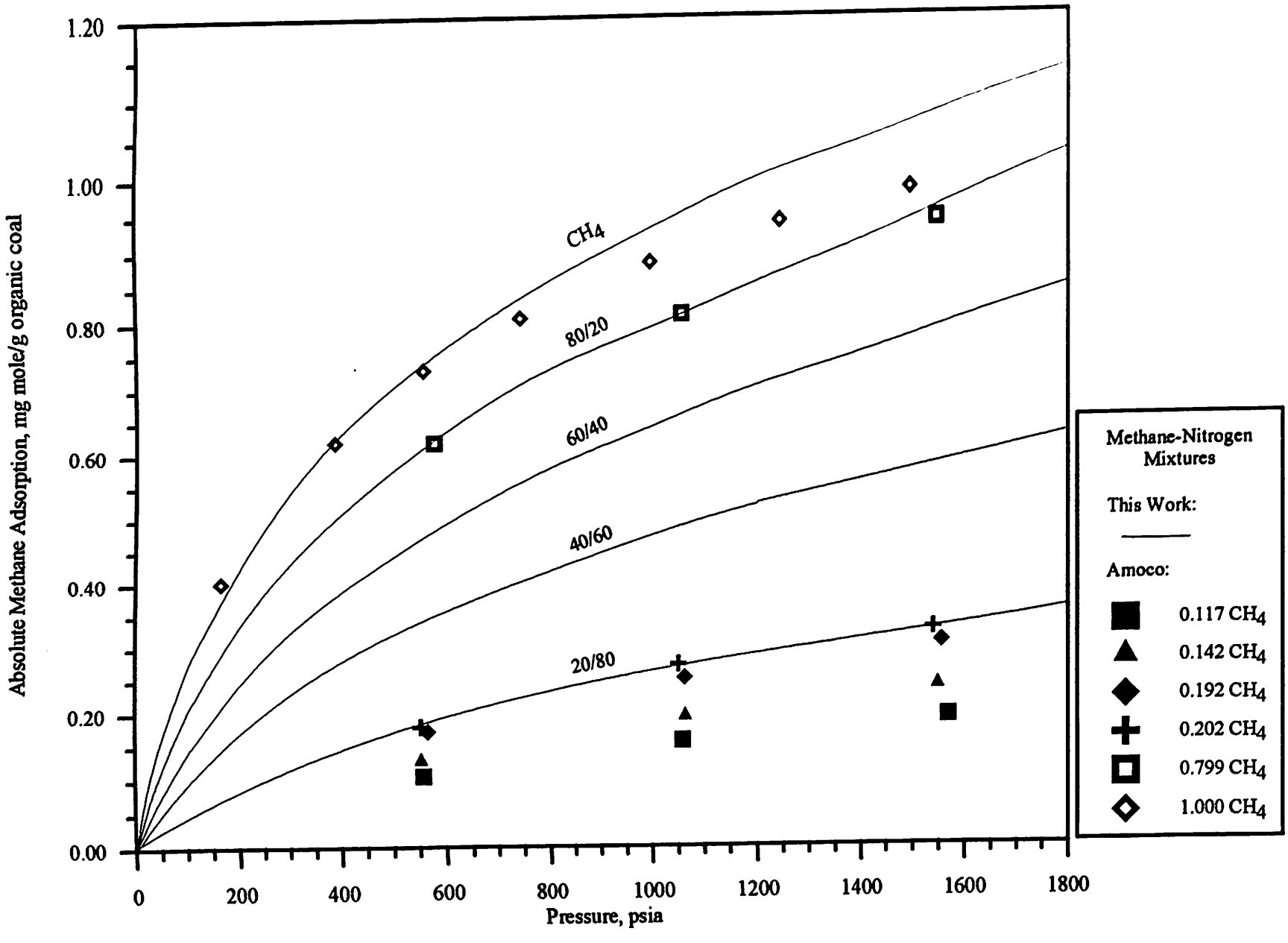

Figure 89. Comparison of Methane Adsorption Data from Methane-Nitrogen Mixtures from OSU and Amoco (Organic Coal Basis)

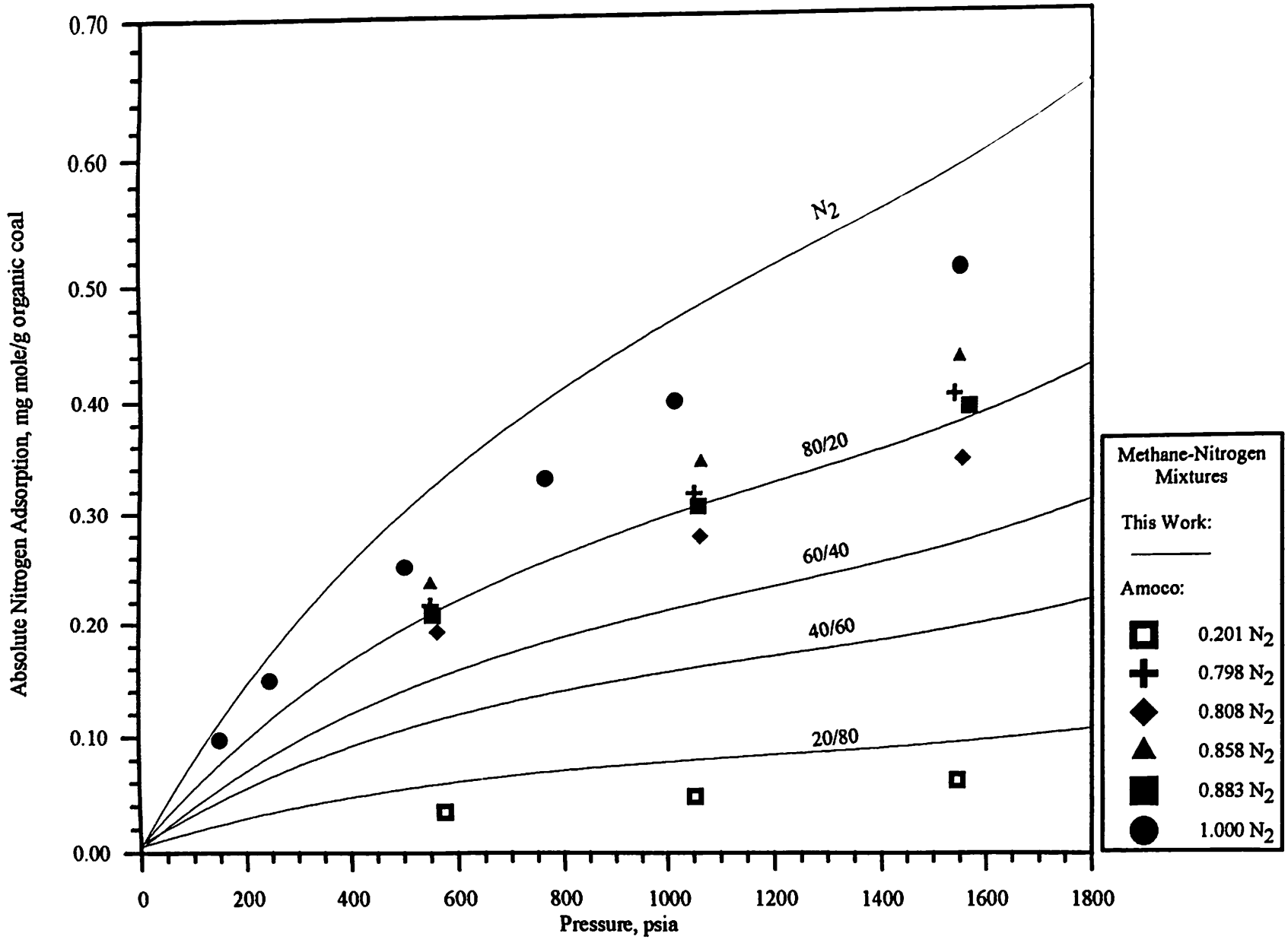

Figure 90. Comparison of Nitrogen Adsorption Data from Methane-Nitrogen Mixtures from OSU and Amoco (Organic Coal Basis)

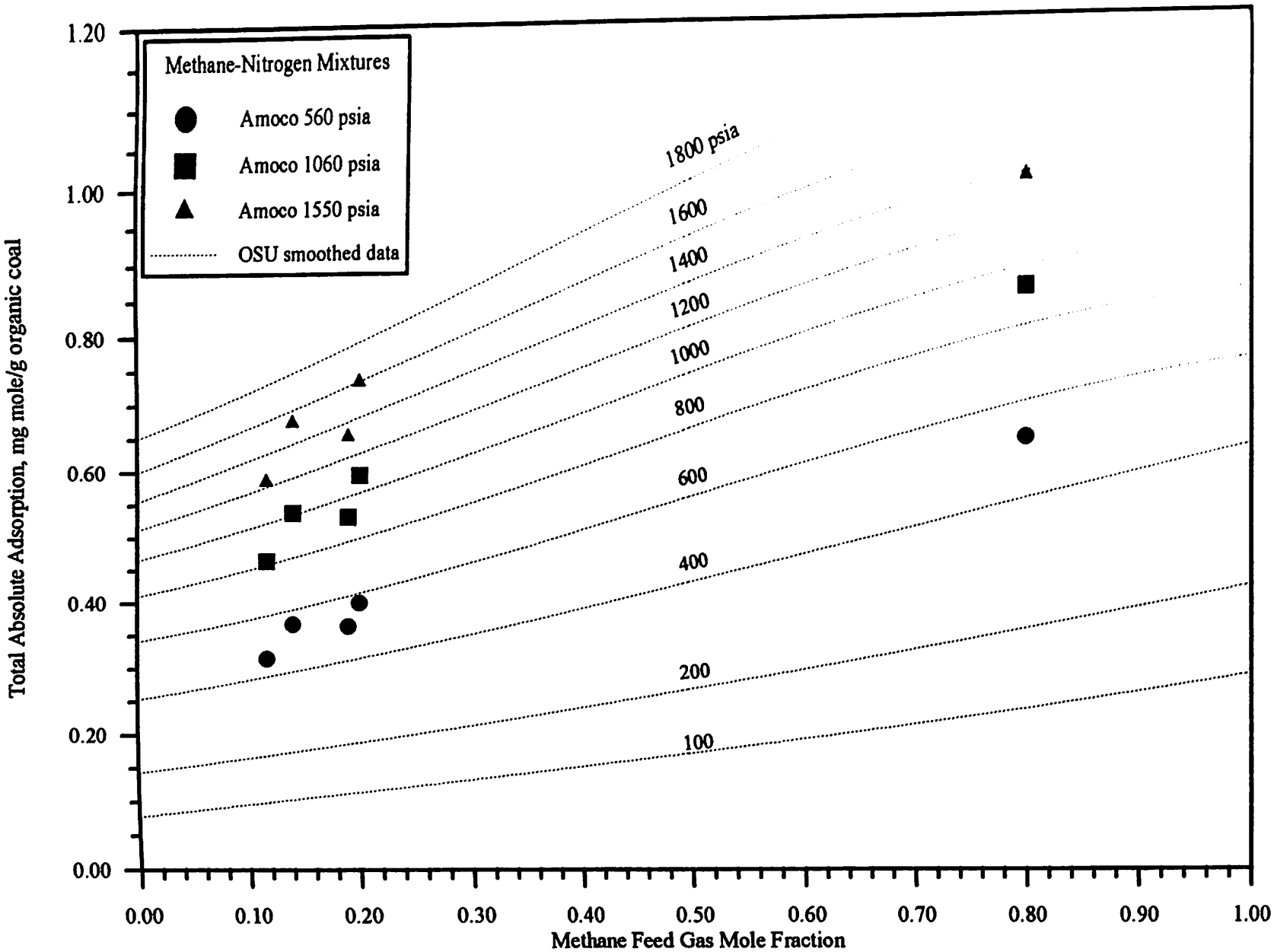

Figure 91. Comparison of Total Adsorption Data from Methane-Nitrogen Mixtures from OSU and Amoco (Organic Coal Basis)

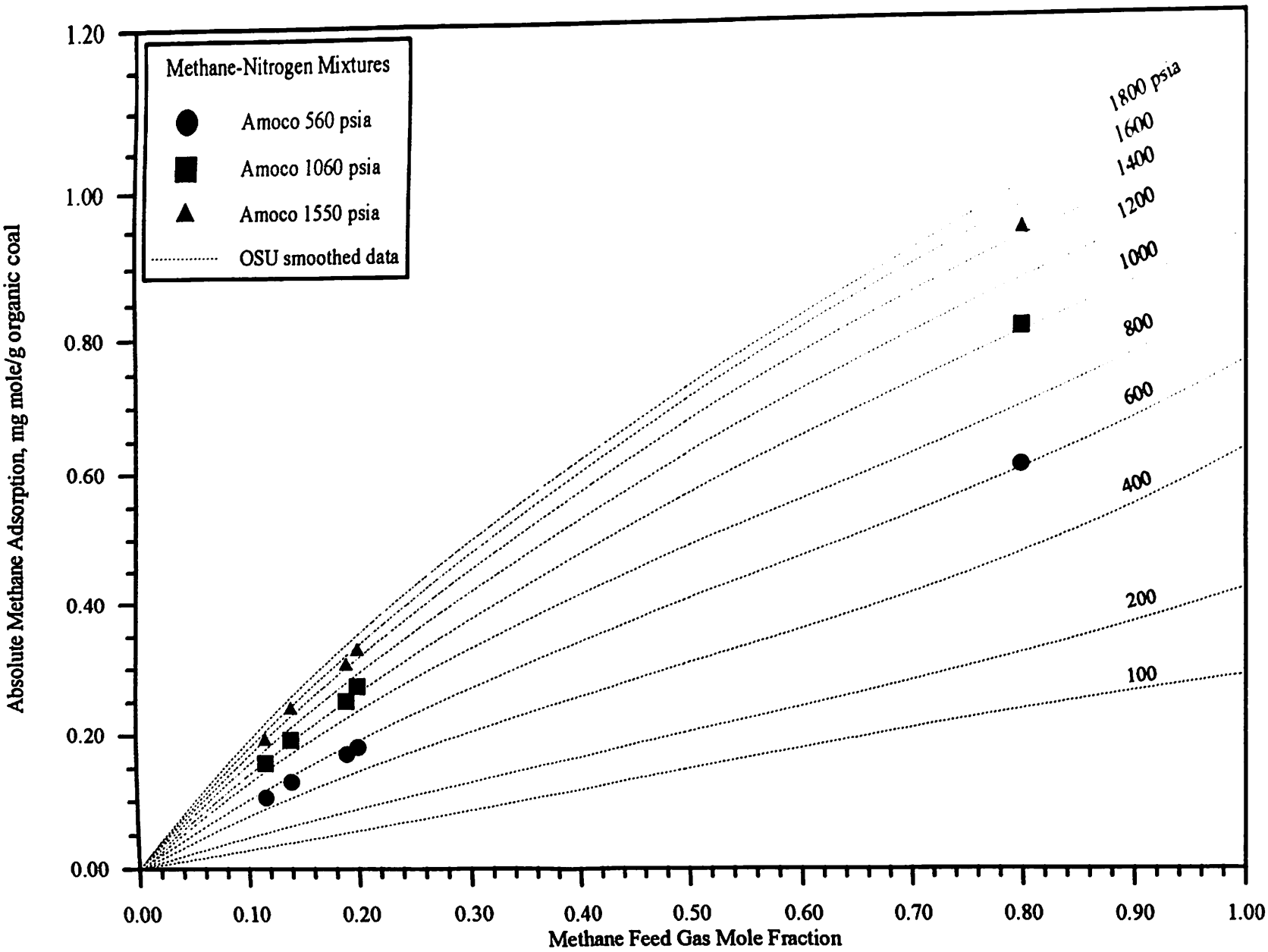

Figure 92. Comparison of Methane Adsorption Data from Methane-Nitrogen Mixtures from OSU and Amoco (Organic Coal Basis)

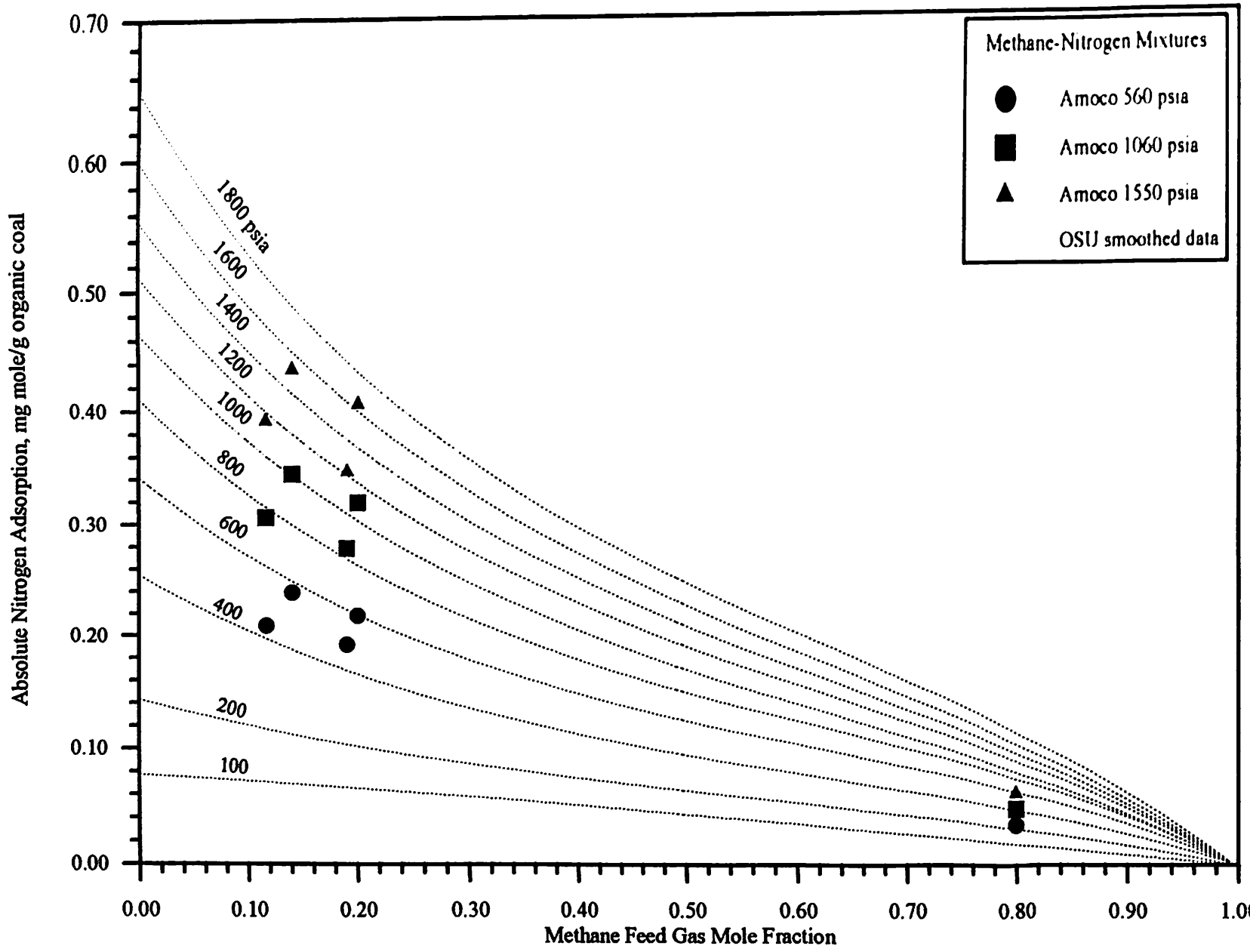

Figure 93. Comparison of Nitrogen Adsorption Data from Methane-Nitrogen Mixtures from OSU and Amoco (Organic Coal Basis)

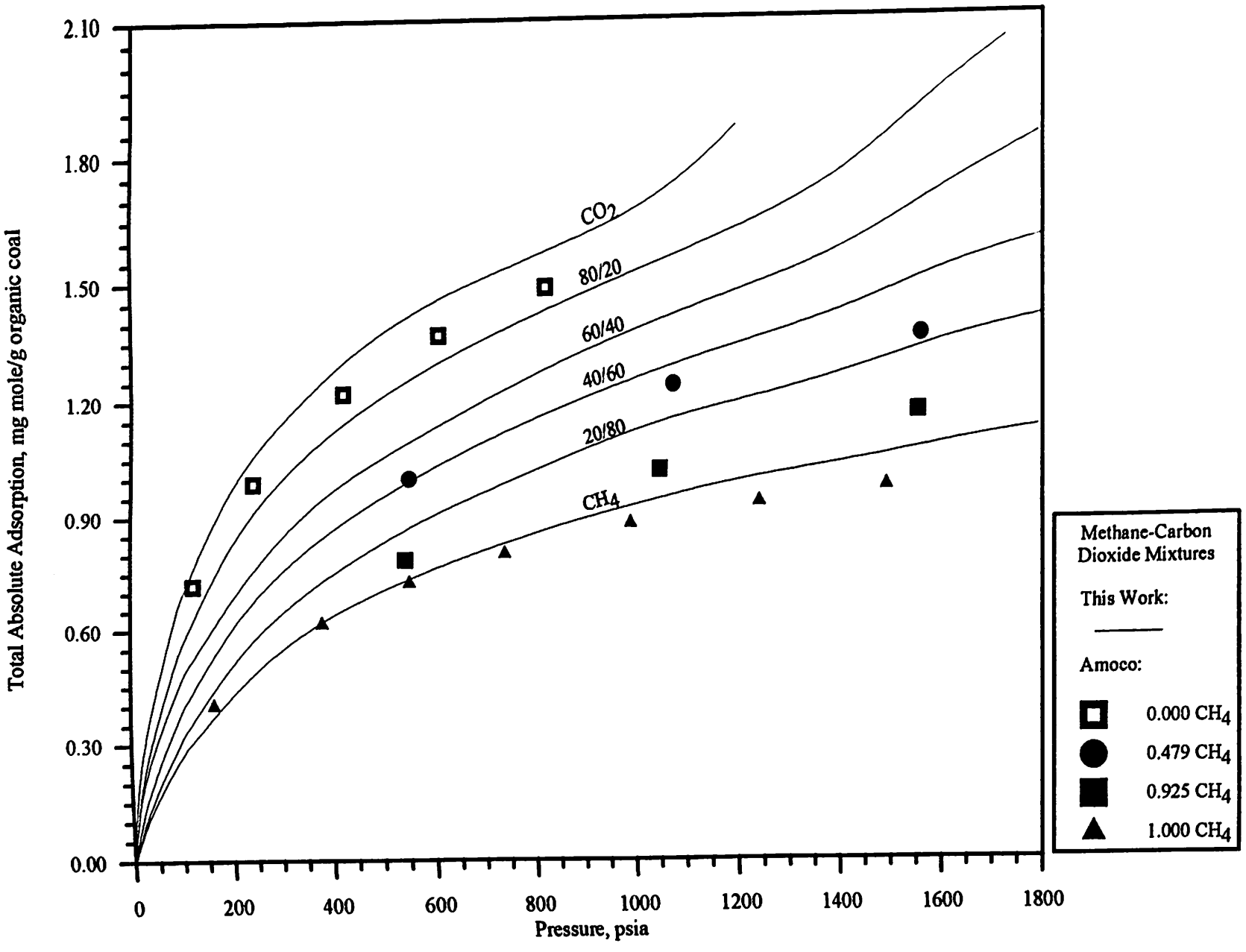

Figure 94. Comparison of Total Adsorption Data from Methane-Carbon Dioxide Mixtures from OSU and Amoco (Organic Coal Basis)

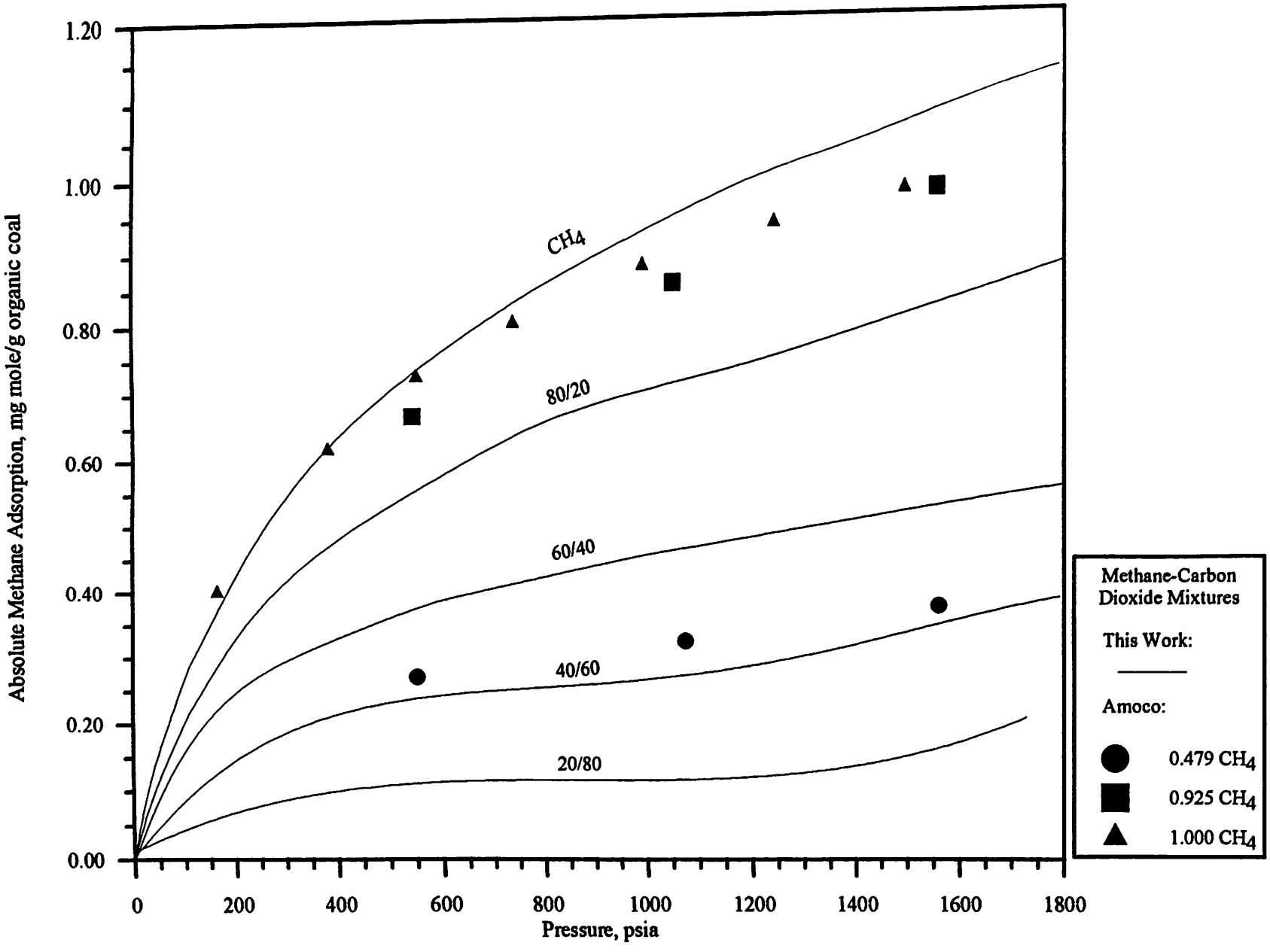

Figure 95. Comparison of Methane Adsorption Data from Methane-Carbon Dioxide Mixtures from OSU and Amoco (Organic Coal Basis)

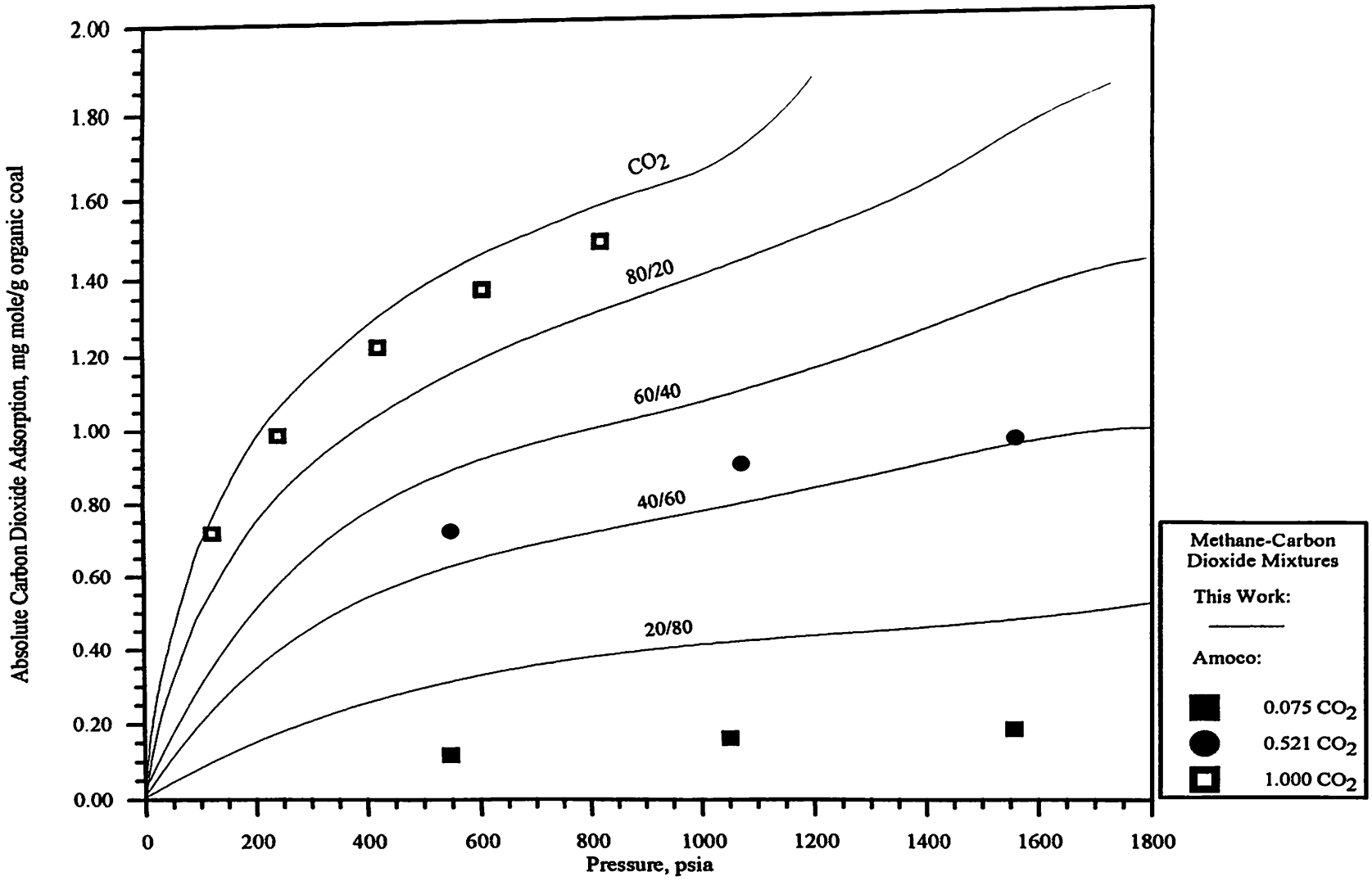

Figure 96. Comparison of Carbon Dioxide Adsorption Data from Methane-Carbon Dioxide Mixtures from OSU and Amoco (Organic Coal Basis)

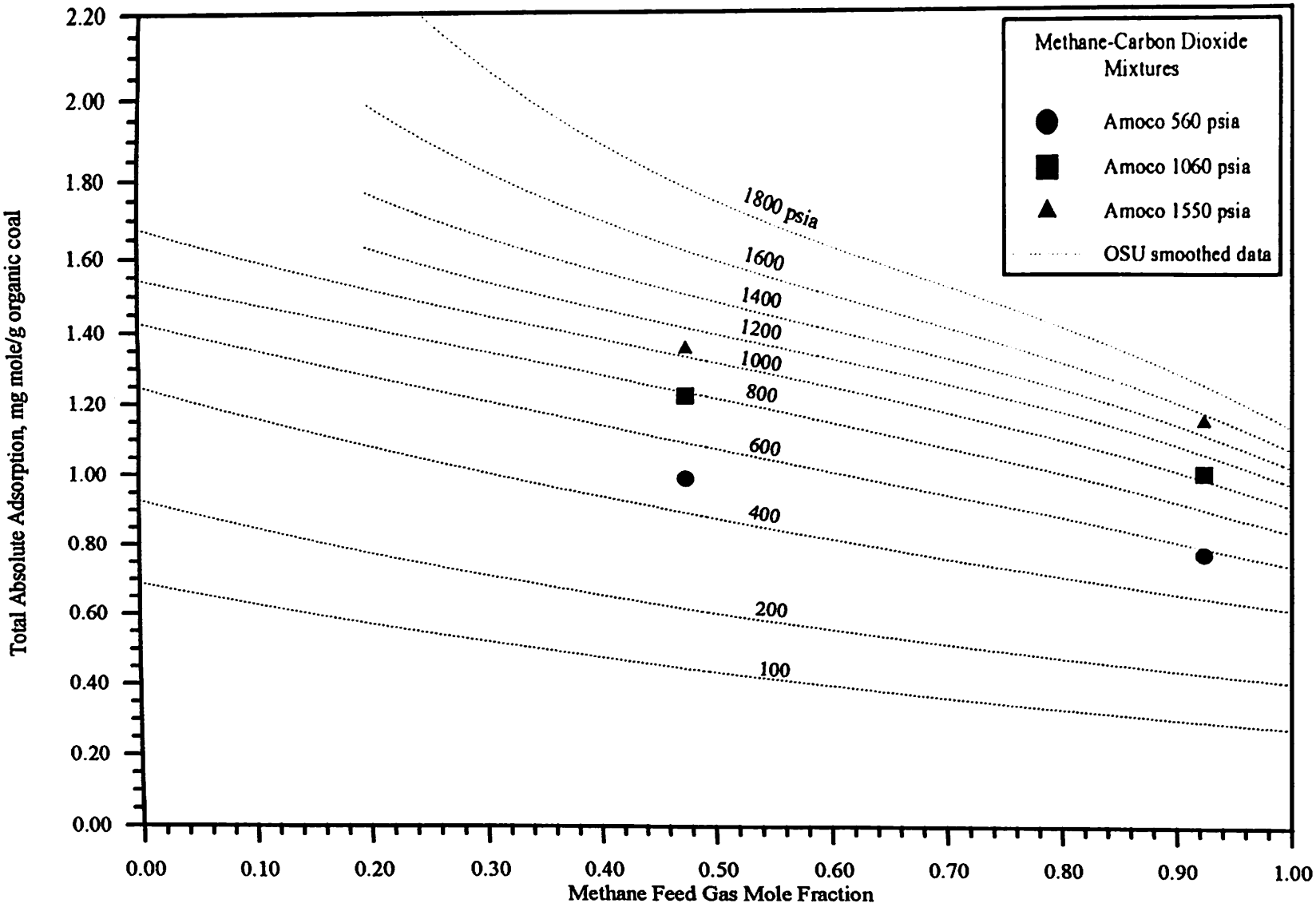

Figure 97. Comparison of Total Adsorption Data from Methane-Carbon Dioxide Mixtures from OSU and Amoco (Organic Coal Basis)

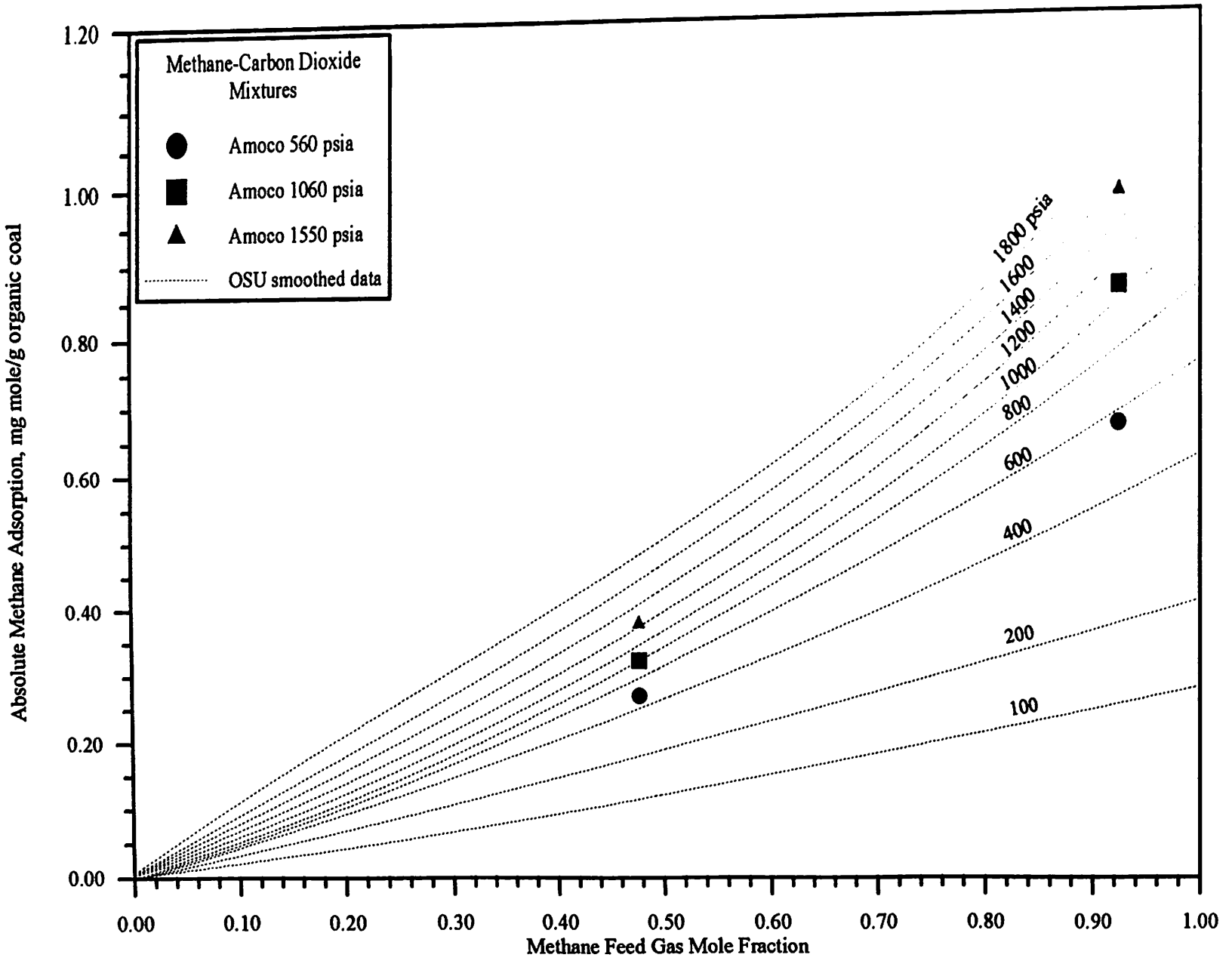

Figure 98. Comparison of Methane Adsorption Data from Methane-Carbon Dioxide Mixtures from OSU and Amoco (Organic Coal Basis)

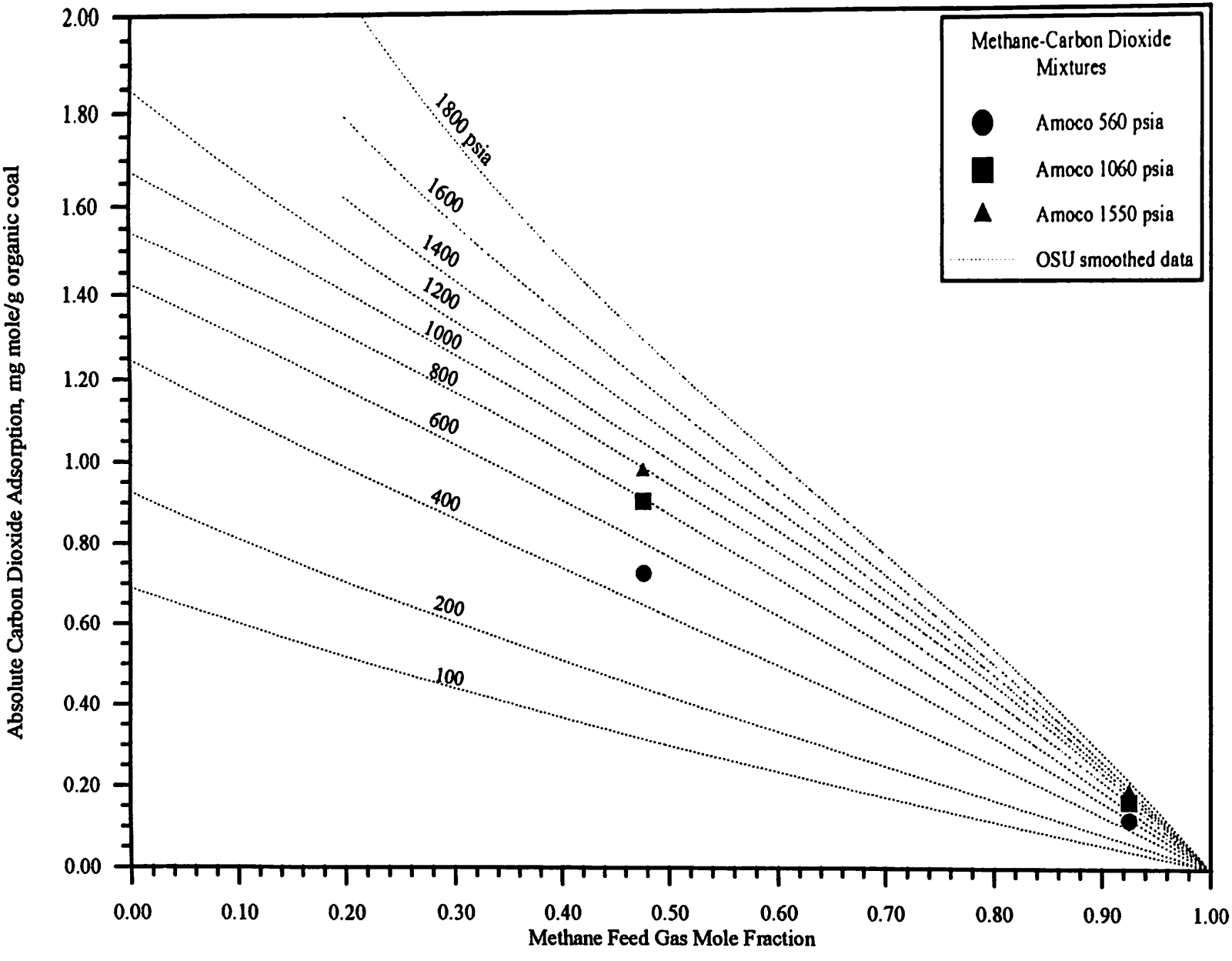

Figure 99. Comparison of Carbon Dioxide Adsorption Data from Methane-Carbon Dioxide Mixtures from OSU and Amoco (Organic Coal Basis)

VITA

Freddie Eddsel Hall Jr.

Candidate for the Degree of

Master of Science

Thesis: ADSORPTION OF PURE AND MULTICOMPONENT GASES ON WET FRUITLAND COAL

Major Field: Chemical Engineering

Biographical:

Personal Data: Born in Oklahoma City, Oklahoma, July 30, 1956, the son of Freddie Eddsel Sr. and Elsie Olive Hall.

Education: Graduated from Crescent High School, Crescent, Oklahoma, in May 1974; attended Mercy Hospitals Radiologic Technology program from June 1977 to June 1979; received radiologic technology license June 1979; received Bachelor of Science Degree in Chemistry, A.C.S. from University of Central Oklahoma at Edmond in May 1986; completed requirements for the Master of Science Degree from Oklahoma State University at Stillwater in December 1993.

Professional Experience: Heart Catheterization Radiologic Technologist, Mercy Hospital, June 1979 to June 1982; Teaching Assistant, Department of Chemistry, Oklahoma State University, August 1987 to December 1989; Research Assistant, Department of Chemical Engineering, Oklahoma State University, May 1991 to December 1993.